

HF
18.5
.A 27
NO.
DOT-
TSC-
UMTA-
79-28

NO. UMTA-MA-06-0100-79-10

✓
**ALLEVIATION OF PRESSURE PULSE EFFECTS
FOR
TRAINS ENTERING TUNNELS**

Jet Propulsion Laboratory
4800 Oak Grove
California Institute of Technology
Pasadena CA 91103



JUNE 1979
FINAL REPORT

DEPARTMENT OF
TRANSPORTATION
SEP 26 1979
LIBRARY

DOCUMENT IS AVAILABLE TO THE PUBLIC
THROUGH THE NATIONAL TECHNICAL
INFORMATION SERVICE, SPRINGFIELD,
VIRGINIA 22161

Prepared for
U.S. DEPARTMENT OF TRANSPORTATION
URBAN MASS TRANSPORTATION ADMINISTRATION
Office of Technology Development and Deployment
Office of Rail and Construction Technology
Washington DC 20590

*Transportation
3*

NOTICE

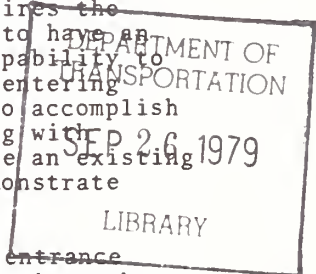
This document is disseminated under the sponsorship of the Department of Transportation in the interest of information exchange. The United States Government assumes no liability for its contents or use thereof.

NOTICE

The United States Government does not endorse products or manufacturers. Trade or manufacturers' names appear herein solely because they are considered essential to the object of this report.

4E
18.5
A37
n0.
DOT-
TSC-
UMTA-
79-28

1. Report No. UMTA-MA-06-0100-79-10		2. Government Accession No.		3. Recipient's Catalog No.	
4. Title and Subtitle Alleviation of Pressure Pulse Effects for Trains Entering Tunnels				5. Report Date June 1979	
				6. Performing Organization Code DTS-222	
7. Author(s) B. Dayman, Jr., A.G. Hammitt, H.P. Holway, C.E. Tucker, Jr., and A.E. Vardy				8. Performing Organization Report No. DOT-TSC-UMTA-79-28	
				10. Work Unit No. (TRAIS) UM948/R9745	
9. Performing Organization Name and Address Jet Propulsion Laboratory* 4800 Oak Grove California Institute of Technology Pasadena CA 91103				11. Contract or Grant No. DOT-RA-N-02-612-0397	
				13. Type of Report and Period Covered Final Report March 1977 - May 1978	
12. Sponsoring Agency Name and Address U.S. Department of Transportation Urban Mass Transportation Administration Office of Technology Development and Deployment Office of Rail and Construction Technology Washington DC 20590				14. Sponsoring Agency Code	
				15. Supplementary Notes * Under contract to: U.S. Department of Transportation Research and Special Programs Administration Transportation Systems Center Cambridge MA 02142	
16. Abstract <p>This study was carried out for the Transportation Systems Center of the U.S. Department of Transportation on behalf of the Urban Mass Transportation Administration in order to determine to what degree it is possible to attenuate the effects of pressure pulses on the passengers in trains entering tunnels. The emphasis of this study is on the approach of modifying the normal, abrupt entry portal of the constant diameter single-track tunnel.</p> <p>In order to understand this approach, which requires the tailoring of a tunnel portal, it was first necessary to have an analytical model in which confidence exists in its capability to predict realistic pressure pulse histories of trains entering tunnels having porous and/or flared entry portals. To accomplish this, the best available theoretical information along with small-scale laboratory experiments were used to update an existing computer program. Then, this program was used to demonstrate effective portal configurations.</p> <p>Although reasonable modifications to the tunnel entrance portal may not decrease the magnitude of the pressure rise, they are very effective in reducing the discomfort to the human ear by decreasing the rate of pressure rise to what the normal ear can accommodate. A brief qualitative comparison was made of this portal modification approach with other approaches: decreasing the train speed during the tunnel entry and sealing the cars. The optimum approach, which is dependent upon the conditions and requirements of each particular rail system, is likely to be the portal modification one for the subway urban transit system.</p>					
17. Key Words Pressure Transients, Tunnel Entry, Sub- way Train Pressure Transients, Passenger Train Pressure Transients, Pressure Pulse Tunnels			18. Distribution Statement DOCUMENT IS AVAILABLE TO THE PUBLIC THROUGH THE NATIONAL TECHNICAL INFORMATION SERVICE, SPRINGFIELD, VIRGINIA 22161		
19. Security Classif. (of this report) Unclassified		20. Security Classif. (of this page) Unclassified		21. No. of Pages 242	22. Price



PREFACE

All five of the primary contributors to this study are listed as authors. Three are from the Jet Propulsion Laboratory (JPL) while the other two are private consultants. The main responsibilities of the contributors are as follows:

Bain Dayman, Jr. (JPL) (Sections 8, 11) coordinated the study and documentation efforts.

Harold P. Holway (JPL) (Section 8) developed the experimental facility and conducted the tests.

Curtis E. Tucker, Jr. (JPL) (Section 8) carried out the data analysis and documentation.

Dr. Andrew G. Hammitt (Palos Verdes Peninsula, CA, USA) (Sections 7, 9) investigated analytical assumptions and developed simplified understandings of the pressure pulse phenomena.

Dr. Allan E. Vardy (Cambridge University, England) (Sections 5, 6, 9, 10) assessed the state-of-the-art and made computer studies to compare with the experimental results and to predict the situation for typical full-scale systems.

The authors are very appreciative of the guidance and stimulation received from Dr. Timothy M. Barrows of DOT's Transportation Systems Center, who monitored this study. Because of his contributions which were based upon his directly related expertise, he really should be considered as one of the co-authors of this study. Much of the material in this report was taken directly from the reports Drs. Hammitt and Vardy prepared for this study. These reports can be obtained directly from the authors. Besides Reference 8, they are:

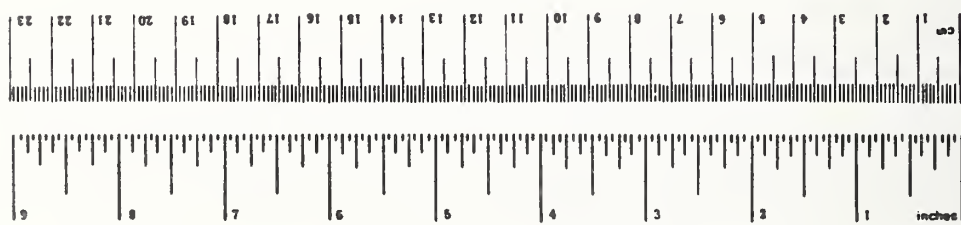
Hammitt, A.G., "Pressure Effect Caused by Vehicle Entering a Tunnel," Report No. 20-001-78, February 1978.

Vardy, A.E., "Tunnel Entry Pressure Transients, Experiments and Theoretical Evidence," December 1977.

METRIC CONVERSION FACTORS

Approximate Conversions to Metric Measures

Symbol	When You Know	Multiply by	To Find	Symbol
LENGTH				
in	inches	2.5	centimeters	cm
ft	feet	30	centimeters	cm
yd	yards	0.9	meters	m
mi	miles	1.6	kilometers	km
AREA				
m ²	square inches	6.5	square centimeters	cm ²
ft ²	square feet	0.09	square meters	m ²
yd ²	square yards	0.8	square meters	m ²
mi ²	square miles	2.6	square kilometers	km ²
	acres	0.4	hectares	ha
MASS (weight)				
oz	ounces	28	grams	g
lb	pounds	0.45	kilograms	kg
	short tons (2000 lb)	0.9	tonnes	t
VOLUME				
teaspoon	teaspoons	5	milliliters	ml
Tablespoon	tablespoons	15	milliliters	ml
fl oz	fluid ounces	30	milliliters	ml
c	cups	0.24	liters	l
pt	pints	0.47	liters	l
qt	quarts	0.95	liters	l
gal	gallons	3.8	liters	l
ft ³	cubic feet	0.03	cubic meters	m ³
yd ³	cubic yards	0.76	cubic meters	m ³
TEMPERATURE (exact)				
°F	Fahrenheit temperature	5/9 (after subtracting 32)	Celsius temperature	°C



Approximate Conversions from Metric Measures

Symbol	When You Know	Multiply by	To Find	Symbol
LENGTH				
mm	millimeters	0.04	inches	in
cm	centimeters	0.4	inches	in
m	meters	3.3	feet	ft
km	kilometers	1.1	yards	yd
		0.6	miles	mi
AREA				
cm ²	square centimeters	0.16	square inches	in ²
m ²	square meters	1.2	square yards	yd ²
km ²	square kilometers	0.4	square miles	mi ²
ha	hectares (10,000 m ²)	2.5	acres	
MASS (weight)				
g	grams	0.035	ounces	oz
kg	kilograms	2.2	pounds	lb
t	tonnes (1000 kg)	1.1	short tons	
VOLUME				
ml	milliliters	0.03	fluid ounces	fl oz
l	liters	2.1	pints	pt
l	liters	1.06	quarts	qt
l	liters	0.26	gallons	gal
m ³	cubic meters	35	cubic feet	ft ³
m ³	cubic meters	1.3	cubic yards	yd ³
TEMPERATURE (exact)				
°C	Celsius temperature	9/5 (then add 32)	Fahrenheit temperature	°F

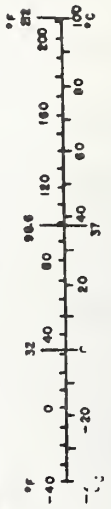


TABLE OF CONTENTS

<u>Section</u>	<u>Page</u>
1. INTRODUCTION.....	1-1
2. BACKGROUND.....	2-1
2.1 Principal Sources of Pressure Disturbances.....	2-1
2.2 Effect on the Human Ear.....	2-2
2.3 Pressure Pulse Problems.....	2-4
3. OBJECTIVE.....	3-1
4. APPROACH.....	4-1
4.1 Theoretical/Analytical.....	4-1
4.1.1 Basic Tunnel.....	4-1
4.1.2 Modified Tunnel and/or Train Design.....	4-1
4.2 Experimental Program.....	4-2
4.3 Other Approaches.....	4-2
4.3.1 Speed Restriction.....	4-2
4.3.2 Sealed Cars.....	4-3
4.3.3 Initiate Flow Through Tunnel.....	4-3
4.3.4 Trade-Off Study.....	4-3
5. STATE-OF-THE-ART ASSESSMENT.....	5-1
5.1 Parameters Influencing Entry Transient Magnitudes.....	5-1
5.2 Reduction of Pressure Transients.....	5-6
5.2.1 Modifications to Trains.....	5-8
5.2.2 Modifications to Tunnel Geometry.....	5-10
5.3 Theoretical Analyses.....	5-17
5.3.1 Evaluation of Additional Terms.....	5-18
5.3.2 Further Simplifications.....	5-20
5.4 Experimental Investigation.....	5-21
5.4.1 Geometric Similarity.....	5-21
5.4.2 Dynamic Similarity.....	5-23
5.5 Identification of Pressure Transients.....	5-24
5.6 Highlights.....	5-31
5.7 Nomenclature.....	5-32

TABLE OF CONTENTS (CONT'D)

<u>Section</u>	<u>Page</u>
6. THE COMPUTER PROGRAM.....	6-1
6.1 Capabilities of the Program.....	6-1
6.1.1 Tunnel System.....	6-1
6.1.2 Trains.....	6-2
6.2 Flow Through Walls of Perforated Portals.....	6-3
7. SIMPLIFIED THEORETICAL ANALYSIS.....	7-1
7.1 Scaling.....	7-1
7.2 Flared Entry Portal.....	7-7
7.2.1 Analysis.....	7-9
7.2.2 Discussion.....	7-15
7.3 Perforated Entry Portal.....	7-22
7.3.1 Analysis.....	7-22
7.3.2 Discussion.....	7-27
7.4 Comparison of Entry Portals.....	7-31
7.5 Nomenclature.....	7-31
8. EXPERIMENTAL PROGRAM.....	8-1
8.1 Purpose.....	8-1
8.2 Description of Facility.....	8-1
8.2.1 Tube.....	8-1
8.2.2 Launcher.....	8-1
8.2.3 Instrumentation.....	8-5
8.3 Configurations Studied.....	8-7
8.3.1 Tube Assembly.....	8-7
8.3.2 Models.....	8-10
8.3.3 Entry Portals.....	8-14
8.4 Run Index.....	8-21
8.5 Raw Data.....	8-21
8.6 Data Reduction.....	8-23
8.6.1 Pressure.....	8-23
8.6.2 Time.....	8-26
8.6.3 Model Speed.....	8-26

TABLE OF CONTENTS (CONT'D)

<u>Section</u>	<u>Page</u>
8.7 Interpretation of Experimental Data.....	8-29
8.7.1 Train Parameters.....	8-29
8.7.2 Tunnel Parameters.....	8-30
8.7.3 Flared Entry Portal.....	8-32
8.7.4 Vent Shafts.....	8-33
8.7.5 Exit Restrictions (Orifices).....	8-34
9. VALIDATION OF ANALYTICAL UNDERSTANDING.....	9-1
9.1 Computer Program.....	9-1
9.1.1 Run 131 (Figure 9.1)*.....	9-1
9.1.2 Run 160 (Figure 9.2)*.....	9-3
9.1.3 Run 162 (Figure 9.3).....	9-5
9.1.4 Run 173 (Figure 9.4).....	9-5
9.1.5 Run 184 (Figure 9.5).....	9-6
9.1.6 Run 186 (Figure 9.6).....	9-7
9.1.7 Run 207 (Figure 9.7).....	9-7
10. APPLICATION TO FULL-SCALE SYSTEMS.....	10-1
10.1 Simple Tunnel Configuration.....	10-2
10.2 Complex Tunnel Configuration.....	10-10
11. TRADE-OFF STUDY.....	11-1
11.1 Cost Estimates for Modified Tunnel Portals.....	11-1
11.1.1 Flared Portal.....	11-1
11.1.2 Summary.....	11-4
11.2 Speed Restrictions.....	11-4
11.2.1 Computer Program.....	11-5
11.2.2 Results.....	11-5
11.3 Sealed Cars.....	11-7
11.4 Initiate Flow in Tunnel.....	11-7
11.5 Comparisons of Approaches.....	11-8
12. SUMMARY.....	12-1
APPENDIX A: RUN INDEX.....	A-1
APPENDIX B: EXAMPLES OF RAW DATA.....	B-1

TABLE OF CONTENTS (CONT'D)

<u>Section</u>	<u>Page</u>
REFERENCES/BIBLIOGRAPHY.....	R-1

LIST OF ILLUSTRATIONS

<u>Figures</u>		<u>Page</u>
1-1	Sketch Showing Tunnel Portal Extensions.....	1-2
5-1	Train Entering Tunnel.....	5-1
5-2	Nose Wave Magnitude.....	5-4
5-3	Train Just After Entry.....	5-5
5-4	Tail Wave Magnitude.....	5-7
5-5	Pressure Distributions Along Tunnel.....	5-25
5-6	Pressure Histories Inside Tunnel.....	5-27
5-7	Reflection of a Ramp - Wavefront.....	5-29
7-1	Diagram of Flow Through Pore.....	7-3
7-2	Unsteady Velocity Through Pore as Function of Dimensionless Time.....	7-4
7-3	Schematic Diagram of Vehicle in Flared Tunnel Entrance.....	7-10
7-4	Pressure Coefficients for Two Flares and Straight Tunnel Entrance (Configurations at Two Vehicle Mach Numbers: $A_0 = 1.309 A_V$, $S = 12.22\sqrt{A_0}$).....	7-17
7-5	Effect of Different Entrance Flare and Tunnel Sizes on Pressure Coefficient as Vehicle Enters Tunnel.....	7-21
7-6	Velocity Through Pores Divided by Velocity Through Annulus Around Vehicle as a Function of Pressure Coefficient.....	7-24
7-7	Schematic Diagram of Vehicle Entering Porous Tunnel.....	7-25
7-8	Pressure Coefficients During Vehicle Entry Into Porous Tunnels.....	7-30
8-1	Tube Configuration.....	8-2
8-2	Complete Tept Facility.....	8-3
8-3	Top View of Launcher.....	8-4
8-4	Side View of Launcher.....	8-4
8-5	Vent Shaft.....	8-6
8-6	Vent-Shaft Configuration.....	8-9

LIST OF ILLUSTRATIONS (CONT'D)

<u>Figure</u>		<u>Page</u>
8-7	Actual Models Tested.....	8-11
8-8	Model Configurations.....	8-12
8-9	Perforated Entrance Portals (Constant Porosity).....	8-15
8-10	Flared Entry Portal.....	8-19
8-11	Flare Configuration.....	8-20
9-1a	Run 131, T19, M55-50.....	9-17
9-1b	TEPT131, T19, M55-50.....	9-18
9-2a	Run 160, T19-V2, M55-50.....	9-19
9-2b	TEPT160, T19-V2, M55-50.....	9-20
9-3a	Run 162, T19-V5 ₀ , M55-50.....	9-21
9-3b	TEPT162, T19-V5*, M55-50.....	9-22
9-4a	Run 173, T19, F1-0, M55-50.....	9-23
9-4b	TEPT173, T19, F1-0, M55-50.....	9-24
9-4a*	Run 173A, T19, F1-0*, M55-50.....	9-25
9-4b*	TEPT173A, T19, F1-0*, M55-50.....	9-26
9-5a	Run 184, T18, M110-50.....	9-27
9-5b	TEPT184, T18, M110-50.....	9-28
9-6a	Run 186, T18, M110-50.....	9-29
9-6b	TEPT186, T18, P1-50, M110-50.....	9-30
9-7a	Run 207, T19, M55-50B.....	9-31
9-7b	TEPT207, T19, M55-50B.....	9-32
9-8	Developing Velocity Profile.....	9-33
9-9	Pressure Coefficient as Vehicle Enters Tunnel; Comparison Between Theory, Vardy's Calculations, and Experiment; $A_0 = 2.116 A_V$, $S = 24.44\sqrt{A_0}$, $c_f = .006$, $M_V = .07225$	9-35

LIST OF ILLUSTRATIONS

<u>Figure</u>		<u>Page</u>
9-10	Pressure Coefficient as Vehicle Enters Flared Tunnel; Comparison Between Theory and Experiments; $A_0 = 4 A_V$, $S = 12.22\sqrt{A_0}$, $c_f = .006$, $M_V = .07225$	9-36
9-11	Pressure Coefficient as Vehicle Enters Flared Tunnel; Comparison Between Theory, Vardy's Calculations and Experiment; $A_0 = 2.116 A_V$, $S = 12.22\sqrt{A_0}$, $c_f = .006$, $M_V = .07225$	9-38
9-12	Pressure Coefficient as Vehicle Enters Flared Tunnel, Comparison Between Theory and Experiments, $A_0 = 1.309A_V$, $S = 12.22\sqrt{A_0}$, $c_f = .006$, $M_V = .07225$	9-39
9-13	Pressure Coefficient as Vehicle Enters Porous Tunnel; Comparison Between Theory, Vardy's Calculations, and Experiments; $A_0 = 2.116 A_V$, $S = 24.44\sqrt{A_0}$, $c_f = .006$, $M_V = .07225$	9-40
10-1	Diagrammatic Representation of Improved Tunnel Entrance Region for a Simple Tunnel.....	10-3
10-2	Berkeley Hills Simulation.....	10-4
10-3	Berkeley Hills and Perforated Extension.....	10-5
10-4	Berkeley Hills and Flared Extension.....	10-6
10-5	Berkeley Hills Extension and Shaft.....	10-8
10-6	Diagrammatic Representation of Complex Tunnel.....	10-11
10-7	Transbay Tube Simulation.....	10-12
10-8	Transbay and Perforated Extension.....	10-13
10-9	Transbay and Orifice Plates in Shafts.....	10-15
10-10	Transbay with Smaller Cross-Dampers.....	10-16
10-11	Transbay and All Three Modifications.....	10-17
11-1	Effect of Train Speed Pressure Transients Experienced by Riders on Trains Entering Tunnels.....	11-9
11-2	Effect of Portal Extension on Pressure Transients Experienced by Riders on Trains Entering Tunnels.....	11-11
B-1	Calibration Traces.....	B-3

LIST OF TABLES

<u>Table</u>		<u>Page</u>
2-1	Pressure Pulse Problems.....	2-6
8-1	Configuration Descriptions (Entrance Portal Extensions).....	8-16
8-2	Perforated Entrance Portal (Linearly Distributed Porosity)....	8-17
8-3	Run Nomenclature.....	8-22
8-4a	Calibrated Pressure Values Statham Transducers (Upper Trace)*.....	8-25
8-4b	Calibrated Pressure Values Piezo Transducers (Lower Trace).....	8-25
8-5	Calibrated Sweep Time Values, True Time Ms/Grid (2% Accuracy).	8-26
8-6	Determination of Model Speed Through Tube.....	8-28
9-1	Computer Output for Run 131.....	9-9
9-2	Computer Output for Run 160.....	9-10
9-3	Computer Output for Run 162.....	9-11
9-4	Computer Output for Run 173.....	9-12
9-4*	Computer Output for Run 173A.....	9-13
9-5	Computer Output for Run 184.....	9-14
9-6	Computer Output for Run 186.....	9-15
9-7	Computer Output for Run 207.....	9-16
11-1	Train Characteristics.....	11-6
11-2	Trade-Off Study Comparison of Approaches (\$K per Year).....	11-12

1. INTRODUCTION

When a train enters a tunnel at speeds in excess of 60 mph for typical ratios of train to tunnel cross-section areas, pressure fluctuations occur which may cause passenger discomfort. Fox and Vardy (Reference 1) and Barrows (Reference 2) examined this issue from a general standpoint and concluded that a perforated entry portal of the type shown in Figure 1.1 can be a very effective means of replacing the sudden pressure jump which occurs at nose entry with a controlled, gradual increase. The advantages of limiting the rate of rise in this fashion were explained, and it was shown that wave reflections from either end of the tunnel are often the most important source of pressure fluctuations. It was assumed for simplicity that waves reflect perfectly from the ends of the tunnel without any change in waveform. However, when the tunnel portals consist of long flared or perforated sections, perfect reflections do not occur and considerable distortion of the waveform results. Reflections of waves from a flared tunnel have been discussed in Reference 1 whereas Reference 2 deals with reflections from a slotted portal. Vardy (Reference 3) has also presented numerical results for what he calls a "ventilated entry region," which is very similar to the slotted entry chamber, the only difference being that he envisions a number of ventilating pores rather than a slot. This distortion introduced into reflected waves is generally a favorable phenomenon since it tends to eliminate abrupt pressure rise, which may be of some utility in the control of pressure transients.

In order to alleviate pressure disturbances upon the passengers, current operating practice on many systems is to reduce the speed of the trains to enter certain tunnels. Although this procedure can successfully cope with the problem, it is far from ideal since it detrimentally impacts the energy requirement and

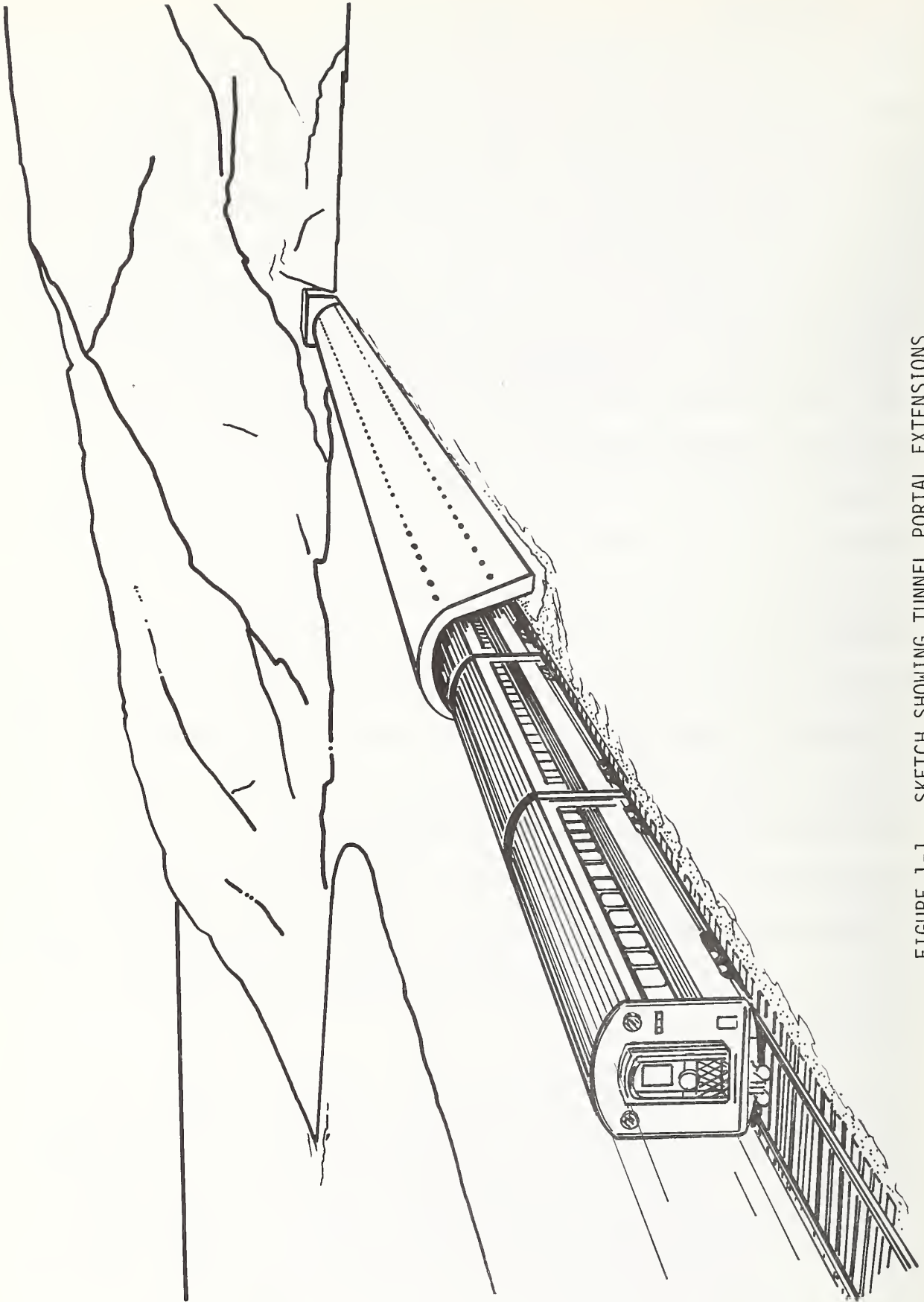


FIGURE 1-1. SKETCH SHOWING TUNNEL PORTAL EXTENSIONS

service capability of the system and thus does not represent an entirely satisfactory solution.

The most direct alleviation approach is sealing (greatly increasing the normal impedance) of the train car interior from the atmosphere. The Japanese National Railways are operating with trains so constructed and British Rail is experimenting with them. However, certain cost and convenience penalties result. An indirect approach is to initiate the flow of air in the tunnel prior to train entry. This is passively done to a degree in systems where the traffic is great enough that a train enters a tunnel while a preceding train traveling in the same direction is still in the tunnel or has just exited (a typical situation for Urban Subways). It also may be done by an existing longitudinal ventilation system.

Another approach which has been around for quite some time, but has not been effectively utilized, is to design the tunnel portals to provide the necessary alleviation of pressure transients. Hara (Reference 4) performed one of the earliest works on the matter. Yamamoto (Reference 5) showed that very little could be done to reduce the peak pressures obtained in a tunnel through modifications to the entrance. However, References 1-3 have pointed out that there are definite benefits to be gained from replacing the abrupt pressure rise of a simple portal with that having a more gradual pressure rise. It is this latter approach that the main effort of this study is focused on.

2. BACKGROUND

2.1 Principal Sources of Pressure Disturbances

The principal causes of pressure disturbances in railway tunnels have been known for many years. From the point of view of passengers on trains, two main types of disturbances can be identified.

The most obvious effect results from unsteady airflows. When the front or rear of a train enters or leaves a tunnel or passes a geometrical discontinuity within the tunnel (a vent shaft for example) pressure waves are generated which pass along the whole length of the tunnel in both directions. These waves travel at approximately sonic speed and they reflect either partially or totally at all discontinuities within the tunnel, including the train itself.

Whenever a wave passes alongside a train, its influence extends to the inside of the vehicle and passengers experience it aurally. The extent to which this can cause passenger discomfort depends upon a) the frequency with which the various waves arrive, b) the manner in which they superimpose on one another, and c) the degree of aerodynamic sealing provided by the body of the train. It is important to realize that passengers detect only a change in pressure and not the direction in which the waves causing the change happen to be traveling. Superposition of waves traveling in opposite directions creates just the same effect as superposition of waves traveling in the same direction as far as passengers are concerned.

The second source of pressure disturbances is a pseudo-steady-state phenomenon. The unsteady wave action described above has the cumulative effect of establishing airflows within the tunnel. In some cases, substantial air velocities (up to 70 m/s, say) can be generated, but it is usual for the

for the velocities inside the tunnel itself to remain less than about 20 m/s. At every geometrical discontinuity within the tunnel, velocity discontinuities must exist, and these are accompanied by pressure discontinuities. When a passenger on a train passes such a discontinuity, its effect is superimposed upon the pressure wave action. Fortunately, except for one special case, these pseudo-steady-state pressure discontinuities are so small as to be negligible.

The exception is that of another train traveling in the opposite direction (or stationary). The pressure alongside a train is always less than that either just in front of it or just behind it (viscous and unsteady effects being neglected). Passengers are always within the low pressure region of their own train and so do not experience this phenomenon directly. They do experience the effect when they pass a second train, however, because the pressure field of the other train interacts with that of their own train. Moreover, this effect may well be the dominant feature of the pressure history experience by these passengers because the magnitude of the pressure fluctuations of two intersecting fields will commonly exceed that of a single field.

2.2 Effect on the Human Ear

It is readily seen that there can be a great many pressure waves and reflections within a tunnel and so the pressure histories experienced by passengers can be highly complex. Moreover, since it is the sum of all the waves which is important and since the relative times of arrival of the various reflections will depend upon such factors as the length and speed of the train and the length of the tunnel, it is virtually impossible to construct a 'typical' pressure history.

Given this situation, it is difficult to find a basis upon which to specify design criteria which will guarantee an adequate comfort level for passengers. Indeed the position is even worse than the above would suggest because, in practice, different people exhibit widely differing responses to identical pressure histories. It appears that these differences can be only partially explained by infections and blocked ear passages. For obvious reasons, comfort criteria must be based upon the reactions of those people who exhibit the greatest sensitivity to pressure fluctuations. In this way, the safety of all passengers can be guaranteed, and most passengers will suffer very little discomfort.

Different railway operators use different methods to prescribe pressure tolerance criteria. In the U.S.A., the recommended method for subway design is to examine the predicted pressure histories in detail and to ensure that a) no sudden pressure change will exceed 0.69 kN/m^2 and also that b) for all pressure changes in excess of this figure, the average rate of change will not exceed 0.41 kN/m^2 per second.

British Rail have adopted an entirely different approach. Instead of looking at pressure histories in close detail, they base their criteria on the overall nature of the pressure history. When the overall nature of the pressure history has a random appearance, they attempt to restrict changes to a maximum of 1 kN/m^2 in any period of 5 seconds, but they will allow occasional changes as large as 3 kN/m^2 in a period of only 3 seconds. In both cases, no restriction is placed on the manner in which the change occurs. That is, a sudden rise, say, of 1 kN/m^2 is regarded as acceptable provided that there are no further pressure rises within 5 seconds.

For regular pulses such as those which would have been generated every 15 seconds in the ill-fated Channel Tunnel, the maximum permitted magnitude is 0.45 kN/m^2 . This situation is not likely to exist in a rapid transit system and so the former criterion is the more relevant.

The differences between the British and American methods of choosing criteria are interesting. On the face of it, the American practice is more restrictive for the random case, but less restrictive for the regular pulses. Whether-or-not this is borne out by passenger reaction is not clear.

A final comment relating to aural response concerns the difference between the above-described pressure disturbances and noise. The only difference between the two from a physical point of view is the frequency. If any particular pressure history was scaled time-wise so that the whole event occurred within, say, 0.01 secs, then an observer would describe the result as noise rather than as a series of discrete pulses. Indeed, unless the magnitudes were also scaled, the noise would be so great as to be painful. For this reason, a proviso must be added to all the above-described comfort criteria, namely, that even 'sudden' changes must not occur so rapidly that they will be interpreted as sound.

2.3 Pressure Pulse Problems

It must be pointed out that these pressure pulse effects on the passengers are not the only pressure transient problems for trains. There are many others, structural as well as physiological, such as trains passing each

other outside or inside tunnels (windows have failed in a number of instances); the pressure transient effect of a train entering or exiting a tunnel on another train, structures, or personnel at some other location in the tunnel; and, as a train passes a communication shaft or abrupt change in tunnel geometry. A wide spectrum of such problems is shown in Table 2.1.

As can be seen from the following table, only a small portion of the possible pressure transients problems were investigated during this study. Actually, only the two indicated with "A's" were within the original scope of the study. Similar information on the four indicated by "B's" was obtained with virtually no additional effort. However, as these are secondary objectives, no analysis of the information was performed. The seven problem areas indicated by the "C's" and "D's" were briefly looked at merely by continuing to record information (both experimentally and analytically on the computer) as the train traversed across an open shaft located about a train length inside the tunnel proper. The 33 areas indicated with "*"s" can be looked into with minor, if any, modification to the experimental setup or the analytical computer model.

The 16 blank areas would require a completely different study since the train(s) is outside of the tunnel. Portions of the experimental work could be carried out in a normal wind tunnel, but a moving-model approach (where the model moves along the ground surface) would be necessary in order to obtain realistic transient effects of the pressure pulses. It is not always possible to convert the steady-state-obtained pressure pulse data to meaningful transient data. The areas marked with "X's" are not relevant to any pressure pulse problems.

TABLE 2-1. PRESSURE PULSE PROBLEMS

Effects On		OPERATING CONDITIONS												
		Enter Tunnel	Pass Structure		Inside Tunnel		Exit Tunnel	Pass Structure		Outside Tunnel				
			Open Shaft	Sealed Shaft etc.	Stopped	Moving		Stopped	Moving	Stopped	Moving			
This Train	Motorman	A	C	X	*	*	*	*	*	*	*			
	Passengers	A	C	X	*	*	*	*	*	*	*			
	Motorman	*	*	X	*	*	*	*	*	*	*	X	X	X
	Passengers	*	*	X	*	*	*	*	*	*	*	X	X	X
Other Train	Users on Platform	B	C	X	*	*	*	*	*	*	*	X	X	X
	Maintenance Personnel	B	C	X	*	*	*	*	*	*	*	X	X	X
Inside Tunnel	This Train	B	C	X	*	*	*	*	*	*	*			
	Other Train	*	*	X	*	*	*	*	*	*	*	X	X	X
Structural	Miscellaneous Structures	B	C	C	*	*	*	*	*	*	*			

A: Primary objectives of this study.
 B: Direct fall-outs during achievement of primary objectives.
 C: Optional objectives of this study.
 *: Problem areas which can be covered by extended application of this study
 Blank: Other possible problem areas.
 X: Not relevant or of no concern.

3. OBJECTIVE

The primary objective of this study was to demonstrate conclusively if tunnel entry pressure transients (TEPT) experienced by riders on high-speed trains could be adequately and practically alleviated. To accomplish this, it was necessary to insure that a satisfactory understanding existed for the generation of such pressure transients. If not, then further development of the understanding would be necessary. The existence of a satisfactory understanding was to be validated by comparison of analytical model with experimental results from a small-scale laboratory test program.

The secondary objective was to perform a trade-off study in order to compare the effectiveness and costs of the various approaches for alleviating the effects of the pressure transient upon the riders of trains entering tunnels.

4. APPROACH

4.1 Theoretical/Analytical

Before this study, the theoretical development of railway tunnel aerodynamics had been accomplished largely in the absence of adequate experimental confirmation. Various modifications to tunnels had been proposed, including the sinking of airshafts and the provision of perforated and/or flared extension tubes upstream or downstream of tunnels. More recently, less obvious modifications had been considered such as the insertion of some form of flow restrictions in airshafts, at tunnel portals, and at the rear of the train. There was a pressing need for physical confirmation of these theoretical proposals.

In this report, theoretical predictions from the computer program (Vardy) are compared with simplified theory (Hammit) in a small-scale facility (at Jet Propulsion Laboratory). The approach taken was:

4.1.1 Basic Tunnel

Available analytical models and computer programs were considered adequate to determine the extent of the pressure transient problem on passengers of a train entering a normal tunnel; the results have been shown to compare well with experimental data. Therefore, they were used to evaluate and demonstrate the basic problem.

4.1.2 Modified Tunnel and/or Train Design

Although some theoretical work had been done on pressure transients of trains entering and traveling through tunnels which had modified (enlarged and/or porous portals or communicating shafts to the surface or adjacent tunnels) there was some question on the applicability to actual conditions of results from computer programs based on this work.

This was mainly due to some differences in the various theories and lack of experimental information to compare with the analytical models. Therefore, this study compared the various theoretical approaches, identified the differences and then resolved them. Whenever there was a question as to which approach was optimum for the purpose of predicting realistic pressure transients, the computer results of the various theoretical approaches were compared to experimental data. This process helped identify which theoretical approach should be taken, or in some cases, that further effort was required on the development of the theory or the computer program. Preliminary results from the existing computer program were used as a guide in developing an experimental program.

4.2 Experimental Program

A small-scale (1%) test facility was developed to carry out the experimental verification. The facility itself and the data acquisition method utilized existing equipment and techniques whenever appropriate. As a consequence, the costs were kept low. Once the development was completed, the time required for the tests was relatively small. So an order of magnitude more tests were made than necessary to demonstrate the validity of the analytical and computer models. The remaining data were not analyzed, but are available in Reference 6.

4.3 Other Approaches

4.3.1 Speed Restriction

The relatively minor effort directed toward this manner of solving the entry pressure pulse problem was on quantifying the extension of running time required to insure alleviation of the problem. Also, the increases in energies (traction effort and braking) were determined.

4.3.2 Sealed Cars

It was intended that use be made of existing information on the costs for sealing subway and passenger train cars. However, we were not able to obtain any firm cost estimate; just that this approach is a very difficult and a costly one.

4.3.3 Initiate Flow Through Tunnel

No analytical work was intended for this approach. However, one run was made to demonstrate the effectiveness.

4.3.4 Trade-Off Study

A brief trade-off study was carried out on the three pressure alleviation approaches, namely 1) modified entrances, 2) speed restrictions, and 3) sealed cars. Although insufficient information is available for a definitive analysis, the important parameters and considerations are identified. Qualitative cost comparisons were made of the various approaches for a number of possible scenarios.

5. STATE-OF-THE-ART ASSESSMENT

5.1 Parameters Influencing Entry Transient Magnitudes

In order to develop a 'feel' for the problem and also as a first step towards overcoming it, there is a need to identify the main factors contributing to the magnitudes of the nose and tail entry waves. For this purpose, a simple theoretical treatment of two cases is presented. This is based upon incompressible flow theory, and it is not as accurate as the program described in Section 6. Nevertheless, it is entirely adequate for the purpose of identifying the major trends.

Using Fig. 5.1, the equation relating conditions across the wavefront is

$$p_1 - p_0 = \rho c (u_1 - u_0), \quad \dots(5.1)$$

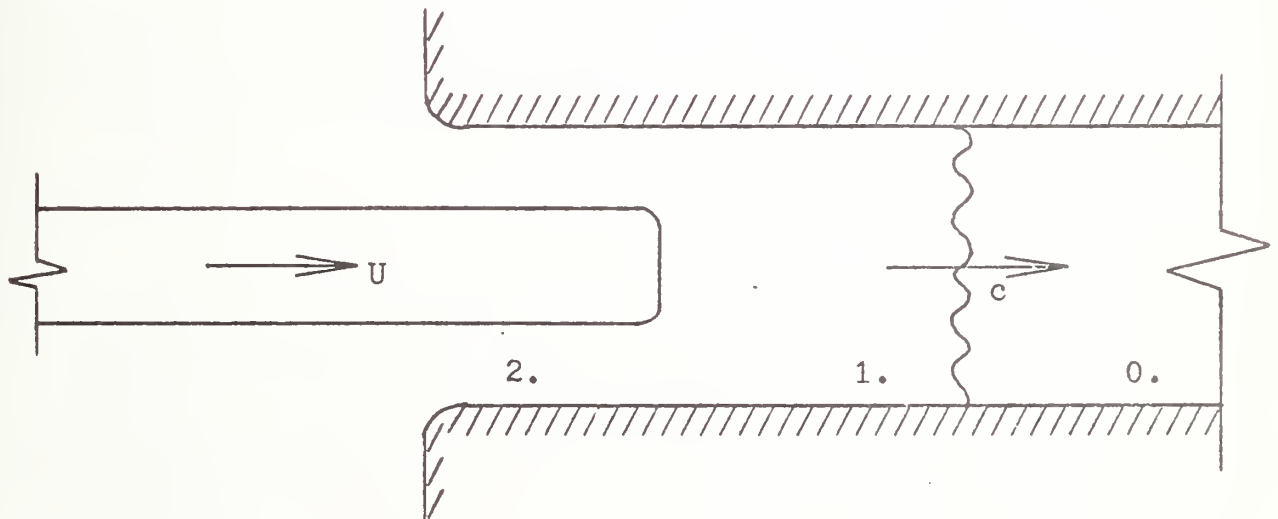


FIGURE 5-1. TRAIN ENTERING TUNNEL

and the steady-state continuity and Bernoulli equations written relative to the moving nose are

$$(u_1 - U) = (1 - \beta)(u_2 - U) \quad \dots(5.2)$$

and

$$\begin{aligned} \left[p_1 + \frac{1}{2} \rho (u_1 - U)^2 \right] - \left[p_2 + \frac{1}{2} \rho (u_2 - U)^2 \right] \\ = \frac{1}{2} k_F \rho (u_2 - U)^2 \quad \dots(5.3) \end{aligned}$$

respectively where β is the blockage ratio and k_F is a pressure loss coefficient describing the degree of streamlining of the train nose.

The conditions at the tunnel entrance are described by

$$p_{AT} - \left[p_2 + \frac{1}{2} \rho u_2^2 \right] = \frac{1}{2} k_E \rho u_2^2, \quad \dots(5.4)$$

where k_E is a pressure loss coefficient describing the degree of streamlining of the tunnel mouth. For the most usual case, air flows out of the tunnel mouth during nose entry and then Eq. (5.4) reduces to

$$p_2 = p_{AT} . \quad \dots(5.5)$$

The velocity u_0 represents the airspeed into the tunnel before the arrival of the train. If we assume that $\frac{1}{2} (1 + k_E) u_0 \ll c$ which is true for all realistic values of u_0 , then it is permissible to approximate p_0 by

$$p_0 \simeq p_{AT} . \quad \dots(5.6)$$

Eqs. (5.1), (5.2), (5.3), (5.5) and (5.6) can be combined to give

$$\frac{p_1 - p_{AT}}{\rho c} = U - u_0 + \frac{c}{2A} \left[1 - \sqrt{1 + \frac{4A(U - u_0)}{c}} \right] \dots(5.7)$$

where

$$A = \frac{1}{2} \left[\frac{1 + k_F}{(1 - \beta)^2} - 1 \right] \dots(5.8)$$

Equation (5.7) has been used to derive the results plotted in Fig. 5.2.

The basic case chosen is marked by an asterisk and it is specified by $U = 35$ m/s, $\beta = \frac{1}{2}$, $k_F = 0$, $u_0 = 0$, $\rho = 1.28$ kg/m³ and $c = 333$ m/s. By inspection, it is immediately obvious why reducing the train speed is such an effective way of reducing the transients. It is also obvious why the blockage ratio should be as small as possible. The variation of the wave magnitude with the nose loss coefficient, k_F , is also marked. These trends are dealt with in more detail in Sections 5.2.1 and 5.2.2.

The analysis of the tail entry wave is handled similarly. In Fig. 5.3, the tail wave is shown progressing into region 2 in which, to fix ideas, the conditions are supposed to be still governed by the nose entry conditions. The equations used are:

wave: $p_3 - p_2 = \rho c (u_3 - u_2) \dots(5.9)$

continuity: $(u_4 - U) = (1 - \beta)(u_3 - U) \dots(5.10)$

Bernoulli: $\left[p_3 + \frac{1}{2} \rho (u_3 - U)^2 \right] - \left[p_4 + \frac{1}{2} \rho (u_4 - U)^2 \right]$
 $= \frac{1}{2} k_R \rho (u_3 - U)^2 \dots(5.11)$

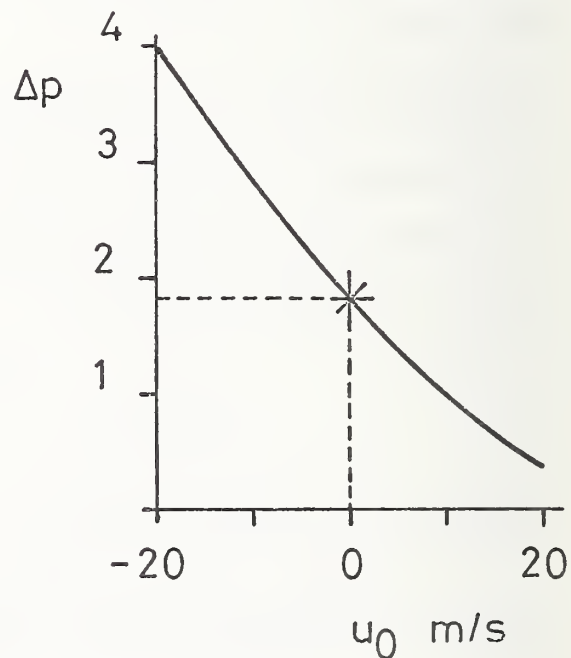
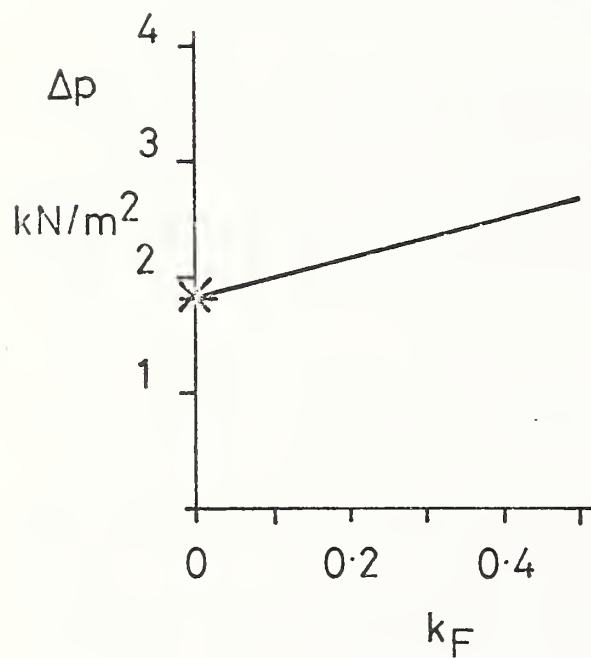
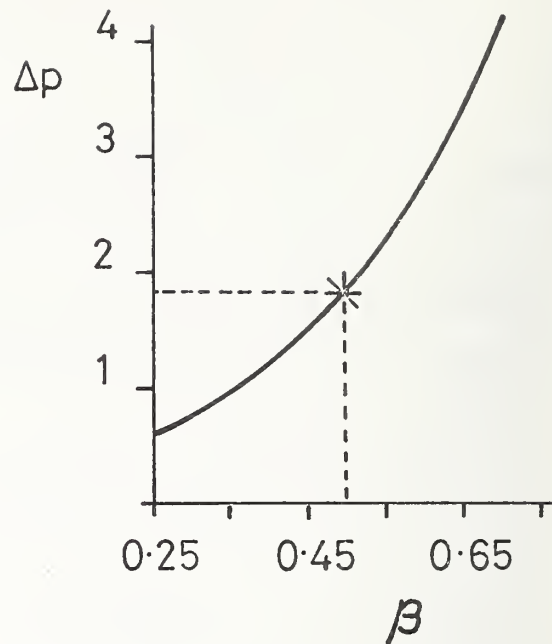
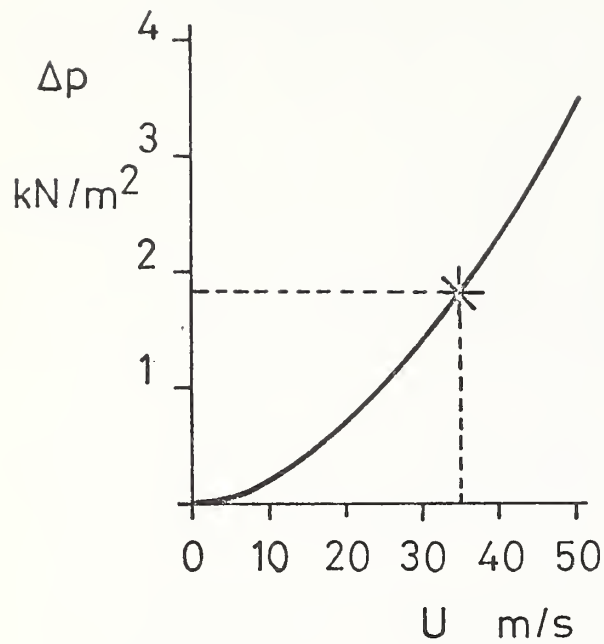


FIGURE 5-2. NOSE WAVE MAGNITUDE

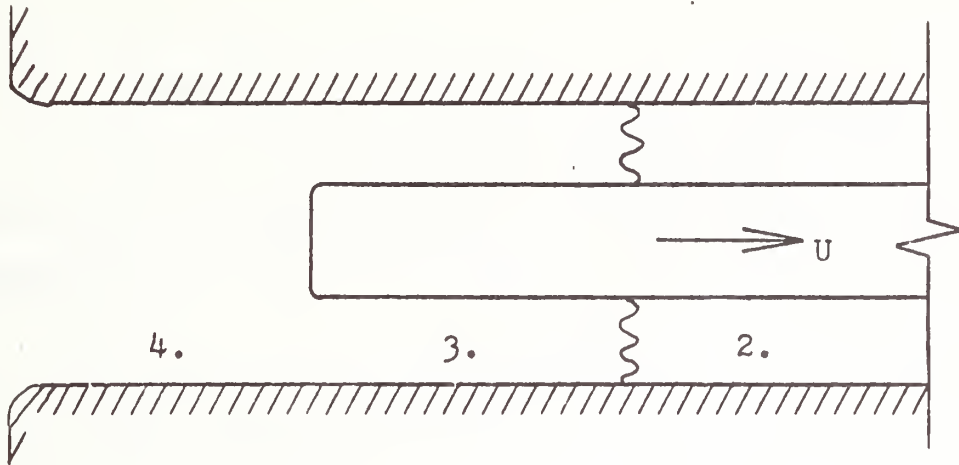


FIGURE 5-3. TRAIN JUST AFTER ENTRY

and
$$p_2 \approx p_4 \approx p_{AT}, \quad \dots(5.12)$$

which may be combined to yield

$$\frac{p_3 - p_2}{\rho c} = U - u_2 + \frac{c}{2B} \left[1 - \sqrt{1 + \frac{4B}{c} (U - u_2)} \right] \quad \dots(5.13)$$

where
$$B = \frac{1}{2} \left[(1 - \beta)^2 - 1 + k_R \right] . \quad \dots(5.14)$$

For the basic case, the parameters are the same as those used for the nose entry calculations. Additionally, the coefficient k_R which describes the pressure loss at the flow expands over the rear of the vehicle is chosen to obey

$$\frac{1}{2} k_R \rho (u_3 - U)^2 = \frac{1}{2} \rho (u_3 - u_4)^2 \quad \dots(5.15)$$

which is the usual assumption for an expansion. Eqs. (5.15) and (5.10) are satisfied by

$$k_R = \beta^2. \quad \dots(5.16)$$

The results are plotted in Fig. 5.4 from which it can be seen that the principal trends are the same as those for the nose entry case. In particular, the dominant parameter is again the train speed, U . An interesting result is that the tail wave is increased when the nose and tail are well streamlined. The implications of this paradoxical result are discussed in detail in Section 5.2.1.

The final graph in Fig. 5.4 is included as an attempt to simulate the effect of the skin friction on the sides of the tunnel and the train. During train entry, the resistance to flow along the vehicle and out of the portal gradually increases so that u_2 may be expected to be a few m/s larger than the value used to derive the other graphs; that is, u_2 will have a smaller magnitude when it is negative.

5.2 Reduction of Pressure Transients

There are a great many ways of reducing the effects of the pressure transients. Entirely feasible possibilities include reducing train speeds especially during entry and exit, aerodynamically sealing trains, reducing the headway between trains (in order to increase u_0), building only large bore tunnels and even, in some circumstances, avoiding the use of tunnels. Such possibilities would be considered in a full feasibility study. Similarly, techniques involving the interconnection of separate running tunnels are not appropriate in a study dealing primarily with entry transients in single tunnels.

In this section, attention is directed principally towards identifying the influence of different tunnel portal designs. However, it is appropriate to begin by summarizing the implications of the previous section with regard to train design.

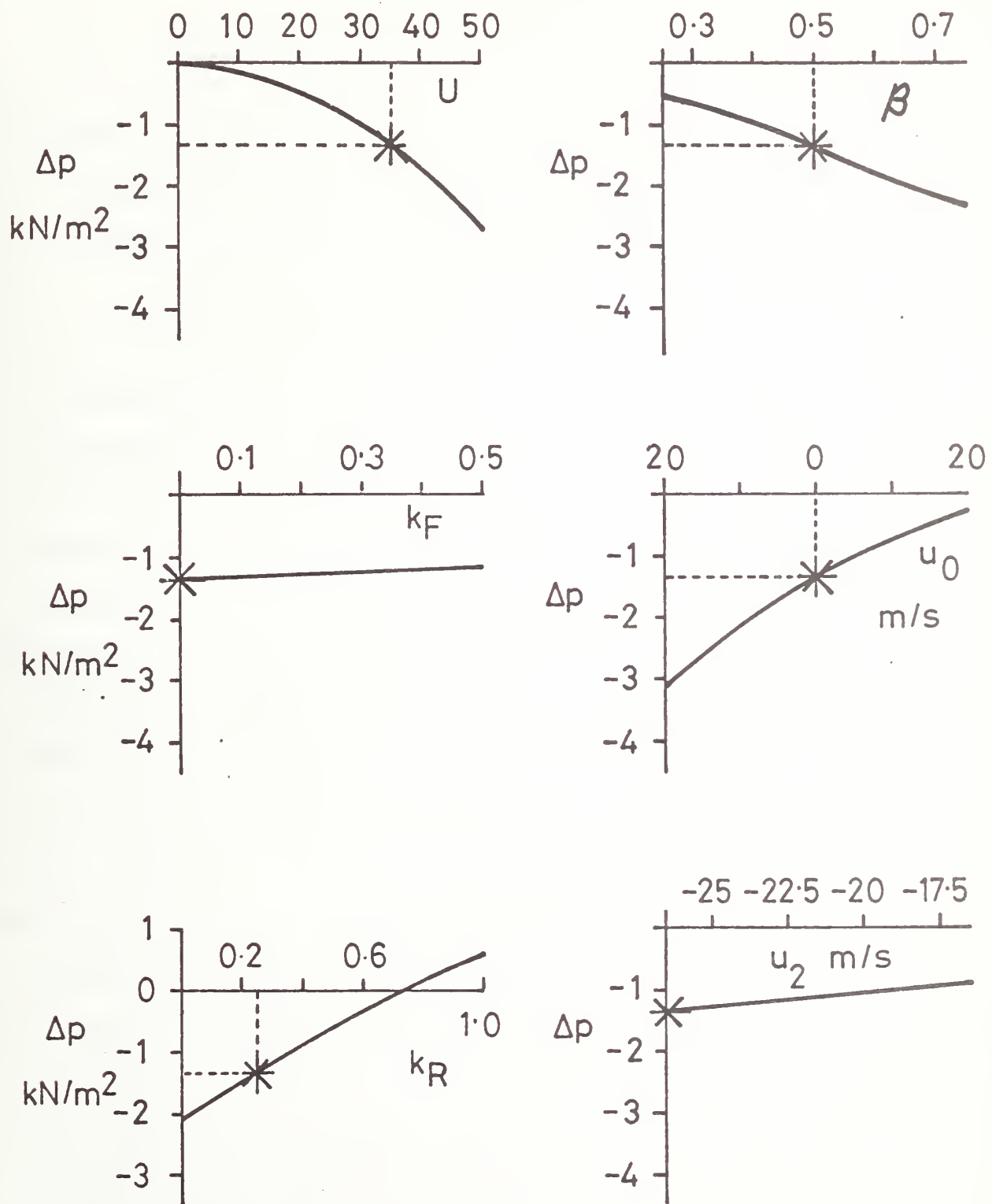


FIGURE 5-4. TAIL WAVE MAGNITUDE

5.2.1 Modifications to Trains

The principal parameters used to describe the geometry of a train are length, cross-sectional area, nose shape, tail shape, and surface roughness (including bogies). Each of these exerts a considerable influence on the pressure histories.

5.2.1.1 Length

The length of the train is of interest because, in conjunction with the train speed, it determines the time interval between the nose and tail waves. When these waves are close together, they are likely to cause greater discomfort than when they are separated by a relatively long interval. Additionally, the manner in which the waves and their subsequent reflections superimpose on one another is strongly dependent upon the train/tunnel length ratio and the train speed. Unfavorable superpositions can lead to pressure fluctuations which are up to 100% greater than those resulting from favorable superpositions.

5.2.1.2 Cross-Sectional Area

The train/tunnel area ratio (blockage ratio, β) has a pronounced influence on the magnitudes of both the nose and the tail waves. This has been demonstrated in Figs. 5.2 and 5.4 and the implication is that new trains should be as small as possible. There is good reason to suppose that by careful design significant train area reductions are possible. For example, British Rail's Advanced Passenger Train has a cross-sectional area of approximately 7.5 m² which is roughly 25% less than that of conventional inter-city vehicles.

5.2.1.3 Nose Shape

A well-streamlined nose leads to smaller nose entry and nose exit waves, but to a larger tail entry wave. The latter effect is relatively small and so the nose should be as well-streamlined as possible.

Evidence about the degree of streamlining necessary to ensure a small value for the loss coefficient in any particular tunnel is scarce. Comparisons of measured data with Fig. 5.2 or Eq. (5.7) are required. A value of 0.15 appears to be typical for older trains on Britain's inter-city routes. This value is encouraging because comparatively little attention has been paid in the past to producing streamlined shapes. It is, therefore, likely that very low values of k_F may be relatively easily achievable.

5.2.1.4 Tail Shape

The tail shape may be the most important single parameter. By varying the degree of streamlining of the tail, it appears to be possible to completely eliminate the tail entry wave (Fig. 5.4). It would be notionally possible to achieve this by equipping the tail with a 'spoiler.'

Alternative possibilities exist. A crude but effective method could be to mount a vertical plate a few train diameters behind the trailing car. Air from alongside the train would expand into the region between the train and the plate before re-accelerating in order to pass around the plate.

Apart from aesthetic considerations, the main disadvantage of such a modification would be that it would lead to an increase drag on the train for the whole of the journey. In order to minimize this adverse effect, the plate could be composed of adjustable vanes.

5.2.1.5 Surface Roughness

Skin friction on the surface of the train and form drag around the suspension units contribute considerably towards the overall drag on the vehicle. Within a tunnel, a pressure gradient develops along the train and this can cause noticeable pressure waves. Fortunately, however, these are not usually of a sufficiently large magnitude to result in unacceptable rates of change of pressure. Instead, air friction helps to dissipate all pressure waves. Also, as is shown in Fig. 5.4, by reducing the backflow along the train, surface roughness tends to reduce the magnitude of the tail entry wave. For the same reason, it also tends to reduce the exit waves. Nevertheless, this is not a desirable way to reduce transients because it leads to increased drag on the vehicle.

5.2.2 Modifications to Tunnel Geometry

The principal parameters describing conventional tunnel geometries are length, cross-sectional area, surface roughness and portal shape. Of these, the cross-sectional area has the most important influence on the magnitudes of the pressure waves. Its influence is described in Figs. 5.2 and 5.4. For the basic case of a blockage ratio of 50% and a train speed of 35 m/s, a 3% increase in the tunnel diameter yields roughly a 20% decrease in the magnitudes of the entry waves. Clearly, when designing new tunnels, serious consideration must be given to the provision of the largest bore of tunnel consistent with the overall design costs - especially if there is a possibility of future tunnel usage at higher vehicle speeds. Tunnel length is important in two ways. Firstly, the longer the tunnel, the greater the time intervals between the arrival of successive wave reflections at the train, and so the smaller the level of discomfort felt by

passengers. Secondly, for any particular train length and speed, the tunnel length determines whether the various reflections of the nose and tail waves will superimpose favorably or unfavorably. Comparatively short alterations to the length of a tunnel can represent the difference between favorable and unfavorable superposition, and so it may sometimes be useful to adjust the length in order to take advantage of this effect. The analysis of this particular effect is best done graphically. It is then a simple matter to determine the optimum tunnel length for any particular train speed (not necessarily constant) through the tunnel. The remaining tunnel parameters, namely, surface roughness and shape, are of lesser importance. Other things being equal, the smaller the roughnesses and the more streamlined the portals, the less resistance there will be to the air flows and so the closer the air speed will be to the train speed. This leads to smaller pressure waves and it also leads to a reduced drag on the vehicle. It may be concluded that attention should be given to ensuring that tunnel induced pressure losses are as small as possible.

It should be noted that the above conclusion takes no account of considerations other than pressure transient minimization. Other considerations might dictate that high air speeds (relative to the train) are desirable - for the discharge of waste thermal energy, for example.

5.2.2.1 Tunnel Entrance Regions

When a tunnel is long, the magnitudes of the nose and tail entry waves (considered separately) cannot be greatly reduced by flaring or ventilating the entrance region. For the case of a ventilated entrance, no reduction at all should be expected. Even for the case of a flared entrance, only small reductions in the nose wave can result from the

pressure recovery in the reversed flow alongside the train. Also, the tail wave will be slightly greater than it would be in the absence of the flare. Both these effects are neglected as a first approximation in the following qualitative discussion.

The major potential benefits from modified entrance regions result from reductions in the rates of change of pressure. The nose entry wave, for example, is not fully developed until after the nose has passed along the whole length of the entrance region. During this time, the pressure at the end of the entrance region increases continuously so that the wave-front in the tunnel is 'ramp-like' rather than 'step-like'.

At realistic train speeds, three main ways of utilizing this effect exist. Firstly, by building a sufficiently long entrance region, the rates of change of pressure associated with the ramp-waves can be reduced to within any desirable limit. At very slow speeds, this could be an effective solution to the whole problem, but it may not be so at high speeds because excessive lengths would be required to reduce pressure gradients to within the comfort criteria.

Secondly, if the train is shorter than the entrance region - or, more exactly, if it is shorter than $(1-M) \lambda_e$ where M is the train Mach number - the tail wave will reach the end of the entrance region before the nose wave has fully developed. Since the two waves are of opposite sign, this is a favorable mode of superposition and it will necessarily reduce the maximum peak to peak pressure fluctuations in the tunnel. Moreover, the longer the entrance, the greater the benefit.

Thirdly, both of the wavefronts will superimpose on themselves when they reflect at the entrance and exit portals. There will therefore be long regions of tunnel adjacent to the portals in which the full magnitudes of the waves will not be experienced. In the time required for the nose to travel along an entrance, a pressure wave can travel λ_e/M and so the length of the ramp wavefront is $\lambda_e (1/M-1)$. The regions of overlap are notionally half this length.

For a train speed of, say, 35 m/s, this means that the full effect of the waves will not be developed within about $4 \lambda_e$ of either tunnel portal. From the point of view of passengers, this is important because the whole of the train will be within this distance from the entrance portal during the first reflection of the nose wave at that portal provided that the tunnel length is less than $(1/M-1)^2 \lambda_e / 4$.

In order to convert this expression into a useful form, we may conveniently interpret it as a statement of the entrance length necessary for the train to be within the region of overlap of the first reflection of the nose wave at the entrance portal. In this form the expression becomes

$$\frac{\lambda_e}{\lambda_t} > \frac{4}{(1/M - 1)^2}, \quad \dots(5.17)$$

which implies an entrance/tunnel length ratio of 2.6% at a train speed of 25 m/s, but of 5.5% at a speed of 35 m/s. For tunnels in excess of 1 or 2 km, unrealistically long entrance regions are required. In that case, only the first two of the above described ways of utilizing the reduced pressure gradients obtainable from the use of entrance regions will be of practical interest.

Flared Entrance Regions

In order to achieve the maximum benefits from a special entrance region, it is important that both the nose and the tail entry waves should be converted from step-to-ramp-waves. With a flared entrance region, this aim appears to be attainable.

The principal parameters describing a flare are its length (already discussed), its portal size and the rate of change of area along its length. The optimum values for these parameters are unknown, but an indication of the likely requirements can be deduced from results obtained for the much lower blockage ratios applicable in double-tracked, single-bore tunnels. In that situation, the portal area should be about 2 or 3 times greater than the tunnel area. Rather surprisingly, the theoretical predictions indicate that the amount of benefit to be expected is not strongly dependent upon the rate of change of area along the flare. It is probable that this degree of freedom may be largely relinquished by the designer so that the longitudinal variation will be dictated instead by structural considerations.

Perforated Entrance Regions

It is at least notionally possible to create a flared entrance by enlarging an existing tunnel bore. In contrast, a ventilated entrance region must be built wholly outside the tunnel as an extension tube. Ventilation through the walls of this tube may be by means of a continuous slot or alternatively by means of a number of discrete holes of any desired shape. In both cases, a 'flare-effect' always exists because the total lateral ventilation in front of a train necessarily decreases as the train progresses along the tube.

For entrance lengths of the order of 100 m, the nose entry wave can be approximately converted into a ramp-wave if the slot width is constant. The total area of the slot (or holes) should be about 30% of the cross-sectional area of the tunnel.

The optimum slot width for converting the tail entry wave into a ramp-wave is as yet unknown. There is evidence that the required amount may differ considerably from that preferred for modifying the nose entry wave. Further results are required before any firm conclusions may be drawn, but if this does prove to be the case, it may be a serious disadvantage in comparison with a flared entrance region.

5.2.2.2 Tunnel Exit Regions

Flared or porous exit regions can be used to modify the exit waves in much the same manner as entrance regions modify the entry waves. For the purposes of the present study, however, exit regions are of interest not because of their influence on train exit but because of their effects on the entry waves. Of course, they cannot modify the generation of entry waves, but they do affect the manner in which these waves reflect from the end of the tunnel. The same amount of wave elongation could alternatively be achieved with an entrance region that is only about one quarter as long (for a train speed of 35 m/s). For economic reasons, therefore, exit regions do not appear to be worthy of extended consideration in a study of train entry waves.

5.2.2.3 Airshafts

Modified entrance and exit regions have many advantages, but they suffer from an important drawback, namely, that their effectiveness decreases with train speed. That is, any particular region will yield a smaller percentage improvement on pressure histories at high speeds than it will

at lower speeds. There is a tendency for most tunnel modifications to be more effective at some speeds than others, but this continuous decrease with speed is surely the most unfortunate type of dependency.

Most tunnels are equipped with airshafts which are normally used for ventilation purposes. These shafts can also be helpful in pressure transient alleviation and, in particular, their position can be chosen so that they have greatest effect at any desired speed (usually the operating speed). For the special case of single-bore, single-tracked tunnels, it can be shown that the effectiveness of a single shaft is greatest if its distance from the entrance portal satisfies

$$\frac{4}{(1/M - 1)^2} < \frac{x_s}{l_t} < \frac{2}{1/M + 1}, \quad \dots(5.18)$$

which for a train speed of 35 m/s reduces to $5.5\% < x_s/l_t < 19.0\%$. Results for main-line tunnels with high speed trains (50 m/s) have indicated that a single shaft within this region and of only about 15% of the tunnel cross-sectional area can yield up to 40% reductions in the peak-to-peak pressure fluctuations experienced by passengers during a complete journey through a tunnel. However, it is not easy to obtain further improvements by the provision of extra shafts, and so the total benefit achievable by this method is of the order of about 50%.

The effect of a shaft is twofold. Firstly, it provides a discontinuity at which waves will reflect, and so it tends to dissipate waves. Secondly, as a discontinuity, it is itself a source of wave generation when it is passed by the nose and tail of the train. The expression (5.18) is chosen to ensure that as many as possible of these extra waves will superimpose favorably with the various reflections of the nose and tail entry waves.

The expression (5.18) has been developed for the case where wave superposition throughout the whole journey through the tunnel is under consideration. Shafts within this region do not normally cause large reductions in the magnitudes of the nose and tail entry waves. However, in the derivation of (5.18), it has been assumed that the shaft is not close to the entrance portal. It is likely that a completely different result will apply if the shaft is allowed to be close to this portal. However, the number of wave reflections that would then have to be taken into consideration is probably so great as to render wave analyses useless except when performed with the aid of computers. There is, therefore, a case for investigating the use of airshafts by means of existing (or new) computer programs. If this option is taken up, emphasis should be placed on shafts which are on the order of one train length from the entrance portal. Consideration should also be given to the possible advantages of using airshafts in conjunction with short flared or ventilated entrance regions. Such a configuration could be highly beneficial, especially if the shaft is very short.

5.3 Theoretical Analyses

The train entry problem involves the three-dimensional, unsteady flow of a viscous, compressible fluid. Even with the aid of modern computers, it would be unrealistic to hope for an exact solution of such a complex flow field. Fortunately, however, considerable simplifications can be made without seriously impairing the value of the results.

From the point of view of passenger comfort, it is reasonable to neglect events which occur within time intervals comparable with those required for the equalization of pressure at a cross-section. This implies that the problem may be regarded as unidimensional even though the analysis

cannot then be used to predict such things as the structural loads around the vehicle nose. It also implies that the detailed manner of diffusion of viscous and heat transfer effects through the body of the fluid need not be known (although their macroscopic behavior must still be specified). The problem thus reduces to one-dimensional unsteady flow with friction and heat transfer. Flares and ventilated entrances can be accommodated by including pseudo-one-dimensional terms describing area change and mass addition.

The equations of continuity, momentum and energy are then

$$\frac{\partial \rho}{\partial t} + u \frac{\partial \rho}{\partial x} + \rho \frac{\partial u}{\partial x} + \frac{\rho u}{a} \frac{\partial a}{\partial x} - \frac{\dot{m}}{a} = 0 \quad \dots(5.19)$$

$$\frac{\partial p}{\partial x} + \rho \frac{\partial u}{\partial t} + \rho u \frac{\partial u}{\partial x} + \rho g \frac{\partial z}{\partial x} + \frac{\tau_s}{a} + \frac{\dot{m}}{a} (u - u_{LX}) = 0 \quad \dots(5.20)$$

and

$$\frac{1}{\gamma-1} \frac{\partial p}{\partial t} + \frac{u}{\gamma-1} \frac{\partial p}{\partial x} - \frac{c^2}{\gamma-1} \frac{\partial \rho}{\partial t} - \frac{u c^2}{\gamma-1} \frac{\partial \rho}{\partial x} = \frac{Q}{a} - \frac{W}{a} + \frac{\tau u_s}{a} + \frac{\dot{m}}{a} \left[c_p (T_L - T) + \frac{u_L^2}{2} + \frac{u^2}{2} - u u_{LX} \right] \dots(5.21)$$

respectively where \dot{m} = mass inflow per unit length,

u_L = velocity of inflow,

u_{LX} = axial component of u_L ,

and T_L = temperature of inflow.

5.3.1 Evaluation of Additional Terms

It is, in principle, possible to solve these equations and so to obtain a solution for the train entry problem without making any further assumptions. However, for this to be the case, it is necessary for the lateral mass inflow rate, the all shear stress and the heat and work to be specified explicitly. In practice, it is always the case that in real problems, some

of these will be unknown quantities. For example, the wall shear stress τ is an unknown which is usually either neglected (inviscid solution) or approximated from empirical steady-state formulae. Attempts have been made by various authors to derive a good approximation for unsteady turbulent shear, but no results suitable for inclusion in a one-dimensional analysis are so far available. This is unfortunate because the work done on the fluid by a moving boundary (train side) is also dependent upon the skin friction.

The heat transfer to, from or between the train and tunnel walls is also usually approximated by steady-state expressions. Its influence on the overall flows in long tunnels is considerable, but it is less important in the train entry problem. Sufficient accuracy will be obtained by assuming a constant tunnel wall temperature and using the Reynolds analogy. In the proposed model tests, a similar assumption will suffice for the heat at the train surface, but in a full scale circumstance considerable heat input from trains may be expected. The total amount of exhaust heat from trains should be available from efficiency considerations, and the distribution of this heat along the train will be known from the geometry of the vehicle. Finally, there is heat conduction along the tunnel within the air itself. This is usually neglected, and only small errors will result provided that the pressures are small. This, in turn, is notably the case when the pressure histories are most satisfactory.

The lateral component of velocity of any lateral inflows or outflows may be assumed to satisfy the equation

$$p = -m_a \frac{du_{LY}}{dt} - \frac{1}{2} \rho u_{LY} |u_{LY}| \dots (5.22)$$

where m_a is an effective mass per unit area. In full size tunnels, it will be permissible to neglect the first term on the right hand side of Eq. (5.22) because large accelerations will exist for only a very small proportion of the time. The axial component of velocity of the lateral flows, u_{LX} , will be a function of the geometry of the holes as well as of u_{LY} . The temperature will be specified externally for the case of inflows, and may be approximated by the free stream temperature for the case of outflows.

5.3.2 Further Simplifications

Although a complete solution can be obtained for the entry problem by means of the above equations and substitutions, a considerable amount of computing effort and time would be required. Further simplifications should be sought and utilized wherever possible. Usually, the aims of any particular investigation are fairly straightforward and then useful approximations can be made. It was therefore possible to obtain sufficient accuracy by regarding the flow as inviscid and by adopting the acoustic assumptions of constant density and constant wavespeed. Furthermore, the flow within each identifiable region was treated as steady except across the principal wavefronts.

When more information is required or when the tunnel is not impervious and of constant bore, less generous assumptions must be made. For the case of the proposed model test, it will certainly be necessary to take account of skin friction and of unsteadiness. However, if interest is restricted to the flows generated during train entry, it may well be acceptable to utilize the acoustic approximations. This will represent a major simplification because it renders the Eq. (5.21) redundant. Additionally, for many of the tests, it may be sufficient to use rigid column theory to describe unsteadiness upstream of the parallel section of the tunnel.

An alternative way to eliminate Eq. (5.21) is to link the continuity and momentum equations by the isentropic condition, $p/\rho^\gamma = \text{constant}$. There is little theoretical justification for the use of this assumption, but it has nevertheless been used successfully by various authors who have justified it by means of experimental agreement. It may be regarded as an implicit assumption about the relative magnitudes of the skin friction and the heat transfers. By inspection of Eq. (5.21), it may be deduced that lateral flows also have a bearing on the accuracy of this approximation.

5.4 Experimental Investigation

By means of dimensional analysis, it is a simple matter to deduce that a true model of the full-scale train/tunnel situation should exhibit both geometrical and dynamical similarity. In practice, however, it is not practical to realize either of these aims exactly. The extent to which this interferes with the investigation is now discussed.

5.4.1 Geometric Similarity

Geometric similarity implies that every linear dimension in the model bears the same relationship to the corresponding dimension in the prototype as does any arbitrarily chosen dimension. If the tunnel height, say, is chosen as the basic dimension, then the ratio of the tunnel lengths, train lengths, train widths, train roughnesses, tunnel roughnesses, etc. should all be numerically equal to the ratio of the tunnel heights. This implies for example that the cross-sectional shapes of the tunnels should be identical and that the distribution of surface roughness around the perimeter of the trains should be identical.

Clearly, such stipulations are unrealistic. Nevertheless, any deviation from them will represent a deviation from a true model, and so great care

must be taken to ensure that any relaxations of geometrical similarity will have only minimal influence on the value of the results obtained.

Major potential simplifications result if the intended use of the model is restricted to verification of the theoretical analyses (as opposed to reproduction of full-scale effects). Then it is sufficient to use any convenient geometry. After verification, the theories may be used with confidence to predict what will happen in the full-scale situation.

Nevertheless, additional benefits will accrue if the model shape resembles the full-scale shape as closely as possible because then the validity of the assumption of one-dimensional flow will be tested for realistic cases.

Geometrical parameters which can be modelled with comparative ease are a) train/tunnel length ratio, b) train/tunnel blockage ratio, and c) train length/'diameter' ratio. Those which are less readily modelled include a) train perimeter/'diameter' ratio, b) tunnel perimeter/'diameter' ratio, c) train roughness size and distribution, d) tunnel roughness size and distribution, e) train nose and tail shapes, and f) train eccentricity within the tunnel cross-section.

In the theoretical analyses, the perimeter and roughness height are used principally for the evaluation of skin friction. It is possible to adjust the roughness height in order to make allowance for discrepancies in the modelling of the perimeters. Similarly, the nose and tail shapes need not be accurately reproduced if their macroscopic effects can be otherwise simulated. Thus, the only important geometrical parameter which cannot be modelled or otherwise accounted for is the vehicle eccentricity (not concentrate with the tube).

Vehicle eccentricity is not a parameter of the theoretical analysis. Greatest accuracy may be expected when the vehicle is centrally positioned within the tunnel, but this is not representative of the full-scale situation. No means exist for determining exactly how much error will be caused by failure to model eccentricity. However, a qualitative assessment can be made by building into the model a facility for varying the eccentricity. The results thus obtained might or might not bear any close resemblance to those which would be obtained at full-scale, but it is likely that the underlying trends will be the same in both cases.

Although the nose and tail shapes need not be reproduced exactly, it is important that the pressure loss coefficients associated with them should be known both in the parallel sections of the tunnel and along the entrance regions, particularly along a flare. It will be of considerable value if these coefficients can be established by means of a series of steady-state tests in which the vehicle would be held stationary within the tunnel which would then be used as a wind tunnel. In the absence of such tests, it will be necessary to deduce the relevant values from the results of the unsteady-state tests. Such a procedure is likely to lead to difficulties in the locations of sources of discrepancies between theory and experiment. Use of the model itself as a wind tunnel will also permit the evaluation of the skin friction coefficients for both the train and the tunnel. At the expected Reynolds numbers, substantial variations in the skin friction may be anticipated between the model and full-scale.

5.4.2 Dynamic Similarity

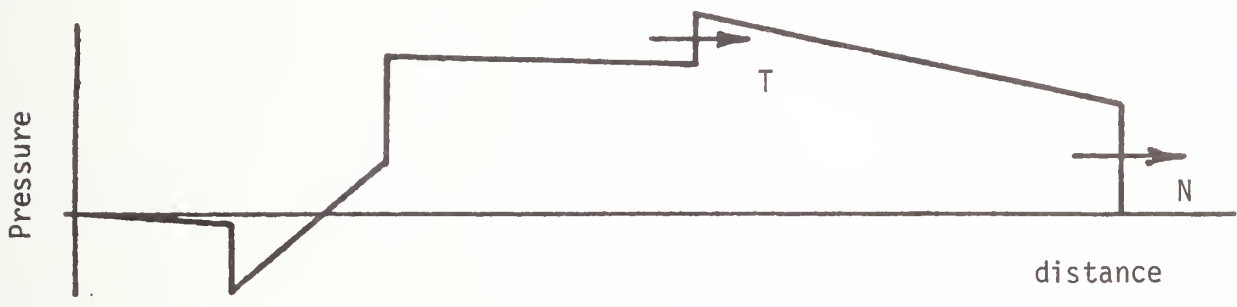
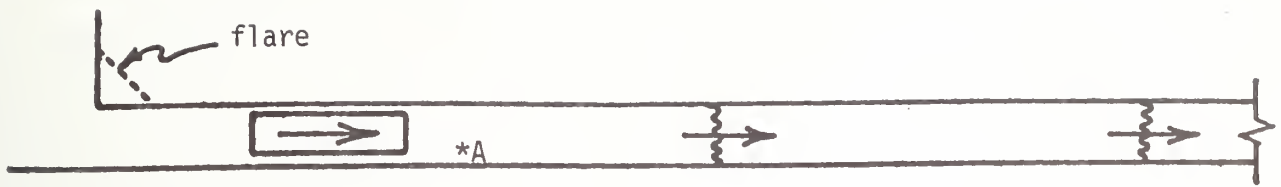
The principal parameters governing dynamic similarity are the Reynolds number and the Mach number. For this study, it is appropriate to model

just the Mach number; that is, to run the model at full-scale speeds. Then compressibility effects including, notably, wave action will be correctly reproduced. In the 1% scale facility, which operates under ambient conditions, the Reynolds numbers will be everywhere 100 times smaller than they are at full-scale. Thus, viscous effects will not be correctly modelled.

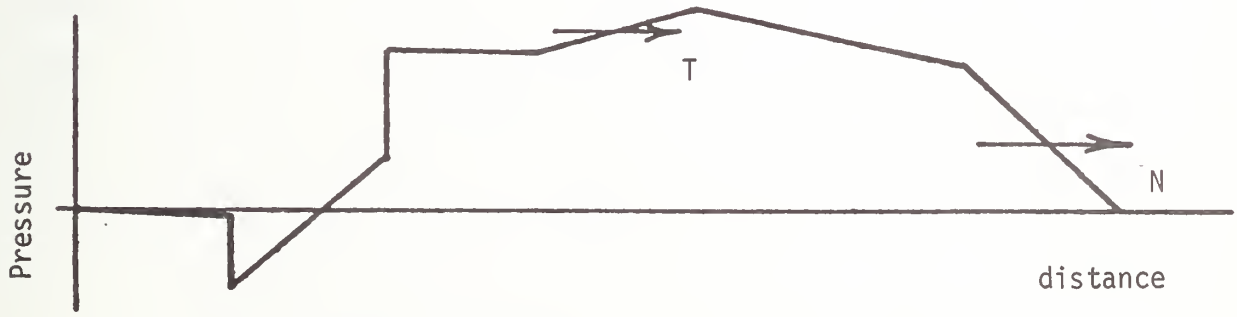
Fortunately, the consequences of this inaccuracy are not considered serious for this study. The greatest contribution to the skin friction is that on the sides of the train. Velocities relative to the train will typically be in excess of 20 m/s and so the Reynolds numbers in the most important region will normally exceed 10,000. For the case of fully developed flows, turbulent conditions may be expected and so it may be notionally possible to adjust the surface roughness of the train in order to reproduce the skin friction coefficient expected at full-scale. In practice, it is not suggested that this adjustment should be made. Instead, the differences between the model and prototype skin friction coefficients should be regarded as simply another reason for treating the model as a small tunnel in its own right. As was indicated above, this does not greatly reduce its value as a means of verifying the theoretical analyses.

5.5 Identification of Pressure Transients

In a simple tunnel, the nose-entry and tail-entry wavefronts are assumed to be generated at the instants when the nose and tail of a train reach the tunnel entrance portal. The resulting pressure distribution in a very long tunnel shortly after tail-entry is illustrated in Figure 5.5a. The wavefronts are step-changes in the pressure, and the figure is simplified by neglecting minor reflections such as that of the tail-entry wavefront at the nose of the train.



(a) Simple Tunnel



(b) Tunnel with Flared Entrance

FIGURE 5-5. PRESSURE DISTRIBUTIONS ALONG TUNNEL

In a tunnel with a modified entrance region - flared or perforated - the wavefronts are assumed to be continuously generated during the periods when the nose and tail pass along the region. The resulting wavefronts are not step-changes but ramp-changes in the pressure, and the situation is illustrated in Figure 5.5b for a case where the train is longer than the entrance region.

At a typical section, A say, in the tunnel, the first pressure change to be experienced is the nose-entry wavefront. This is followed by the tail-entry wavefront and later (in this example) by a period when the train itself passes by. The resulting pressure history is shown in Figure 5.6a for a simple tunnel and in Figure 5.6b for a tunnel with a flared entrance. After sufficient time has elapsed, the pressure histories will be influenced by reflections of the nose-entry and tail-entry wavefronts from the exit portal. As a first approximation, these may be regarded as linear superpositions on top of the basic pressure histories. The superpositions can occur at any position in the pressure histories, depending upon the length and speed of the train as well as upon the length of the tunnel and the position of the measuring station along the tunnel. There is, therefore, no such thing as a typical superposition. However, the effect is illustrated by Figure 5.6c.

In all of Figure 5.6, the following notation is used:

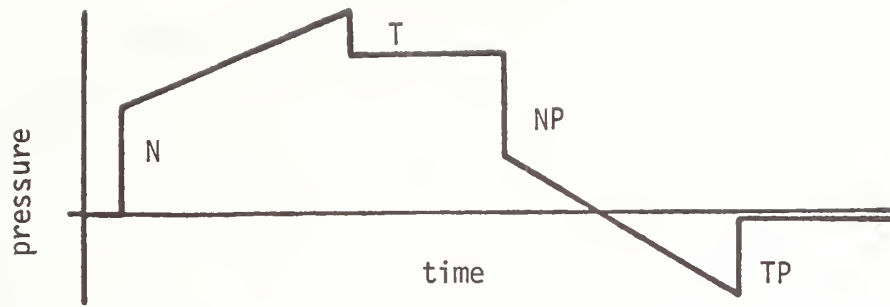
N = Nose-entry wavefront

NP = Nose passing measuring station

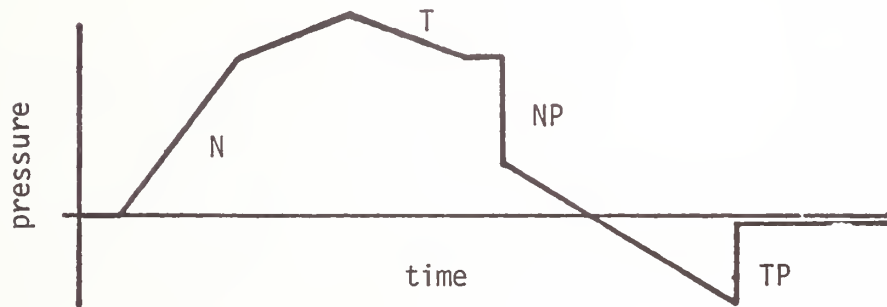
NR = Reflection of nose-entry wavefront from exit portal

N2 = Subsequent reflection from entrance portal, i.e.
second downstream pass of nose-entry wavefront

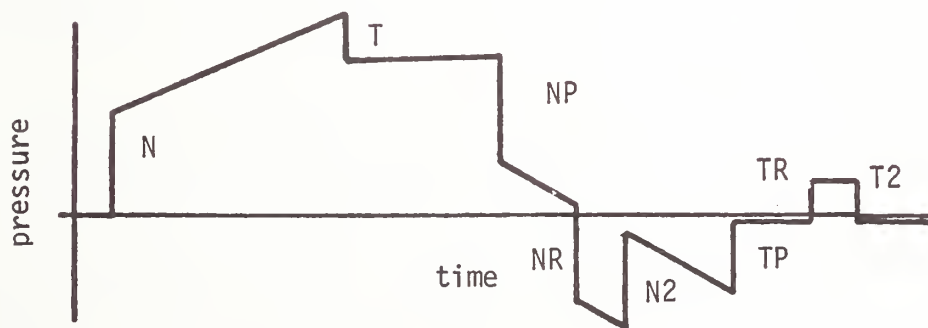
T, TP, TR, T2 = Ditto for tail



(a) Simple Tunnel



(b) Tunnel with Flared Entrance



(c) Simple, Short Tunnel

FIGURE 5-6. PRESSURE HISTORIES INSIDE TUNNEL

The major effect of perforated and flared entrance regions is to reduce the rates of change of pressure associated with the nose-entry and tail-entry wavefronts. Substantial reductions in the magnitudes of these wavefronts are not to be expected. However, reductions can occur in the peak-to-peak pressure excursions experienced by personnel as a result of superpositions of wavefronts and their reflections. For example, the frontmost part of the tail-entry wavefront will overlap with the rear-most part of the nose-entry wavefront if the train is significantly shorter than the entrance region.

It is also possible for useful superpositions of waves to occur with their own reflections. Suppose for example that a train travelling at a speed V (35 m/s say) enters a tunnel which has an entrance region of length λ_e (200 m say). In the time required for the nose of the train to pass completely along the entrance region, i.e. λ_e/V (5.714 s), the frontmost part of the wavefront will have moved a distance $\lambda_e c/V$ (1885.72 m if $c = 330$ m/s). The total length of the wavefront generated by nose-passage along the entrance region is thus $\lambda_e(c/V - 1)$ which is 1685.72 m in the numerical example.

When the frontmost part of the wavefront reaches the exit portal - see Figure 5.7a - the rearmost part is still $\lambda_e(c/V - 1)$ meters away (neglecting wavefront steepening effects). After a half of the time required for the whole wavefront to reflect, the frontmost part of the reflected wavefront coincides with the rearmost part of the incident wavefront - see Figure 5.7c. Both are $\frac{1}{2}\lambda_e(c/V - 1)$ from the exit portal. Subsequently the situations depicted in Figures 5.7d and 5.7e are reached. By inspection of Figure 5.7 it is seen that within the region of length $\frac{1}{2}\lambda_e(c/V - 1)$

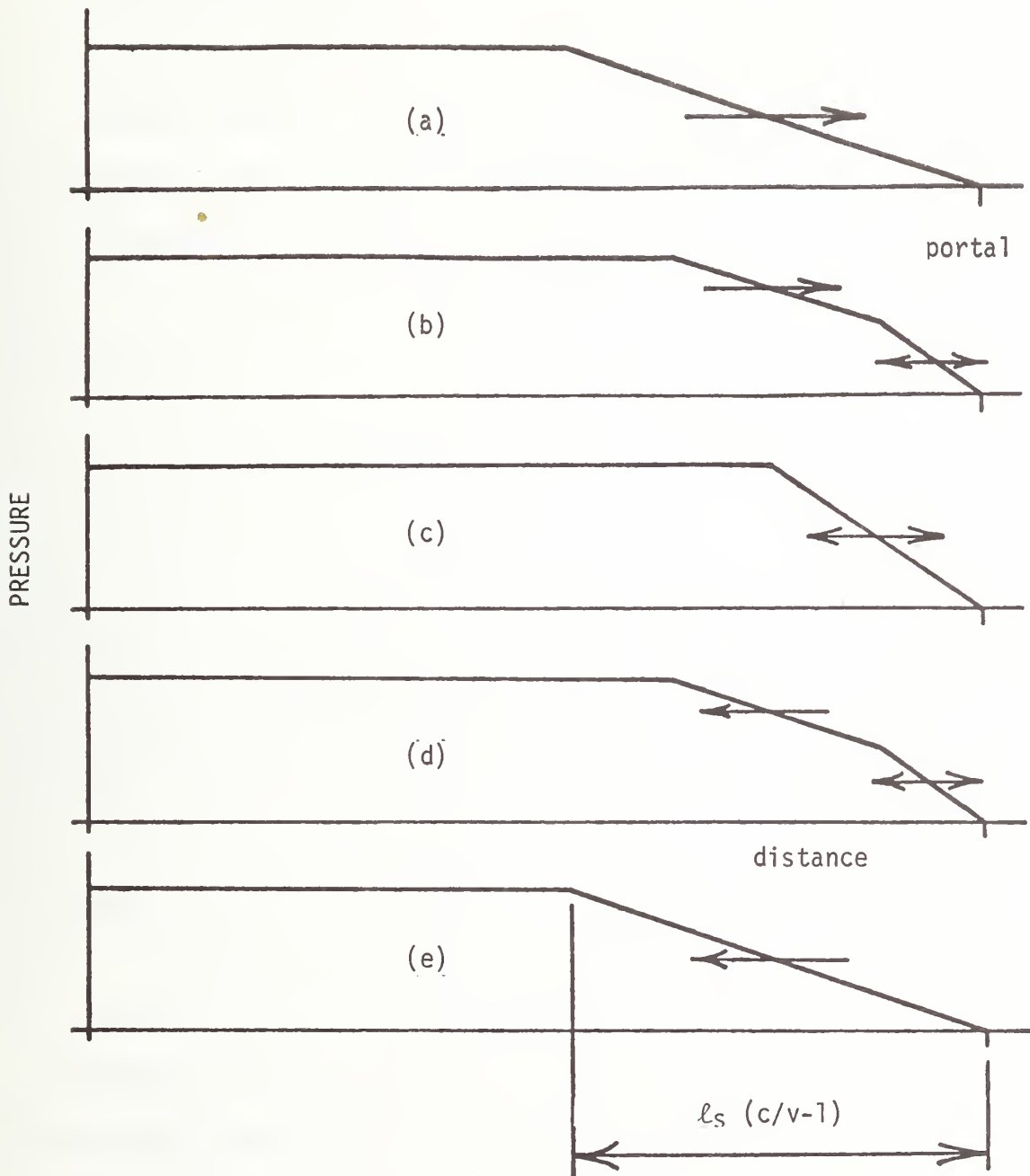


FIGURE 5-7. REFLECTION OF A RAMP - WAVEFRONT

next to the exit portal, the full magnitude of the incident wavefront is never developed. Quite simply, the returning wavefront begins to lower the pressure before the incident wavefront has finished raising it.

In short tunnels, it is possible for the train to be partly or wholly within this region during the period when the wave reflects. By extending the above reasoning, it can be shown that at least the nose of the train will be within this region whenever

$$\lambda_e > \frac{2\lambda_t}{(c/V + 1)} \quad \dots(5.23)$$

which is 19.18% of the tunnel length in the numerical example.

After the wavefront has reflected from the exit portal, it passes back along the tunnel and subsequently reflects at the entrance portal. Once again there is a region of length $\frac{1}{2}\lambda_e(c/V - 1)$ in which the full peak-to-peak pressure excursion does not occur. Also, it is again possible for the train to be within this region. This time, the appropriate requirement is that

$$\lambda_e > \frac{4\lambda_t}{(c/V - 1)^2} \quad \dots(5.24)$$

which is 5.63% of the tunnel length when $c = 330$ m/s and $V = 35$ m/s.

By comparison of Figures 5.5 and 5.6, it is found that it is more like that passengers will benefit from this latter effect than from the previous one. This conclusion remains true for all train speeds below about 78 m/s.

The importance of these effects depends upon the length of the tunnel because it is only with sufficiently short tunnels that the required entrance lengths are practical. With the more advantageous example, the

required entrance length is 56.3 m for each 1000 m of tunnel length. Even then, however, passengers at the front of the vehicle are only just inside the region of overlap and they receive relatively little benefit. For all passengers to receive substantial benefit, the entrance length should be much longer, say 80 m per 1000 m of tunnel length. For a train speed of 35 m/s, therefore, it may not be realistic to attempt to take advantage of this phenomenon when the tunnel length exceeds about 2500 m.

It must be stressed that the whole effect is strongly dependent upon the train speed. Considerably shorter entrance lengths are sufficient at lower speeds while there is a rapid drop-off in the effectiveness of modified entrance regions at higher speeds.

5.6 Highlights

- a. The principal waves generated by a train passing through a single-tracked tunnel originate at the instants when the nose and tail of the train enter and leave the tunnel or pass a discontinuity such as an airshaft. Of these, the most important for the purposes of this study are the nose and tail entry waves.
- b. The degree of aural discomfort experienced by passengers depends upon the magnitudes of the pressure fluctuations and upon the time intervals between successive pulses.
- c. The major parameters influencing the magnitude of the nose entry wave are the train speed, the blockage ratio, the nose shape and the air speed in the tunnel prior to train entry.
- d. The major parameters influencing the magnitude of the tail entry wave are the train speed, the blockage ratio, the tail shape, the surface roughness of the train and the air speed in the tunnel prior to train entry.

- e. In order to cause least passenger discomfort, trains should have small cross-sectional areas, well-streamlined noses, poorly streamlined tails and rough surfaces.
- f. Pressure gradients within tunnels are reduced if the entrance and exit regions are flared or ventilated. If these regions are sufficiently long, the magnitudes of the pressure fluctuations are also reduced.
- g. No information is available concerning the influence of shafts very close to tunnel entrances. Provided that the shafts are short, it is likely that this would be a useful position for them. Existing computer programs could be used to obtain information about this possibility.
- h. One-dimensional considerations are sufficient to describe the transmission of pressure waves in tunnels.

5.7 Nomenclature

a	cross-sectional area
c	local sonic velocity
c_p	specific heat at constant pressure
g	gravitational acceleration
k	pressure loss coefficient
ℓ	length
m	mass flow rate (lateral flows)
M	train Mach number
p	pressure
Q	heat transfer per unit length
s	cross-sectional perimeter
t	time co-ordinate
T	absolute temperature

u	air velocity
U	train speed
W	external work per unit length
x	distance co-ordinate
z	elevation
β	blockage ratio
γ	ratio of specific heats
ρ	density
τ	wall shear stress

Subscripts

AT	atmospheric conditions
e,E	tunnel entrance
ex	tunnel exit
F	train nose (front)
L	lateral flows
R	train tail (rear).

6. THE COMPUTER PROGRAM

Neither of two computer programs which existed prior to this study were suitable. One could handle trains in simple or complex tunnel systems, but dealt with lateral flows in an inelegant manner. The second dealt rigorously with lateral flows, but was not capable of handling the discontinuities presented by trains.

The second of these programs (written in FORTRAN 4) was modified so that it is capable of everything required of it in the current experimental investigation. It is written more efficiently than the previous global program and has therefore superseded it. The current cost of a typical run on Cambridge University's IBM 370/165 is approximately \$25, which represents about 40 secs of CPU time. In general, runs in which the tunnel has no flared or perforated section are much cheaper than those in which such a section is present. This is a direct consequence of the large reduction in grid size which is necessary in order to properly describe flows in non-uniform entrance regions. The new program is, however, less sensitive to this reduction than was the previous global program because a novel numerical scheme has been developed. The time-steps of integration can be up to four times as great as the nominal maximum values deduced from standard stability criteria. Even greater steps may be feasible.

6.1 Capabilities of the Program

6.1.1 Tunnel System

a. There may be any number of tunnels, which may be joined together to form any desired network.

- b. When appropriate, three or more ducts may meet at a single junction so that airshafts or cross-overs can be accommodated. Pressure loss coefficients for every possible flow combination at a junction may be input if necessary. In particular, this permits the introduction of flow restrictions into the system.
- c. Intervening between two adjacent tunnels may be specified in the form of discrete adits of any length and cross-section. At present, perforated dividing walls may not be specified, but this capability could be made available.
- d. Tunnels may have stepped or gradual area changes.
- e. Tunnels may have perforated walls connecting to the atmosphere. In this case, account is taken of the dimensions of the ventilating holes.
- f. Changes in elevation along the tunnels and shafts may be specified.

6.1.2 Trains

- a. The trains are regarded as constant area, impervious objects. Local increases in area at the front or rear of a train may be specified in order to correctly reproduce the pressure differences at these boundaries. In particular, this permits the simulation of built-up tails.
- b. The speed history is specified in any one of three forms: 1) constant speed, 2) pre-determined acceleration history, or 3) acceleration determined from aerodynamic drag.
- c. There may be any number of trains, and each may be routed through the tunnel system in any desired manner. Two (but not more) trains are permitted alongside one-another in any tunnel.
- d. Stationary trains may be specified as present anywhere inside the system before a run begins. They may subsequently be routed through the system in any desired manner.

6.2 Flow Through Walls of Perforated Portals

The laboratory model can be regarded as a true dynamic model of full-scale tunnels. An example is the case of a step-wavefront reflecting at a perforated tube on the end of an impervious tube. The following results are of special interest to the TEPT study:

- a. The reflected wavefront profile can be made to approximate a ramp which is three times longer than the length of the perforated region. This result demonstrates the importance of non-linear terms in the equations describing the flow through the holes in the tube walls. If the non-linear terms are neglected, the ramp is falsely predicted as being only twice as long as the perforated region.
- b. The optimum total porosity varies with the square-root of the magnitude of the incident wavefront. This causes little difficulty from a tunnel designer's point of view because only a narrow range of pressure is of interest.
- c. The ventilating holes may be evenly distributed along the perforated region without causing the profile of the reflected wavefront to differ significantly from the optimum shape. This means that a well designed perforated entrance region will also act usefully as perforated exit region for vehicles travelling in the opposite direction.

7. SIMPLIFIED THEORETICAL ANALYSIS

A simple analysis of scaling was undertaken to help resolve questions of simulating the full scale situation with a model experiment, especially in relation to size of the holes in the porous walls. It was also planned to produce simplified analytic models by the use of appropriate simplifying assumptions that would better explain the physical phenomena and lead to a means of evaluating different entry concepts more readily than the Vardy computer model. Simplified models of flared and porous entries have been developed.

7.1 Scaling

The purposes of this analysis are twofold. The first purpose is to establish the criterion for designing a correctly scaled experiment involving porous walls and, second, to determine if such an experiment can be practically carried out. At the start of this program there was a question of whether the unsteady inertia term played an important role in the flow through the passages of a porous wall and whether the importance of this term depended upon the scale of the experiment or the velocity of the vehicles, References 7 and 8. It was necessary to resolve this question in order to properly understand the meaning of the experiments and to judge the accuracy of the existing theory.

In Reference 9, an examination was made of the scaling laws for tunnel flows and it was concluded that proper scaling could be accomplished if geometry were scaled and the usual dimensionless aerodynamic parameters, such as Mach number and Reynolds number, were preserved. The unsteady aspects of the flow are scaled by using a dimensionless time, $\tau = \frac{tu_t^*}{L}$, and acceleration, $\alpha = \frac{aL}{u_t^2}$. There appears to be no real difficulty with this scaling except for the usual problems with Reynolds number. The

* See Section 7.5 for definition of nomenclature.

scaling of porosity was not specifically considered in this analysis, but the analysis would appear to be general enough to cover this case also. The conclusion would be that geometric similarity for the porous wall would be adequate except for the obvious difficulties with Reynolds number if the pores become too small.

A better understanding of why the scaling leads to no difficulties and the importance of the unsteady inertia term can be obtained by examining the unsteady flow through an orifice. The analysis developed in Reference 10 is appropriate. Consider the flow through a tube and include the stream-tube around the entrance to the tube in the quasi one dimensional model, Figure 7.1. For incompressible flow, the dynamic relation is:

$$\frac{\partial u}{\partial t} - \frac{u^2}{A} \frac{dA}{dx} + \frac{1}{\rho} \frac{\partial p}{\partial x} = 0 \quad \dots(7.1)$$

Integrate this relation from a station ahead of the tube where flow area is essentially ∞ (1) to the exit (2) using the continuity equation to obtain u as a function of A .

$$\frac{du_2}{dt} \int_1^2 \frac{dA_2}{A} dx + \frac{1}{2} \left(1 - \frac{A_2^2}{A_1^2} \right) u_2^2 + \frac{p_2 - p_1}{\rho} = 0 \quad \dots(7.2)$$

If the initial and final pressure difference is independent of time, this equation integrates with respect to t to yield

$$\frac{(t-t_i) u_f}{2L} = \left(\tanh^{-1} \frac{u_2}{u_f} - \tanh^{-1} \frac{u_{2i}}{u_f} \right) \quad \dots(7.3)$$

where

$$L_e = \int_1^2 \frac{A_2}{A} dx \quad \text{and} \quad u_f = \sqrt{\frac{2(p_1 - p_2)}{\rho} \left[\frac{1}{1 - \left(\frac{A_2}{A_1} \right)^2} \right]}$$

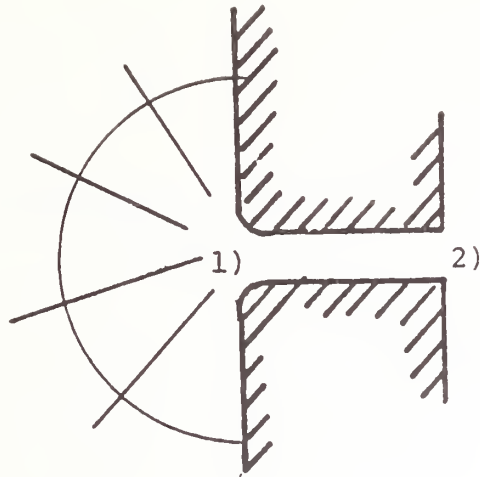


FIGURE 7-1. DIAGRAM OF FLOW THROUGH PORE

For the simple case in which station 1 is in a large reservoir, $\frac{A_2}{A_1} = 0$, the expression for u_f is simplified. For a fluid entering a straight tube from a reservoir, the effective length, L , is simply the length of the tube plus the effective length of the entrance flow. The apparent mass for the flow into a round hole is

$$M_a = \frac{1}{16} \pi^2 d_p^3 \rho. \quad \dots(7.4)$$

Dividing by the area of the hole and the density gives the effective length

$$L_a = \frac{\pi d_p}{4}. \quad \dots(7.5)$$

The effective length of the tube is then

$$L_e = L + \frac{\pi d_p}{4}. \quad \dots(7.6)$$

as shown in Figure 7.2. The characteristic time for obtaining steady

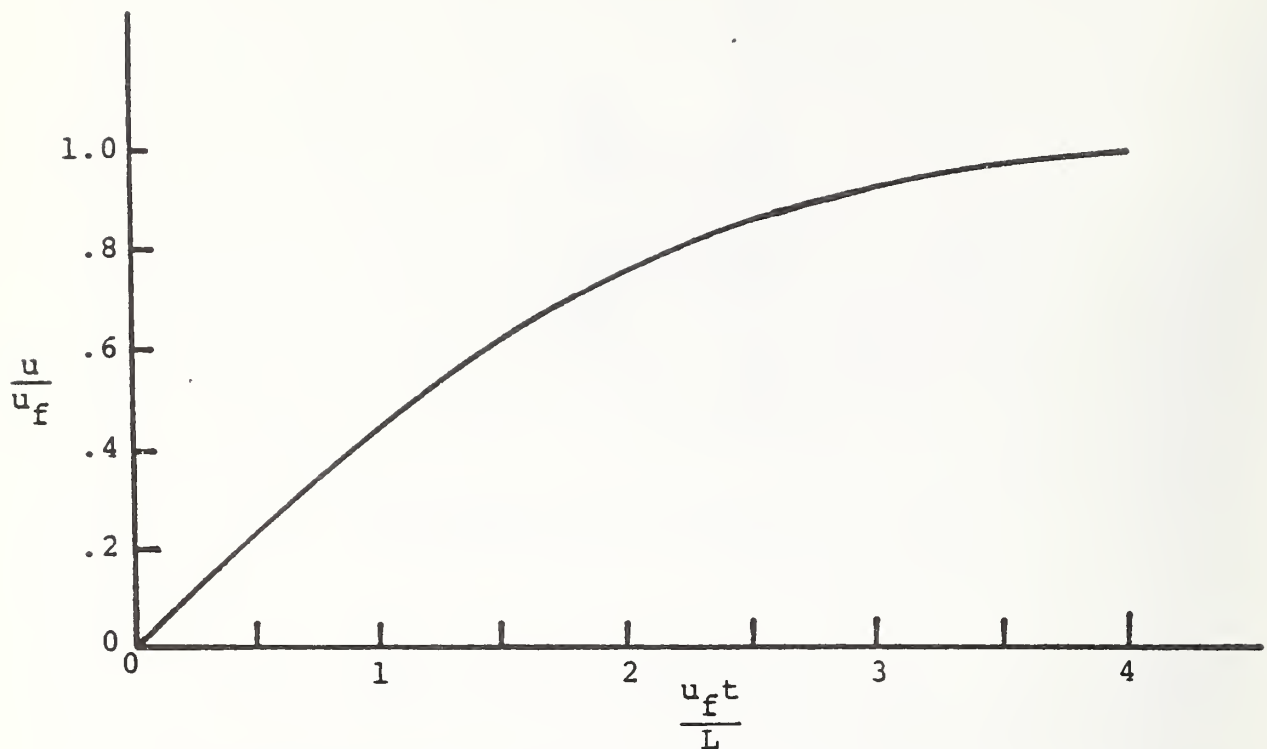


FIGURE 7-2. UNSTEADY VELOCITY THROUGH PORE AS FUNCTION OF DIMENSIONLESS TIME

state velocity is $\frac{L}{u_f}$ or $L \sqrt{\frac{\rho}{2\Delta p}}$. If the rate of change of the pressure within the tube is small in this characteristic time, then the flow through the pores will be given by the steady state velocity and, if not, the velocity will be considerably different and the unsteady inertia term will be important.

To reconsider the scaling problem in the light of this result, note that the characteristic time varies inversely as the effective length of the pore, L . The scaling analysis previously discussed shows that all times vary inversely as the length. The time for the flow through the pore varies in the same way as all the other times and there is no change in the relation of these times between model and full scale.

The parameter for judging the importance of the unsteady inertia term is $\frac{1}{p} \frac{dp}{d\tau}$ where $\tau = \frac{tu_f}{L}$. Therefore,

$$\frac{1}{p} \frac{dp}{d\tau} = \frac{L}{u_f p} \frac{dp}{dt} = L \sqrt{\frac{\rho}{2p^3}} \frac{dp}{dt} \quad \dots(7.7)$$

The unsteady term is important if this parameter is small. However, in a numerical analysis of this problem performed on a computer it may not be necessary to decide if this parameter is large or small. Equation 7.7 is suitable to predict the flow through the pore and is valid for all values of τ .

The pressure change which generates the flow through the pores is caused by the vehicle entering and passing through the tunnel. The most important pressure effect is caused by the vehicle entering the tunnel. The pressure rise can be related to the drag coefficient of the vehicle, Reference 8.

$$\Delta p = \frac{1}{2} \rho v^2 C_D (1 - C_{D_t} + \dots) \quad \dots(7.8)$$

This pressure rise takes place in three steps, the first is a rather steep one caused by the nose entering the tunnel. The time for the pressure rise is the time for the vehicle to travel a characteristic distance which is related to the diameter of the tunnel. An additional pressure rise takes place as the vehicle continues to enter the tunnel and the characteristic length for this process is the length of the vehicle. A decrease in pressure occurs when the rear of the vehicle enters the tunnel and the characteristic length for this process is again the diameter of the

tunnel. The pressure rise is proportional to the change in drag associated with each of these processes. The most rapid pressure rise is probably that associated with the nose entering the tunnel and its characteristic time and magnitude are given by the expressions:

$$\tau_R = \frac{D}{v} \quad \dots(7.9a)$$

$$\Delta p = \frac{1}{2} \rho v^2 C_{DN}, \quad \dots(7.9b)$$

neglecting the Mach number correction. The characteristic time period for the pore to establish steady flow is

$$\tau_p = \frac{L_p}{u_f} = L_p \sqrt{\frac{\rho}{2p}}. \quad \dots(7.10)$$

If the pressures at the pore and in front of the vehicle are taken as the same, then

$$\tau_p = \frac{L_p}{v \sqrt{C_{DN}}}. \quad \dots(7.11)$$

The ratio of the characteristic pore steady flow time to the pressure rise time is

$$\frac{\tau_p}{\tau_R} = \frac{L_p / v \sqrt{C_{DN}}}{D / v} = \frac{L_p}{D \sqrt{C_{DN}}}. \quad \dots(7.12)$$

The first conclusion is that the ratio is independent of vehicle velocity and the scale of the experiment. The next conclusion is that, if the effective length of the pore is small compared with the tube diameter, the unsteady inertia effects need not be considered. The effective length of the pore is given by Equation 7.6. Unless the porosity is achieved by vent shafts, the physical length of the pore would be the tube wall thickness which would be small compared with the tube diameter. The effective entrance length can be large if the pore is of the order of the

tube diameter but then the pore flow analysis is no longer valid. However, if the concept of a porous entry is limited to pores small with respect to the tunnel diameter than the unsteady effect is not important. The drag coefficient does have an effect and the above conclusion will be in error for very low drag coefficients. However, such low drag coefficients do not apply to real vehicles and if they did the pressure pulse generated would be too weak to be of practical importance.

7.2 Flared Entry Portal

The objective of this analysis is to perform a simplified analysis of a flared entrance to supplement the more complete computer solution being performed by Vardy. The objectives of such a simplified solution are to gain a better understanding of the dominant physical effects. Also, a simplified means of computing the effects of an entrance flare would allow the effects of different configurations or the initial pressure wave to be determined with greater ease than by means of experiments or the full computer program.

The principal assumptions of this analysis are as follows:

- a. The flow in the flared inlet and around the model can be considered incompressible. The flow is considered incompressible up to the end of the inlet or nose of the vehicle, whichever is further from the entrance.
- b. The flow in the tunnel in front of the model is compressible and the tunnel is long enough so that a reflected wave cannot return from the other end of the tube during the period for which this analysis is valid.
- c. Friction is considered in the flow about the vehicle but not in the tunnel ahead of or behind the vehicle.

Before settling on this set of assumptions, other possibilities were considered such as an entirely incompressible analysis. This assumption requires a slug concept for the fluid in front of the vehicle in which the initial pressure is high and drops off as the slug of fluid accelerates. The incompressible concept is more appropriate to a short tube in which reflections return from the far end before the vehicle has appreciably entered the tunnel. For the vehicle speeds and entrance to tunnel length ratios used in the experiments this concept was not appropriate. The incompressible model, however, is reasonable for the flow around and behind the vehicle. The principal disturbances occur as the vehicle enters the tunnel. Wave travel time between the vehicle and the entrance is short and there is time for multiple reflections. Wave effects quickly disappear and a slug flow concept is appropriate. These arguments are somewhat less applicable as the vehicle undergoes the transition from the flare to the straight section. Waves generated at this time have a greater distance to travel to the entrance and back. However, continuous reflection will occur as a wave travels through the flared section. One would expect some smoothing of the predicted results at this junction because of the neglect of the wave effects.

The effects of friction with the vehicle and the tunnel wall are not important in the entrance process except for the flow passing around the vehicle. The velocities with respect to the tunnel in the sections ahead of and behind the vehicle are small so the friction forces with the tunnel are also small and should not have an important effect during the limited time of the entering process. In accelerating around the vehicle, the flow velocities relative to the tunnel wall are increased and the velocity

relative to the vehicle is also augmented by the speed of the vehicle. For a long vehicle, a substantial part of the pressure drop about the vehicle is caused by the friction effects and these effects must be included.

7.2.1 Analysis

Consider the configuration shown in Figure 7.3. In the straight section of the tunnel, pressure and velocity can be related by the expression across a simple wave.

$$\frac{\Delta u}{c_\infty} = \frac{2}{\gamma-1} \frac{\Delta c}{c_\infty} \quad \dots(7.13)$$

and

$$\frac{c}{c_\infty} = \frac{p}{p_\infty} \frac{\gamma-1}{2\gamma} = 1 + \frac{\gamma-1}{2\gamma} \frac{\Delta p}{p_\infty} + \dots$$

Combining these expressions, the result is

$$\frac{u_0}{c_\infty} = \frac{1}{\gamma} \frac{p_0}{p_\infty} \quad \dots(7.14)$$

which can be expressed in the form of a pressure coefficient based on vehicle velocity as

$$c_{p_0} = \frac{2u_0}{vM_v} \quad \dots(7.15)$$

From Station 0 to 1 the flow can be considered incompressible. The Bernouli and continuity expressions apply giving:

$$\frac{p_1}{\rho} + \frac{u_1^2}{2} = \frac{p_0}{\rho} + \frac{u_0^2}{2} \quad \dots(7.16)$$

$$\dots(7.17)$$

$$A_0 u_0 = A_1 u_1$$

$$c_{p_1} = c_{p_0} + \frac{u_1^2}{v^2} \left(\frac{A_1^2}{A_0^2} - 1 \right) \quad \dots(7.18)$$

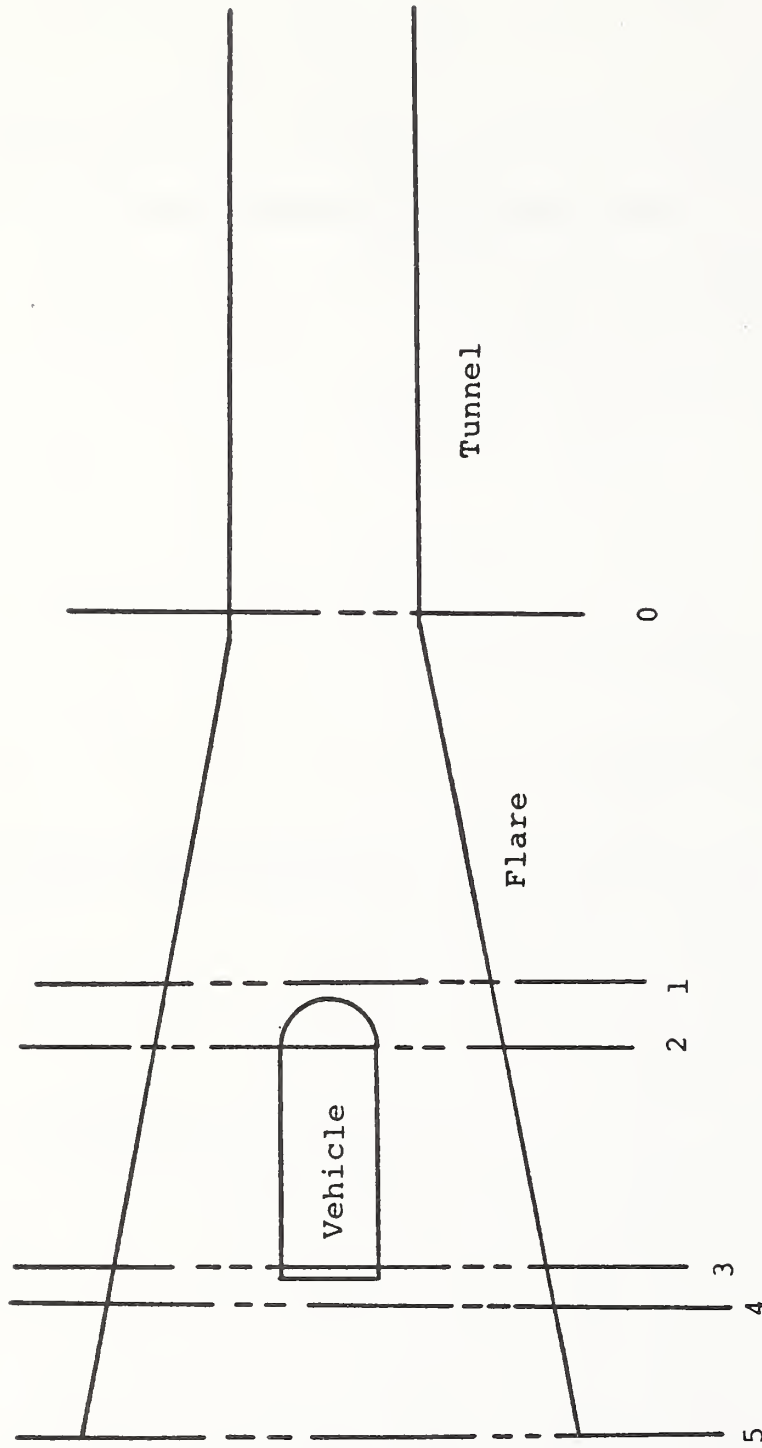


FIGURE 7-3. SCHEMATIC DIAGRAM OF VEHICLE IN FLARED TUNNEL ENTRANCE

The flow around the nose takes place between Stations 1 and 2. This section may be treated using the steady Bernouli and continuity relations as the equations are written in a coordinate system fixed with respect to the nose of the vehicle. The resulting relations are:

$$\frac{p_2}{\rho} + \frac{(u_2-v)^2}{2} = \frac{p_1}{\rho} + \frac{(u_1-v)^2}{2} \quad \dots(7.19)$$

$$(u_2-v)A_2 = (u_1-v)A_1 \quad \dots(7.20)$$

$$c_{p_2} = c_{p_1} + \left(\frac{u_2}{v} - 1\right)^2 \left(1 - \frac{A_2^2}{A_1^2}\right) \quad \dots(7.21)$$

and

$$c_{p_1} = \frac{2}{M_v} \left[\frac{A_1}{A_0} + \left(\frac{u_2}{v} - 1\right) \frac{A_2}{A_0} \right] + \left[1 + \left(\frac{u_2}{v} - 1\right) \frac{A_2}{A_1} \right]^2 \left(\frac{A_1^2}{A_0^2} - 1 \right) \quad (7.22)$$

Unsteady incompressible relations will be used to treat the section between Station 2 and the rear of the vehicle, Station 3. The unsteady Bernouli equation is

$$\frac{\partial u}{\partial t} + u \frac{\partial u}{\partial x} = -\frac{1}{\rho} \frac{\partial p}{\partial x} - \frac{c_f u^2}{2} \frac{C}{A} \quad \dots(7.23)$$

and the continuity equation

$$m = uA \quad \dots(7.24)$$

Since m is constant with respect to distance in this section, it is convenient to replace u with m.

$$\frac{1}{A} \frac{\partial m}{\partial t} - \frac{m^2}{A^3} \frac{\partial A}{\partial x} = -\frac{1}{\rho} \frac{\partial p}{\partial x} - \frac{c_f}{2} \left[\frac{m|m|C_0}{A^3} + \left(\frac{m}{A} - v\right) \left| \frac{m}{A} - v \right| \frac{C_v}{A} \right] \quad (7.25)$$

This relation can be integrated with respect to x between 2 and 3 and written in the form

$$v \frac{dm}{dx} \int_2^3 \frac{dx}{A} - m^2 \int_2^3 \frac{1}{A^3} \frac{dA}{dx} dx = - \frac{p_2}{\rho} - \frac{c_f}{2} \left[m |m| \int_2^3 \frac{C_0}{A^3} dx + \int_2^3 \left(\frac{m}{A} - v \right) \left| \frac{m}{A} - v \right| \frac{c_v}{A} dx \right] \dots(7.26)$$

In order to evaluate these integrals, a relation between A and x is required. If the flare is conical, the relation is:

$$\frac{A_1}{A_0} = \left(1 + \frac{L-x_v}{A_0} F \right)^2 \quad x_v < L \quad \dots(7.27a)$$

$$\frac{A_1}{A_0} = 1 \quad x_v > L \quad \dots(7.27b)$$

Using this relation the integrals can now be evaluated for the case where $\left(\frac{m}{A} - v \right) < 0$. It is convenient to divide all areas by A_v , all lengths by $\sqrt{A_v}$, and all velocities by v to give dimensionless quantities. The same symbols will be used for these dimensionless quantities.

When the rear of the vehicle enters the tunnel, a pressure recovery occurs and the velocity with respect to the tunnel wall is reduced. In general, the fluid velocity will be away from the entrance ahead of the vehicle, towards the entrance while passing by the vehicle and again away from the

entrance behind the vehicle after the rear has entered the tunnel. The volume flow away from the entrance will be the same ahead of and behind the vehicle but the flow velocity behind the vehicle will be reduced because of the greater area of the flare at this point. Until the vehicle has fully entered the tunnel, air will be being expelled from the entrance. This expulsion is caused by the displacement effect of the entering vehicle. Once the vehicle has fully entered, air is pulled into the flare since the drag of the vehicle induces a flow down the tunnel.

The pressure recovery at the rear of the vehicle is calculated by the relation for a sudden expansion. This relation has generally been found acceptable for blunt based vehicles, Reference 8. Using this relation gives the pressure difference between Stations 3 and 4:

$$C_{p_3} - C_{p_4} = -u_4^2 - \left(\frac{2}{A_4-1}\right)(1-u_4)^2 \quad \dots(7.28a)$$

where

$$u_4 = \left[1 + \left(\frac{m}{A_1-1} - 1\right) \left(\frac{A_1-1}{A_1}\right) \right] \frac{A_1}{A_4} \quad \dots(7.28b)$$

Since the flow is into the flare after the vehicle is completely entered, the stagnation pressure of the air at Station 4 is the same as the free stream static pressure.

Including all of these effects results in the final differential equation for the flare entrance. In this equation the vehicle velocity and vehicle cross sectional area are used to make the other quantities dimensionless.

$$\begin{aligned}
& \left[\frac{1}{F} \ln \left(\frac{1 - \sqrt{A_1}}{1 + \sqrt{A_1}} \right) \left(\frac{1 + \sqrt{A_4}}{1 - \sqrt{A_4}} \right) - R \right] \frac{dm}{dx_V} = m^2 \left[\frac{1}{(A_1 - 1)^2} - \frac{1}{(A_4 - 1)^2} \right] \\
& + \frac{2}{M_V} \left(\frac{m-1}{A_0} \right) + \left[1 + \left(\frac{m}{A_1 - 1} - 1 \right) \left(\frac{A_1 - 1}{A_1} \right) \right]^2 \left(\frac{A_1}{A_0} - 1 \right) \\
& + \left(\frac{m}{A_1 - 1} - 1 \right)^2 \left[1 - \frac{(A_1 - 1)^2}{A_1^2} \right] + \frac{c_f \sqrt{\pi}}{F} \left\{ \frac{m|m|}{2} \left[\frac{1}{(A_1 - 1)^2} - \frac{1}{(A_4 - 1)^2} \right] \right. \\
& - \frac{m^2}{2} \left[\frac{\sqrt{A_1}}{(A_1 - 1)^2} - \frac{\sqrt{A_4}}{(A_4 - 1)^2} \right] + \left(\frac{3}{4}m^2 + 2m \right) \left(\frac{\sqrt{A_1}}{A_1 - 1} - \frac{\sqrt{A_4}}{A_4 - 1} \right) \\
& \left. + \left(\frac{3}{8}m^2 + m + 1 \right) \ln \left(\frac{1 - \sqrt{A_1}}{1 + \sqrt{A_1}} \frac{1 + \sqrt{A_4}}{1 - \sqrt{A_4}} \right) \right\} + S \\
& + \left[1 + \left(\frac{m}{A_1 - 1} - 1 \right) \left(\frac{A_1 - 1}{A_1} \right) \right]^2 \left(\frac{A_1}{A_4} \right)^2 \\
& + \frac{2}{A_4 - 1} \left\{ 1 - \left[1 + \left(\frac{m}{A_1 - 1} - 1 \right) \left(\frac{A_1 - 1}{A_1} \right) \right] \right\} \frac{A_1}{A_4}
\end{aligned} \tag{7.29}$$

where for $x_V < L$

$$R = 0 \quad S = 0 \tag{7.30a}$$

and for $x_V > L$

$$R = \frac{2(x_V - L)}{A_0 - 1}$$

$$S = 2c_f \sqrt{\pi} (x_V - L) \left[\frac{m|m|\sqrt{A_0} - m^2}{(A_0 - 1)^3} + \frac{2m}{(A_0 - 1)^2} - \frac{1}{A_0 - 1} \right] \tag{7.30b}$$

This equation has been solved by numerical integration. The integration has been continued until the vehicle has proceeded beyond the end of the flare. Since the returning waves are neglected in this model, the model would not predict any additional changes after this point.

7.2.2 Discussion

The effect of the flare is to spread out the pressure rise caused by the vehicle entering the tunnel and to limit it to the total value which occurs for a straight tube once the vehicle has fully entered the tunnel. It removes the overshoot in pressure which occurs when a vehicle enters a straight tunnel and the subsequent drop as the rear of the vehicle enters. When a vehicle first enters the large end of the flare, the initial pressure on the nose of the vehicle is quite similar to that which would be felt by the same vehicle entering a straight tunnel of the same diameter as that of the large end of the flare. The strength of the initial pressure pulse or the pressure generated at the nose of the vehicle has to be enough to cause the displaced flow to escape around the vehicle or down the tunnel. The flow down the tunnel is controlled by the wave equation

$$\frac{p_0}{p_\infty} = \frac{\gamma u_0}{c_\infty} \quad \dots(7.31)$$

The flow around the model is governed by the steady flow equation

$$\frac{2p_2}{\rho} + (u_2 - v)^2 = \frac{2p_1}{\rho} + (u_1 - v)^2. \quad \dots(7.32)$$

The wave relation is linear in u while the steady flow relation depends on u^2 . For conditions which produce only low pressure rises in the tunnel most of the flow escapes out the end of the tunnel and the flow

carried along with the wave is small. However, as the strength of the wave increases, the fluid carried with the wave increases and relatively less escapes around the vehicle. If the pressure rise is expressed as a pressure coefficient this coefficient would be independent of the velocity of the vehicle until the pressure rise becomes large enough so that the fluid carried with the wave becomes an appreciable part of the entire displaced fluid. The pressure does not rise as rapidly as the square of the vehicle velocity because of this relieving effect of part of the air being carried with the pressure wave. If the flare is made large enough so that the initial pressure rise is small, the initial pressure rise coefficient is independent of vehicle Mach number. This is demonstrated in Figure 7.4 by comparing the results at the two different flare sizes and the straight tunnel at the two different Mach numbers. As the vehicle passes through the flare, the pressure rises and the wave relieving effect becomes more important so that the pressure coefficient does not rise as rapidly for the higher Mach number case. For a given flare size greater relief is obtained for low Mach number vehicles than for high Mach number.

As the nose of the vehicle enters the flare, the pressure required to cause the fluid to escape around the vehicle increases since the velocity through the narrower forward end of the annulus must increase. However, the velocity out of the entrance remains low. The fluid diffuses along the flare with a consequent increase in pressure. Some of the pressure drop which occurs as the fluid flows around the nose of the vehicle is recovered in the flare. As the vehicle proceeds into the flare, the pressure continues to rise because of the decreased size and the increased friction. The pressure on the nose is never higher than it would be for

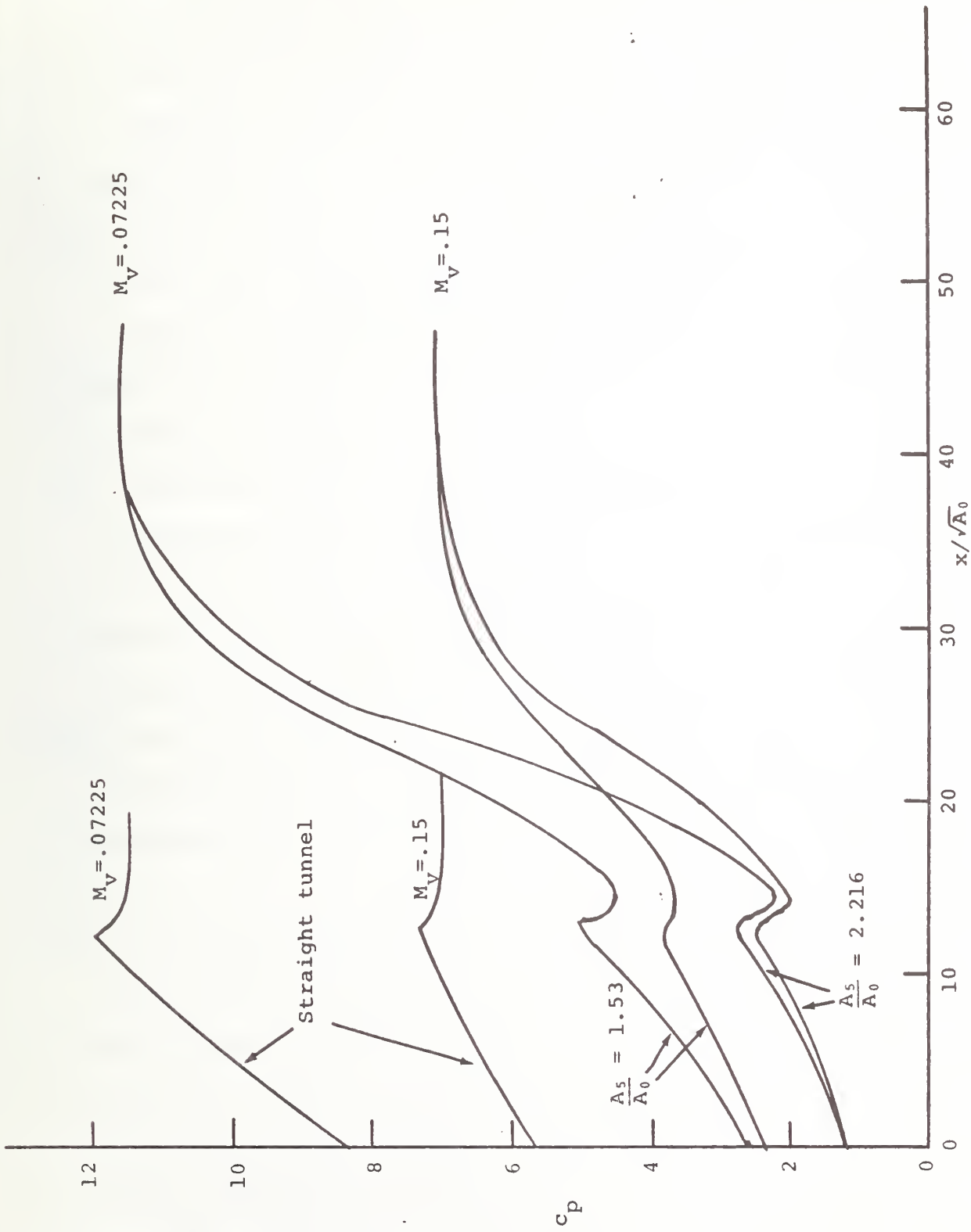


FIGURE 7-4. PRESSURE COEFFICIENTS FOR TWO FLARES AND STRAIGHT TUNNEL ENTRANCE
 (Configurations at Two Vehicle Mach Numbers: $A_0 = 1.309 A_V$, $S = 12.22/\sqrt{A_0}$)

a vehicle entering a tunnel of the same size without a flare, since the friction in the flared section is less than in a straight section and because of the diffuser action of the flare.

When the rear of the vehicle enters the flare, there is a further increase in pressure recovery. The pressure recovery around the rear of a blunt based vehicle is not very efficient because of the separation losses. However, the effect of a decrease in vehicle cross-sectional area is quite different than a similar increase in annular cross-sectional area caused by an increase in tunnel diameter. The difference is in the relative velocity; the relative velocity with respect to the vehicle being considerably higher than with respect to the tunnel. The effect of the rear of the vehicle entering the end of the flare is reduced over what it would be for a straight tunnel because of the increased diameter of the end of the flare. Since the total friction and nose drag of the vehicle have not yet reached their final value, because the vehicle is not entirely in the straight section of the tunnel, any overshoot which occurs before the rear has entered the tunnel is likely to be less than the final pressure. This has been true for all the cases calculated except the 25% blockage ratio case (see Figure 9.10.). Because of the discrepancies between theory and experiment for this case, any conclusions drawn must be considered with this in mind. However, if the theoretical results are accepted, it would seem that the flare is incorrectly designed for this size of vehicle. For this small blockage ratio vehicle, the pressure recovery at the rear is quite efficient and is a large part of the pressure drop at the nose of the vehicle. The friction loss in the flow through the annular passage between the vehicle and the tunnel wall is largely responsible for the final pressure. The drop in

pressure as the rear of the vehicle approaches the beginning of the straight section is caused by the pressure recovery at the rear increasing more rapidly as the rear enters increasingly small sections of the flare than the increase caused by friction as more of the vehicle enters the straight section. It is not clear at this time how the flare should be modified to alleviate these overshoots. No calculations have been made for different designs to explore the effects of such changes. When the rear of the vehicle enters the straight section, the friction and the rear pressure recovery stabilize at their values in a straight tunnel. It takes a little while for the flow to settle down to the final conditions because of the inertia effect. In the theory presented here, the flow around the model is considered to be incompressible so that the inertia of the whole slug must be considered. In the real case, compressible wave phenomena would exist and the fluid would be brought to the final conditions by the waves reflecting between the vehicle and the entrance. The final condition is the same as that achieved by the train entering a straight tunnel if the tunnel is long enough so that no reflected waves have returned from the far end of the tunnel.

At first one might think that the total pressure rise would be less because the time available before the air in the tunnel reaches its final velocity is much longer for the flared entry than for the straight entry. This is not true if the time is not long enough for the waves to return from the far end of the tunnel. The acceleration of the flow through a series of weak waves gives the same result as the acceleration through one stronger wave (as long as the stronger wave still obeys the weak wave relations). If the flow were incompressible in the tunnel, the slower

acceleration would result in a lower total pressure rise. The incompressible assumption gives an infinite sound speed so that there is time for the waves to return from the far end of the tunnel. An increase in the time for the pressure rise is only significant in effecting the total pressure rise if the time of pressure rise is longer than the time required for a wave to return from the far end of the tunnel.

Figure 7.4 also shows the predicted pressure rises for tunnels with no flare. It is interesting to compare these results with those for the case of flare. For the no flare case there is a definite overshoot as the vehicle enters the tunnel and then a drop as the rear enters. The final pressure is the same for the flare and no flare cases. The case of the flare eliminates the overshoot in all cases calculated except for the 25% blockage ratio vehicle. The initial pressure rise with a flared entrance is almost the same as the entry into a straight tunnel with a diameter equal to the maximum flare diameter. This result is shown in Figure 7.5 where the initial pressure coefficient is plotted against maximum flare diameter for a variety of straight tunnel diameters. The figure shows that the diameter of the straight tunnel had little effect on the initial pressure. The flare seems to be an effective method of decreasing the initial pressure effect on tunnel entry and in spreading out the total pressure rise over a longer time and distance. The overshoot and consequent reduction caused by the entry of the rear is also effectively reduced or virtually eliminated in most cases.

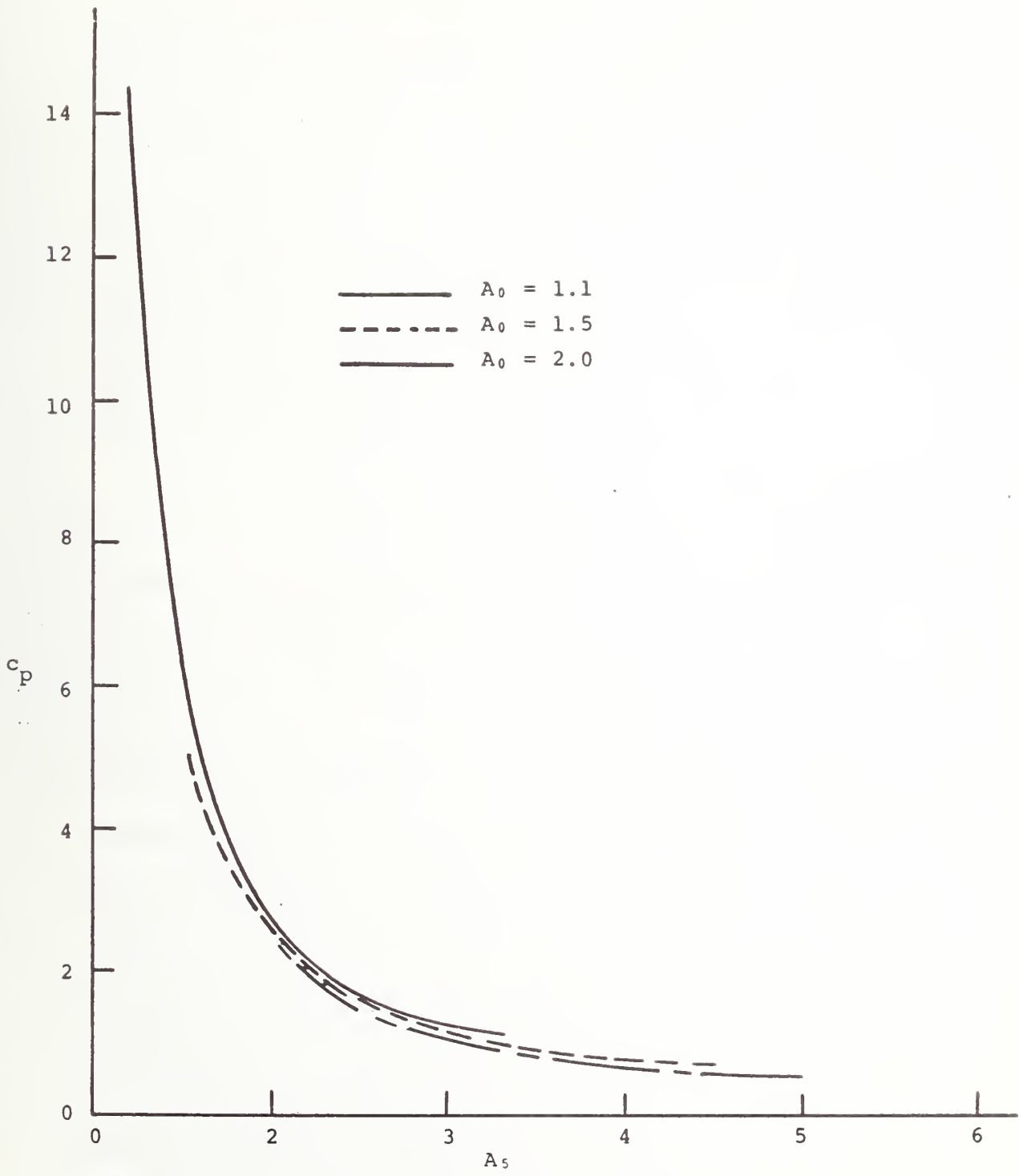


FIGURE 7-5. EFFECT OF DIFFERENT ENTRANCE FLARE AND TUNNEL SIZES ON PRESSURE COEFFICIENT AS VEHICLE ENTERS TUNNEL

7.3 Perforated Entry Portal

7.3.1 Analysis

A porous (perforated) entry portal is another method of increasing the effective size of the tube as the vehicle first enters the tunnel and an effective gradual reduction as the vehicle travels through the porous section to the final tube diameter. The essential feature of the porous entry problem is that when the vehicle first enters the mouth of the porous section, the air can escape not only down the tube and out of the entrance around the model but also through the porous wall of the tube. In the porous walls that are generally considered, the holes are of sufficient size so that the flow may be considered essentially inviscid, similar to the flow about the vehicle. This means that the area of the pores effectively adds to the annular area about the model and the velocity is proportional to the square root of the pressure difference. In fact, the pore area provides a more effective release of air from ahead of the vehicle than the annular area around the vehicle. The velocity of the air which flows through the pores is governed by the steady state Bernouli equation from nearly stationary conditions in the tube. The flow through the annulus about the vehicle is also governed by the steady state Bernouli equation, but, in this case, written in a coordinate system steady with respect to the vehicle. The pressure drop from the value in front of the vehicle to the exterior ambient pressure must accelerate the flow around the vehicle which is already moving at close to vehicle velocity with respect to the vehicle. Under this circumstance the increase in velocity for a given pressure difference is not as large as it would be if starting from stationary

conditions. The conclusion is that pores provide a more effective venting scheme, on an area basis, than the annular area between the vehicle and the tunnel wall. Figure 7.6 shows a comparison between the velocity in the pores and annular area around the model. This comparison suggests that a porous entry may be a more effective method for effecting the entrance transient than a flared entrance, based on the pore area compared to the increased entrance area of the flare.

A proper analysis of the porous wall problem should involve the way in which the pressure varies along the tunnel as illustrated in Figure 7.7. The differential equation to describe this situation is as follows:

$$u_p = \sqrt{\frac{2p_0}{\rho}} \quad \dots(7.33a)$$

$$\frac{\partial u}{\partial x} = K \sqrt{\frac{2p_0}{\rho}} \quad \dots(7.33b)$$

$$\frac{\partial u}{\partial t} + u \frac{\partial u}{\partial x} = - \frac{1}{\rho} \frac{\partial p}{\partial x} \quad \dots(7.33c)$$

Attempts to find simplified ways of solving this set of equations which preserve the essential qualities have not been successful. However, many of the important aspects of the porous wall problem can be treated by approximating the pressure along the porous section as a constant. It is then possible to perform a simplified analysis which does account for the venting through the pores on the mass flow balance within the tube. The air in front of the vehicle being displaced by the vehicle as it enters the tunnel must escape by any of three different means: down the tunnel, through the pores, or through the annular space around the vehicle. The volume flow down the tunnel is given by Equation 7.19 the same as for

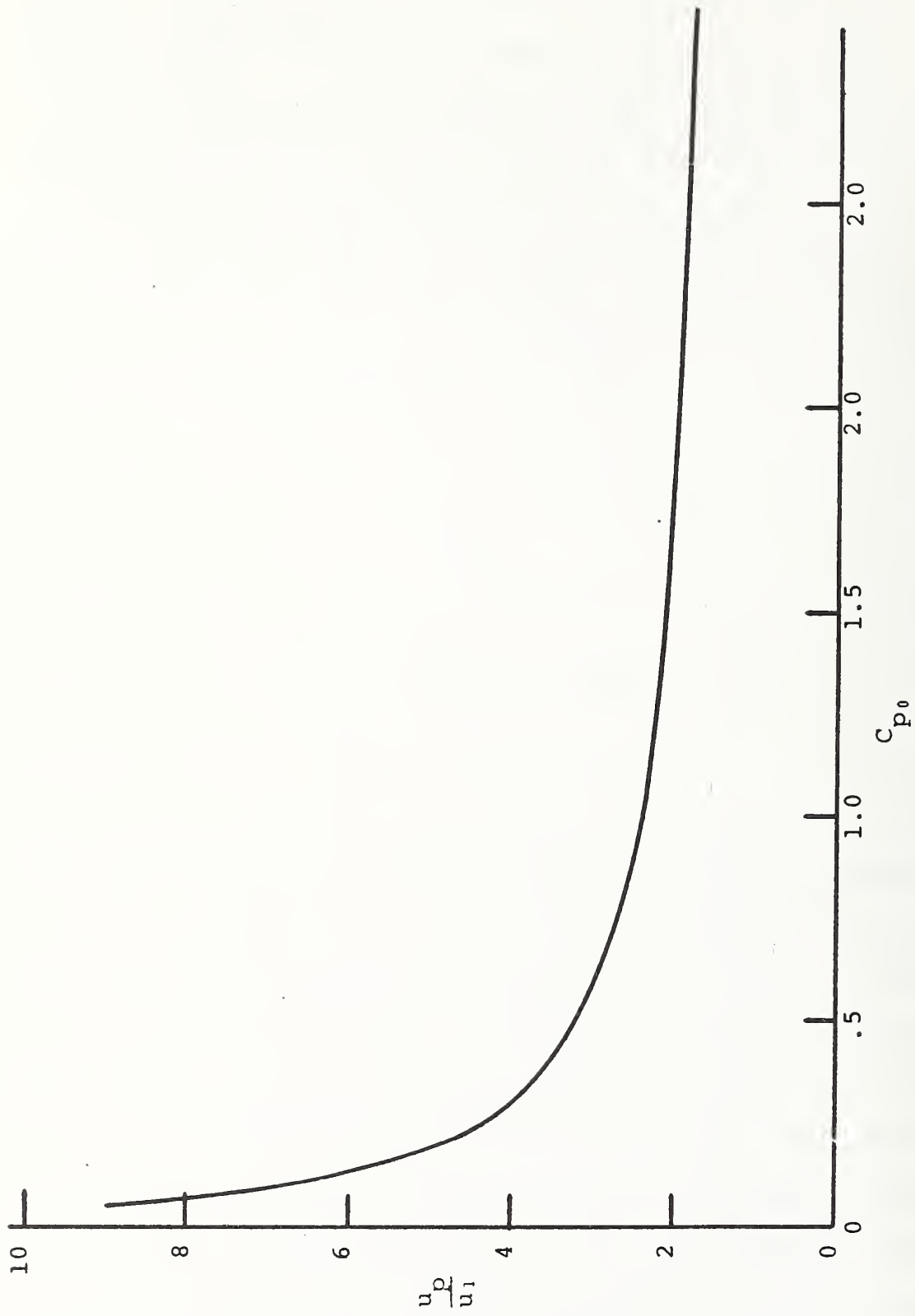


FIGURE 7-6. VELOCITY THROUGH PORES DIVIDED BY VELOCITY THROUGH ANNULUS AROUND VEHICLE AS A FUNCTION OF PRESSURE COEFFICIENT

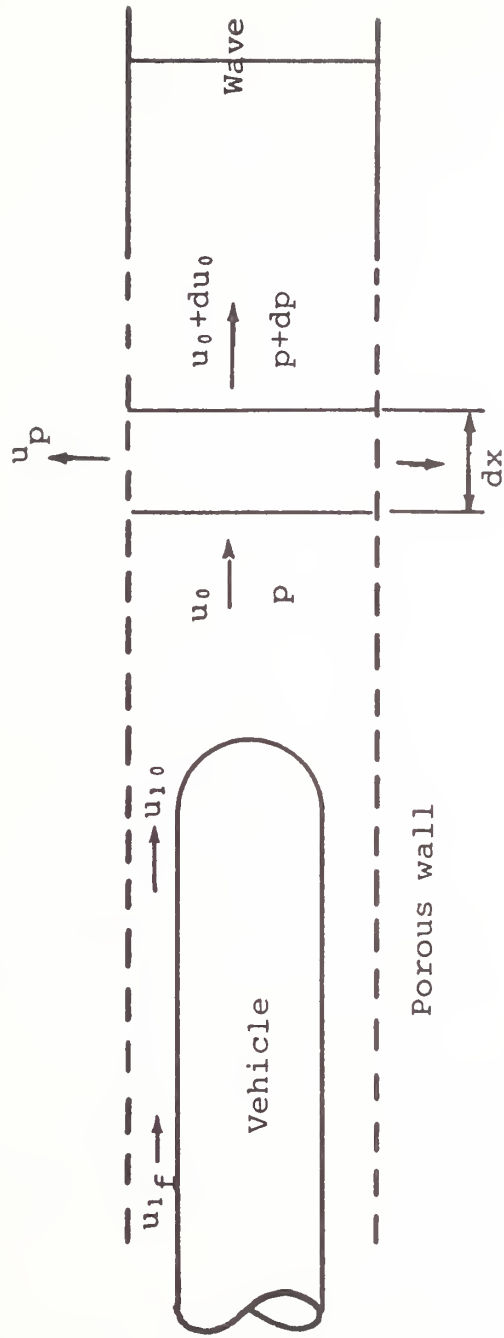


FIGURE 7-7. SCHEMATIC DIAGRAM OF VEHICLE ENTERING POROUS TUNNEL

the flare entrance case. To calculate the flow through the pores, the pressure will be taken as uniform along the entire length of porous tunnel ahead of the vehicle and equal to the value behind the wave transmitted down the tunnel. For the flow through the annular area around the vehicle, both the velocity head and the friction loss must be considered. The friction loss calculation is complicated by the fact that the velocity through the annular area will be decreased by flow outward through the pores until the rear of the vehicle has left the porous section entirely. To properly handle this situation, a solution to an equation of the type of Equation 7.33 is necessary. Lacking this solution it was necessary to resort to a rather crude approximation for a vehicle which has not yet completely entered the tunnel. The pressure at the inlet to the annular area can be related to the pressure ahead of the model by the Bernouli relation (7.19) and the pressure at the rear of the vehicle must be equal to the external ambient pressure. The ambient velocity through the pores can then be taken as equal to half the velocity at the entrance to the annular section. The assumption of a linear average of the velocity through the pores along the annular passage can be faulted for several reasons but it is an acceptable simplification for present purposes. The frictional pressure drop through the annulus is given by the relation:

$$\frac{2p_1}{\rho v^2} = \frac{\sqrt{\pi} C_f x}{(A_0 - A_V)} \left[\sqrt{A_0} \frac{u_{10}^2 + u_{1f}^2}{v^2} + \sqrt{A_V} \frac{(u_{10} - v)^2 + (u_{1f} - v)^2}{v^2} \right]. (7.34)$$

The velocity in the annulus is

$$\frac{u_{1f}}{v} = \frac{u_{10}}{v} + \sqrt{\frac{2p_1}{\rho v^2}} \frac{A_0 P}{2(A_0 - A_v)} \frac{x}{L} \quad \dots(7.35a)$$

or $\frac{u_{1f}}{v} = 0$ whichever is greater. $\dots(7.35b)$

The volume flow balance in front of the vehicle is as follows:

$$\frac{1}{2} \frac{2p_0}{\rho v^2} M_v \frac{A_0}{A_v} + \sqrt{\frac{2p_0}{\rho v^2}} \frac{A_0}{A_v} \frac{L-x}{L} - \frac{u_{10}}{v} \left(\frac{A_0}{A_v} - 1 \right) = 1. \quad \dots(7.36)$$

The first term is the volume flow down the tunnel, the second is the volume flow through the porous wall, the third the volume flow into the annulus around the vehicle, and the right hand side is the rate of volume being displaced by the vehicle as it enters the tunnel.

7.3.2 Discussion

The porous tunnel entrance is another way of reducing the initial pressure effect and stretching out the time and distance for the entire rise. To cause these effects, only a small amount of porosity is required, an amount somewhere on the order of the tunnel cross section area spread out over the entire length of porosity. One of the reasons that so small an amount of porosity is important is because of the greater effectiveness of the pores in venting the tunnel than the annular area around the model. This point has already been discussed in Section 7.3.1 and is related to the fact that the quantity of accelerated flow in the annular passage is growing at a rate proportional to the sum of vehicle and fluid velocities while that in the pores only at the rate of the fluid velocity.

If the porous section is exposed to the atmosphere, then the air flowing from the pores is vented directly. However, if a porous entrance is submerged in the ground the way in which the venting occurs must be considered. A possible configuration might be a vent tube running back along the tunnel in a configuration which might look like a porous tube section built into a flared tunnel. A thorough consideration has not yet been given to such a situation, but there seems to be no reason to expect that the area of the flare outside of the porous tube around the vehicle will be a more effective vent with the porous tube present than it was without the porous tube. Although it is less obvious, the same considerations of the venting length growing at the rate of vehicle velocity are still valid. However, this is an interesting point that needs further consideration.

Another point to be considered with respect to a porous inlet section is its effect on the initial wave strength. From a strictly one dimensional point of view, when the vehicle first enters the tunnel, the wave created will be independent of the porosity of the section. As this wave travels through the porous section it will be attenuated and reduced in strength. The time for this reduction to be achieved is approximately that required for the wave to travel the length of the porous section. A measuring station located beyond this point, as in the experiment, will not sense the initial wave but only the attenuated one. For an actual case, the initial pressure rise is spread out over a time of the order of that required for the vehicle to travel one tunnel diameter. During this time in which the wave is building, the initial small waves developed will have

traveled a distance equal to one tunnel diameter divided by the vehicle Mach number. In the experimental case the tunnel diameter is about 5 cm and the vehicle Mach number is about .072 giving a wave travel during the entry process of about 70 cm, a substantial part of the porous entry section length. This initial pressure effect does not show at the measuring stations but should effect the pressure on the nose of the vehicle. However, for the experimental case, it should be considerably less than in the ideal one dimensional case and may be of little importance in most real cases.

The distribution of porosity in the entrance section should also be considered. Based upon the limited theory presented here, it would appear that the pressure initially rises slowly and then more rapidly towards the end of the porous section. If the ideal pressure rise is a linear one, a reducing porosity along the length of the section would appear to be better than the constant one. The effect of the rear of the vehicle entering the tunnel has not been considered for the case of the porous section by the present theoretical model. It would appear that the porous section would reduce this wave and reduce the size of the overshoot. Both the theoretical results of Vardy and the experiments seem to bear this out.

The effect of porosity for different diameter tunnels and different wall porosities is shown in Figure 7.8. In this figure, the pressure divided by the pressure when the vehicle has reached the end of the porous section is shown as a function of how far the vehicle nose has progressed down the porous section. The change in tunnel diameter seems to have only a small effect while a change in porosity has a major effect.

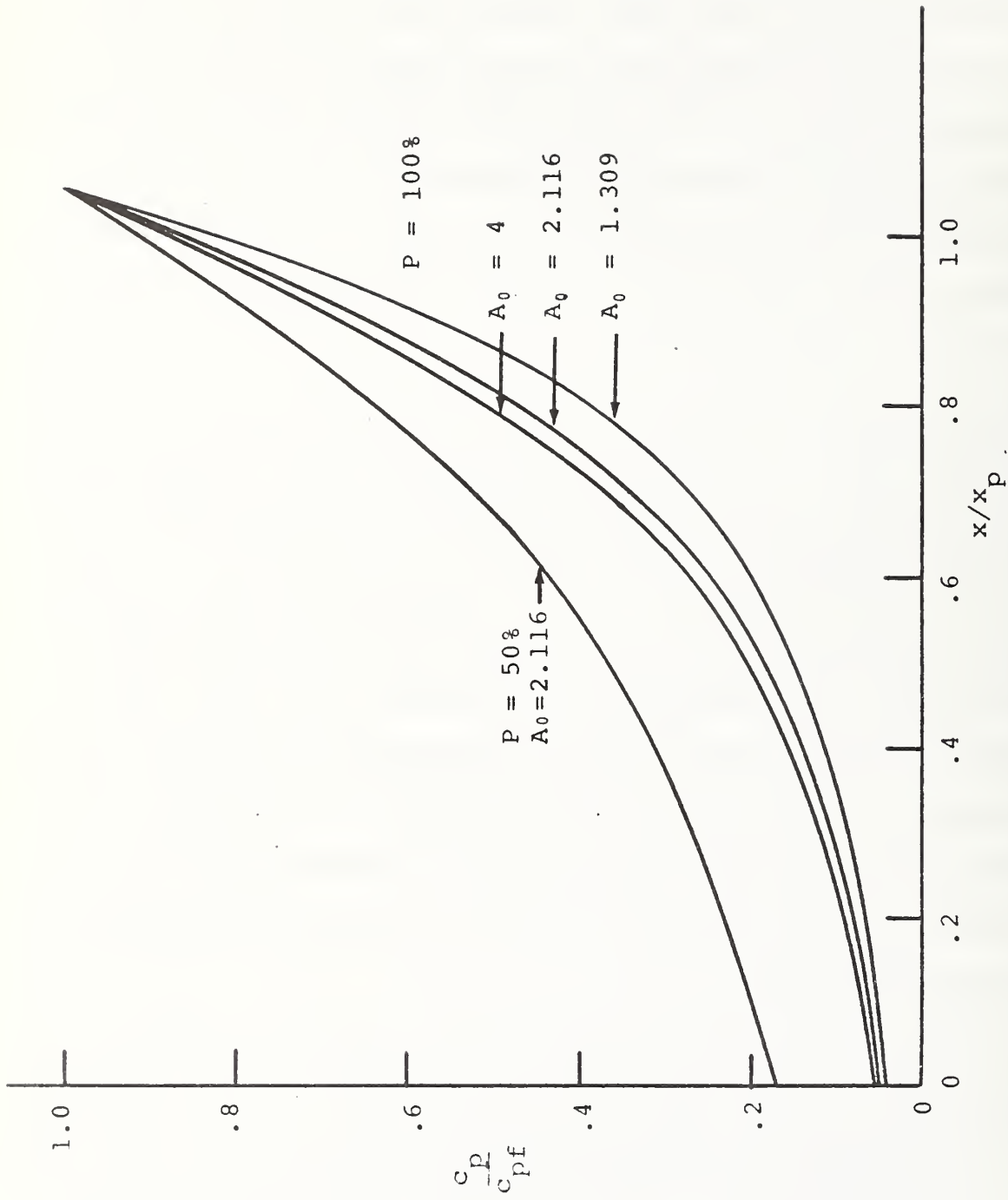


FIGURE 7-8. PRESSURE COEFFICIENTS DURING VEHICLE ENTRY INTO POROUS TUNNELS

7.4 Comparison of Entry Portals

A flared entrance reduces the size of the initial pressure jump to that which would occur if the entire tunnel were increased to the size of the flared entrance. The overshoot in pressure which occurs before the rear of the vehicle enters a straight tunnel is eliminated. The final pressure rise is the same as for a straight tunnel. A porous entrance has similar effects. For the same total area, pores in the tunnel are more effective than a flared entrance.

7.5 Nomenclature

A	cross sectional area of tunnel, vehicle, or pore
c	speed of sound
c_f	friction coefficient
c_p	pressure coefficient
C	circumference
C_{DN}	vehicle nose drag coefficient
d_p	diameter of pore
L	length of pore, vehicle, or porous tunnel
m	volume flow (Au)
M	Mach number
M_a	apparent mass
p	pressure
P	porosity: total pore area divided by tunnel cross sectional area
Δp	pressure difference across pore
t	time
u	fluid velocity relative to wall
u_f	final velocity through pore
v	vehicle velocity

x distance from entrance of tunnel or along pore
γ specific heat ratio
ρ density
τ dimensionless time

Subscripts:

∞ undisturbed
0 in straight section
1 just ahead of vehicle nose or ahead of pore
2 just behind vehicle nose or at exit of pore
3 just ahead of rear of vehicle
4 just behind rear of vehicle
5 at mouth of flare
v vehicle
10 at entrance to annular area round vehicle in porous tunnel
1_f at rear of annular area around vehicle in porous tunnel.

8. EXPERIMENTAL PROGRAM

8.1 Purpose

The purpose of the experimental program is to obtain precise pressure transient information that can be used to assist the development of an adequate and effective analytical computer model. This naturally includes the confirmation of several critical aspects of the final computer program. Should there be some aspects of the tunnel design tailoring that are not amenable to modeling (at least not within the scope of this study), experiments can be used to obtain the necessary pressure transient information since the scale effects are shown not to invalidate the results when applied to the full-scale conditions.

8.2 Description of Facility

8.2.1 Tube

A 1% scale was selected for the tube. This results in a tube diameter of approximately 5 cm (5 meters full-scale) with a maximum overall length of about 21 m (2.1 km or 1.3 miles). About 1 m from the entrance end of the tube assembly is a provision for vent shaft. The tube was open to atmosphere with air as the only fluid medium. Figure 8.1 shows a sketch of the facility; a photograph of it is in Figure 8.2.

8.2.2 Launcher

A simple spring catapult launcher was used to accelerate the models up to 35 m/s (see Figures 8.3 and 8.4). The smaller blockage ratio models lost less than 10% of their launch velocity by the time they passed completely across the vent shaft. The larger blockage models lost more speed in going through the tubes. The models were guided in the launcher and to the tube by three circumferentially-located grooved rails. Tri-skids located on the fore and aft ends of the models rode in these grooves

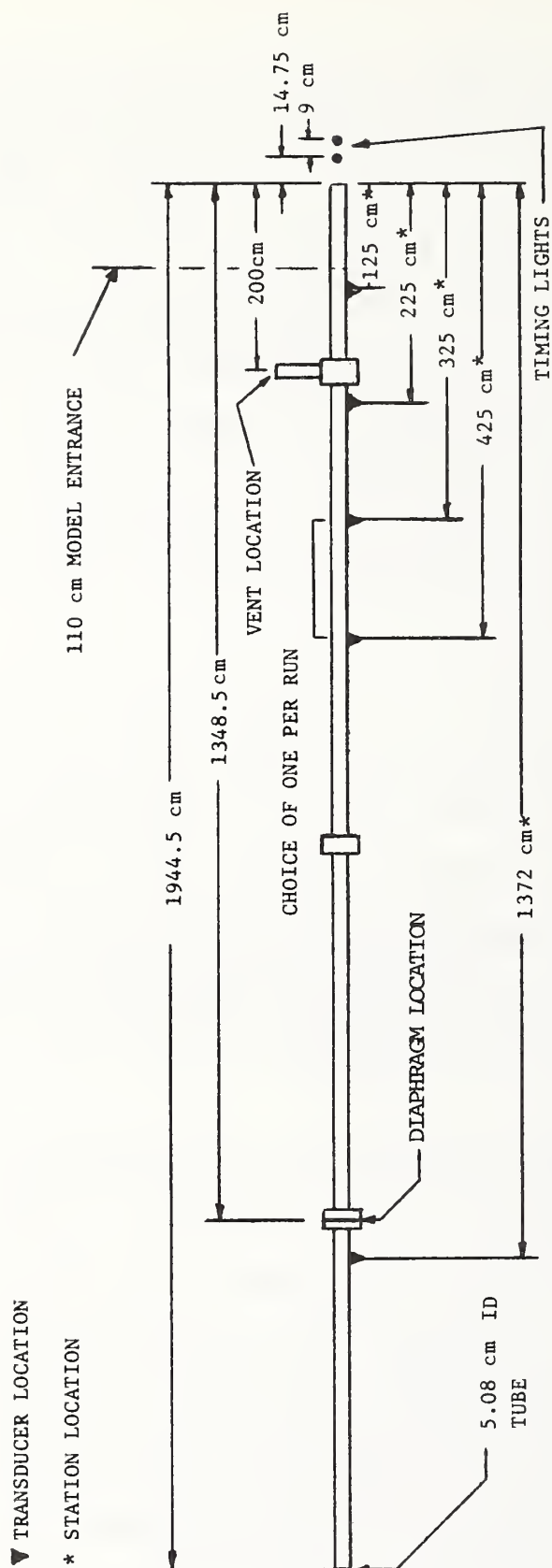


FIGURE 8-1. TUBE CONFIGURATION

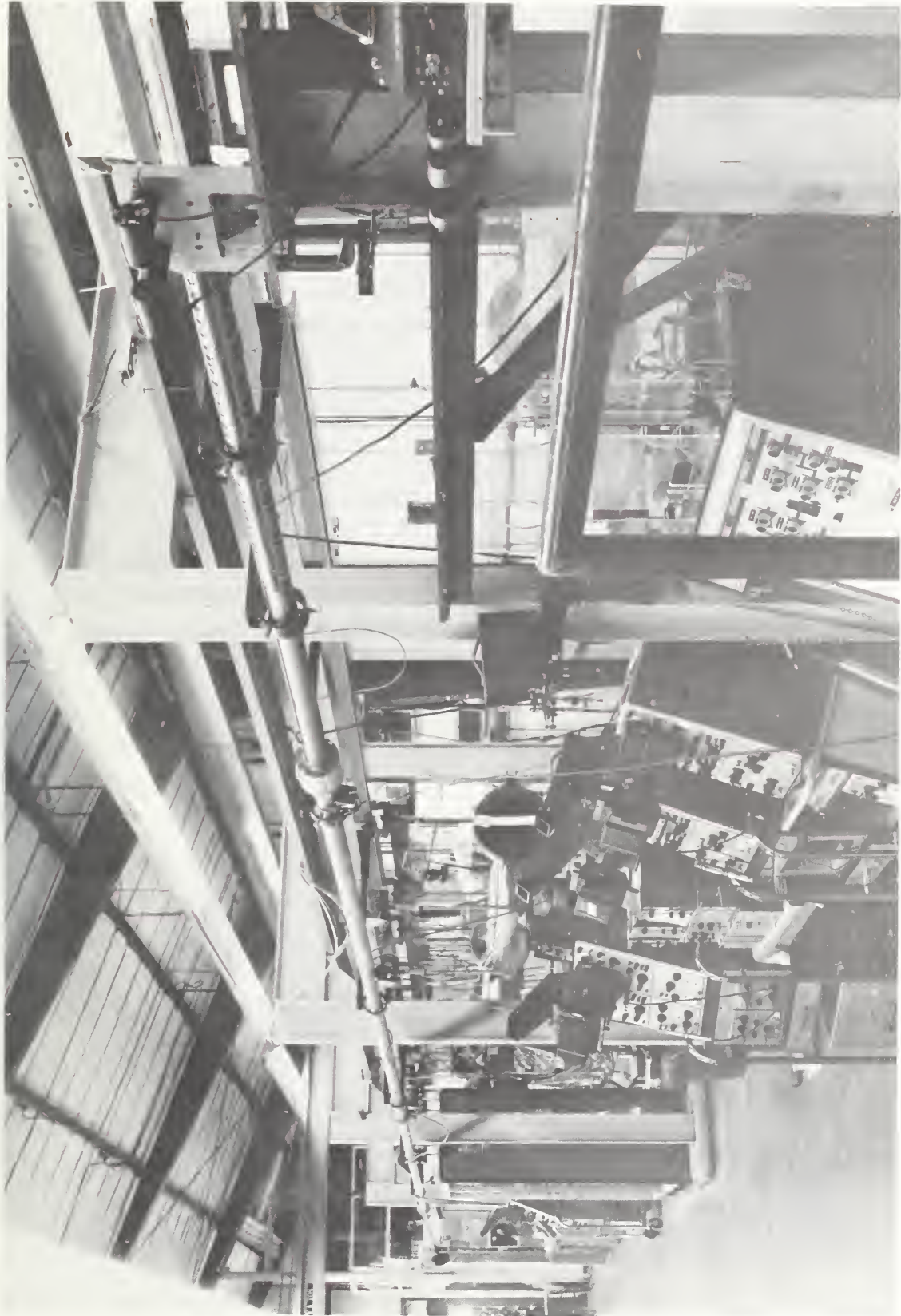


FIGURE 8-2. COMPLETE TEPT FACILITY

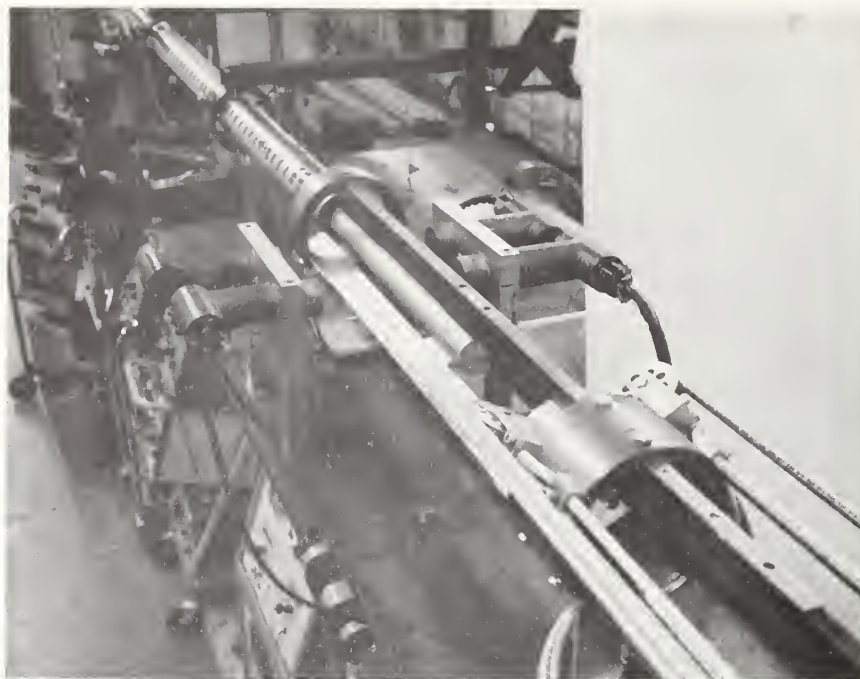


FIGURE 8-3. TOP VIEW OF LAUNCHER

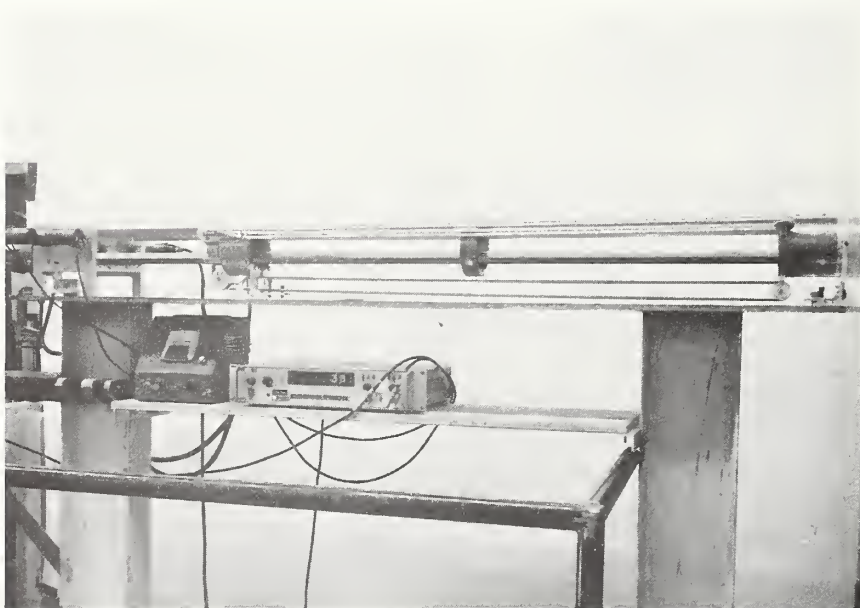


FIGURE 8-4. SIDE VIEW OF LAUNCHER

and also on the inside walls of the tube. There were some minor mechanical problems in extending the guide rails through a flared portal to the tube entrance. The models were retrieved by catching them in a padded container.

8.2.3 Instrumentation

The tube-wall pressures at each of the stations (Figure 8.1) were generally recorded with a pair of transducers see. See Figure 8.5 for transducers mounted at Station 225. Statham diaphragm-type (upper trace) gave an accurate overall magnitude of pressure while Kistler piezo electric-type (lower trace) allowed accurate indication of rapid change that Stathams, due to longer response time and ringing, were unable to cope with. Unfortunately, these Kistler transducers could not record a constant pressure level over 5 ms without a considerable drop-off in the recorded measurement. Hence the reasons for including the Statham transducers at these critical forward stations. The last station (1372) far down the tube had only a Kistler transducer.

For Run 234, A Kulite transducer was installed at Station 25. Numerous other transducer changes were made during the program. Also, it should be noted that all stations are measured from the actual entrance. To accomplish this, it was necessary to move some transducers for the few runs when the tube was shortened at the entrance end. These and other changes are included in the Run Index and should be checked prior to data reduction and analysis. The Kulite transducer was used in the attempt to measure pressures on the moving model.

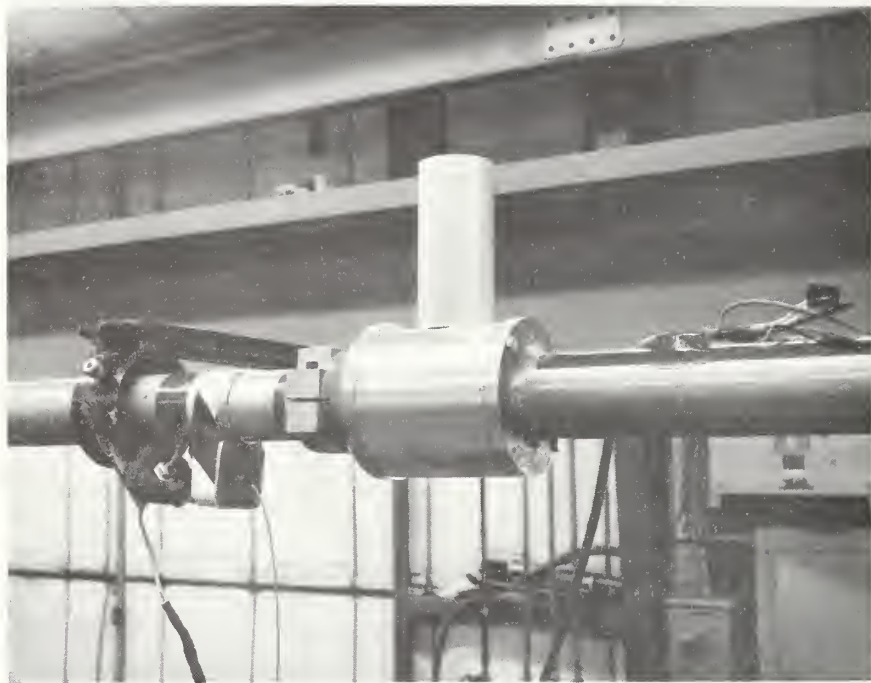


FIGURE 8-5. VENT SHAFT

8.3 Configurations Studied

A wide variety of configurations were tested. The configurations fall into three main divisions: Tube (including vent-shaft and orifice at end); model; entry portal. The basic elements were made as versatile as possible in order to minimize the pieces of hardware. It is believed that this versatility had no deleterious effects on the quality of the results. For example, the basic tube (5.08 cm D) had all required hole patterns drilled into the 6 mm tube wall. Only the particular holes required to produce the desired perforation pattern were left open; all others were taped over on the outside. A check was made on this for the zero-porosity case; several runs were made with an alternate tube section which had no holes drilled. The resulting data compared well.

8.3.1 Tube Assembly

8.3.1.1 Basic Tube

The four-section aluminum tube was 5.08 cm I.D. with walls of 6.35 mm. The inside surfaces were finely honed. Three flanges were used to attach the sections together. Flange (B) was the only normal flange. Flange (A) was extra wide in order to incorporate a vent-shaft; Flange (C) was modified in order to accommodate the diaphragms. (See Figure 8.1 for location of Flanges)

8.3.1.2 Orifices

Various diameter orifices were used at the exit end of the tube in order to demonstrate the effects upon wave reflection. Orifices were also used at the entrance end for the diaphragm-burst runs for the same reason.

8.3.1.3 Diaphragm

The thin milar diaphragm was located in Flange (C). It sealed off 1.05 or 1.10 atmosphere of pressure in the exit end of this tube, giving a pressure differential of 0.05 or 0.10 atmosphere. Thin nichrome wire encircled the diaphragm about 2 mm inside the tube wall. A 12v battery was used to heat the wire which in turn caused the diaphragm to rupture in a fairly repetitive, uniform manner. Proper timing was done in order that the resulting pressure waves were recorded on the oscilloscopes.

8.3.1.4 Vent-Shaft

A 15 cm long, 5 cm D vent-shaft was located within Flange (A). Normally, it was sealed off flush to the tube I.D. It could be open fully to its 5 cm D, or have orifices located either at the upper end or the tube-wall end. Also, its I.D. could be decreased along its entire length. A photograph of the vent shaft is in Figure 8.5, the various configurations are shown in Figure 8.6.

8.3.1.5 Instrumentation Ports

Provision was made for a considerable number of ports to which pressure transducers could be attached. A typical arrangement is shown in Figure 8.1. A single port was located at Station 1372 and 1272; double ports at Station 125, 325, 425; eight ports, used for comparative purposes, were at Station 225. Again, double ports were at Station 825 and 525 which were used for the diaphragm-burst runs. For Run 203, two pressure transducers were located at Station 25 in order to observe the development of the pressure pulse close to the end of the perforated entry portal.

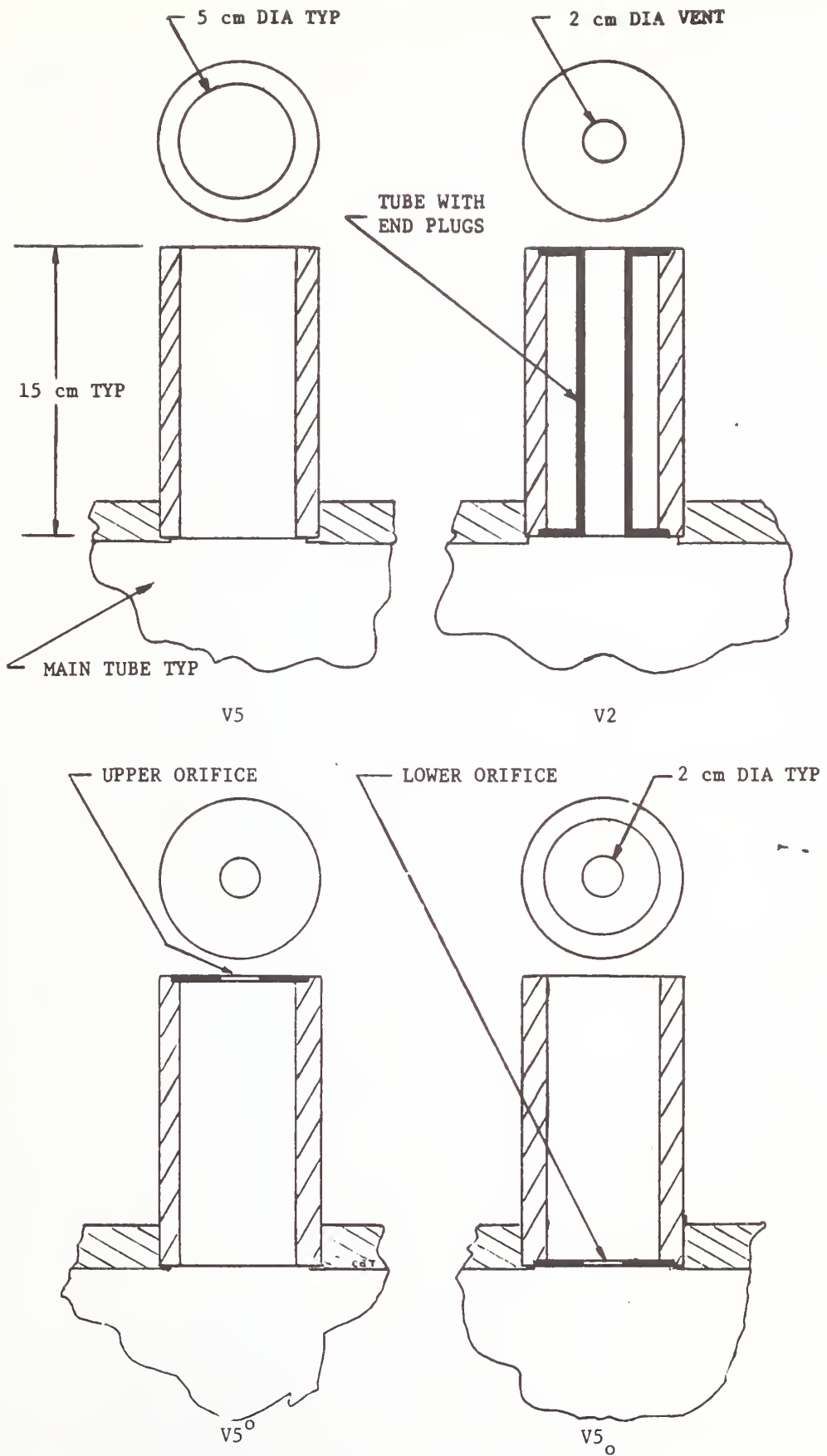


FIGURE 8-6. VENT-SHAFT CONFIGURATION

8.3.2 Models

Four actual models were used (see Figure 8.7). They were made from normal thin-wall aluminum tubing. The basic model, M55-50, was the only one that was modified. A ray of holes were drilled in order to simulate a train with normal leaks. Also, four separate base build-ups were added to it. This is the model that was used in the attempt to obtain pressures on the nose. For this purpose, the base was left open in order to allow the signal wires to pay out after launch. Otherwise, the base was sealed flat, as was always the case for the other three models. The details of the model can be seen in Figure 8.8. Tube entry speeds of the model and oscilloscope triggering were obtained by a pair of photocells located just ahead of the tube entrance. These cells activated a timer and readings were made for each run. Caution should be exercised in using the launch speeds indicated by these cells as the sabot was not clear of the base of the models prior to their nose passing this pair of cells. For a 55cm model, the sabot was still accelerating the model for 20 cm of its length. This resulted in the model traveling at a higher speed once its tail entered the tube than the speed at the time the nose entered the tube. For the tube shortened at the entrance end, the 55cm long models experienced no clearing problem and the above problem did not occur. Naturally, the model speed decreased during its passage. However, it was not necessary to set up any special timing devices to determine the exact speed loss; this can be determined from the pressure pulse histories. The model blockage was defined as:

$$\frac{\text{Cross Section of Model}}{\text{Cross Section of Tube ID}}$$

Several attempts were made to obtain direct measurements of the pressure



FIGURE 8-7. ACTUAL MODELS TESTED



MODEL	L	D	% BLOCKAGE	WT, GRAMS
M55-25	55 cm	2.54 cm	25	169.7
M55-50	55 cm	3.49 cm	47½	175.5
M55-75	55 cm	4.44 cm	76½	221.8
M110-50	110 cm	3.49 cm	47½	328.4

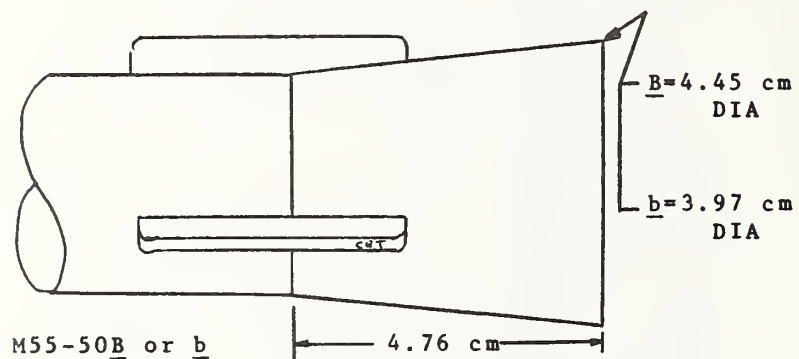
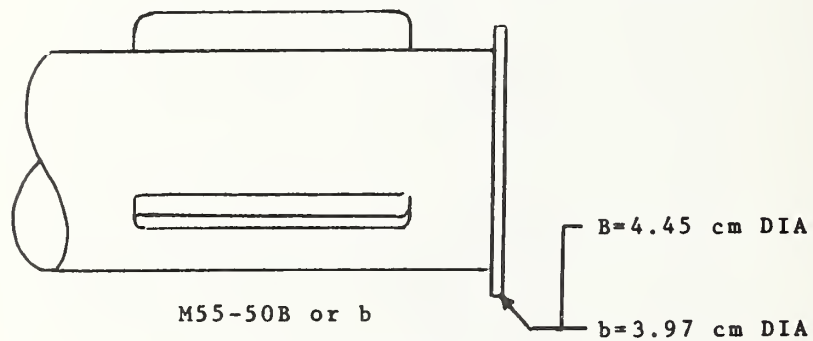
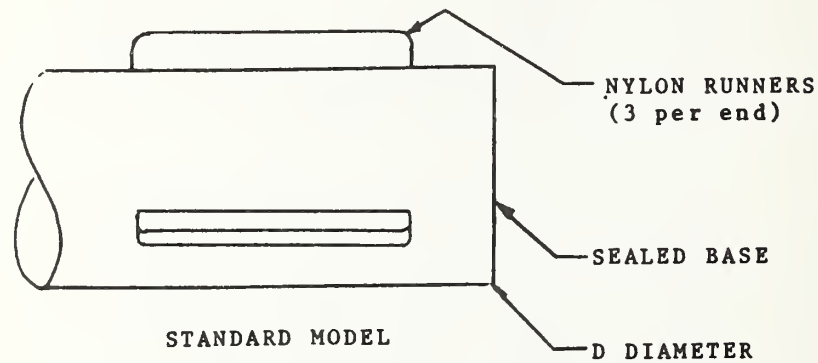


FIGURE 8-8. MODEL CONFIGURATIONS

transients on the model nose and sidewall. These attempts were successful during the shakedown period proceeding the formal experimental program (prior to Run 100). However, the Kulite pressure transducer used was inadvertently damaged later before it was calibrated and the intended extensive set of model pressure runs were carried out. Comparable success was not achieved with the replacement Kulite transducer. The results are shown in Runs C253 and 254. In Runs C253A, power supply (small battery) was installed in the model to activate the transducer attached to a port in the nose of model M55-50. This port, in turn, was attached to an open port at Station 225 on the outside of the tube. Then model M55-75 was launched into the tube to create a known pressure wave at the nose of model M55-50. As can be seen by the trace, no intelligible information was obtained. Switching to an external power source, good results were obtained during this procedure (Run C253B). The trace labeled Station 225 is the normal recording by the Statham transducer. The upper trace (labeled nose) is equivalent to the trace shown for Run C253A. The comparison of the two traces of Run C253B is good.

However, when model M55-50 was launched into the tube with the exact same set-up as it had for Run C253B, the results were not satisfactory; the noise was too great to make it possible to infer the pressure transient with sufficient accuracy. This was surprising because the similarly conducted shake-down run had little noise. It was not possible to correct this problem in the short period available for this phase of the experimental program. Because of the initial success, it is believed that, given reasonable development time, it should be possible to make measurements directly on the model. It should be noted

that such measurements can be obtained only for the first several meters of model travel through the tube. The signal is carried from the model to the oscilloscope by wire which is pulled out of the base of the model shortly after it leaves the launcher.

8.3.3 Entry Portals

8.3.3.1 Normal

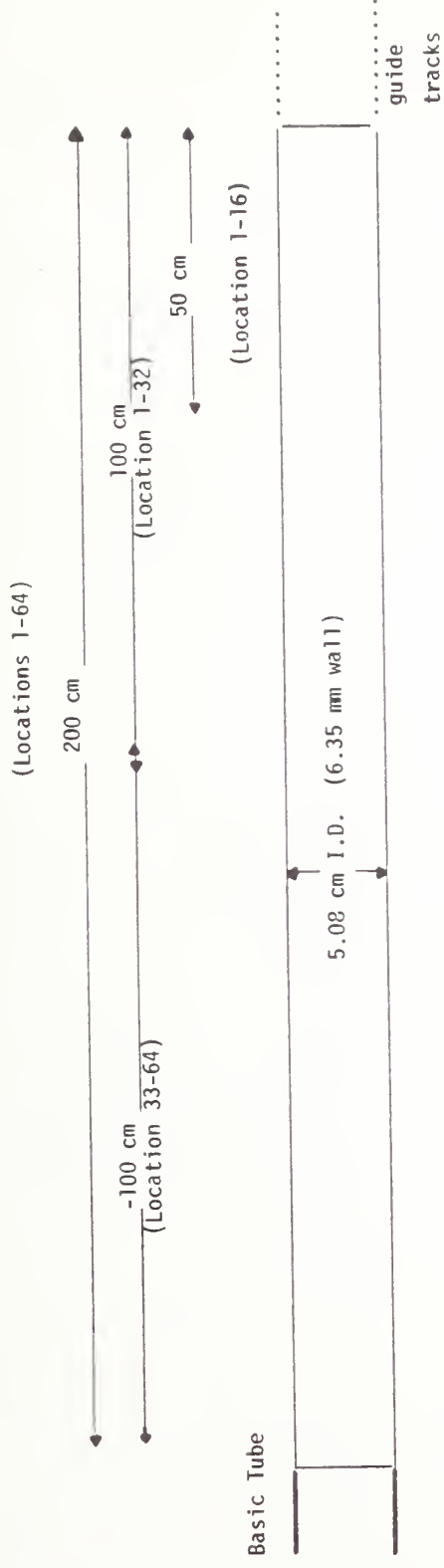
The normal entry portal was simply an extension of the basic tube. It was constant diameter and had no perforations. As was the case for all portals, it was a tube end in free air; there was no attempt to simulate the tunnel entrance in the side of a mountain

8.3.3.2 Perforated

The perforated entry portals started at the same point in space as the normal entry portals. This does not simulate an actual condition where the perforated portal would most likely be added ahead of the normal portal. This approach made for convenient variation of the porosity of the perforated portals in which the only change required was to tape and/or untape the proper pre-drilled hole patterns. The basic hole patterns for the uniform porosity portals are shown in Figure 8.9 and Table 8.1. The hole pattern for the linear porosity is shown in Table 8.2.

The porosity of the perforated portals is based on the sum of the physical area of the open (unsealed) holes in relation to cross section area of the basic tube (5cm D). The aerodynamic porosity is about one-third less.

The holes were left sharp-edged, except the inner edges were deburred moderately in order not to affect the performance of the model skids.



Hole Patterns

Hole locations start at right (entrance) and 1; cm from end and are 3 cm apart, 64 stations in all




- Loc. 17-32 At each location: six 3.18 mm D holes  6 holes at each loc.
- Loc. 33-64 At each location: four 3.18 mm D holes:  4 holes at each loc.
- Loc. 1-16 At each location: eight 3.18 mm D Holes  8 holes at each loc.

FIGURE 8-9. PERFORATED ENTRANCE PORTALS (Constant Porosity)

TABLE 8-1. CONFIGURATION DESCRIPTIONS (Entrance Portal Extensions)

CALLOUT	LENGTH (m)	POROSITY * (%)	HOLE CONFIGURATION
(Blank)	-	-	None (all sealed)
P _{1/2} -25	1/2	25	F
P _{1/2} -50	1/2	50	G
P1-25	1	25	C
P1-50	1	50	A
** P1-75	1	75	B
P2-50	2	50	E
P2-100	2	100	D
P1-50L	1	50 Lin. Distr.	See Table 1
*** F1-0	1	0	None (all sealed)
F1-25	1	25	H

If no callout given, normal tube end is portal.

- A ~ 4 Holes spaced 90° apart at each of locations 1-32
- B ~ 6 Holes at each of locations 1-32
- C ~ 2 Opposing holes at each of locations 1-32
- D ~ 4 Holes spaced 90° apart at each of locations 1-64
- E ~ 2 Opposing holes at each of locations 1-64
- F ~ 4 Holes spaced 90° apart at each of locations 1-16
- G ~ 8 Holes spaced 45° apart at each of locations 1-16
- H ~ 2 Opposing holes at each of locations 1-32

* Porosity is defined as the total physical area of perforations relative to the cross-section area inside the basic tube.

** These configurations are obtained from one physical 2m tube section that contains all of the hole configuration. Undersized holes are sealed in order to obtain selected hole configuration. For the normal portal, all holes are sealed.

*** F1-0 is obtained by sealing all holes in F1-25.

TABLE 8-2. PERFORATED ENTRANCE PORTAL (LINEARLY DISTRIBUTED POROSITY)

Portal Length: 100 cm I.D. = 5.08 cm

Same 32 location spacing as before (constant porosity) (except start at 3 cm from tube entrance end). At each location 4 opposing holes drilled (90° apart).

Location	Hole Diam.		Relative Area
	Inches	mm	
1-6 (entrance end)	3/32	2.38	0.562
7-13	7/64	2.78	0.765
14-19	1/8	3.18	1.000
20-26	9/64	3.57	1.265
27-32	5/32	3.97	1.562

As a consequence, the holes had a length-to-diameter ratio of two. This is substantially larger than what would be the likely situation for a full-scale version in which the 30 cm D holes would have an L/D of only one-half.

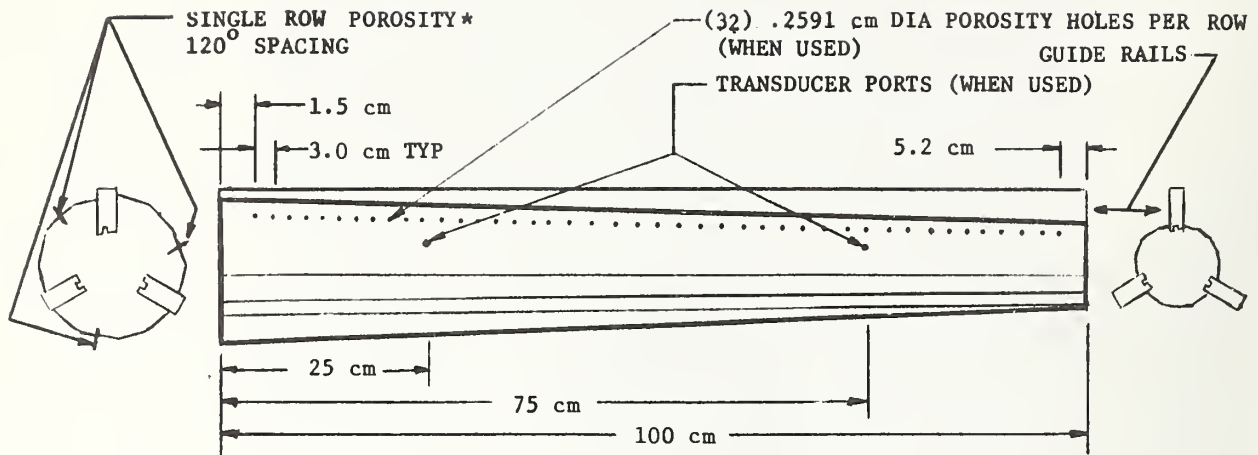
8.3.3.3 Flared

In order to incorporate the 1m long flared entry portal, it was necessary to replace the portions of the tube upstream of Flange (A). It was replaced with a section of tube that was 1m less in length to which the extended guide rails were attached. The three-segment flare entry portal was installed in between the guide rails (see photograph in Figure 8.10; design details are shown in Figure 8.11). As can be seen, the guide rails decrease the effective area of the flared portal. The ratio of the net entrance area to the tube area is 2.21. Three rays of holes along the flare portal could be left open to yield 25% porosity based upon the tube cross-sectional area (20.268 cm^2).

The three elements of the flared portal were removed in order to launch the 110 cm long models. The model was completely clear of the sabot when it entered the tube. Also the 55 cm long model was run in this shortened tube configuration in order to obtain data to compare with the usual configuration where the sabot was still accelerating the model even after the model nose had entered the tube portal.



FIGURE 8-10. FLARED ENTRY PORTAL



FLARE

* 25% POROSITY BASED ON TUBE
CROSS-SECTION AREA

LOCATION	AREA
ENTRANCE	44.809 cm ²
EXIT	21.286 cm ²
TUBE	20.268 cm ²

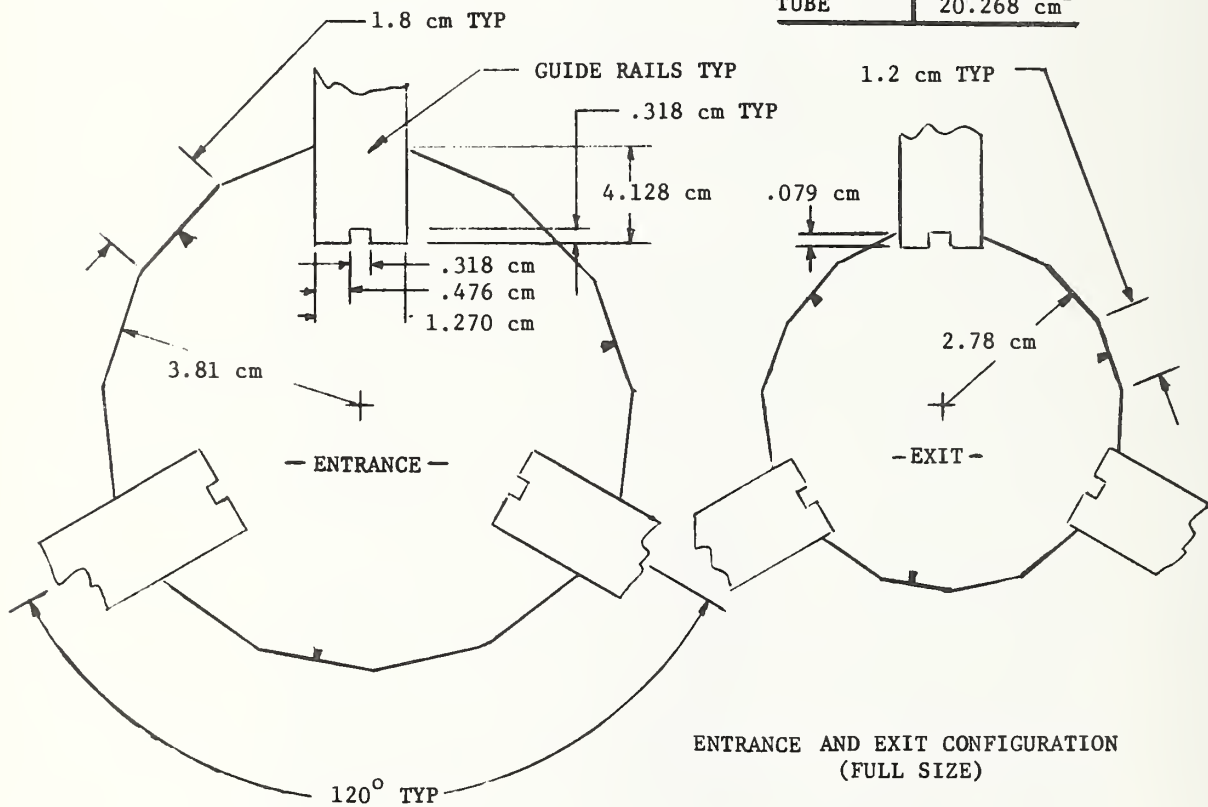


FIGURE 8-11. FLARE CONFIGURATION

8.4 Run Index

The Run Index may be found in Appendix A. Based upon the previous description of the configuration tested, a concise nomenclature format was used in the Run Index. Details appear in Table 8.3.

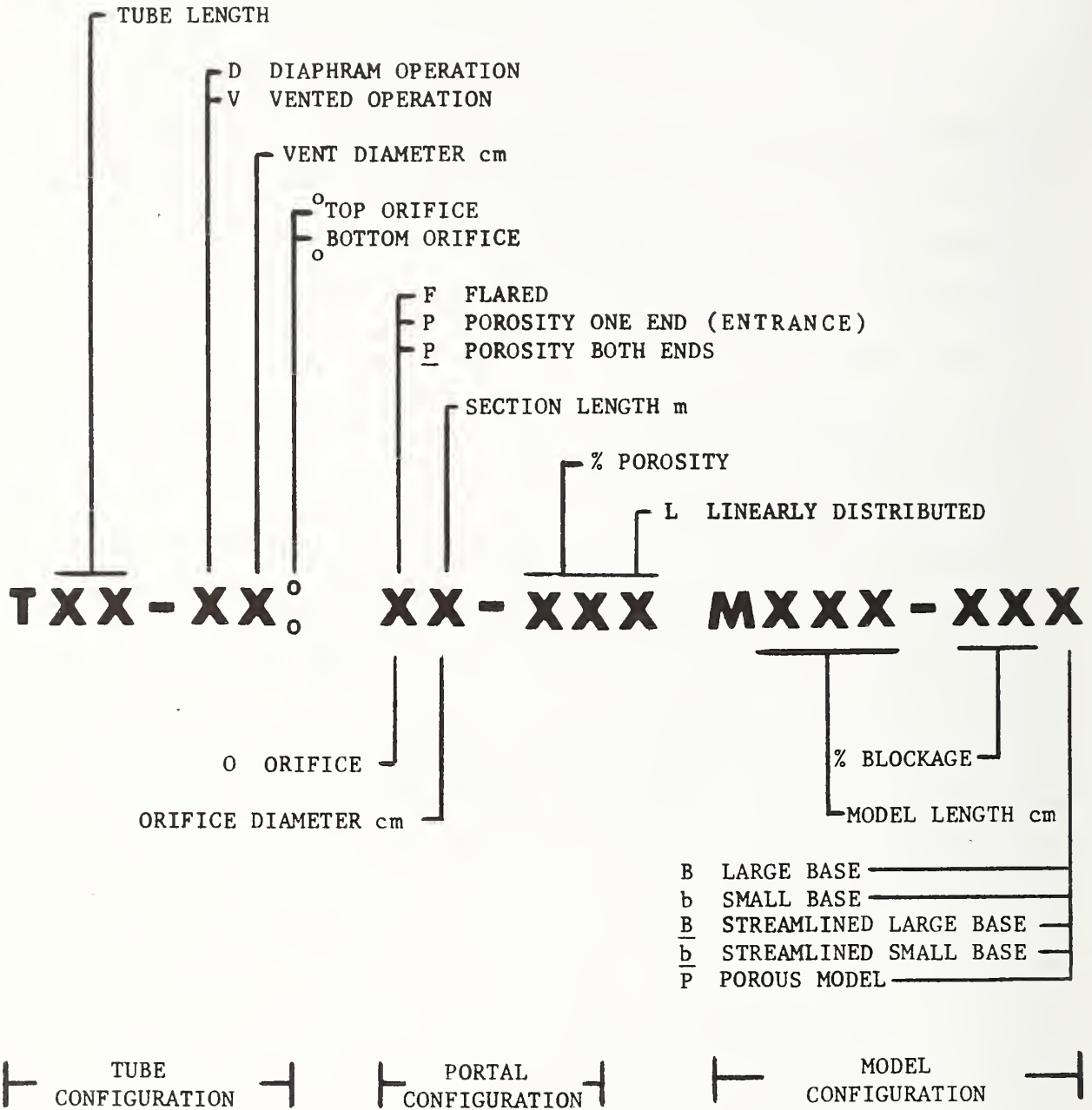
8.5 Raw Data

Reference 6 contains all of the experimental data as oscilloscope traces. Several examples of the oscilloscope data of Reference 6 are presented in Appendix B in order to demonstrate the various types and quality of data obtained. The oscilloscope traces for each run have been arranged on single pages, labeled appropriately, photographed, and then printed,

For the most part, these reproductions of the original Polaroid oscilloscope traces are no more difficult to read and interpret than the original pictures. Therefore it is practical to use this assembly of the data for further analysis. However, the originals are on file with the JPL authors and they can be contacted in order to clear up any ambiguities.

Occasionally, a particular pressure transducer was not included on an oscilloscope picture. Unless this omission was considered critical, this run was not rerun.

TABLE 8-3. RUN NOMENCLATURE



8.6 Data Reduction

In order to properly interpret the experimental data, it is necessary to deduce appropriate scaling factors. The four dual-beam Tectronix oscilloscopes used in recording the pressure data could have been calibrated in indirect ways. However, the expense is great and the need is often. Therefore, this indirect procedure was performed only once, just prior to the start of the test program, and was only approximate. The primary calibration procedure, which was used continuously throughout the entire test program, was based upon the direct approach in which the calibration procedure was on-site with the equipment in near-normal hook-up. Some error will be introduced because such measurements involve subjective decisions. In order to minimize these errors, large dimensions have been measured wherever possible.

As a matter of convenience, the pressure and time calibration factor are based on the grid squares (approximately 1 cm x 1 cm) of the Oscilloscope. Because of the reproduction process involved, these spacings are not 1 cm in this printed report.

8.6.1 Pressure

One Statham transducer (located at Station 225) was calibrated against an oil (DC-200) manometer by removing the transducer from the tube and hooking it up to the manometer. This was done for a range of pertinent pressures...and turned out to be linear. In order to check the response time of this transducer, it was suddenly disconnected from the manometer. It responded to the pressure setup in about 5 m/s with a moderate amount of ringing and subsequently stabilized at atmospheric pressure with a horizontal, steady trace.

This procedure for establishing the calibration factor for the Kistler transducers was not satisfactory as they could not maintain a constant oscilloscope trace at any pressure level other than atmospheric because of the excessive charge-leak-rate for the high pressure range (3000 psi) transducers that were available for this test program. However, the response characteristics were checked in the same manner as was done for the Statham transducers and showed them to respond within a milli-second with no ringing. Actually, calibration factors can be obtained during this procedure, but were not because of the convenience to obtain them in the following manner for both the Kistlers and the Kulites.

All seven transducers were located at the same station (Station 225) on the tube. A 50% blockage model (55cm long) was launched at about 25 m/s into the tube in its normal non-perforated constant diameter portal configuration. Since all transducers were recording the same pressure, it was then a simple matter to determine the respective calibration factors as well as compare the response characteristics of each. The results of this calibration process (based upon Runs C161A, B,C) are shown in Table 8.4.

TABLE 8-4a. CALIBRATED PRESSURE VALUES STATHAM
TRANSDUCERS (UPPER TRACE)*

STATION	PRESSURE kN/m^2 PER GRID (3% ACCURACY)			
	@ 20 mv/cm	@ 50 mv/cm	@ 100 mv/cm	@ 200 mv/cm
125	.204	.511	1.022	2.044
225	.209	.523 **	1.047	2.094
325/425	.189	.472	.945	1.890
225 ***	.184	.460	.920	1.840

* Average values based upon independent interpretation by the various authors.
 ** Base calibration
 *** Kulite Transducer

TABLE 8.4b. CALIBRATED PRESSURE VALUES PIEZO
TRANSDUCERS (LOWER TRACE)

STATION	PRESSURE kN/m^2 PER GRID (5% ACCURACY)			
	@ 20 mv/cm	@ 50 mv/cm	@ 100 mv/cm	@ 200 mv/cm
125	.25	0.63	1.27	2.54
225	.15	0.38	0.76	1.52
325/425	.17	0.53	0.86	1.72
1372	.26	0.64	1.28	2.56

8.6.2 Time

The time scales of the oscilloscope traces were calibrated by observing the passage of pressure waves along the length of the tube. The waves were weak enough that the usual assumption of the speed of sound in air was adequate (about 346 m/s at 24⁰c). Specifically, this was done by observing the signal at a single upstream station, and noting the time for the wave to travel to and from the downstream end of the tube. The time scale calibration are shown in Table 8.5.

TABLE 8-5. CALIBRATED SWEEP TIME VALUES, TRUE TIME MS/GRID (2% ACCURACY)

STATION	@ 5 ms/cm	@ 20 ms/cm	@ 50 ms/cm
125	4.92	19.68	49.20
225	4.82	19.27	48.17
325/425	4.90	19.60	49.00
1372	4.90	19.61	49.03

8.6.3 Model Speed

The model speed, just prior to entering the tube, was measured in real time by the use of a pair of photoelectric cells and a time counter. As was previously mentioned, the launcher sabot was still accelerating the model at this point. The launch velocity values that appear on the Run Index are nominal values for operation purposes only. Furthermore, due to aerodynamic and model skid-wall resistances, the model velocity decreases as the model travels through the tube. Therefore, it is necessary to obtain the model velocity history from the pressure traces as

the model nose passes each transducer station.

The model speed may be deduced at various stages of its journey by measuring the distances between identifiable events on the experimental traces. The positions where the model nose and tail pass the transducers and the positions where their entry wave fronts pass these points are especially useful. In practice, some of these events do not appear clearly on all the traces. Also, small distances cannot be accurately measured.

For example, it is not a good procedure to measure the distance between the nose-entry and tail-entry wavefronts because the inaccuracies in the resulting average entry speed are too great. The chosen procedure is to measure the time between the arrival of the nose-entry wavefront and the arrival of the nose (or tail) of the model. By adding the time required for the wave to reach the transducer, the time taken for the nose (or tail) of vehicle to reach the transducer can be obtained.

From this, an average speed is deduced. It is somewhat higher near the tube entrance than the speed recorded by the photocells. See Table 8.6 for details of the process used to determine the model speeds for several example runs.

TABLE 8-6. DETERMINATION OF MODEL SPEED THROUGH TUBE

MEASUREMENT	131	160	162	173	184	186	207
nose wave to nose at 125, mm EED paper	-	19.2	19.2	19.7	~20	~20	18.2
nose wave to tail at 225, mm EED paper	14.3*	47.4	47.2	49.0	59.4	59.2	35.4*
nose wave to nose at 425, mm EED paper	24.3†	70.3	70.0	-	-	-	78.7
avrg. speed, 0-125, m/s	-	26.70	26.70	26.08	25.72	25.72	28.06
avrg. speed, 0-280, m/s	26.82*	25.67	25.77	24.88	24.80	24.88	27.07*
avrg. speed, 0-425, m/s	26.66†	25.56	25.66	-	-	-	23.01
approx entry speed, m/s	27.21	25.99	26.11	25.20	25.14	25.21	28.23
* = nose wave to nose at 225 † = nose wave to tail at 325							

8.7 Interpretation of Experimental Data

In addition to its use for comparison with theoretical models, the experimental data can be used to establish the influence of various train/tunnel parameters on the pressure histories.

8.7.1 Train Parameters

The influence of the train length is well illustrated by Runs 130 (0.55m) and 184 (1.10m) in which the tunnel is a simple parallel tube. The pressure traces in the two cases are built-up of the same basic elements, but the resulting patterns exhibit considerable differences. The complete picture depends upon the superpositions of the waves and upon the times at which the transducers are passed by the nose and tail of the train. It is possible for these superpositions to be either favorable or unfavorable, and the designer can choose to adjust the tunnel length to his advantage.

Runs 101, 130 and 102 deal with the basic configuration for 0.55m long trains of 25%, 50% and 75% blockage ratio respectively. The shapes of the pressure histories are very similar to one another, but the pressure magnitudes are highly sensitive to the blockage ratio. In particular, the nose-entry wavefront varies approximately in the ratio 1:2:8 for the three cases. The tail-entry wavefront will vary similarly, but its importance is shown to be less great because of attenuation in the annulus alongside the train.

In Run 143, the train sides are perforated in order to simulate leakage around doors etc. on full-scale trains. By comparison with Run 130, it is seen that this has negligible effect on the flow structure in the tunnel. This is because only tiny quantities of air are required to change the air pressures inside the vehicle. For the leakage to significantly influence the tunnel airflows, it would be necessary for

the axial velocities through the train to attain high values. The effective blockage area of the vehicle would then be reduced.

There are three runs, namely 142, 150, and 207, with a built-up vehicle tail. The latter two both deal with a large build-up and they give similar results. It is noticeable that the streamlined case (207) produces a much more clearly defined pressure history at each transducer. This is convenient for the purposes of analysis, but it is less desirable in a full-scale circumstance. The non-streamlined case might then be preferred because it involves slightly smaller pressure gradients. Run 142 illustrates the influence of a smaller build-up. Even this, however, is sufficiently large to cause tail-entry to generate a compression wavefront and so the results are broadly similar to the other two runs. It would be possible to use a slightly smaller build-up to completely eliminate the tail-entry wavefront (except for three-dimensional effects). This would be highly desirable because passengers close to the rear of the train are subjected to the full magnitude of this wavefront even though those at the front benefit from the subsequent attenuation in the annulus.

It is worth noting in passing that the elimination of the tail-entry wavefront can be achieved in alternative manners. All that is required is for some modification to be made to the tail in order to cause the aerodynamic drag at that position to be increased.

8.7.2 Tunnel Parameters

The most extensively investigated tunnel modification in the laboratory test series was the perforated entrance region. A range of lengths of the region and also a variety of wall porosities have been covered.

The influence of the length of the region may be seen in runs 107 (0.5m), 132 (1.0m) and 113 (2m), for each of which the total porosity is 50% of the tunnel cross-sectional area. The shape of the nose-entry wavefront can be seen to be roughly the same in each case, but the rate of change of pressure in the tunnel is approximately inversely proportional to the entrance length. This is a highly desirable feature because it indicates that advantage can always be gained from longer regions even when these exceed the length of the train.

In addition to the immediate advantages resulting from the reduced pressure gradients, there is a reduction in the magnitudes of some of the pressure fluctuations. This occurs whenever the elongated wavefronts overlap with themselves or with one-another. It is this effect which is responsible, for example, for the reduced wave activity in the later stages of Run 132 in comparison with Run 131. The effect is more pronounced in Runs 170 and 171 in which a shorter tube was used. In order to witness the reduction in the pressures, the measurements at Station 225 in Run 171 should be compared with the data for Run C161C.

A less fortunate property of perforated entrance regions is also demonstrated, namely that the tail-entry wavefront is not elongated as much as the nose-entry wavefront. It has been an important requirement of this study that this predicted feature should be verified. The evidence is two-fold. In Run 113, for example, the tail-entry wavefront can be seen at Station 325 to occupy only about 0.5m of tunnel even though the perforated region is 2 m long. Additionally, by inspection of the computed pressure histories alongside the train- (Figures 9.5b and 9.6b)-it is seen that the tail-entry wavefront is reduced by only about 25% at entry. Passengers close to the rear of

of the train will experience relatively little immediate benefit.

It is useful to note that this difficulty could be overcome by building-up the tail of the train. Then the nose-entry effects would be alleviated by the perforated region, but the tail-entry effects would not require alleviation. It may be deduced that these two modifications complement one another very well.

The optimum total porosity is deduced from Runs 119, 122, 128 and 132 to be about 75% of the tunnel cross-sectional area. The pressure histories are not very sensitive to moderate changes in this value or to changes in the distribution of the porosity (run 135). This is fortunate because the optimum total value will depend upon such things as the skin friction in the annulus as well as upon the train speed and blockage ratio. The object is to minimize overall pressure gradients caused by wave activity due to all sources including friction.

8.7.3 Flared Entry Portal

The most natural alternative to a perforated entrance region is a flared entrance region. These two devices have much in common and their respective influences on the pressure histories are broadly similar. Nevertheless, important differences can be seen by comparing, say, Runs 119 and 173. It is clear that the maximum pressure rise in the latter case (flare) is considerably smaller than that in the former. This is because of the different manners in which the two devices influence the tail-entry wavefront. We have already seen that the influence of tail-entry is not felt downstream of a perforated region until the tail has almost reached the end of the region. In contrast, the flared entrance elongates this wavefront approximately as effectively as the nose-entry wavefront. The fall in pressure due to tail-entry counterbalances the rise due to nose-entry. Of course, this property will not be so important when the train is longer than the entrance region.

Even in that case, though, reduced skin friction in the annulus as well as diffuser action of the flared entrance will lead to a smaller peak pressure than that found with a perforated entrance.

It has already been shown that the flare in the laboratory apparatus did not act as an efficient diffuser. This should not be taken as an absolute guide to the behavior in a full-scale tunnel. However, it is reasonable to suppose that little pressure recovery will occur at full-scale unless care is taken to provide a smooth join between the tunnel and the flare. It is possible that it will be found to be uneconomical to aim for this additional benefit in practice.

Run 181 deals with an entrance region which is both flared and perforated. Since the porosity is small, the flare effect dominates, but there is evidence of a reduced elongation of the tail-entry wavefront. It would appear that there is little point in using the combined device.

8.7.4 Vent Shafts

The influence of airshafts has been well demonstrated. Broadly speaking, they can reduce the effects of the entry transients, but only at the expense of creating additional sources of wave activity. A delicate balance must be maintained in which the size and position of the shafts must be matched with the size and speed of the train. In Runs 160 and 162, the airshaft provided very useful attenuation, but the short, large-bore shaft in Run 156 was of little help. The wavefronts generated at the shaft in that run were almost as great as those generated by train-entry in the basic configuration. This run illustrates very clearly why large pressure wavefronts are generated in the Transbay Tube on the BART system when the trains travel at 80 mph.

8.7.5 Exit Restrictions (Orifices)

For Run 155, the tube exit was blanked-off except for a 1 cm diameter orifice. It was expected that this would inhibit the reflection of the nose-entry wavefront, and this expectation was fully realized. A simple explanation for its effectiveness is that a fully open end causes a total negative reflection whereas a fully closed end causes a total positive reflection. Intermediate openings cause intermediate reflections.

The blockage ratio at the exit can be chosen so that no reflection occurs when a design wavefront of any stipulated magnitude reaches the orifice. Wavefronts of other magnitudes will reflect either positively or negatively depending upon whether they are of greater or smaller magnitude than the design wavefront. Analysis of this phenomenon is straightforward.

There are important practical restraints on the design of suitable restrictions. For example, the diameter of the blockage used in Run 155 was only 20% of the tube diameter. Such a restriction cannot be provided as a permanent rigid fixture in a real tunnel. Two alternatives exist. Either the blockage must be removed before the arrival of the vehicle--by opening roller doors for example--or the blockage must be in the form of a flexible device which the train can safely penetrate. Water curtains and air curtains have been suggested as possible restrictions partly because they can fit into either category. They might prove to be feasible, but they also have undesirable side effects.

The use of flow restrictions in tunnels is a topic which merits attention. Important advances could be made with such devices, especially if they are modulated by means of active controls which respond to air pressures or to the presence of trains.

9. VALIDATION OF ANALYTICAL UNDERSTANDING

9.1 Computer Program

The experimental program has made available a comprehensive series of data on tunnel entry pressure transients. Much of the data is of immediate value in its own right because firm conclusions may be drawn from it about the effectiveness of various tunnel entrance configurations in the attenuation of the entry transients. Additionally, the data is valuable as a means of testing the validity of theoretical models which have been proposed for prediction of the phenomenon. Satisfactory models may then be used to predict full-scale phenomena.

In this section, the experimental data for seven runs is compared with numerical predictions from the computer program. Agreement is generally good, but certain discrepancies are identified and are critically discussed.

9.1.1 Run 131 (Figure 9.1)*

The numerical (solid) and experimental (dotted curves) results for Run 131 are presented in Figure 9.1. By inspection, the correlation is satisfactory except that the waves appear to be somewhat smaller in practice than in the theoretical model. This result is attributed to inaccuracies in the representation of skin friction, and a critical examination of the theoretical procedure is therefore required for dynamic skin friction.

In a unidirectional model, no direct account can be taken of lateral velocity distributions which are the source of the skin friction. This difficulty can be overcome in steady-flows because numerous experiments have demonstrated that a unique relationship exists between the skin friction and velocity in any particular duct. Different ducts are

*All figures appear at the end of Section 9.1.

categorized by the ratio of the effective roughness height to the hydraulic radius.

No similar experimental relationships exist for the case of unsteady flows. Indeed, there is considerable reason to doubt that such relationships will be found within the foreseeable future because the class of unsteady flows far exceeds that of steady flows. The principal difficulty is that the true skin friction must depend upon the velocity history as well as upon the local velocities and accelerations.

Figure 9.8 gives an idealized illustration of a developing velocity profile close to a wall following the passage of a step-wavefront. Immediately after the wavefront has passed (Curve 1), the velocity at every part of the cross-section (except very close to the wall) is equal to U . The velocity gradient at the wall is extremely large. Vorticity diffusion into the flow from the wall serves to gradually reduce this velocity gradient until the steady-state velocity distribution is eventually reached. Since the instantaneous skin friction depends upon the velocity gradient at the wall, it follows that it is greatest close to the wavefront.

In the computer program, the skin friction is represented by a steady-state expression which is a function of the local velocity, but not of the acceleration or the velocity history. Consequently, a crude overall average value is all that can be found and this must be equivalent to one of the intermediate curves (2 or 3) in Figure 9-8. It follows that we expect the skin friction to be underestimated close to wavefronts and overestimated in regions of more steady-state flows.

This provides a plausible explanation for the features displayed in Figure 9.1a. The overall damping is everywhere reasonably well reproduced,

but the discrepancies in the magnitudes of the wavefronts is greatest at Station 125 where the dependency upon the true profile of the wavefront is greatest.

The empirical values used to obtain the numerical predictions for this run are also used for the remainder of the comparisons. They are:

- (a) train nose pressure loss coefficient = zero,
- (b) train effective Moody roughness height = zero,
- (c) tube wall effective Moody roughness height = 0.5 mm.

Before discussing the comparisons for the other runs, attention is drawn to two features in Figure 9.1a. Firstly, the very sharp impulse predicted at Station 325 after approximately 0.12 second does not appear on the measured trace. Such features can form a valid part of the solution of a unidirectional analysis, but they rarely exist in a three-dimensional environment. This particular "impulse" results from the superposition of two step-wavefronts travelling in opposite directions. Secondly, a sudden pressure rise was measured at Stations 225 and 325 approximately 0.064 second after the nose-entry wave. This feature also appears in Runs 128, 130, 132, 134, 135, 143, 155, and 173 and to a lesser extent in several other runs. Since no wave was expected to arrive at this time, it is likely that there was a leak in the apparatus. If this interpretation is correct, the leak was between 1.75 m and 1.85 m from the tube entrance and the wavefront was produced when the train nose passed that region.* No attempt has been made to simulate this effect in the computer program.

9.1.2 Run 160 (Figure 9.2)*

For this run, the tube had a 20 mm bore airshaft 2 m from the entrance. This can be represented in the computer program either as a duct in its own right or a tube in which the wavespeed is regarded as infinite. In

*The existence of an occasional leak was verified.

both cases, unsteady flows are analyzed, but in the latter case, only smooth accelerations result. For short shafts, no significant difference can be found in the main tunnel between results obtained from the two types of analyses.

Agreement between the predicted and measured traces is generally good. The magnitudes of the wavefronts generated by nose-entry and by the nose passing the shaft are all well predicted. So are the pressure signatures when the train passes the transducer positions. However, at least four discrepancies are apparent.

Firstly, the tail-entry wavefront is not as sharp fronted as the theory predicts. This is at least partly explained by the nature of tail-entry. Immediately before this event, air is exhausting through the entrance portal from the annulus around the train. In a one-dimensional representation, the flow through the portal must immediately reverse in direction as the tail enters. In practice, however, there is considerable large-scale turbulence for several diameters behind the tail, and this will tend to elongate the wavefront.

Secondly, the pressure magnitude following tail-entry is underestimated. The reason for this is not fully understood, but it is likely that the theory permitted too much flow through the airshaft. This would imply that the pressure loss coefficient (unity) introduced to describe the flow at the base of the shaft was too small. It is also possible that the magnitude of the tail-entry wavefront is overestimated or that it is not sufficiently attenuated as it passes alongside the vehicle.

Thirdly, at Station 425, the pressure is wrongly predicted between 0.10 and 0.12 second. This does not imply an error in the theory. Instead

it is a measure of the accuracy of the data presented to the program. A very small increase in the assumed train speed would eliminate this discrepancy. It is important to note that equally small changes to a train speed can have a big influence on the pressure histories experienced by personnel in tunnels.

Fourthly, the wave activity predicted at all three stations between about 0.12 second and 0.14 second is greatly overestimated. These wavefronts are simply the reflections of the wavefronts originating at the entrance portal and at the shaft during tail-entry, and so this discrepancy is a necessary consequence of the previously discussed phenomenon.

9.1.3 Run 162 (Figure 9.3)

The conditions for this run are similar to those for Run 160. The differences are that the shaft is of 50 mm bore and that it has a restriction at its lower end in the form of a 20 mm bore orifice. This is simulated by a pressure loss coefficient of 105, which represents the square of the ratio of the shaft area to the area of the vena contracta formed downstream of the orifice.

Rather surprisingly, agreement is generally better for this more complex situation than it is for Run 160. The same general comments apply, but their importance is less great. It may be inferred that the representation of this shaft is better than that of the smaller bore shaft.

9.1.4 Run 173 (Figure 9.4)

With a flared entrance region, the main features are well predicted, but the pressures are underestimated when a significant proportion of the vehicle is within the flare. It is almost certain that this is due to the failure of the flare to yield the expected pressure recovery alongside

the train. In the annulus, the flow relative to both the train and the tunnel is towards the entrance portal. If the flow remained fully attached, the flare would act as a diffuser and a pressure recovery would result. This would manifest itself as a reduced pressure in front of the train.

In the numerical simulation, the diffuser action has been assumed present. Also, no account has been taken of the small pressure loss which will occur at the area discontinuity between the flare and the main tunnel.

It would be a relatively simple matter to modify the computer program so that nonattached flows could be simulated. However, a simple test of the validity of the above assumption about the cause of the discrepancy between theory and experiment has been made without this modification. Instead, a pressure loss coefficient of 0.80 has been introduced at the junction of the flare and the main tunnel. The loss takes effect only while the vehicle is alongside this junction. The assumed loss is too small (zero) when the train has travelled less than 1 m, approximately correct immediately after that point, and too great thereafter until the tail passes.

The resulting pressure histories are presented in Figure 9.4a*, and the tendency is for the pressure to be under- and overestimated in the regions just described. This strongly supports the hypothesis that the flare in the model did not act as a diffuser.

9.1.5 Run 184 (Figure 9.5)

Run 184 is a simple configuration in which a long (1.10 m) train enters a basic tunnel. Agreement between theory and experiment is very good indeed, and this leads to confidence in both. In particular, the magnitude of the tail-entry wavefront is correctly predicted. It is

because of this that considerable effort has been made to find alternative explanations for the apparent overestimation of this wavefront in two of the preceding runs.

9.1.6 Run 186 (Figure 9.6)

For Run 186, the tube was equipped with a 1-m long perforated entrance region with a total porosity of 50% of the tube cross-sectional area. In the numerical analysis, the effective area at the vena contractas is taken as 30.5% of the tube area. The effective thickness of the wall was chosen as 10 mm, which includes an allowance for the apparent mass of the flow adjacent to the holes.

Agreement between theory and experiment is again very good. The small discrepancies at Stations 125 and 225 as well as the larger variation at Station 325 can be accounted for by an error in the assumed vehicle speed at entry. By inspection, the true vehicle speed was slightly slower than the assumed value.

9.1.7 Run 207 (Figure 9.7)

In the state of the art section, it was stated that a vehicle with a built-up tail could generate a smaller than usual tail-entry wavefront or even a compression wavefront. Run 207 tests this hypothesis in a circumstance where the build-up is so great that the tail wavefront is a strong compression wavefront.

At Station 125, the computed solution differs significantly from the measured pressure trace only as the tail passes the transducer. Then there is a pronounced fall in pressure due to the additional restriction and the resulting velocity increase. No attempt is made to simulate this area change explicitly in the computer program because considerable extra complexity is introduced if the train area is not regarded as a constant.

The overall effect is simulated by the same boundary condition as that used for all the preceding runs except that account is taken of the increased blockage when the expansion pressure loss is estimated.

At Stations 225 and 425, the qualitative agreement is as good as that at Station 125, but the experimental results indicate a large reduction in the pressure magnitudes as the wavefronts pass down the tunnel. No theoretical explanation for this effect is obvious and so it is assumed to be due to a change in the calibration of the gauges. It is possible that not all the gauges have a linear calibration curve.

Basic Computer Results

Tables 9.1 to 9.7 tabulate the computer output for the seven runs just discussed. Besides listing the tubewall pressures at the four experiment stations, it also lists the pressures that are on the train-model.

Figures 9.1b to 9.7b are plots of these predicted pressures on the train-model: on the model nose (upper curve); on the side of the model just aft of the nose (middle curve); and just forward of the base (lower curve).

TABLE 9-1. COMPUTER OUTPUT FOR RUN 131

TEPT131. T19. M55-50.		PRESSURE, kN/m ²				nose front 'Rear (Side of Train)	VELY. m/s	
TIME secs	125cm	225cm (Along Tube)	325cm	1372cm				
0.00	-0.00	-0.00	-0.00	-0.00	0.98	0.02	0.0	27.21
0.03	1.03	1.38	1.32	-0.00	1.02	0.08	-0.65	27.05
0.05	-0.15	0.92	0.92	1.20	0.92	-0.01	-0.65	26.81
0.08	-0.01	0.91	0.91	-0.05	0.90	-0.03	-0.65	26.59
0.10	-0.00	-0.52	0.90	-0.00	0.90	-0.01	-0.63	26.37
0.12	-0.07	-0.09	-0.15	0.01	0.55	-0.09	-0.52	26.22
0.15	-0.06	-0.08	-0.08	-0.10	0.56	-0.11	-0.54	26.06
0.18	-0.03	-0.04	-0.05	0.67	0.57	-0.10	-0.51	25.90
0.20	-0.03	-0.03	0.11	-0.13	0.67	-0.01	-0.39	25.75
0.23	-0.59	-0.66	-0.70	0.04	-0.11	-0.70	-1.23	25.61
0.25	0.00	0.07	0.15	-0.14	0.47	-0.08	-0.34	25.48
0.28	-0.06	-0.08	-0.11	0.51	0.42	-0.14	-0.52	25.35
0.30	-0.03	0.08	0.04	0.03	0.56	-0.01	-0.40	25.21
0.33	-0.05	-0.01	-0.02	0.08	-0.01	-0.52	-0.80	25.09
0.35	-0.13	-0.12	-0.14	-0.01	0.00	-0.54	-0.82	24.97
0.37	-0.07	-0.06	-0.08	0.03	0.40	-0.10	-0.39	24.85
0.40	-0.03	-0.06	-0.08	0.35	0.32	-0.19	-0.49	24.73
0.43	-0.08	-0.08	-0.03	-0.02	0.02	-0.46	-0.68	24.62
0.45	-0.23	-0.29	-0.34	0.06	0.07	-0.42	-0.73	24.51
0.48	-0.05	-0.05	-0.04	0.05	0.06	-0.44	-0.72	24.39
0.50	-0.03	-0.04	-0.07	0.27	0.29	-0.18	-0.43	24.28

TABLE 9-2. COMPUTER OUTPUT FOR RUN 160

TEPT160. T19-V2. M55-50.		PRESSURE, kN/m ²				nose front rear (Side of Train)		VELY. m/s
TIME secs	125cm	225cm (Along Tube)	425cm	1372cm	nose	front	rear	
0.00	-0.00	-0.00	-0.00	-0.00	0.89	0.01	0.0	25.99
0.01	0.84	0.68	-0.00	-0.00	1.07	0.23	0.0	25.95
0.02	0.77	0.59	0.58	-0.00	0.90	0.22	0.0	25.90
0.03	0.50	0.54	0.73	-0.00	0.51	-0.18	-0.52	25.83
0.04	0.59	0.60	0.54	0.83	0.59	-0.09	-0.50	25.77
0.05	-0.13	0.58	0.58	0.53	0.58	-0.09	-0.50	25.71
0.06	-0.32	0.58	0.58	0.69	0.57	-0.09	-0.50	25.64
0.07	-0.03	0.58	0.58	0.59	0.57	-0.09	-0.50	25.58
0.08	-0.02	0.80	0.58	0.00	0.83	-0.03	-0.44	25.52
0.09	0.11	0.12	0.91	-0.12	1.02	0.20	-0.34	25.45
0.10	0.16	-0.14	0.94	0.05	1.01	0.20	-0.39	25.37
0.11	-0.56	-0.42	0.13	0.01	0.26	-0.47	-0.92	25.30
0.12	0.20	0.30	0.30	0.39	0.38	-0.31	-0.18	25.24
0.13	-0.04	-0.07	0.68	0.42	0.63	-0.06	-0.51	25.17
0.14	-0.09	-0.02	0.63	0.22	0.69	0.01	-0.30	25.11
0.15	-0.01	0.00	0.55	0.14	0.57	-0.12	-0.52	25.04
0.16	0.00	0.00	0.62	0.16	0.61	-0.06	-0.52	24.98
0.17	0.00	-0.04	-0.13	0.56	0.61	-0.06	-0.50	24.92
0.18	-0.04	-0.20	-0.60	0.15	0.22	-0.40	-0.72	24.86
0.19	-0.06	-0.20	-0.28	-0.03	0.24	-0.37	-0.70	24.80
0.20	-0.03	-0.03	0.20	-0.05	0.53	-0.08	-0.28	24.75

TABLE 9-3. COMPUTER OUTPUT FOR RUN 162

TEPT162. T19-V5-*. M55-50.									
TIME secs	PRESSURE, kN/m ²								VELOCITY m/s
	(Along Tube)				(Side of Train)				
	125cm	225cm	425cm	1372cm	nose	front	rear		
0.00	-0.00	-0.00	-0.00	-0.00	0.89	0.01	0.00		26.11
0.01	0.54	0.45	-0.00	-0.00	1.08	0.24	0.00		26.07
0.02	0.92	0.72	0.50	-0.00	0.99	0.32	0.00		26.02
0.03	0.63	0.63	0.82	-0.00	0.58	-0.10	-0.51		25.96
0.04	0.60	0.63	0.65	0.65	0.60	-0.10	-0.53		25.89
0.05	-0.13	0.63	0.62	0.44	0.61	-0.09	-0.51		25.82
0.06	-0.33	0.62	0.62	0.75	0.61	-0.08	-0.51		25.76
0.07	-0.03	0.62	0.62	0.68	0.61	-0.08	-0.51		25.69
0.08	0.14	1.00	0.61	0.14	1.00	0.17	-0.33		25.62
0.09	0.05	0.16	1.03	-0.17	1.06	0.24	-0.36		25.55
0.10	0.33	-0.10	1.08	-0.01	1.21	0.43	-0.41		25.47
0.11	0.01	-0.26	0.19	0.02	0.41	-0.35	-0.79		25.39
0.12	-0.10	-0.24	0.20	0.45	0.20	-0.50	-0.69		25.33
0.13	-0.01	-0.13	0.56	0.56	0.59	-0.09	-0.54		25.27
0.14	-0.10	-0.07	0.57	0.18	0.61	-0.06	-0.47		25.20
0.15	-0.09	-0.01	0.58	-0.05	0.59	-0.09	-0.49		25.14
0.16	-0.02	-0.04	0.58	0.09	0.58	-0.09	-0.50		25.07
0.17	0.01	-0.02	-0.17	0.50	0.59	-0.09	-0.52		25.01
0.18	-0.07	-0.20	-0.69	0.22	0.15	-0.46	-0.81		24.95
0.19	-0.06	-0.14	-0.27	0.03	0.18	-0.40	-0.67		24.90
0.20	-0.10	-0.03	0.16	-0.06	0.56	-0.05	-0.33		24.84

TABLE 9-4. COMPUTER OUTPUT FOR RUN 173

TEPT173. T19. F1-0. M55-50.									
TIME secs	PRESSURE, kN/m ²						nose front rear (Side of Train)	VELY. m/s	
	125cm	225cm	425cm	1372cm	(Along Tube)				
0.00	-0.00	0.0	0.0	0.0	0.0	0.22	0.00	0.0	25.20
0.01	0.27	0.29	-0.00	-0.00	-0.00	0.30	0.02	0.0	25.19
0.02	0.39	0.36	0.29	-0.00	-0.00	0.41	0.04	0.0	25.17
0.03	0.33	0.27	0.41	-0.00	-0.00	0.36	-0.17	-0.24	25.14
0.04	0.55	0.47	0.36	0.32	0.32	0.59	-0.27	-0.30	25.10
0.05	-0.12	0.70	0.61	0.32	0.32	0.72	-0.11	-0.39	25.04
0.06	-0.29	0.78	0.74	0.44	0.44	0.79	-0.03	-0.50	24.97
0.07	-0.52	0.81	0.80	0.40	0.40	0.81	-0.00	-0.56	24.90
0.08	0.00	0.81	0.81	0.37	0.37	0.80	-0.01	-0.56	24.82
0.09	-0.00	-0.02	0.80	0.36	0.36	0.79	-0.01	-0.56	24.74
0.10	-0.00	-0.26	0.77	0.44	0.44	0.80	-0.00	-0.55	24.66
0.11	-0.25	-0.73	0.38	0.21	0.21	0.51	-0.24	-0.77	24.59
0.12	-0.02	0.05	0.35	0.08	0.08	0.44	-0.28	-0.41	24.52
0.13	-0.08	0.04	0.64	0.01	0.01	0.64	-0.06	-0.47	24.45
0.14	-0.13	-0.08	0.34	-0.04	-0.04	0.41	-0.25	-0.55	24.39
0.15	-0.16	-0.20	0.21	0.02	0.02	0.27	-0.37	-0.70	24.33
0.16	-0.06	-0.05	0.35	0.18	0.18	0.37	-0.24	-0.53	24.28
0.17	-0.02	-0.05	0.46	0.26	0.26	0.46	-0.13	-0.48	24.22
0.18	0.00	-0.03	-0.23	0.23	0.23	0.49	-0.09	-0.45	24.16
0.19	-0.01	-0.02	-0.36	0.18	0.18	0.52	-0.06	-0.42	24.11
0.20	-0.02	-0.02	0.04	0.30	0.30	0.52	-0.06	-0.38	24.05

TABLE 9-4.* COMPUTER OUTPUT FOR RUN 173A

TRIP 173A. T19. F1-0*. M55-50.								
TIME secs	PRESSURE, kN/m ²						VFLY. m/s	
	125cm	225cm (Along Tube)	425cm	1372cm	rose front (Side of Train)	rose front, rear (Side of Train)		
0.00	-0.00	0.0	0.0	0.0	0.22	0.00	0.0	25.20
0.01	0.27	0.29	-0.00	-0.00	0.30	0.02	0.0	25.19
0.02	0.39	0.36	0.29	-0.00	0.41	0.04	0.0	25.17
0.03	0.33	0.27	0.41	-0.00	0.36	-0.17	-0.24	25.14
0.04	0.56	0.47	0.36	0.32	0.65	-0.20	-0.30	25.10
0.05	0.02	0.83	0.67	0.32	0.84	0.02	-0.39	25.04
0.06	-0.15	0.89	0.85	0.44	0.90	0.10	-0.49	24.96
0.07	-0.52	0.84	0.91	0.40	0.80	-0.01	-0.56	24.88
0.08	-0.00	0.81	0.81	0.46	0.80	-0.00	-0.56	24.80
0.09	-0.00	-0.01	0.80	0.48	0.80	-0.00	-0.56	24.72
0.10	-0.00	-0.26	0.77	0.49	0.80	-0.00	-0.55	24.65
0.11	-0.25	-0.72	0.39	0.16	0.51	-0.24	-0.77	24.57
0.12	-0.02	0.05	0.35	-0.02	0.44	-0.28	-0.41	24.50
0.13	-0.08	0.04	0.64	-0.09	0.64	-0.06	-0.47	24.44
0.14	-0.13	-0.07	0.27	-0.04	0.33	-0.32	-0.56	24.38
0.15	-0.22	-0.29	0.10	0.02	0.16	-0.46	-0.78	24.32
0.16	-0.05	-0.05	0.32	0.18	0.34	-0.25	-0.52	24.27
0.17	0.02	0.03	0.54	0.24	0.54	-0.03	-0.38	24.21
0.18	0.00	-0.01	-0.16	0.22	0.56	-0.02	-0.39	24.16
0.19	-0.02	-0.03	-0.37	0.25	0.52	-0.06	-0.43	24.10
0.20	-0.01	-0.02	0.04	0.37	0.52	-0.07	-0.38	24.05

TABLE 9-5. COMPUTER OUTPUT FOR RUN 184

TEPT184. T18. M110-50.		PRESSURE, kN/m ²				nose front rear (Side of Train)	VELY. m/s	
TIME secs	125cm	225cm (Along Tube)	425cm	1272cm				
0.00	0.0	0.0	0.0	0.0	0.83	0.01	0.0	25.14
0.01	0.96	0.90	-0.00	-0.00	1.01	0.22	0.0	25.12
0.02	1.14	1.09	0.98	-0.00	1.18	0.42	0.0	25.09
0.03	1.31	1.27	1.17	-0.00	1.33	0.60	0.0	25.05
0.04	1.46	1.42	1.32	0.88	1.47	0.76	0.0	25.00
0.05	0.52	1.49	1.48	1.07	1.27	0.53	-0.49	24.94
0.06	0.25	1.23	1.27	1.24	1.23	0.48	-0.53	24.87
0.07	0.01	1.22	1.22	1.12	1.22	0.47	-0.53	24.81
0.08	-0.21	1.21	1.21	0.42	1.21	0.47	-0.52	24.75
0.09	-0.44	0.46	1.21	0.06	1.20	0.47	-0.52	24.68
0.10	-0.01	0.16	0.34	-0.09	0.50	-0.17	-0.52	24.62
0.11	-0.59	-0.85	-0.15	-0.23	0.07	-0.54	-1.19	24.58
0.12	-0.11	-0.35	0.30	0.01	0.41	-0.11	-0.46	24.55
0.13	-0.20	-0.56	0.22	-0.22	0.27	-0.22	-0.59	24.51
0.14	-0.14	-0.16	0.52	-0.15	0.43	-0.03	-0.49	24.48
0.15	0.06	0.03	0.70	0.40	0.72	0.24	-0.28	24.44
0.16	-0.01	-0.02	0.79	0.41	0.80	0.32	-0.40	24.40
0.17	-0.09	-0.10	0.65	0.82	0.64	0.15	-0.45	24.36
0.18	-0.05	-0.05	0.06	0.39	0.65	0.15	-0.39	24.32
0.19	-0.06	-0.06	0.25	0.31	1.04	0.52	-0.24	24.27
0.20	0.17	0.07	-0.15	0.05	0.39	-0.10	-0.31	24.23

TABLE 9-6. COMPUTER OUTPUT FOR RUN 186

TEPT186. T18. P1-50. M110-50.									
TIME secs	PRESSURE, kN/m ²								VELY. m/s
	(Along Tube)				(Side of Train)				
	125cm	225cm	425cm	1272cm	nose	front	rear		
0.00	-0.00	-0.00	-0.00	-0.00	0.81	0.01	0.0		25.21
0.01	0.30	0.15	-0.00	-0.00	0.55	0.03	0.0		25.20
0.02	0.65	0.59	0.37	-0.00	0.72	0.19	0.0		25.18
0.03	0.89	0.84	0.69	-0.00	0.96	0.33	0.0		25.15
0.04	1.18	1.11	0.95	0.14	1.10	0.32	0.0		25.12
0.05	0.48	1.21	1.13	0.57	1.24	0.49	-0.45		25.07
0.06	0.37	1.31	1.25	0.83	1.33	0.59	-0.48		25.00
0.07	0.24	1.38	1.33	1.03	1.38	0.66	-0.52		24.94
0.08	-0.19	1.34	1.39	0.73	1.33	0.60	-0.58		24.87
0.09	-0.46	0.45	1.23	0.56	1.21	0.46	-0.53		24.80
0.10	-0.01	0.22	0.96	0.40	1.07	0.34	-0.52		24.74
0.11	-0.12	-0.35	0.52	0.20	0.62	-0.06	-0.66		24.69
0.12	-0.13	-0.46	0.38	-0.02	0.53	-0.08	-0.63		24.64
0.13	-0.14	-0.59	0.27	-0.11	0.36	-0.19	-0.63		24.60
0.14	-0.11	-0.21	0.35	-0.21	0.41	-0.12	-0.58		24.56
0.15	-0.12	-0.18	0.41	0.09	0.43	-0.07	-0.54		24.52
0.16	-0.11	-0.15	0.43	0.22	0.44	-0.04	-0.51		24.49
0.17	-0.09	-0.12	0.61	0.49	0.61	0.13	-0.44		24.45
0.18	-0.01	0.02	0.12	0.44	0.72	0.23	-0.32		24.41
0.19	-0.05	-0.05	0.01	0.41	0.80	0.31	-0.39		24.37
0.20	-0.01	0.02	-0.19	0.36	0.65	0.15	-0.37		24.33

TABLE 9-7. COMPUTER OUTPUT FOR RUN 207

TEPT207. T19. M55-50B.		PRESSURE, kN/m ²				nose front rear (Side of Train)		VEHY. m/s
TIME secs	1372cm				nose	front	rear	
	125cm	225cm (Along Tube)	425cm	425cm				
0.00	-0.00	-0.00	-0.00	-0.00	1.03	0.01	0.0	28.23
0.01	1.20	1.12	-0.00	-0.00	1.27	0.29	0.0	28.18
0.02	1.44	1.37	1.23	-0.00	1.48	0.55	2.29	28.10
0.03	3.03	3.03	1.47	-0.00	3.04	2.39	2.02	27.75
0.04	3.00	3.00	3.00	1.04	3.00	2.36	2.00	27.41
0.05	2.23	2.96	2.96	1.28	2.96	2.32	1.97	27.06
0.06	2.02	2.92	2.92	2.75	2.92	2.29	1.94	26.72
0.07	-0.04	2.87	2.88	2.88	2.87	2.26	1.91	26.40
0.08	-0.04	2.83	2.84	1.68	2.83	2.23	1.88	26.07
0.09	-0.04	2.07	2.79	1.43	2.79	2.20	1.86	25.74
0.10	-0.03	1.88	2.73	0.11	2.75	2.17	1.83	25.43
0.11	-0.55	-0.75	1.30	0.10	1.41	0.94	0.75	25.15
0.12	-0.23	-0.44	0.54	0.09	1.12	0.68	0.64	24.90
0.13	-0.68	-0.96	0.16	0.08	0.23	-0.05	-0.14	24.74
0.14	-0.26	-0.50	0.28	-0.17	0.22	-0.06	-0.18	24.59
0.15	-0.01	-0.13	0.87	-0.20	0.89	0.66	0.54	24.47
0.16	-0.22	-0.30	0.95	0.08	0.95	0.72	0.55	24.35
0.17	-0.25	-0.24	0.57	0.40	0.86	0.62	0.49	24.21
0.18	-0.17	-0.18	0.53	0.94	0.90	0.65	0.50	24.08
0.19	-0.18	-0.19	-0.26	0.71	0.95	0.70	0.54	23.95
0.20	-0.16	-0.19	-0.07	0.67	1.19	0.92	0.78	23.80

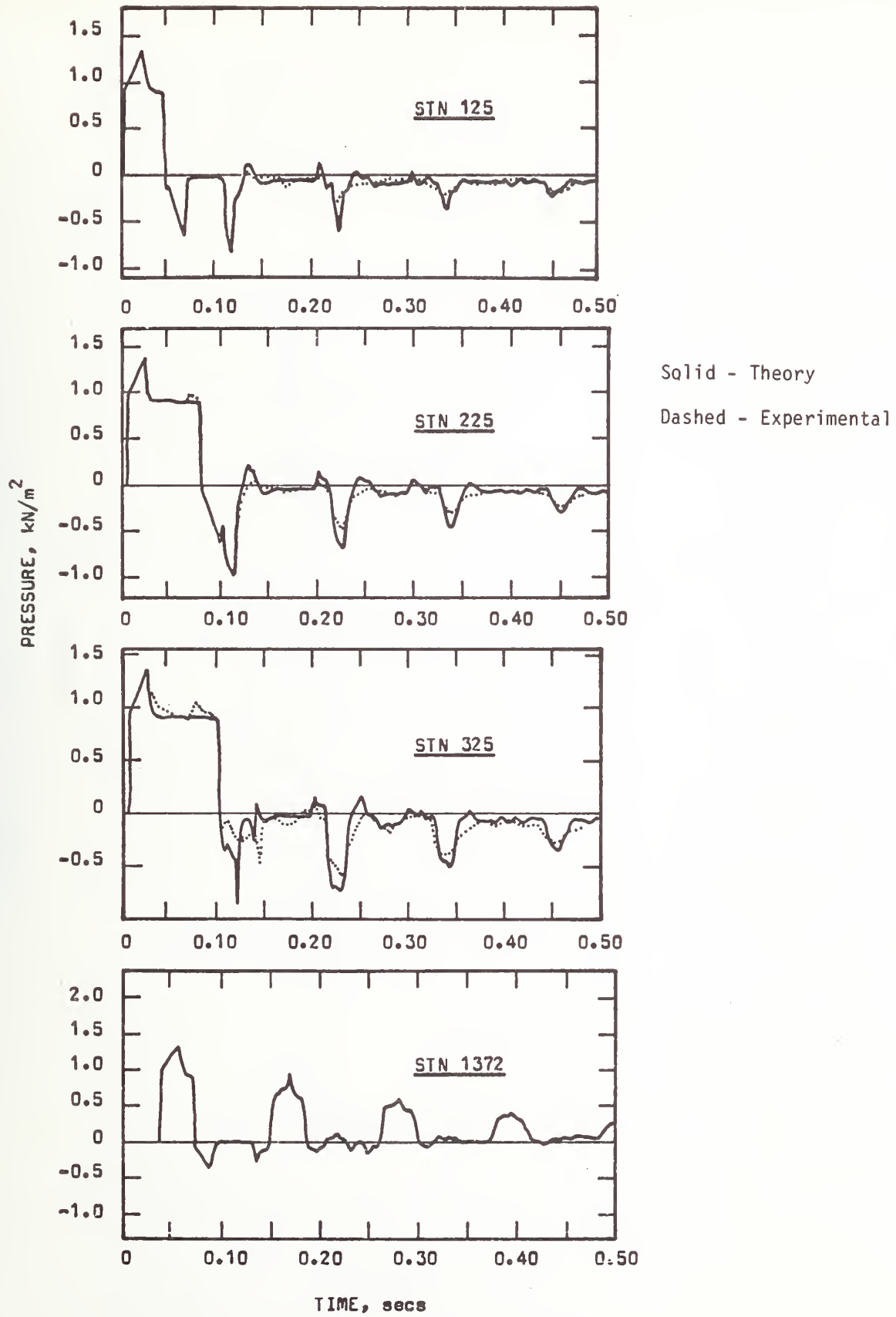


FIGURE 9-1a. RUN 131, T19, M55-50

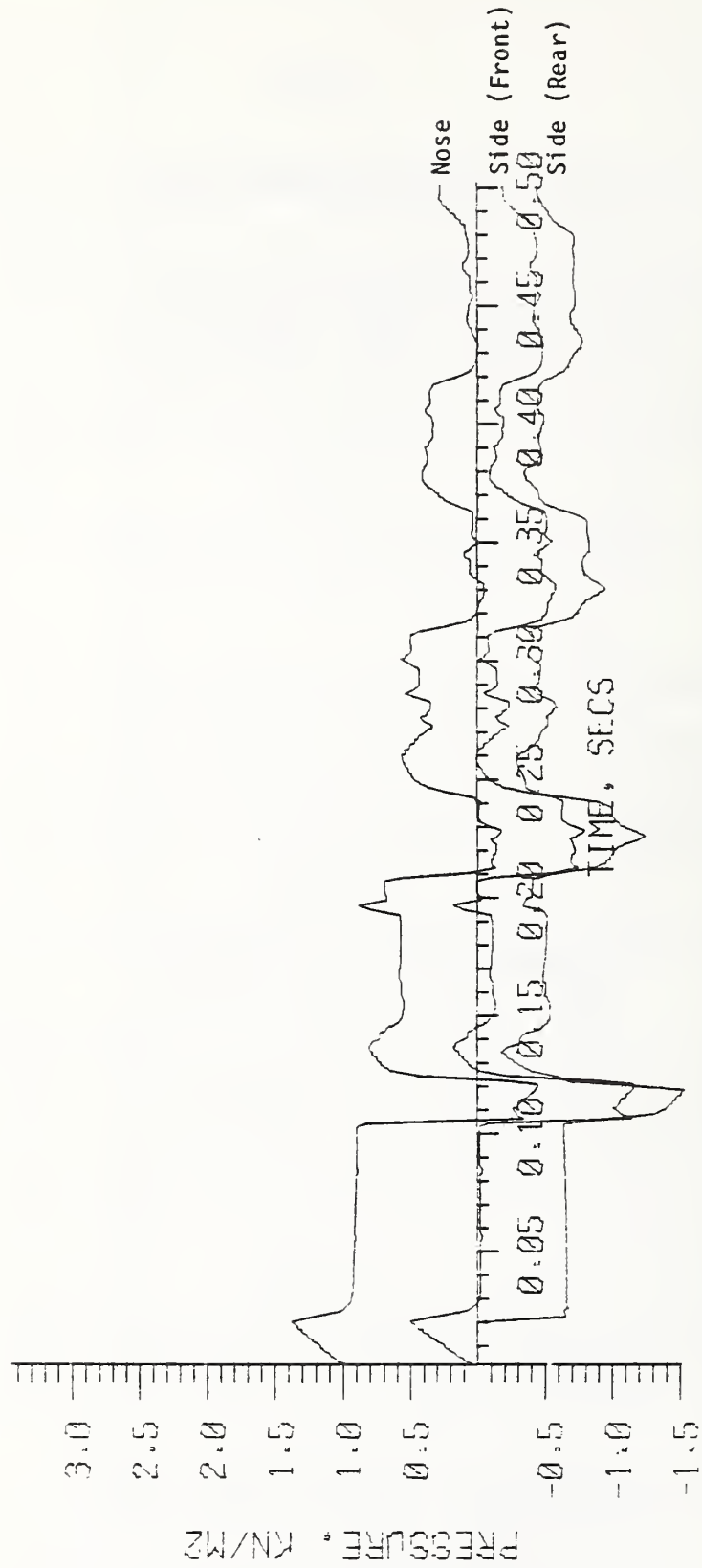


FIGURE 9-1b. TEPT131, T19, M55-50

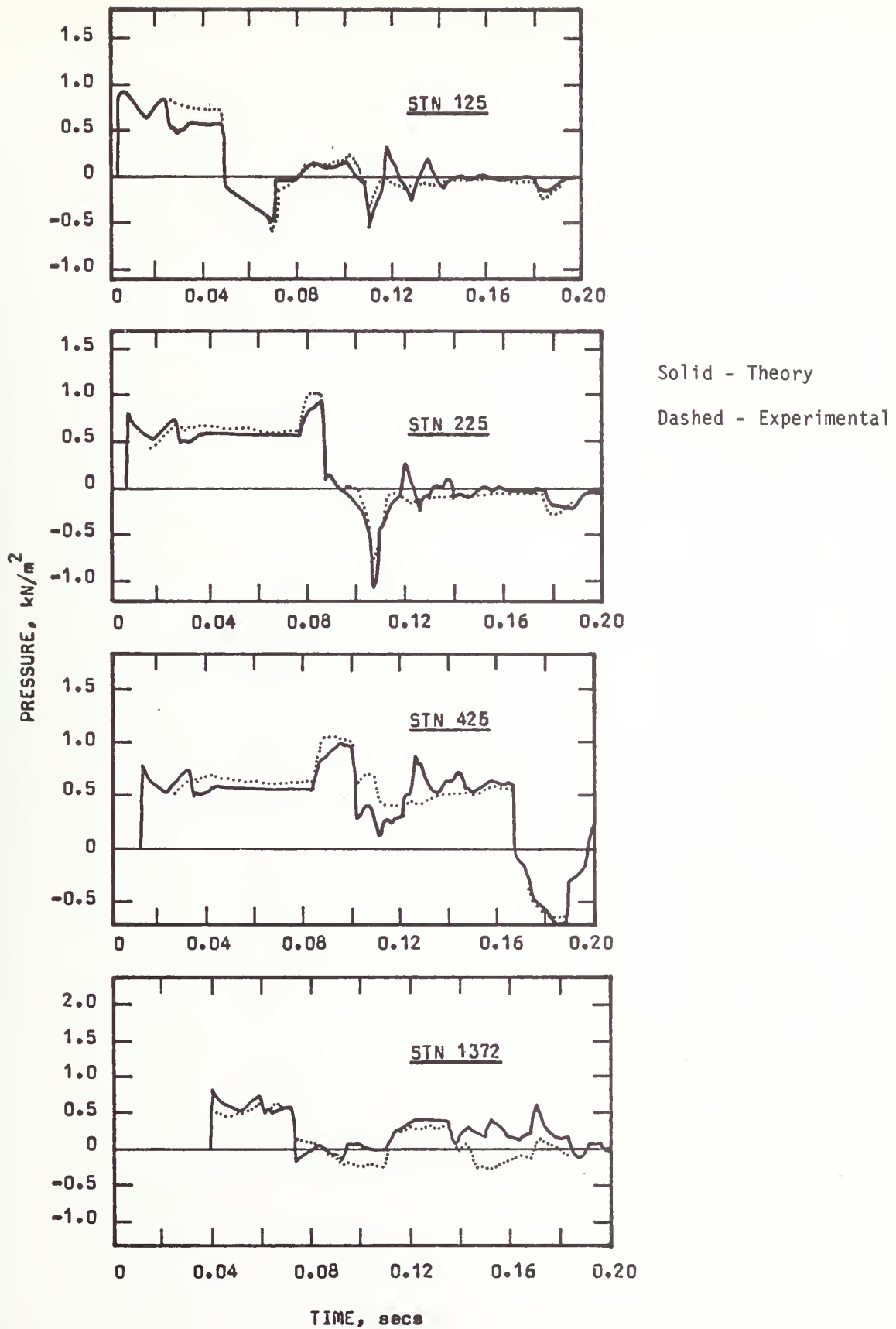


FIGURE 9-2a. RUN 160, T19-V2, M55-50

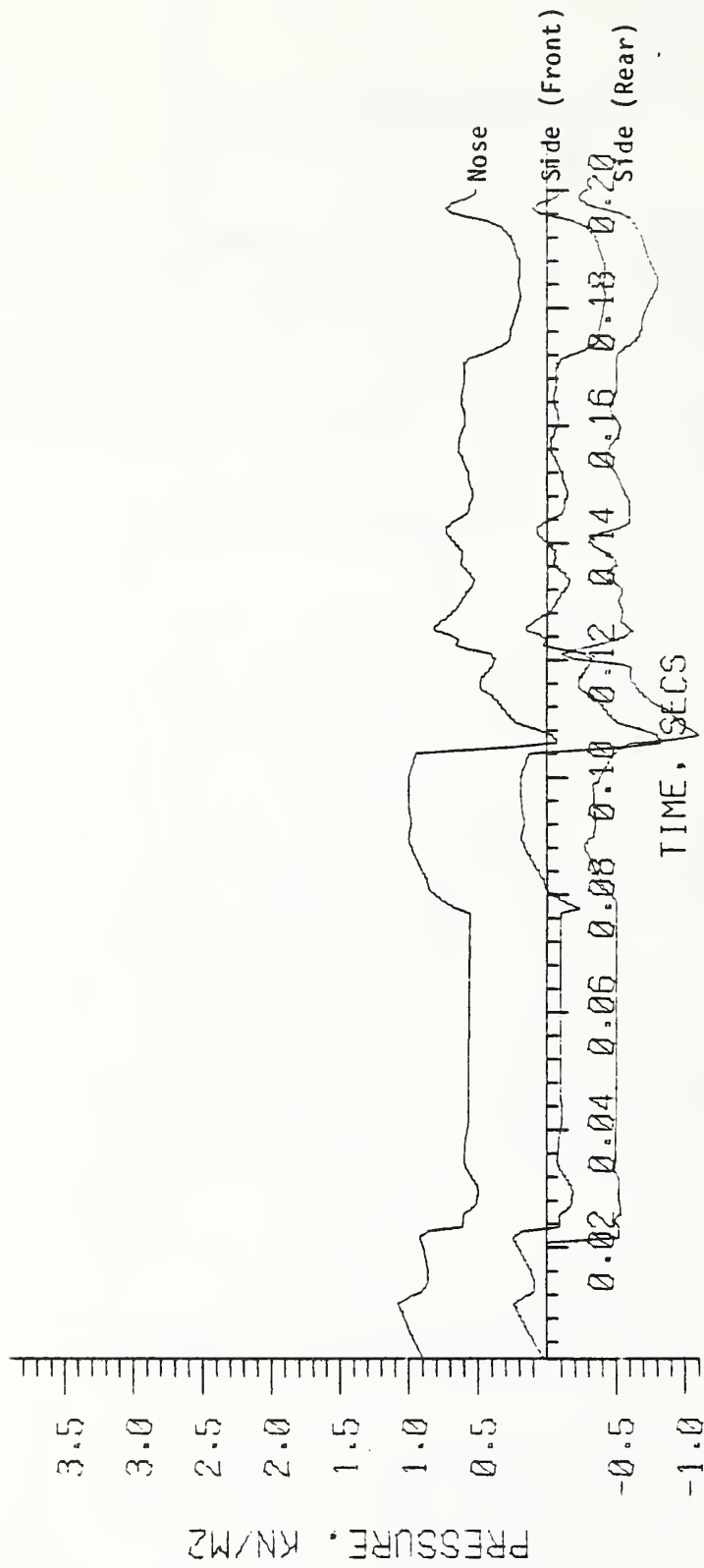


FIGURE 9-2b. TEPTI60, T19-V2, M55-50

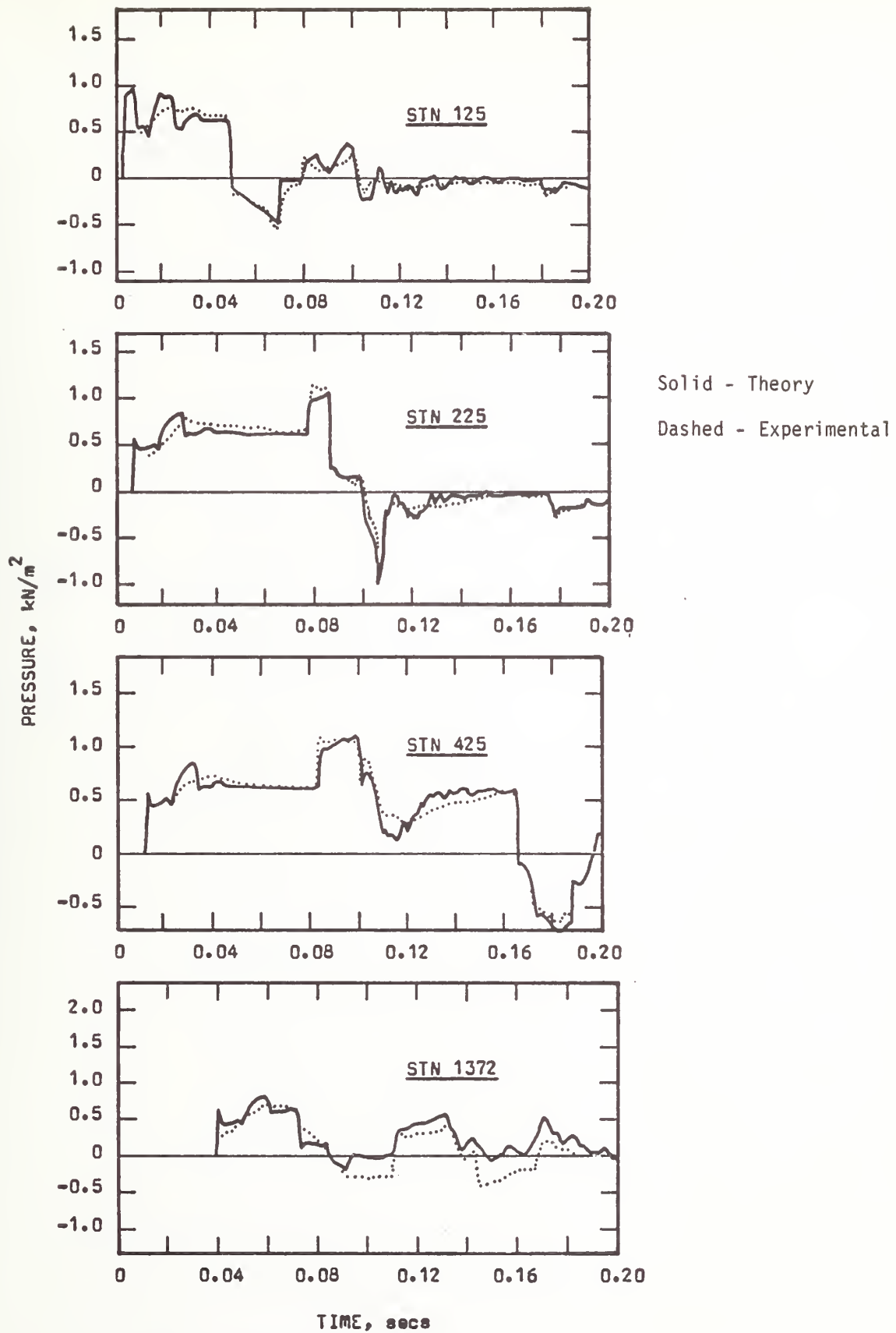


FIGURE 9-3a. RUN 162, T19-V5₀, M55-50

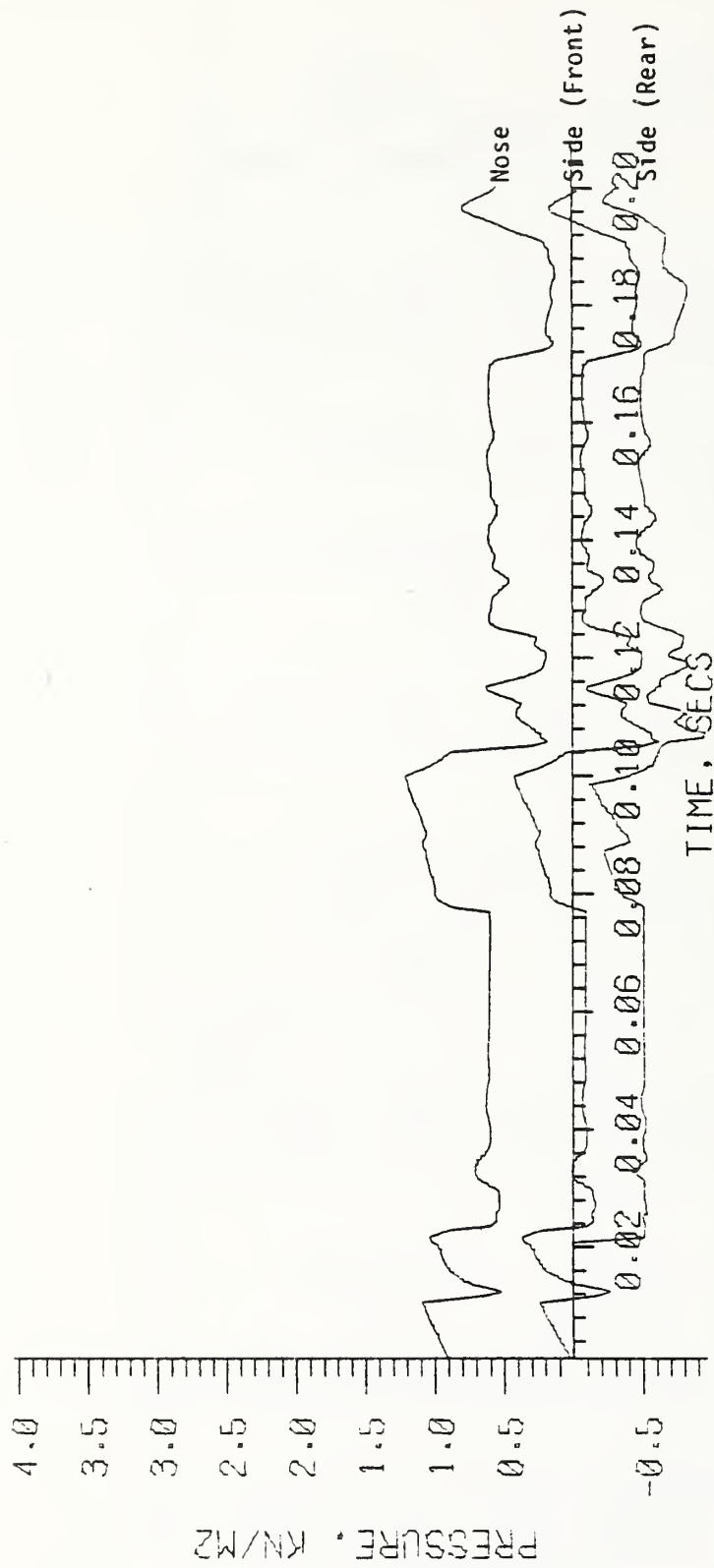


FIGURE 9-3b. TEPT162, T19-V-5*, M55-50

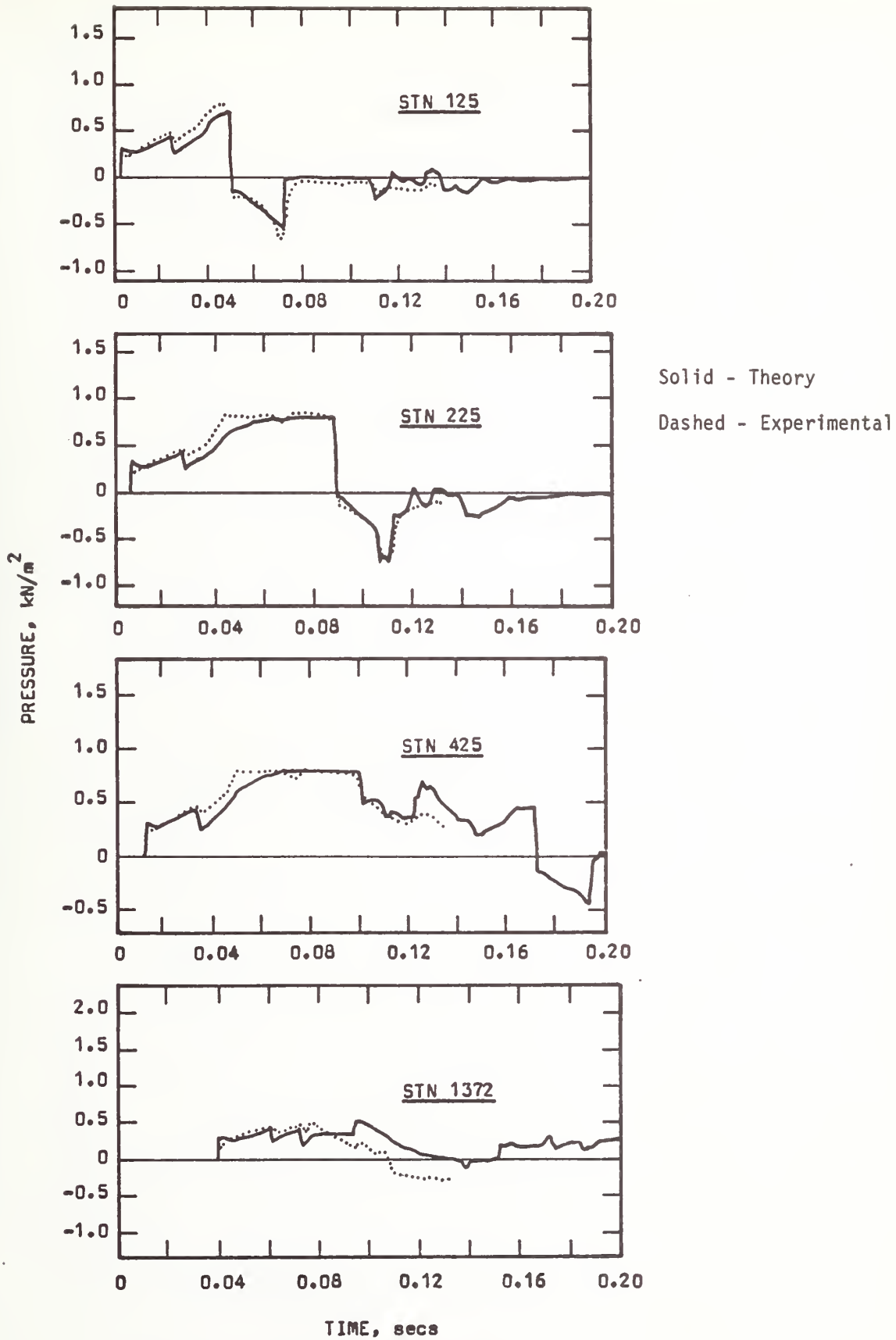


FIGURE 9-4a. RUN 173, T19, F1-0, M55-50

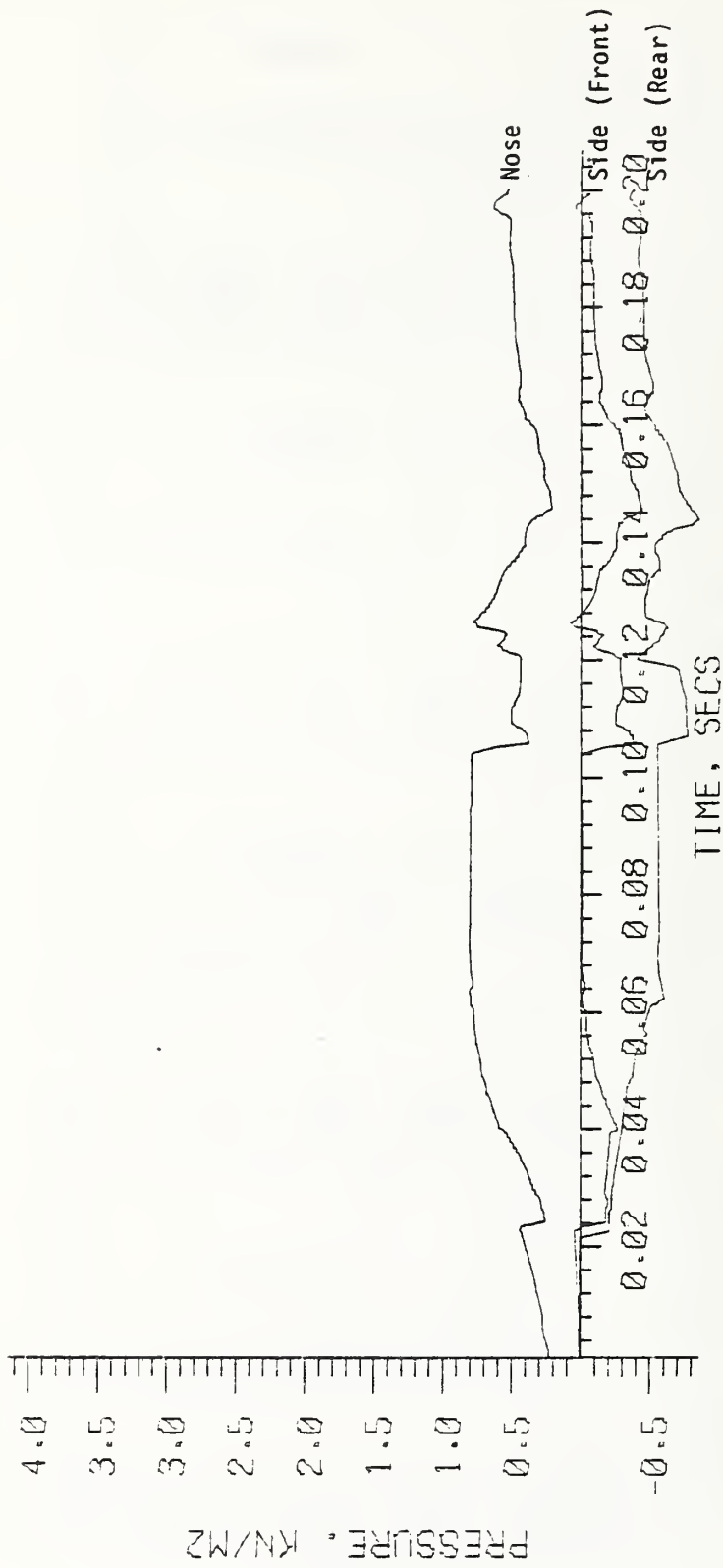


FIGURE 9-4b. TEPT173, T19, F1-0, M55-50

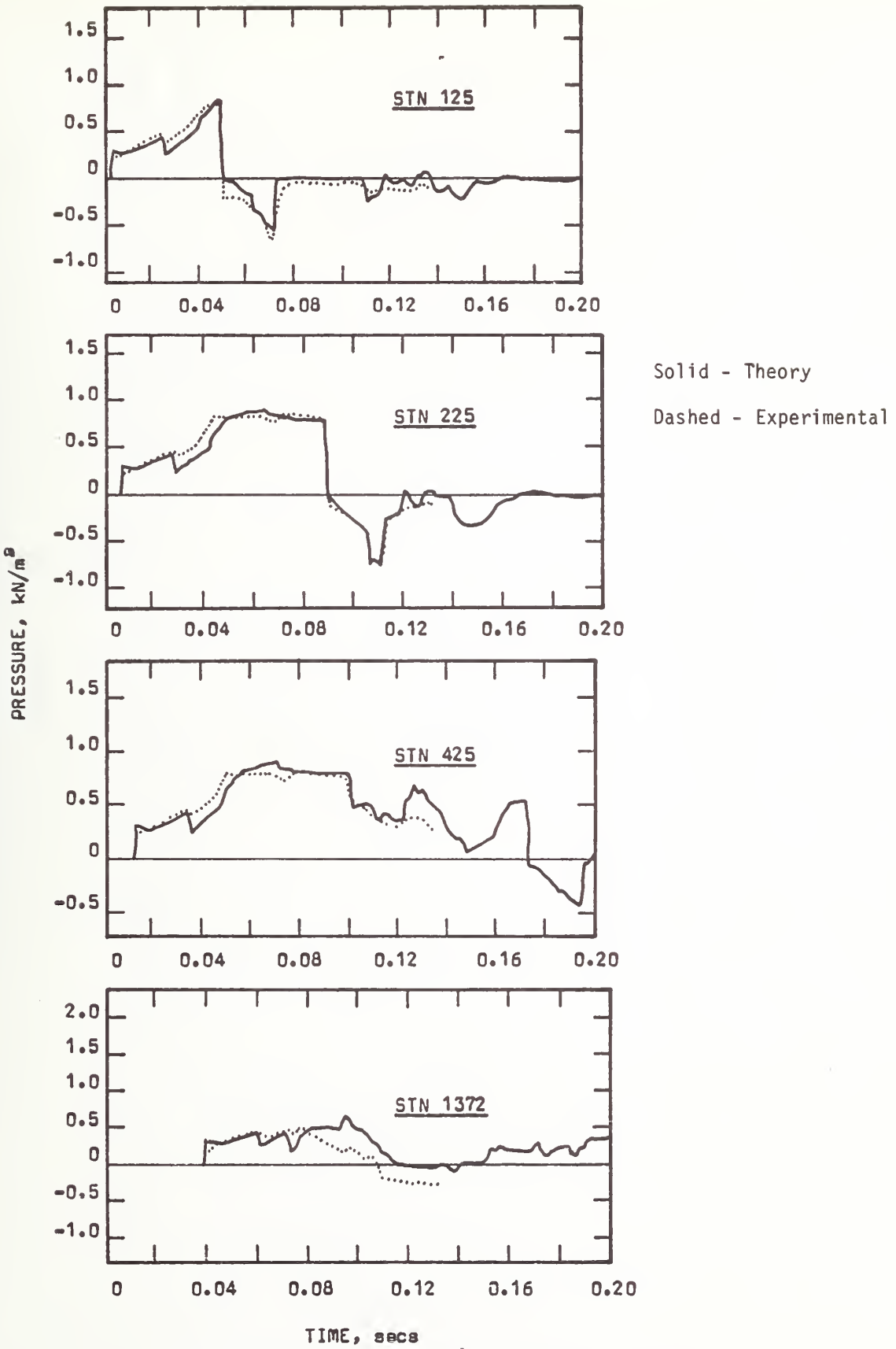


Figure 9-4a.* RUN 173A, T19, F1-0*, M55-50

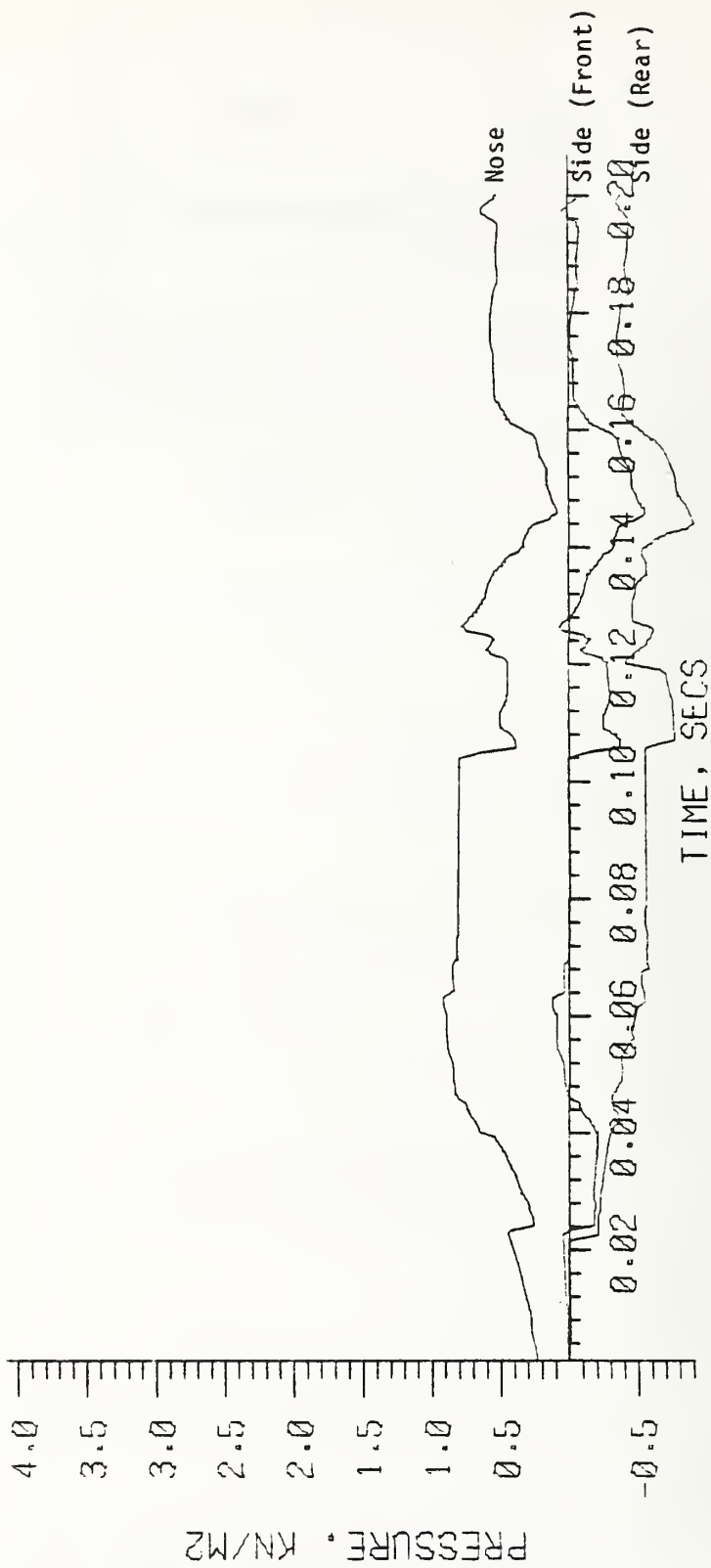


FIGURE 9-4b.* TEPT173A, T19, F1-0*, M55-50

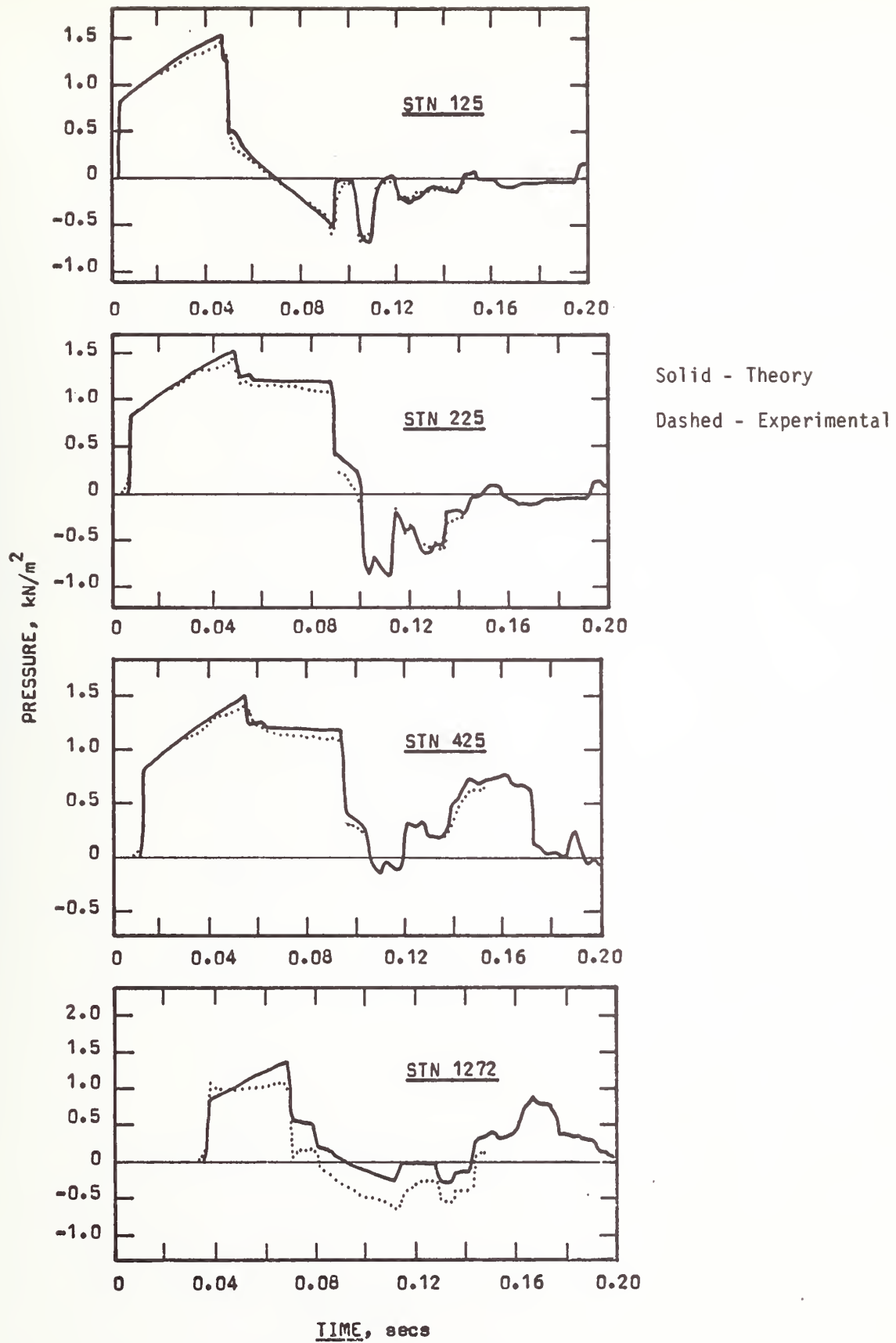


FIGURE 9-5a. RUN 184, T18, M110-50

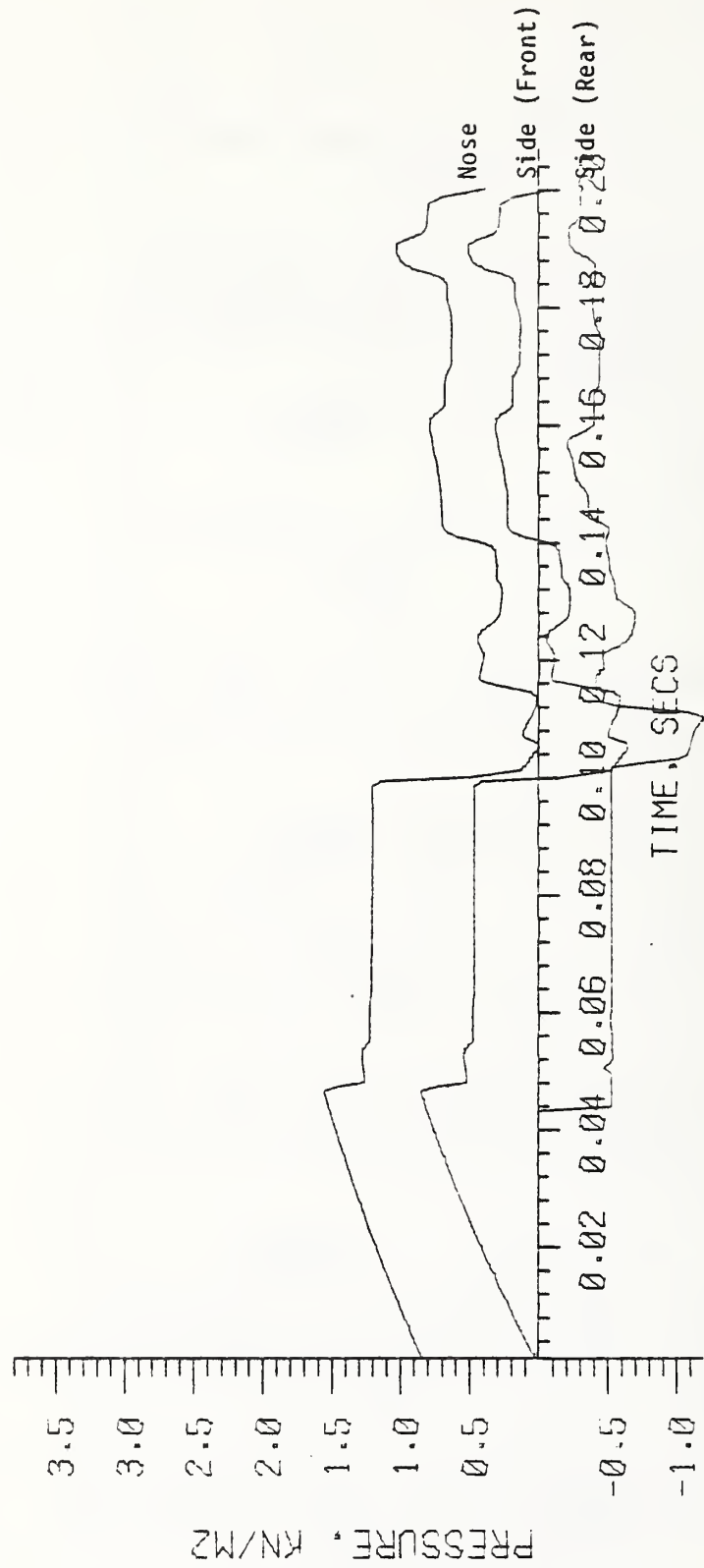


FIGURE 9-5b. TEPT184, T18, M110-50

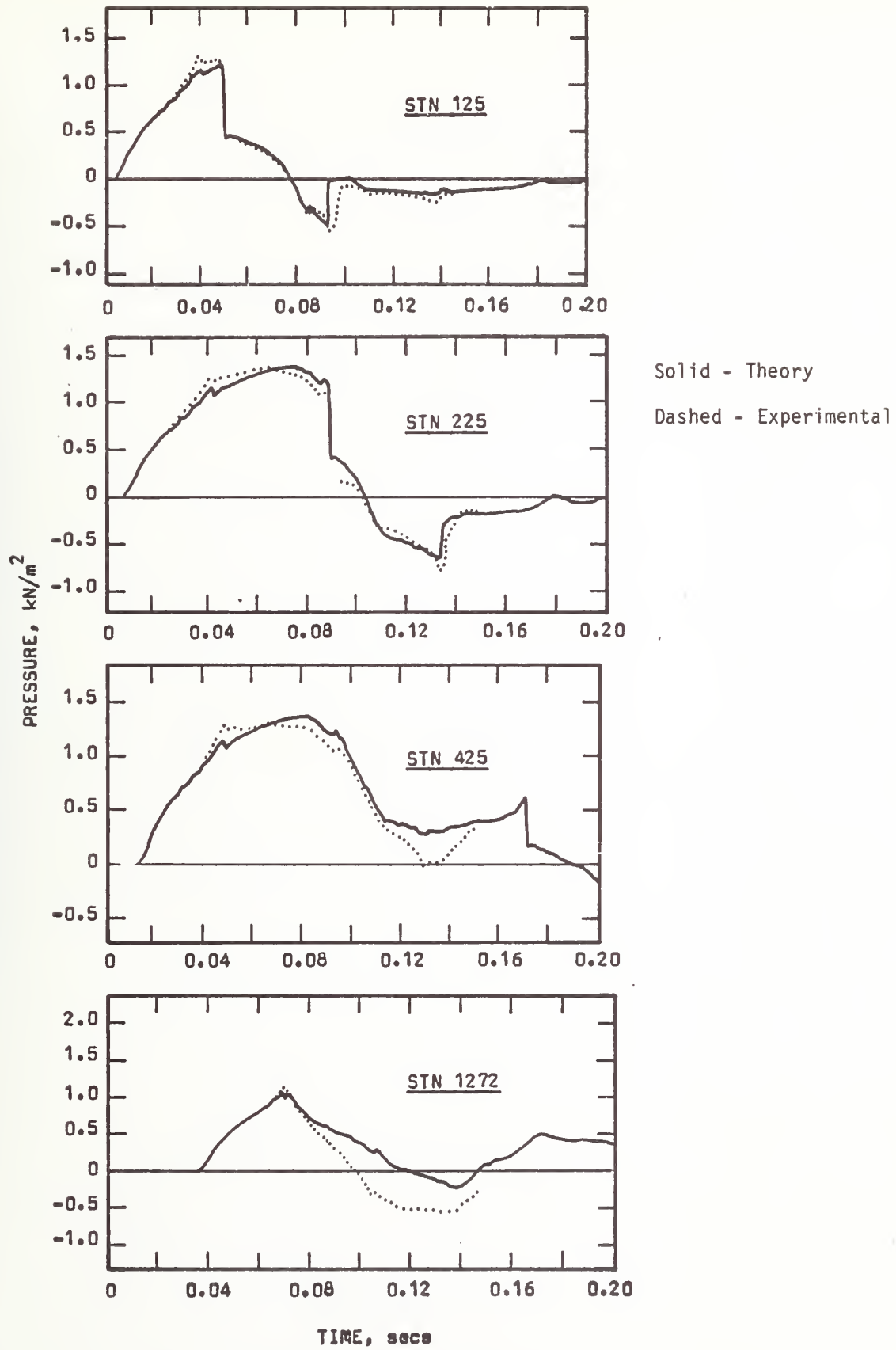


FIGURE 9-6a. RUN 186, T18, M110-50

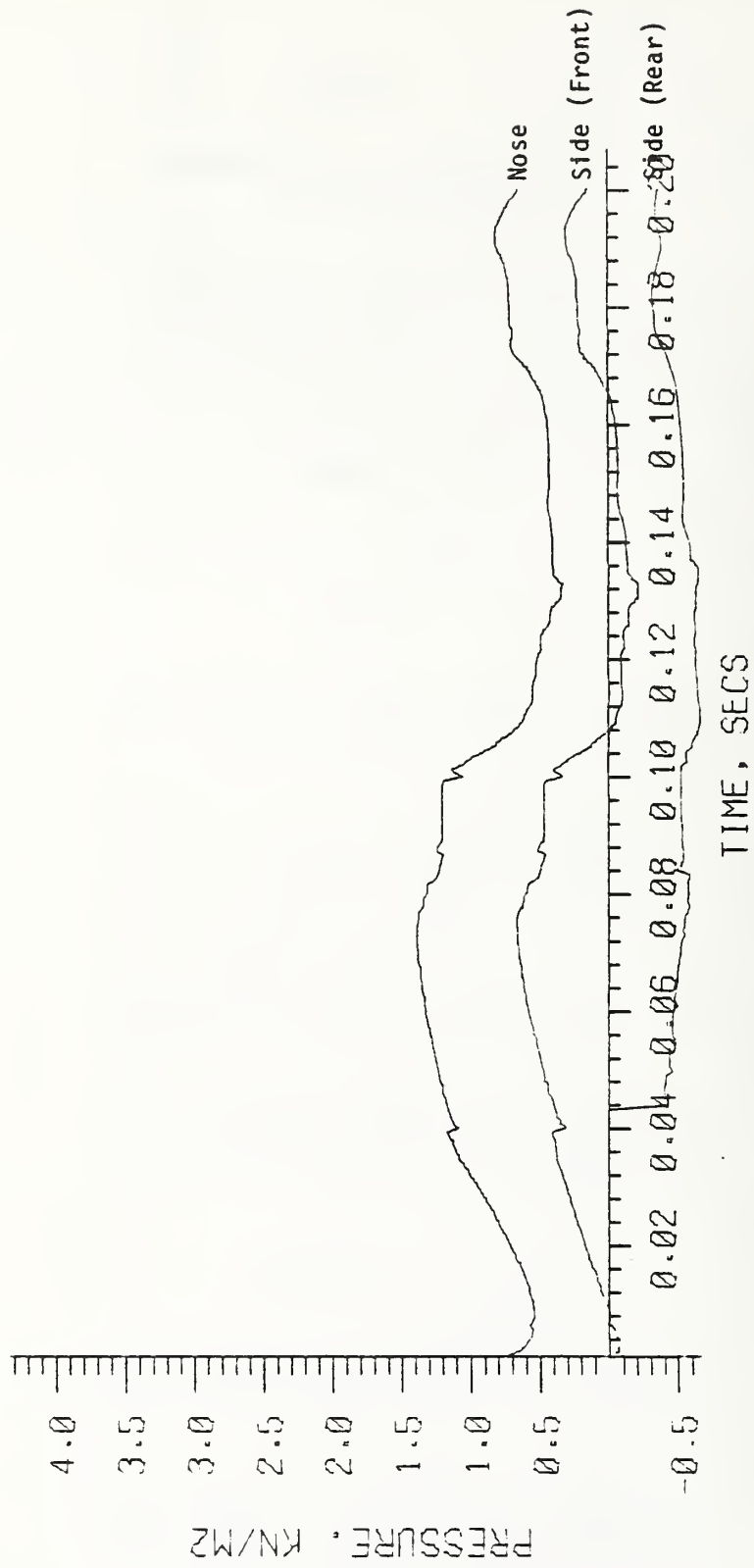


FIGURE 9-6b. TEPT186, T18, P1-50, M110-50

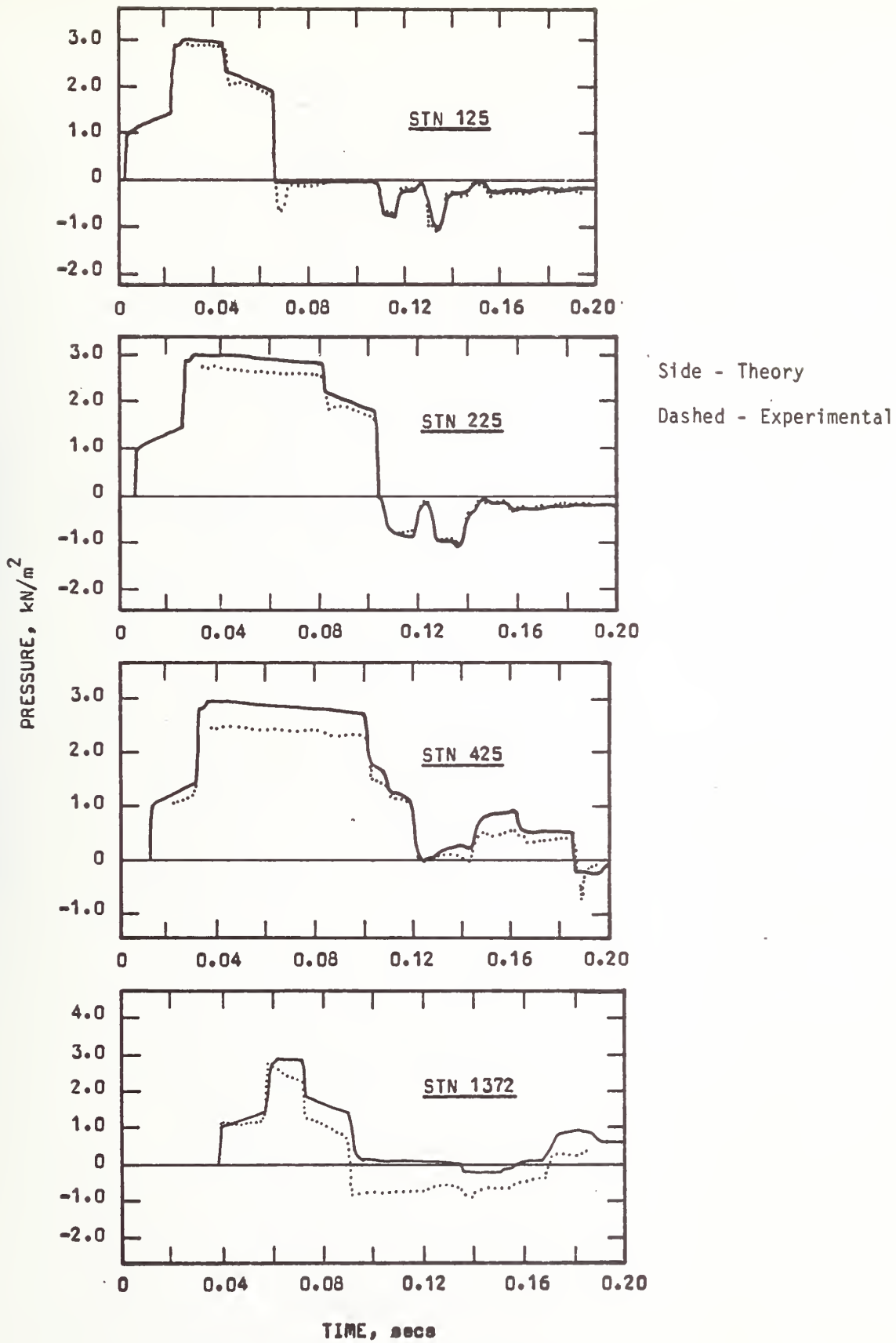


FIGURE 9-7a. RUN 207, T19, M55-50B

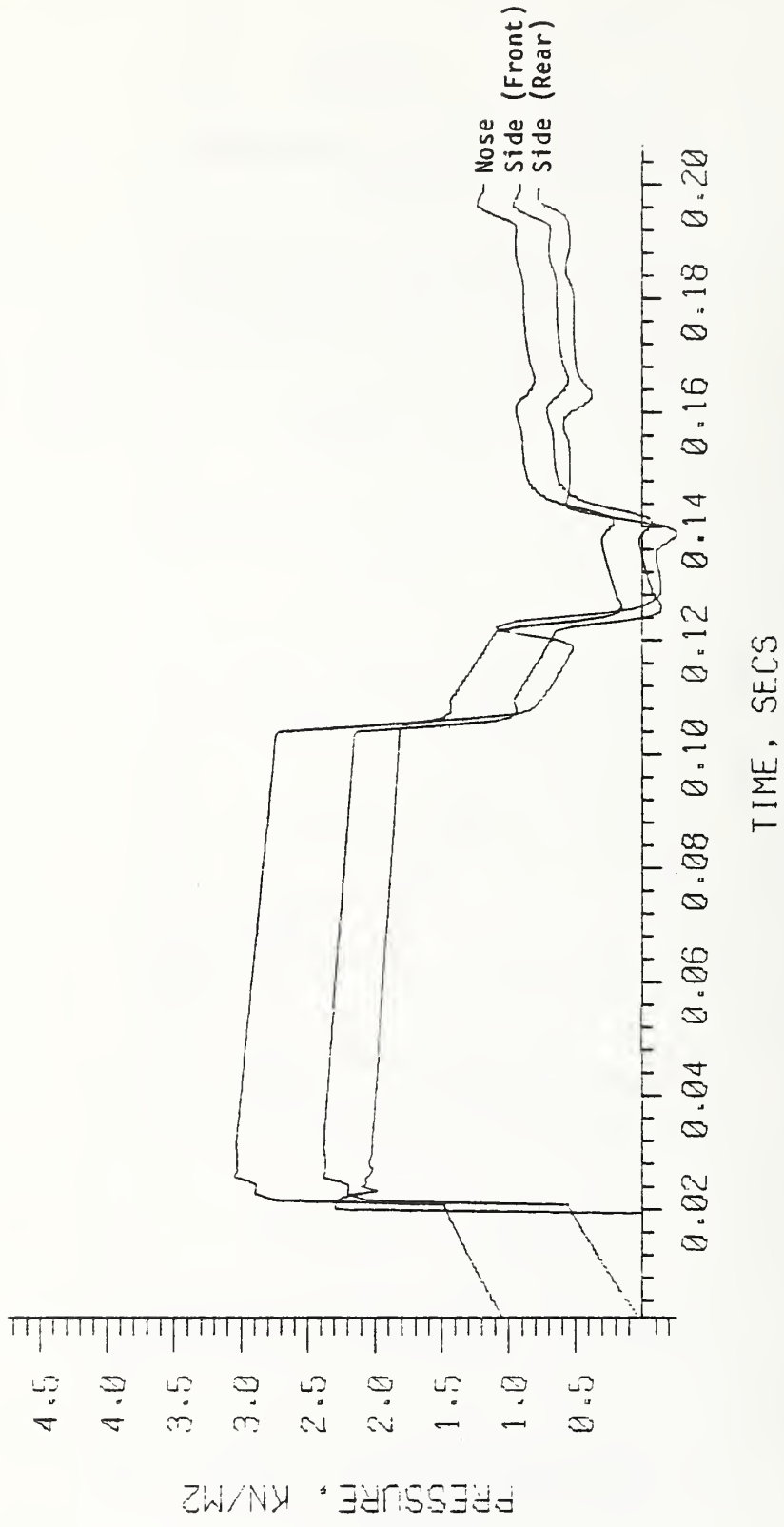


FIGURE 9-7b. TEPT207, T19, M55-50B

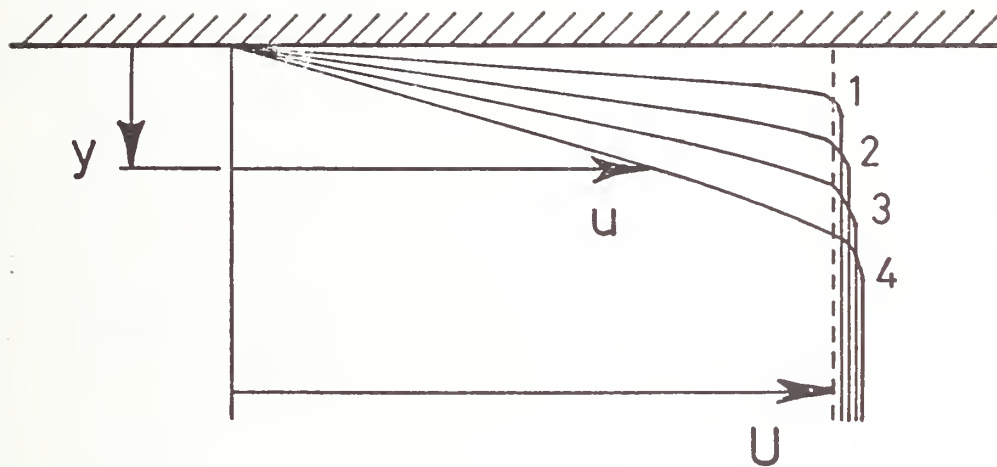


FIGURE 9-8. DEVELOPING VELOCITY PROFILE

9.2 Simplified Theoretical Analysis

9.2.1 Normal Tunnel

The flare prediction model can also be applied to a straight tube. This has been done for the 50% blockage ratio, 110-cm long model. This case has been selected since it corresponds to the experimental Run 184 and one of the cases calculated by Vardy. The comparison between these three results, Figure 9.9, shows reasonably good agreement. It is somewhat ambiguous how to select the zero point on the length scale for the experimental and Vardy's results to give the proper comparison with the present calculation. In the present calculation, the flow about the model is considered to be incompressible and the speed of sound infinite. The pressures calculated by the model are plotted as if they were transmitted instantaneously to the station at which they are compared with the experimental and Vardy's calculated results. A refinement on this point is possible but has not been made. Therefore, an exact comparison on the length scale should not be expected.

9.2.2 Flared Entry Portal

Calculations are made for the three different model sizes run in the flare. Results for the 25% blockage ratio model are shown in Figure 9.10. Since Vardy did not provide results for this case, only comparison with experiment is possible. This comparison is not quite as good. The experiments give a somewhat lower pressure than the theory. One difficulty with this case is that the experimental results are not good. The trace shows a rather broad band instead of a well-defined line. The reason for this is the low pressure level which must be measured. Except for this experimental difficulty, it is not known why the agreement is not any better.

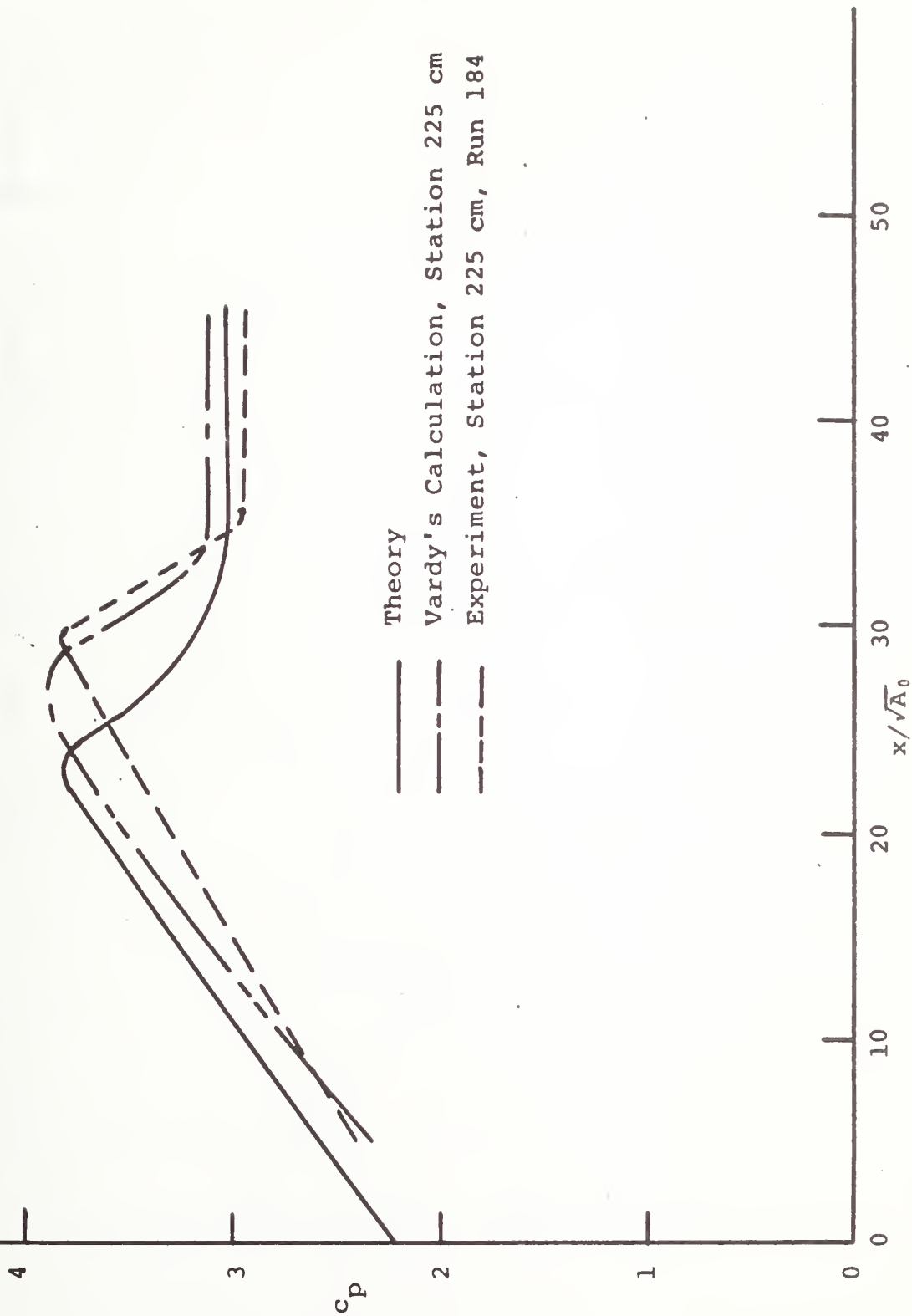


FIGURE 9-9. PRESSURE COEFFICIENT AS VEHICLE ENTERS TUNNEL; COMPARISON BETWEEN THEORY, VARDY'S CALCULATIONS, AND EXPERIMENT; $A_0 = 2.116 A_v$, $S = 24.44\sqrt{A_0}$, $c_f = .006$, $M_v = .07225$

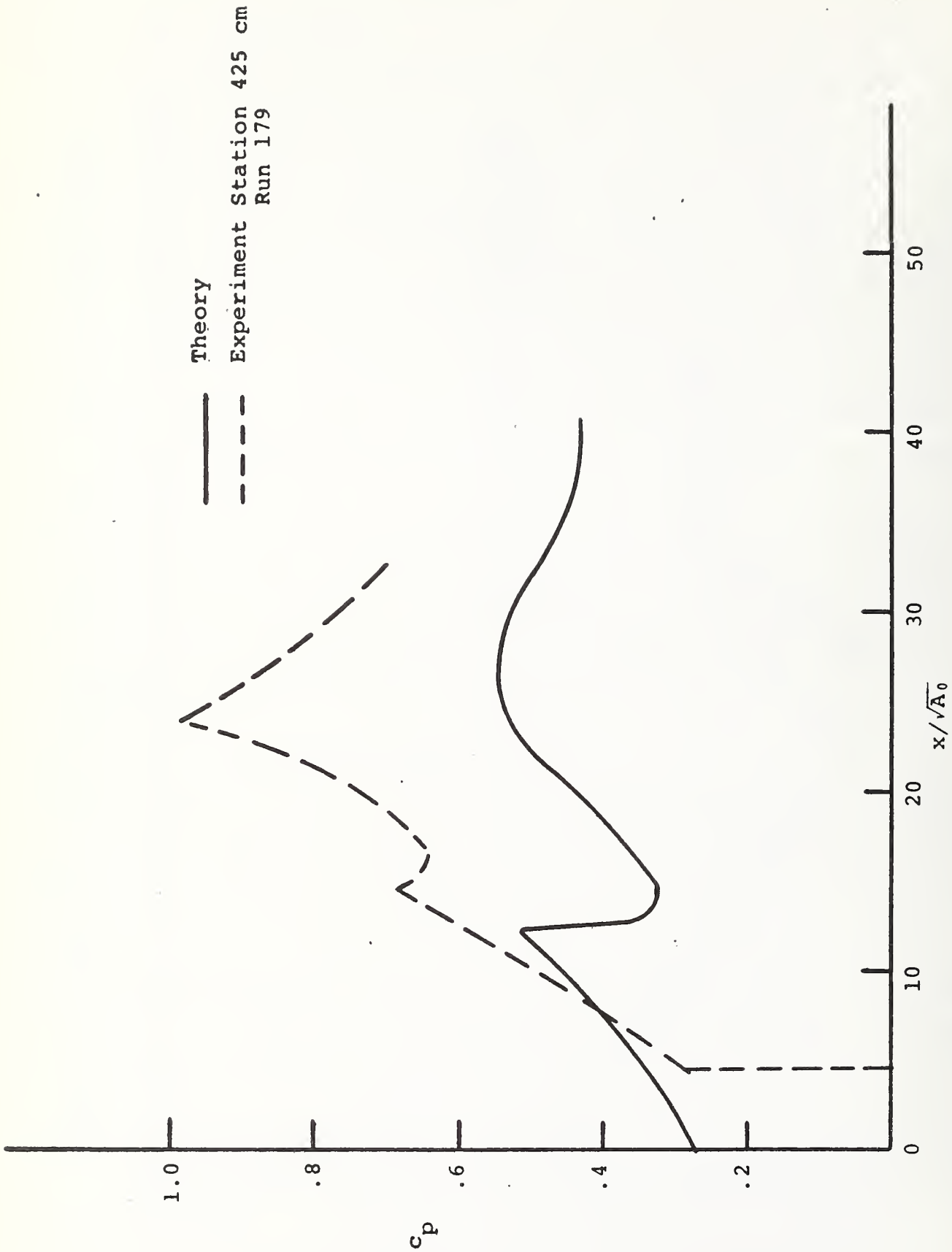


FIGURE 9-10. PRESSURE COEFFICIENT AS VEHICLE ENTERS FLARED TUNNEL; COMPARISON BETWEEN THEORY AND EXPERIMENTS; $A_0 = 4 A_v$, $S = 12.22\sqrt{A_0}$, $c_f = .006$, $M_v = .07225$

The 50% model case has also been calculated with much better results (Figure 9.11). Vardy's results show very good agreement with the experiment, and the present results agree well in the final pressure level but show some difference during the pressure rise as the model passes through the flare. The dip in pressure shown at $X/\sqrt{A_0}$ of about 12 to 14 is larger for the present theory than either of the other results and there is some discrepancy in the length scale as previously discussed.

The results for the 75% blockage ratio case are shown in Figure 9.12. Again, only a comparison with experiment is possible. The final pressure is somewhat above the experimental results, and the dip caused by the entry of the rear of the model is larger in the theory than the experiment. The agreement here is similar to that found for the 50% blockage ratio case.

9.2.3 Perforated Entry Portal

The pressure transients that are predicted for this case are compared with experiment in Figure 9.13. The results from the predictions by the computer model (Vardy) are included. The most important difference is the reduced rate of pressure rise as the vehicle enters the porous section. The slow rate of pressure increase as the vehicle passes down the porous section is caused by the fact that the rate of volume flow through the pores and annular area goes as the square root of the pressure. If all of the air must escape through the pores and the pore area is decreasing linearly as the vehicle approaches the end of the porous section, then it might be expected that the pressure would vary as the reciprocal of the square of the remaining porous length.

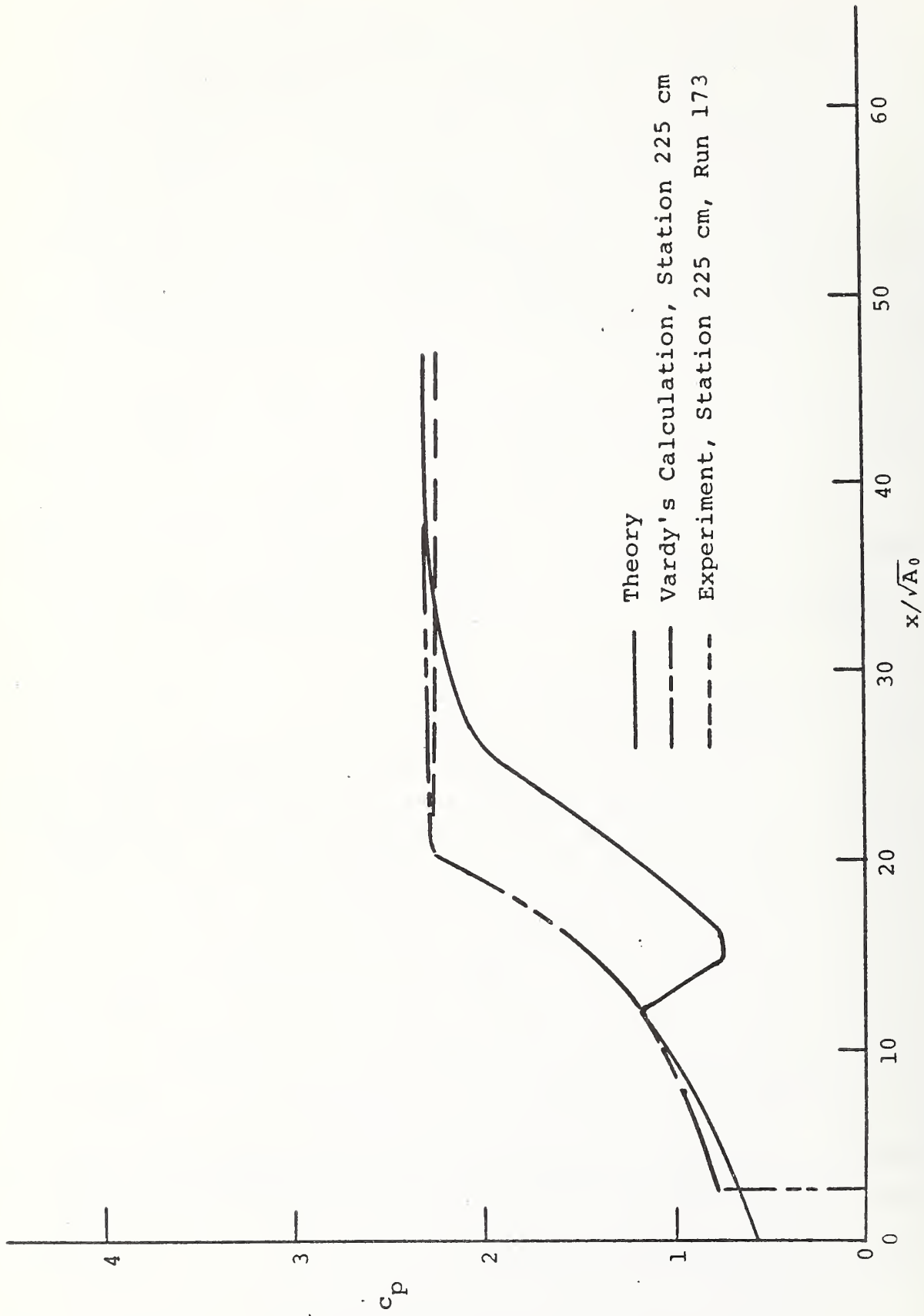


FIGURE 9-11. PRESSURE COEFFICIENT AS VEHICLE ENTERS FLARED TUNNEL; COMPARISON BETWEEN THEORY, VARDY'S CALCULATIONS AND EXPERIMENTS; $A_0 = 2.116 A_V$, $S = 12.22\sqrt{A_0}$, $c_f = .006$, $M_V = .07225$

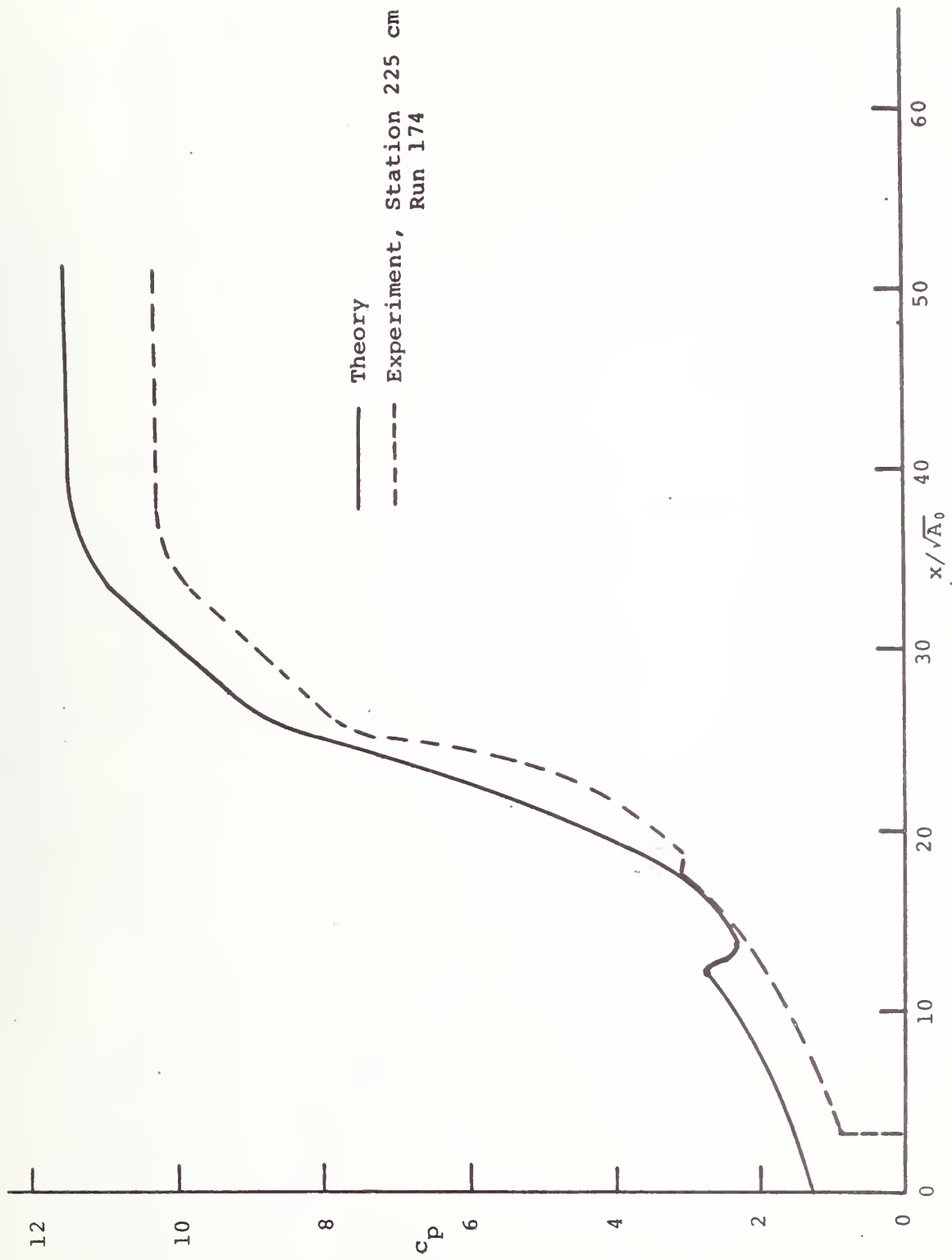


FIGURE 9-12. PRESSURE COEFFICIENT AS VEHICLE ENTERS FLARED TUNNEL, COMPARISON BETWEEN THEORY AND EXPERIMENTS, $A_0 = 1.309A_V$, $S = 12.22\sqrt{A_0}$, $c_f = .006$, $M_V = .07225$

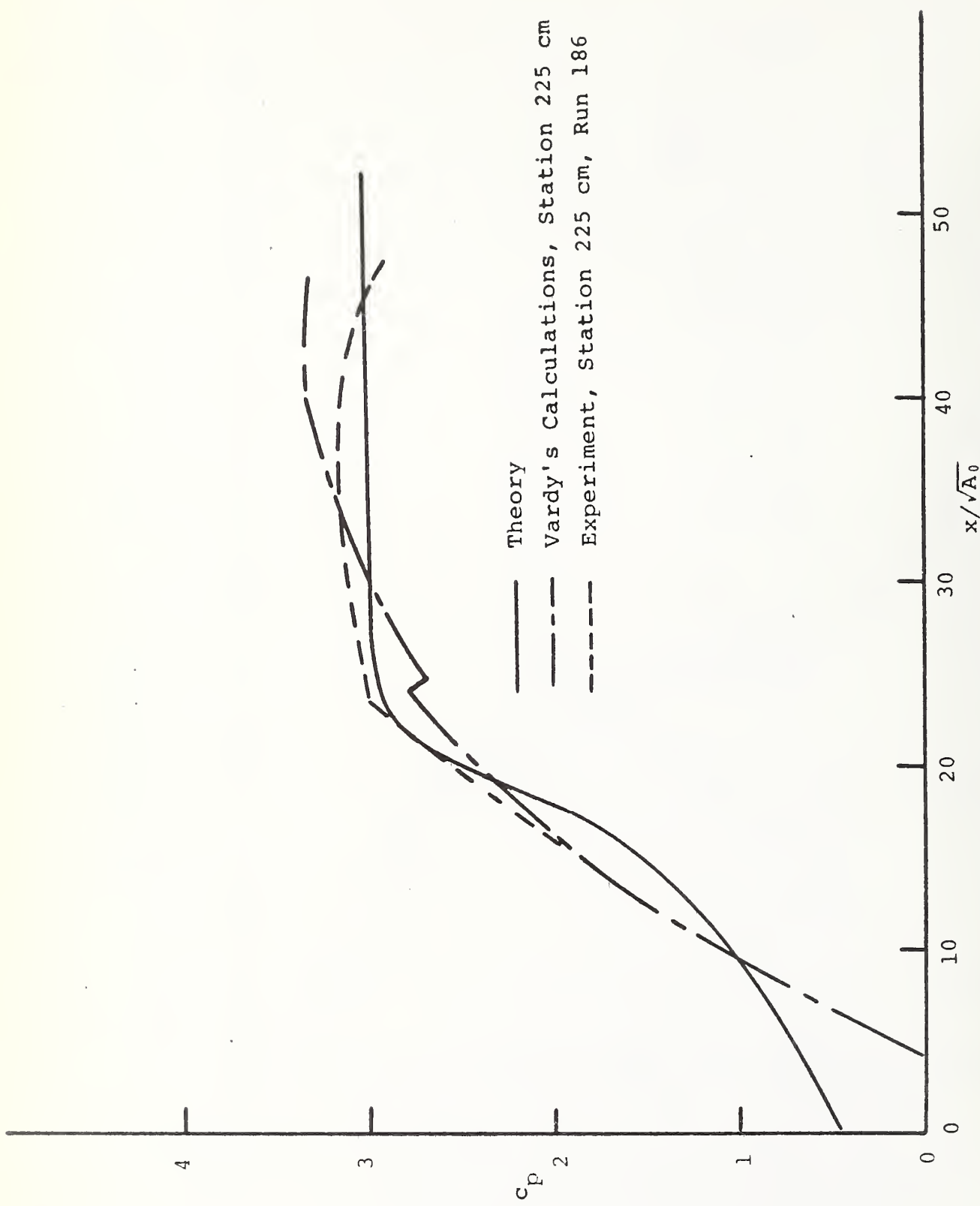


FIGURE 9-13. PRESSURE COEFFICIENT AS VEHICLE ENTERS POROUS TUNNEL; COMPARISON BETWEEN THEORY, VARDY'S CALCULATIONS, AND EXPERIMENTS; $A_0 = 2.116 A_V$, $S = 24.44/\sqrt{A_0}$, $c_f = .006$, $M_V = .07225$

10. APPLICATION TO FULL-SCALE SYSTEMS

The model used in the laboratory experiments is representative of a full-scale tunnel with the same length/"diameter" ratio. The results obtained from it may be regarded as indicative of the pressure histories in the full-scale tunnel except for probable differences in the skin friction. Additionally, those parts of the pressure traces which precede the arrival of wave reflections from the exit portal are typical of any tunnel whose length/diameter ratio is at least as great as that of the model. For the purposes of this study, these early portions of the traces are especially valuable.

In the extension of the work to full-scale situations, it is equally useful to retain generality by avoiding complications due to reflections arriving from downstream. All the results presented in this section refer to this situation. Thus, only waves generated in the upstream region of the tunnel systems are considered, and this is achieved by treating the tunnels as semi-infinite ducts.

Two systems are considered, one simple and one complex. Neither is an exact simulation of any known system, but the two closely resemble the conditions found in the Berkeley Hills Tunnel and the Transbay Tube under San Francisco Bay of the BART system.

Skin friction coefficients on the train and tunnel walls are again specified by means of effective roughness heights which are used in steady state expressions based upon instantaneous unsteady velocities. Values of 10 mm and 50 mm have been chosen for the train and tunnel, respectively. It is believed that these are reasonable approximations, but full-scale measurements are required before accurate figures can be deduced. Until then, no confidence can be placed in the exact values

predicted for the pressure magnitudes in the tunnels. Nevertheless, this does not detract significantly from the usefulness of the conclusions drawn in the remainder of this section. These will remain valid for real tunnels even if they have very different roughnesses.

10.1 Simple Tunnel Configuration

A simple tunnel (Figure 10.1) is considered with no airshafts or special entrance region. This situation is representative, for example, of the Berkeley Hills Tunnel in which entry effects are largely independent of downstream departures from this simple configuration. The flared entrance region on that tunnel is too short to be effective.

Figure 10.2a depicts pressure histories when a 150-m long, 10-m^2 train enters a 20-m^2 simple tunnel at 35.763 m/s (80 mph). The graph shows the pressures on the nose of the train (upper curve) and at the front (middle curve) and rear (lower curve) of the annulus. Figure 10.2b shows the pressure histories at various positions in the tunnel, 150 m from the original entrance portal (left), 300 m (middle), and 450 m (right). The histories are very simple. They are similar to those for Run 184 in the laboratory tests. It is clear that the recommended comfort criteria are violated both along the train and inside the tunnel.

We now consider how these pressure histories might be improved by modifications of the type considered in the laboratory program.

Figures 10.3 and 10.4 illustrate the pressure histories at the same positions when the tunnel is equipped with 200-m long perforated and flared entrance regions respectively. The length of 200 m is currently believed to be within sensible economic limits. The total porosity in the walls of the perforated region is 50% of the tunnel cross-section

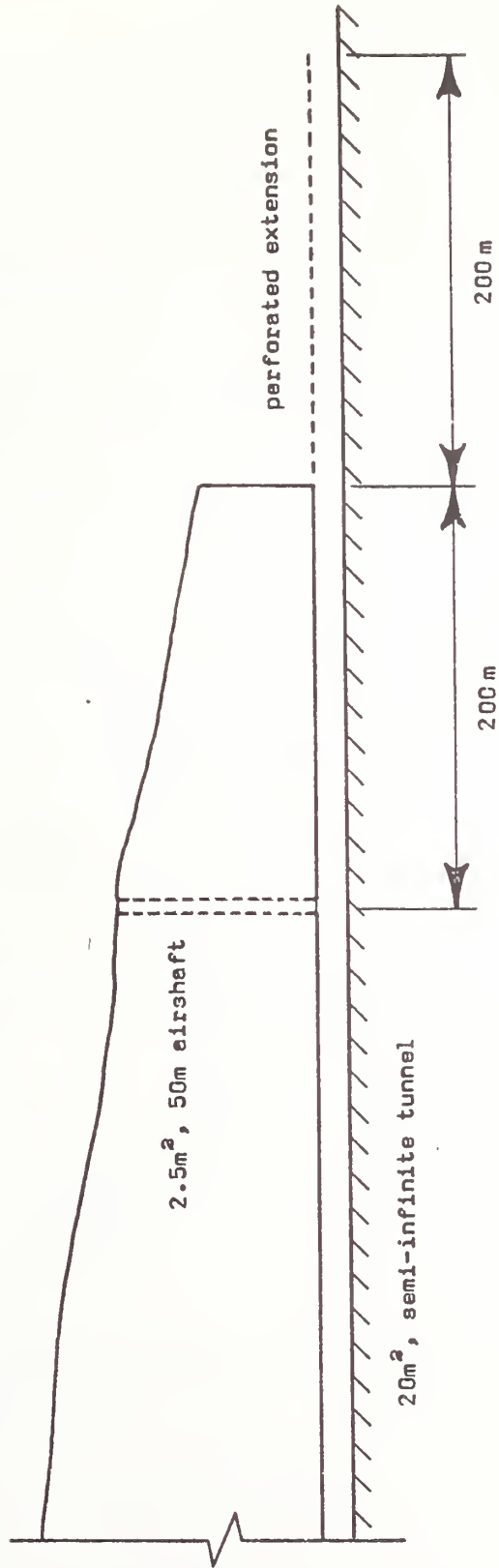


FIGURE 10-1. DIAGRAMMATIC REPRESENTATION OF IMPROVED TUNNEL ENTRANCE REGION FOR A SIMPLE TUNNEL

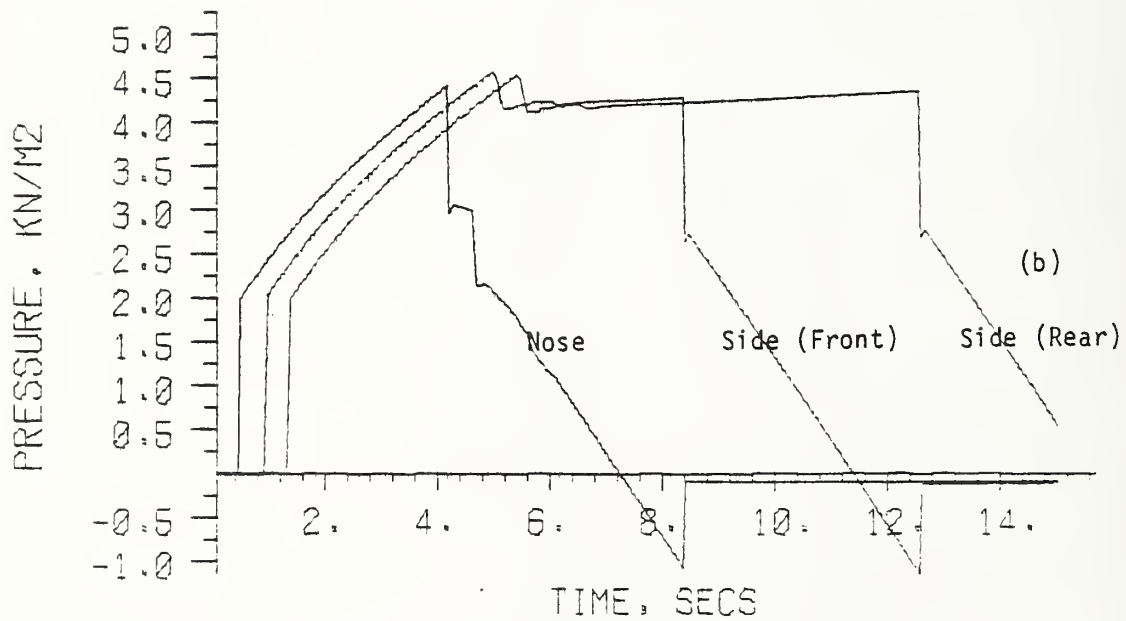
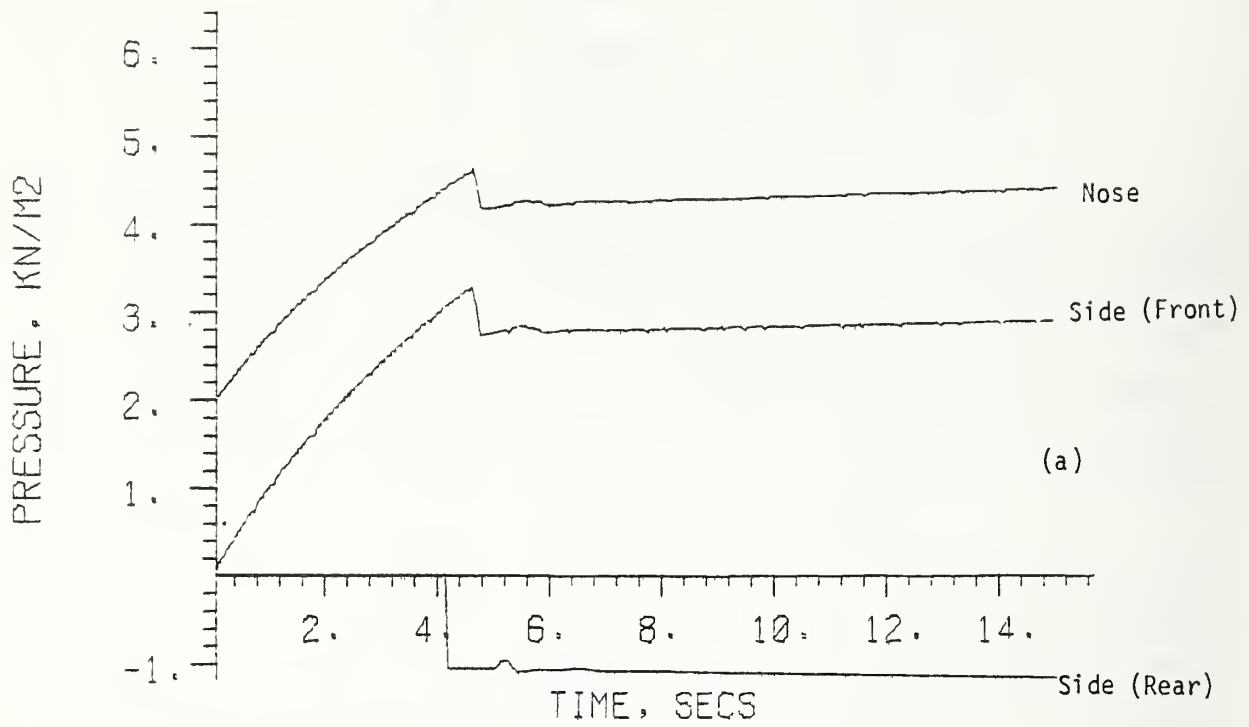


FIGURE 10-2. BERKELEY HILLS SIMULATION

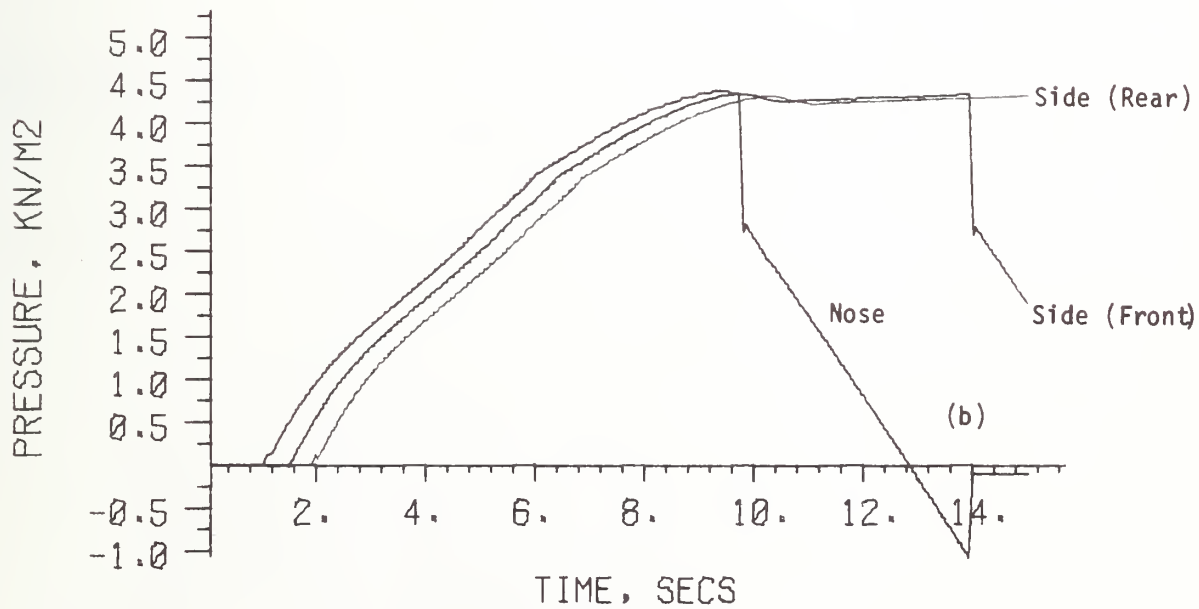
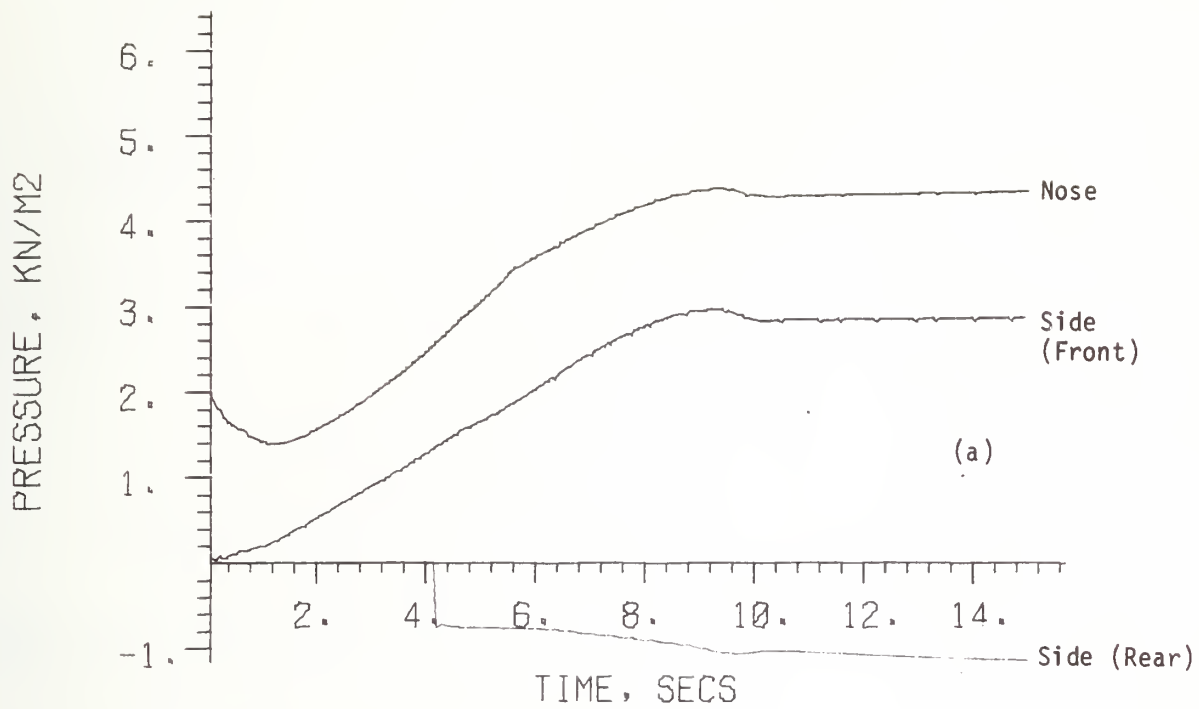


FIGURE 10-3. BERKELEY HILLS AND PERFORATED EXTENSION

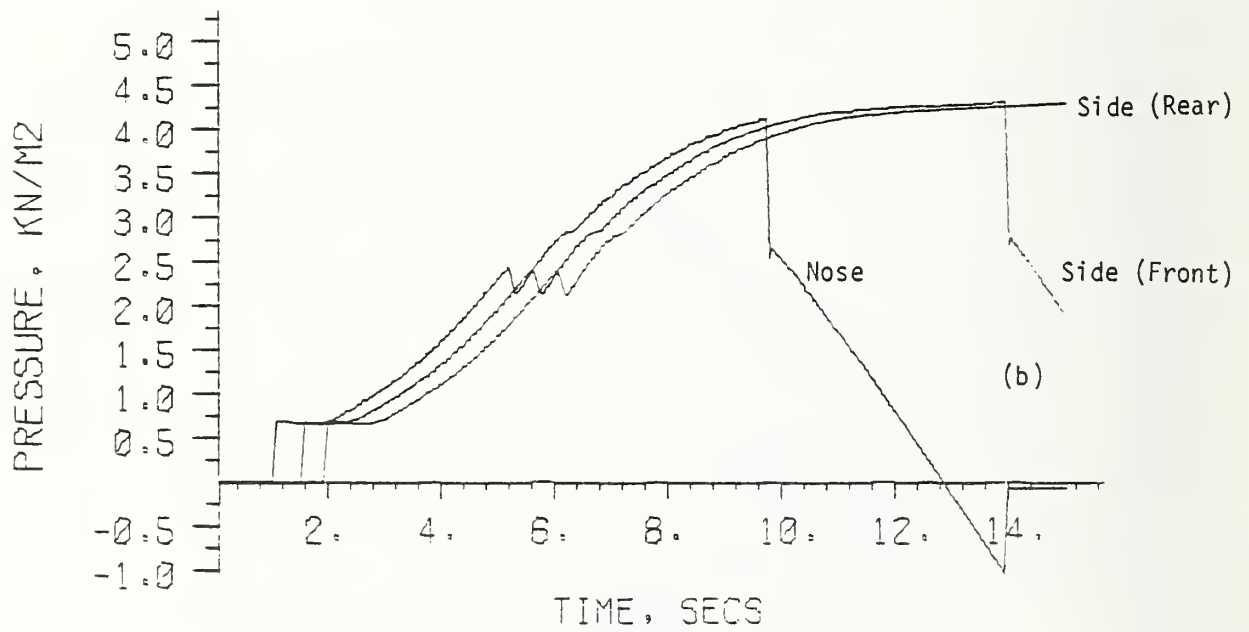
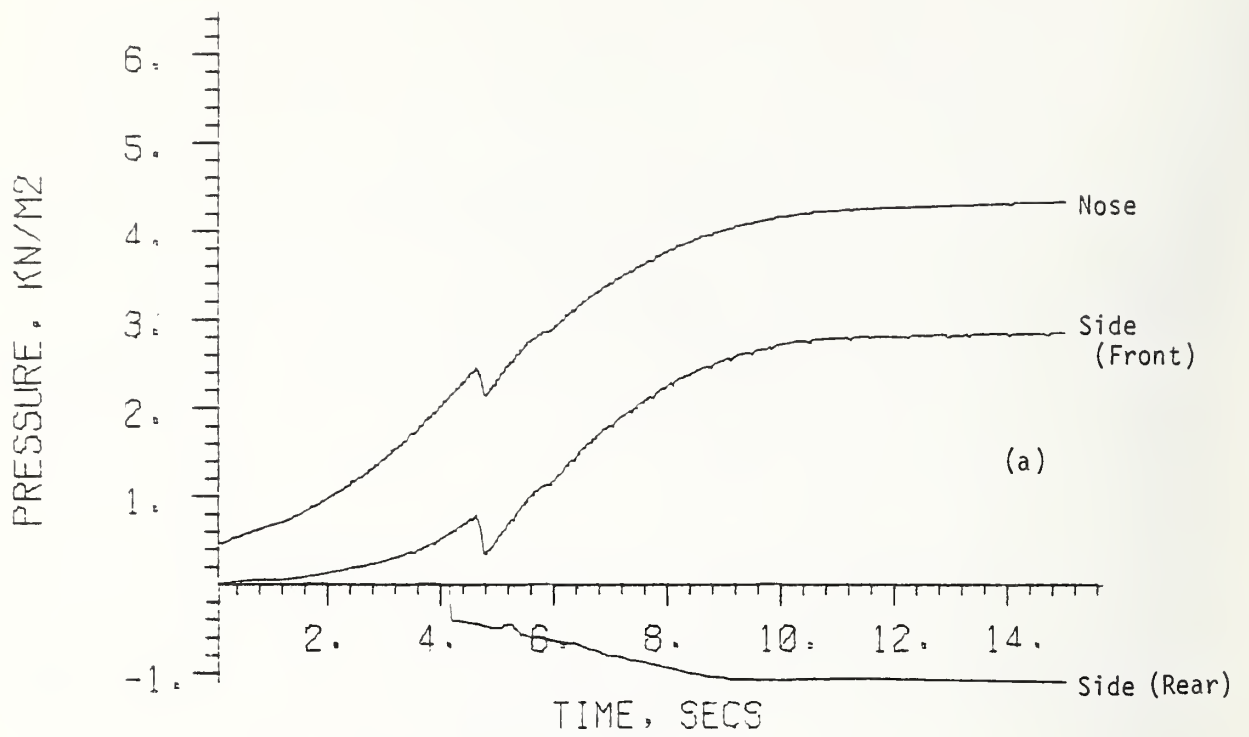


FIGURE 10-4. BERKELEY HILLS AND FLARED EXTENSION

and this is evenly distributed along the region. The portal area of the flared entrance is 50 m^2 and the increase in area along the flare is proportional to the square of the distance from the original portal.

Both modifications yield a considerable improvement in the pressure histories. Along the train, the histories are well within the comfort limits except for the rear of the train at entry into the perforated extension. That special case just violates the step-change criterion, but this could be remedied by a small build-up at the tail. Inside the tunnel, the improvement is sufficient to render the pressure histories acceptable except during the period when the train passes the point in question.

Further improvements to the pressure histories can obviously be gained by using longer entrance regions because smaller pressure gradients will result. An alternative method of achieving the same result, however, is to include a small-bore airshaft downstream of the entrance region. Such a circumstance is illustrated in Figure 10.1, and the corresponding pressure histories are shown in Figure 10.5. It is clear that the pressure fluctuations alongside the train take place only very gradually. So do those in the tunnel except when the train passes by. Even then, the situation upstream of the airshaft is far more satisfactory than in the simpler tunnels. It should be noted that no attempt has been made to optimize the position of the shaft along the tunnel.

The choice between a long perforated or flared extension and a shorter extension in conjunction with an airshaft will be based upon economic as well as aerodynamic considerations. Usually, shafts are comparatively expensive, but this may not be the case when a total cross-sectional area

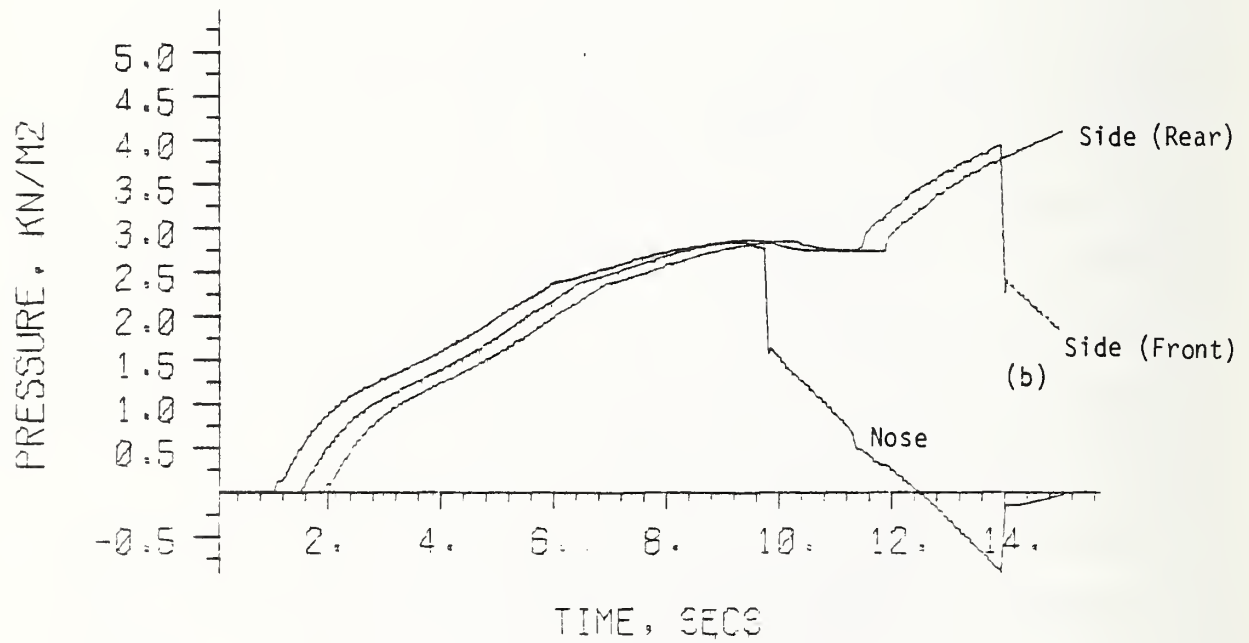
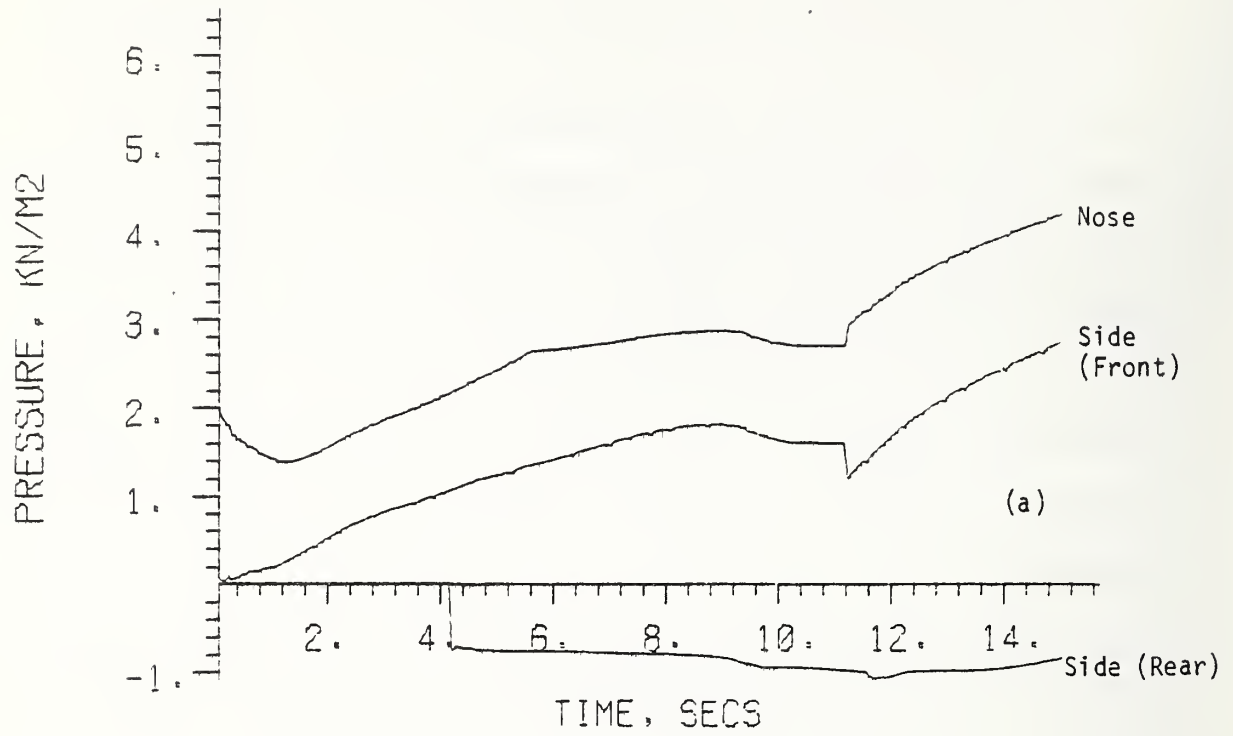


FIGURE 10-5. BERKELEY HILLS EXTENSION AND SHAFT

as small as 2.5 m^2 is all that is required. This might well be provided by means of several very small bore shafts which could be produced very cheaply. Of course, it is not necessary for the shafts to be close together. Indeed, there would be aerodynamic advantages to be gained from spacing them several tunnel diameters apart.

10.2 Complex Tunnel Configuration

The computer program has been shown to handle the entry of a train into a tunnel very well even when the tunnel is not simple. It is therefore reasonable to place confidence in its predictions for configurations which are even more complex than those investigated in the laboratory program. The tunnel system shown in Figure 10.6 is chosen as an example of a complex network. It may be recognized as resembling the Transbay Tube under San Francisco Bay, particularly the Oakland end where high-speed entry would currently cause very large pressure transients inside trains. It would be desirable to modify that tunnel to permit vehicle entry at 80 mph.

Figure 10.7a shows the pressure histories on a train (upper curve for nose; middle for side-front; lower for side-rear). Figure 10.7b shows the pressure histories in the tunnel complex at the positions A, B, C, of Figure 10.6 when an 80-mph train enters the basic system with no entrance extension. Violations of the comfort criteria for passengers occur at entry and also when the train passes by the airshafts. Also, rapid pressure changes occur when the vehicle passes by the three dampers in the dividing wall between the main running tunnels downstream of the shafts. Even bigger violations occur inside the tunnel, particularly when the vehicle itself passes by the point considered.

The equivalent pressure histories are shown in Figures 10.8 through 10.11 for cases in which the tunnel system is modified in various ways. In Figure 10.8, the influence of a 206.25-m long perforated entrance in front of the original portal is shown. By inspection, it is seen that this greatly improves the pressure histories caused by train entry, but that it

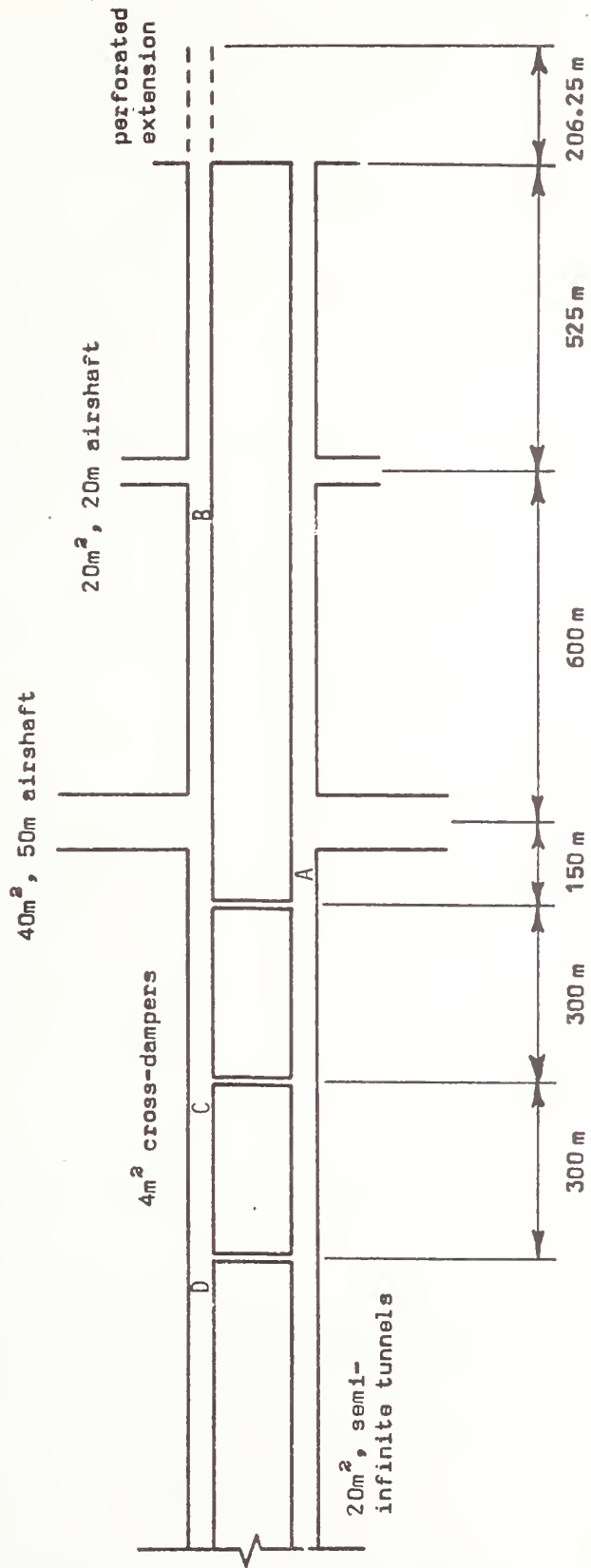


FIGURE 10-6. DIAGRAMMATIC REPRESENTATION OF COMPLEX TUNNEL

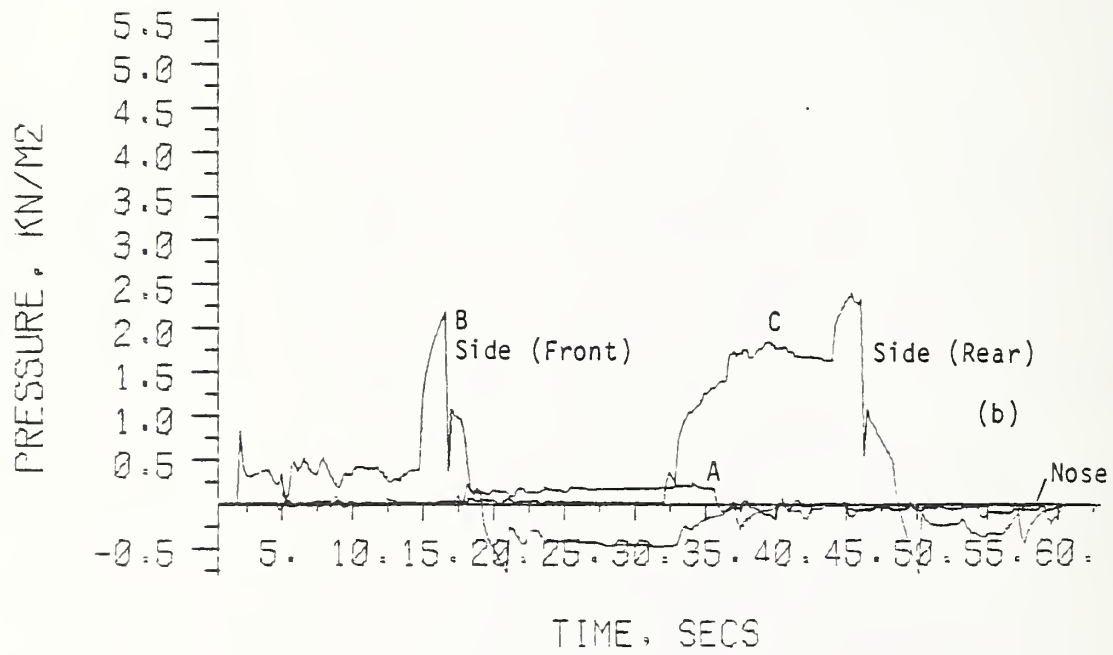
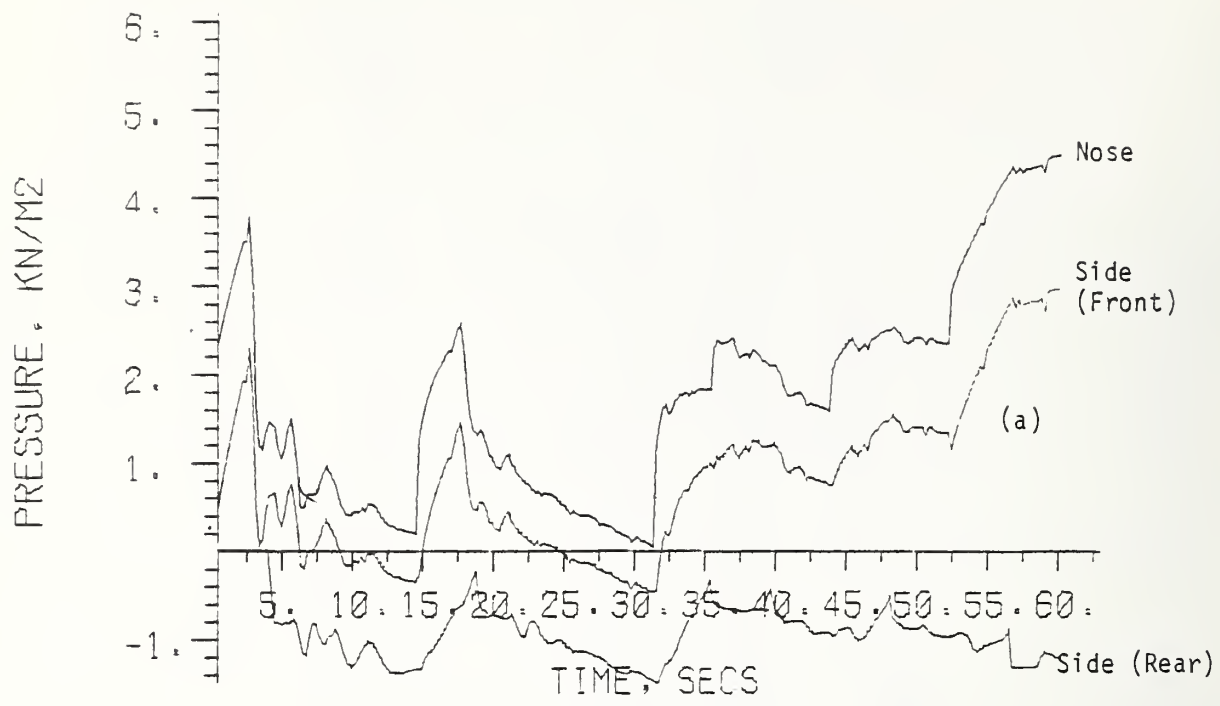


FIGURE 10-7. TRANSBAY TUBE SIMULATION

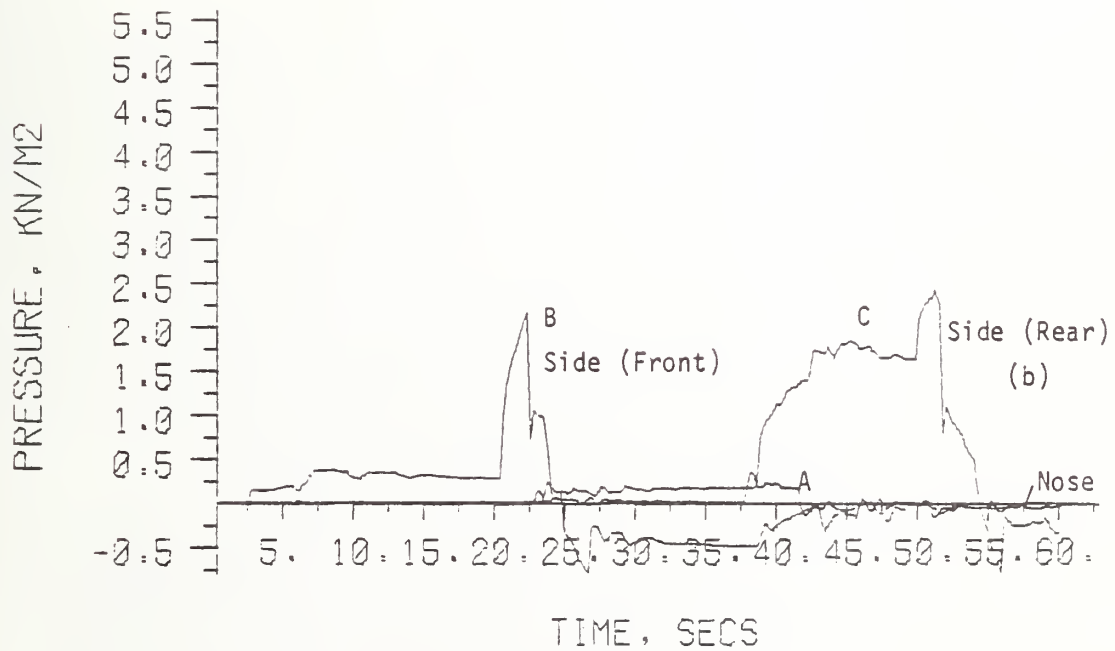
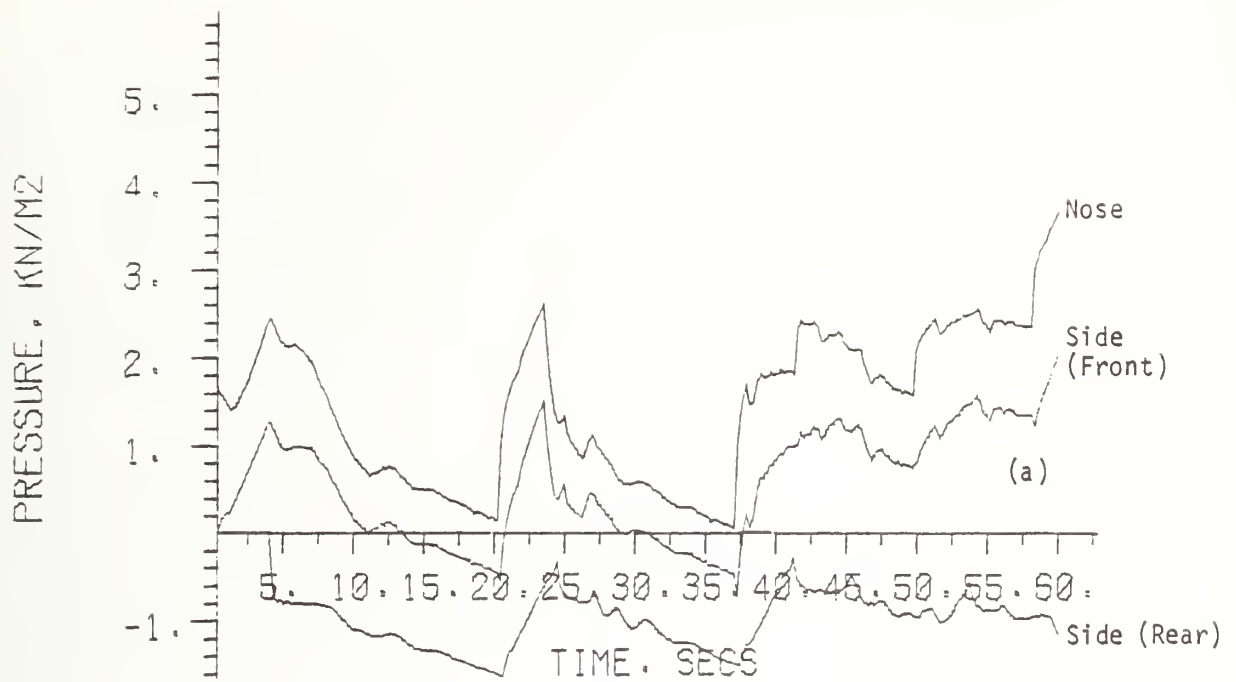


FIGURE 10-8. TRANSBAY AND PERFORATED EXTENSION

has negligible influence on the subsequent parts of the pressure histories. Clearly the pressure fluctuations produced at the shafts will be best alleviated by modifications to the shafts themselves. Figure 10.9 shows the histories when the flow through the shafts is restricted by means of orifice plates in which the holes are only 2.5 m^2 in cross-section. A considerable improvement is apparent, but once again the pressure histories at other parts of the journey are negligibly different from the original case.

The advantages to be gained from reducing the area of each of the cross-dampers from 4 m^2 to 2 m^2 are shown in Figure 10.10, and the combined influence of all three types of modification is illustrated in Figure 10.11. It appears to be a general rule that each trouble spot must be tackled separately from the others when they are initially greatly separated from one another.

No attempt has been made to optimize either the areas of the dampers or the areas of the orifices in the shafts. Nevertheless, a big improvement has already been obtained in the pressure histories experienced by passengers. It is reasonable to suppose that additional improvements could be obtained with relative ease, for example by building up the train rear. Also, a sensible compromise between ventilation requirements and the need to reduce pressure transients is within reach.

With the single exception of the tail-entry wavefront close to the rear of the train, the pressure histories alongside the train (in Figure 10.11) satisfy the recommended comfort criteria. As with the simple tunnel configuration, however, the pressure histories at points inside the tunnel system do not satisfy these criteria, especially when the train passes by.

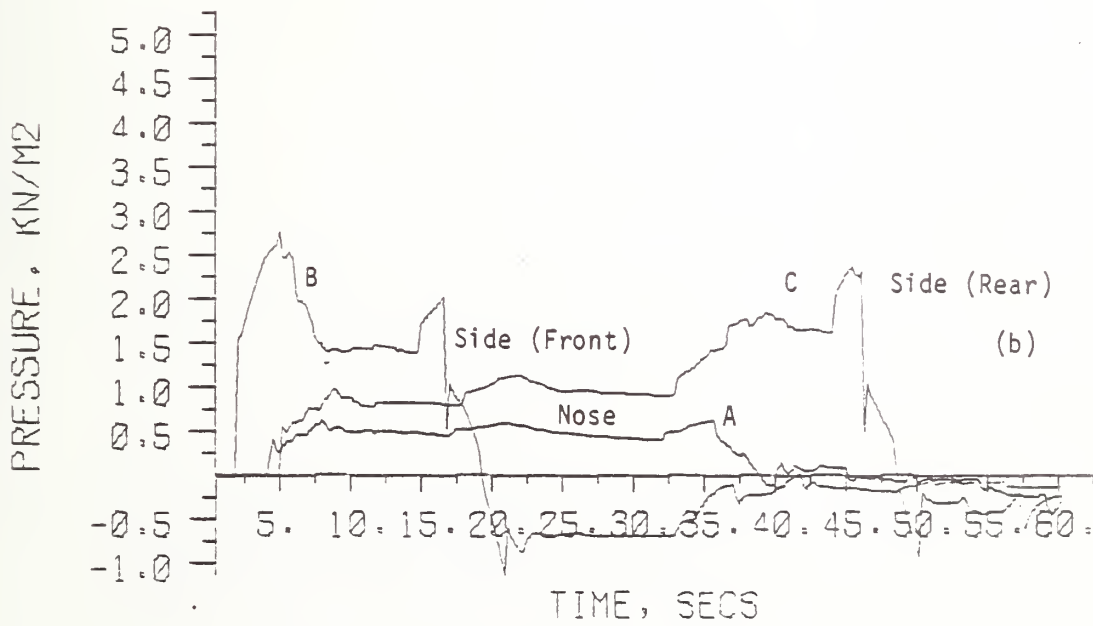
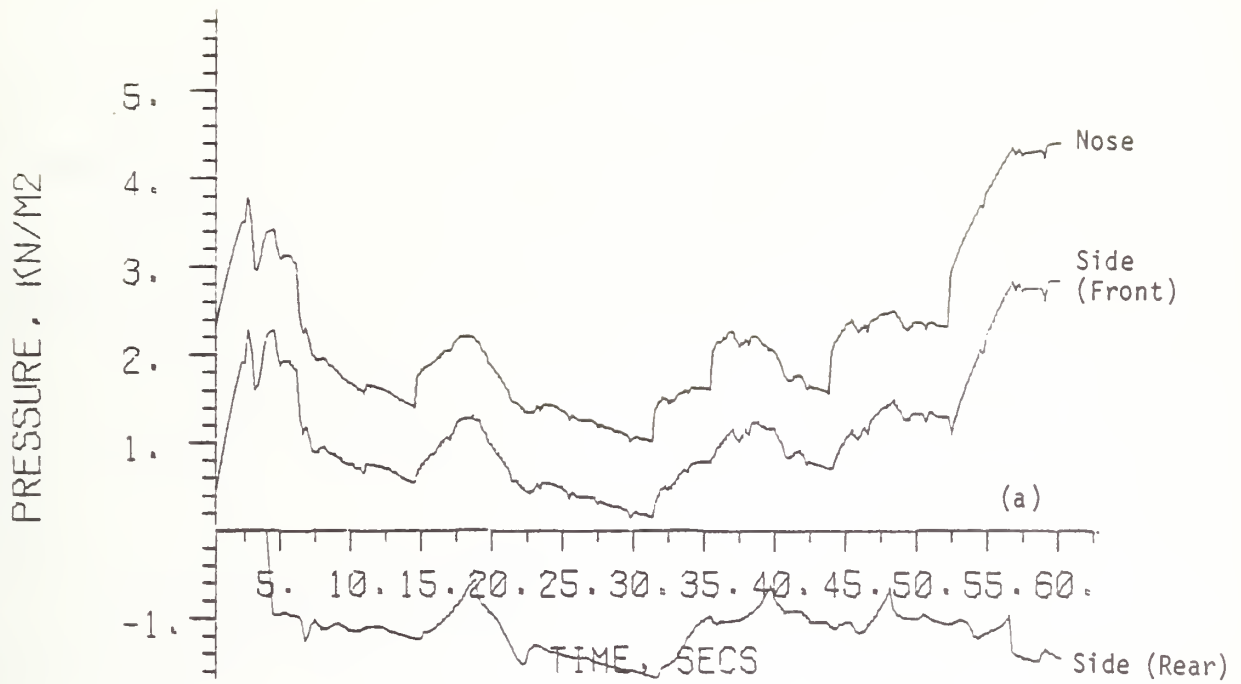


FIGURE 10-9. TRANSBAY AND ORIFICE PLATES IN SHAFTS

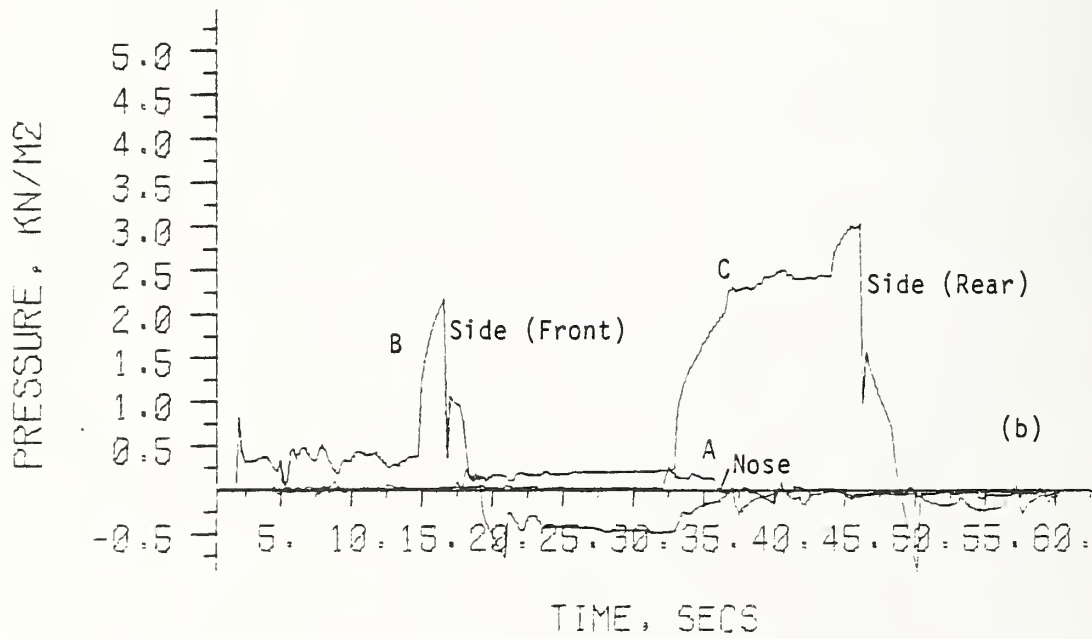
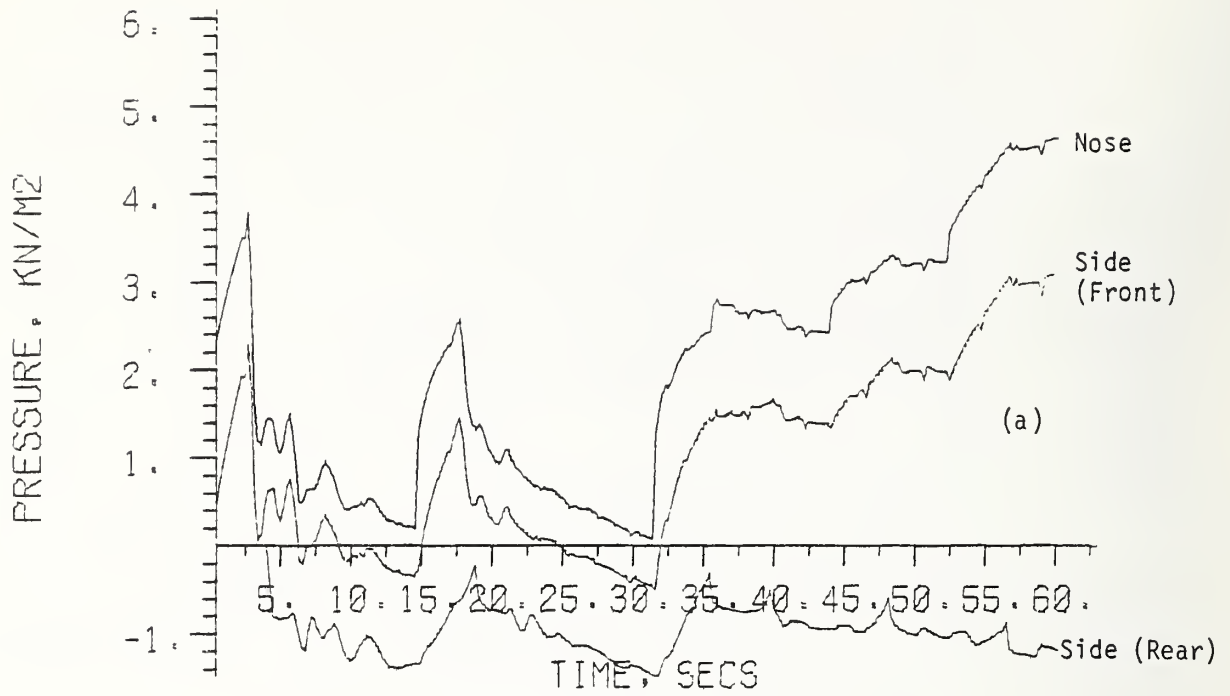


FIGURE 10-10. TRANSBAY WITH SMALLER CROSS-DAMPERS

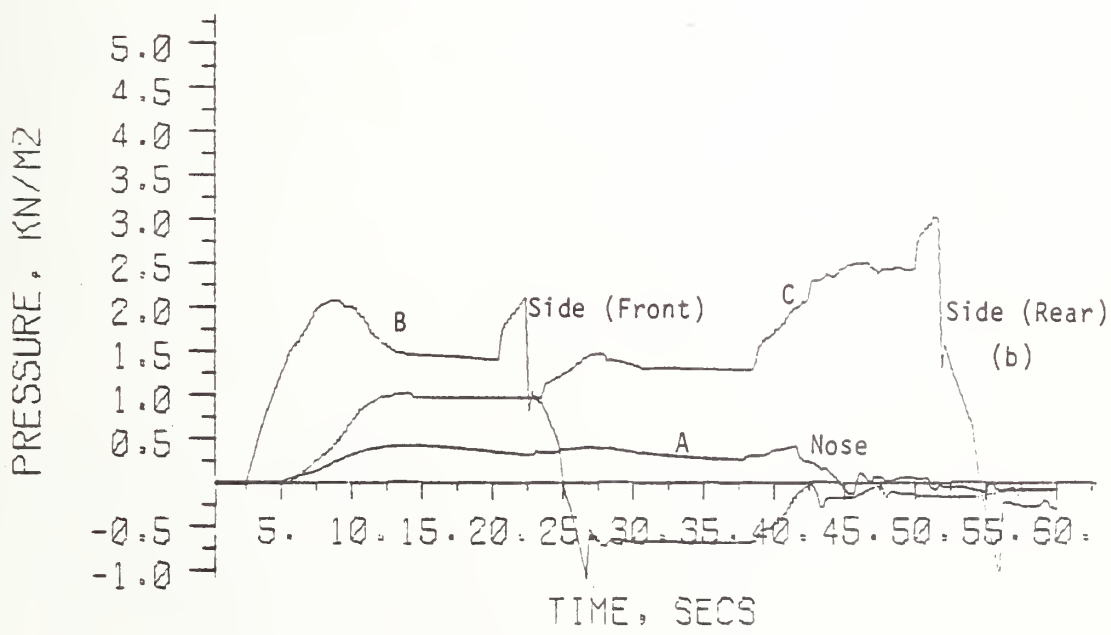
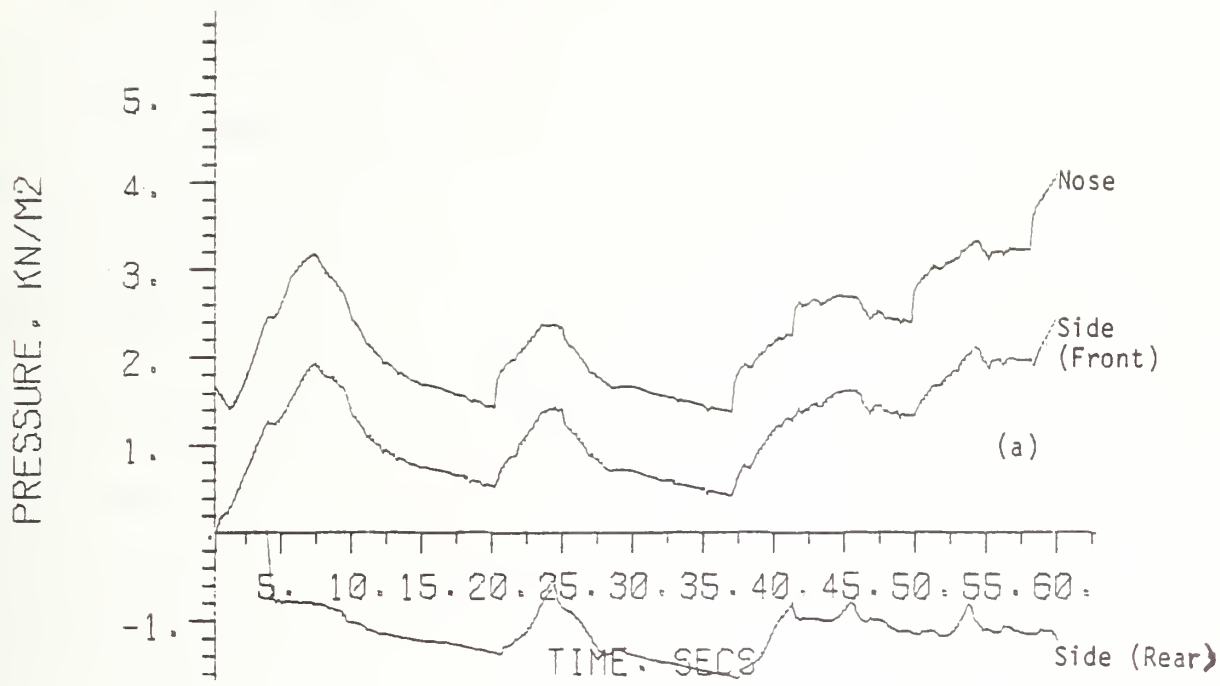


FIGURE 10-11. TRANSBAY AND ALL THREE MODIFICATIONS

It is not currently obvious how this difficulty may be overcome except by reducing the train speed. However, it may be argued that these pressure histories are of less importance than those alongside the train because personnel will not normally be present within the tunnel. It would appear to be entirely realistic to specify less restrictive comfort criteria for situations which will rarely occur than for events which will be experienced daily by thousands of passengers. With this proviso in mind, it may be concluded that adequate methods of alleviating pressure transients in both simple and complex tunnel systems have been demonstrated.

11. TRADE-OFF STUDY

In order to determine the effectiveness of the tunnel portal modification approach to the alleviation of pressure transients, it is necessary to make comparison with other possible approaches. The comparison was based upon already existing information. As a consequence, it is preliminary, but is considered adequate to give a general magnitude of the costs of each approach.

11.1 Cost Estimates for Modified Tunnel Portals

No formal estimates were made during this study on the costs of various approaches to modifying a tunnel portal to incorporate the flared or perforated sections. However, during several studies (Reference 11 and 12), related cost information was generated that was applied to this study.

These cost estimates should not be considered to be any more than indications of the general magnitudes. Nevertheless, they should be adequate for assessing the feasibility of portal modification.

11.1.1 Flared Portal

1.1.1.1 Internal to Tunnel

The original design of a tunnel can incorporate a flared portal that results from an increase in the cross-section area of the end of a mined tunnel. This is a fairly expensive feature as it requires specialized construction (handmining) procedures for a relatively short length of the overall tunnel. From Reference 11, the hand mining cost of a 5m D concrete-lined tunnel is estimated to be about \$8,200 per m in comparison to \$5,700 mined by a tunnel boring machine (TBM). The cost of hand mining a flared portal which gradually increases the effective diameter from 5 m to 8 m ($A_{\text{entrance}}/A_{\text{tunnel}} = 2^{1/2}$) over a length of 200 m, is assumed to on the average around \$10,700 per m. Since

the basic cost of the 5 m tunnel mined by a TBM is \$5,700 per m, the additional cost of one internally flared end is \$5,000 per m, which is the difference. This comes out to an additional cost of about one million dollars for a 200 m long internally flared portal.

11.1.1.2 External to Tunnel

Aside from the high cost of the internal flared portal, a more fundamental drawback exists. It may not be practical to retrofit an existing tunnel that is in operation with an internal flare. Train operation would have to be degraded if not interrupted. Therefore, the more practical approach for having a flared portal is probably to add an extension outside of the basic tunnel.

One approach to the design is to use precast concrete segments that make up into semi-circles of constant diameter. The variation in the cross-section area of the extended "tunnel" would be accomplished by placing this segment upon sloping walls. These walls would vary from 1.8 m high at the normal entrance to the tunnel to 7.2 m high at the tunnel entrance.

The cost of the upper semi-circle concrete segments can be estimated from information developed in Reference 12. The volume of concrete required would be

$$200 \text{ m} \times 2.5 \text{ m} \times 3.14 \times 0.2 \text{ m} = 3.14 \text{ m}^3$$

(length) (radius) (π) (thickness)

Assuming a foundation depth of 0.7 m with a thickness of 0.3 m, the volume of concrete required for the two sloping walls would be

$$200 \text{ m} \times (1.8 + 7.2) \text{ m} \times 0.3 \text{ m} = 540 \text{ m}^3$$

(length) 2 x (avg. ht.) (thick.) .

The total cost of concrete at \$45/m³ would be about \$40K. Using the Reference 6 ratio of 2.5 of total material costs to concrete costs (this includes the cost of reinforcing rod) the total material cost is about \$100K.

The cost to build the pre-cast sections and install them inside a tunnel is about \$40K per 200 m. Assume that this \$40K would apply to the curved portions with another \$40K for the sloping walls and \$20K for the foundation giving a total labor cost of \$100K. But because of the shorter length (200 m vs 3050 m), the labor is assumed to be doubled (i.e \$200K). Hence the total cost for one 200 m externally flared portal would be around \$300K. Even including reasonable estimation errors, the cost of an external portal is considerably less than an internal one.

11.1.1.3 Perforated Portal

It would not be practical to build an internal perforated portal as that would require a greatly enlarged tunnel diameter that would be fitted with a perforated inner liner of the same diameter of the rest of the tunnel. The cost of such a portal would be about the same cost as the internal flared one. Therefore, only an external extension will be considered.

The cost of the material would be arrived at as follows: The volume of concrete for the side wall and foundation would be

$$\begin{array}{r} 200 \text{ m} \times 2 \times 1.8 \text{ m} \times 0.3 \text{ m} = 216 \text{ m}^3 \\ , \\ (\ell) \qquad \qquad (\text{ht}) \qquad \qquad (\text{t}) \end{array}$$

Including the volume of the curved section, the total volume would be 265 m³. At 45/m³, the cost of the concrete would be \$24K. Applying the 2.5 factor to obtain the cost of all materials, the material cost estimate is \$60K.

The labor cost can be derived from the flared portal by eliminating the cost of the sloping walls, thus giving $2 \times (40 + 20) = \$120K$. The total cost estimate comes out to be \$180K.

11.1.2 Summary

The following tabulation summarizes the cost estimates (\$K) for one 200 m long external portal:

<u>TYPE</u>	<u>EXTERNAL</u>	<u>INTERNAL</u>
Perforated	180	1000
Flared	300	1000

From the analytical and experimental results of this study, the peak pressure pulse with a flared portal is some 20% less than that for a perforated portal of the same length. Hence a flared portal need be only 80% the length of a perforated portal, thereby dropping its \$300K cost down to \$240K. As this is still a third greater than the cost estimate for the perforated portal, the perforated portal extension is the most economical one.

11.2 Speed Restrictions

Historically, the approaches used to alleviate the tunnel entry pressure pulse effects on the train passengers was simply to restrict the train speed at entry. However, if this is accomplished by a decrease followed by an increase in the train's speed, the schedule time as well as the energy requirements increase. On the other hand, if the entire trip is made at the restricted speed, the energy requirements go down, but the schedule time increases even more. This latter aspect of speed restriction is not considered in the brief study of restricted speed that was carried out; neither is the aspect of allowing the train to coast down to the restricted speed.

The only aspect considered is the deceleration from cruise speed down to the restricted speed at the normal braking rate and the immediate acceleration at full power back up to cruise speed. However, consideration must be given to the necessary tolerances in order to insure that the train is at the restricted speed at the time of tunnel entry or exit. This can be accomplished by lowering the restricted speed below that of the threshold of alleviating the pressure pulse problems; or by initiating the deceleration phase somewhat in advance, thereby allowing the train to travel at the restricted speed for a nominal distance.

11.2.1 Computer Program

A computer program (called TEPTRR) was derived from the study of Reference 6. Realistic train characteristics such as weight, rotational inertia, aerodynamic and mechanical rolling resistances, motor and braking characteristics were used. No account was included for tapering the ends of the braking or the acceleration phases as the effects upon both time and energy are quite small. The basic Davis coefficients were used for the mechanical rolling resistance.

11.2.2 Results

In order to develop a better perspective on the effects of the speed restriction approach, two train configurations were included in the study: An 80 mph subway system and AMTRAC. A brief description of the characteristics of these trains appears in Table 11.1.

TABLE 11-1. TRAIN CHARACTERISTICS

TRAIN TYPE		CARS		
		TYPE	WEIGHT (KLB)	NBR
U.S. High-Performance Subway (BART, MARTA, WMATA)		MU 4-Axles each Axle powered	75	4
AMTRAK	Standard (Current	"	170	6
N-E Corridor (NY-DC)	High Performamnce	"	170	6

The 80 mph subway train would lose at least 3.5 seconds each time in order to restrict its speed to 60 mph at tunnel entry. Assuming a 1-second contingency (352 ft), the increase in travel time per slow-down would be 4.5 seconds. The traction effort energy increase would be about 12.7 KWH $[(10.65-0.09) \times 1.2]$ while the net braking would be about 7.3 KWH. The corresponding quantities for the current AMTRAK N-E Corridor (NY-DC) train would be about 43 seconds and 125 KWH for slowing down to 60 mph from 120 mph (assuming 1,000 feet of contingency). These examples represent typical situations.

11.3

Sealed Cars

One way of alleviating pressure pulses for the train passengers during tunnel entry is to have the cars sealed when they enter the tunnel. This is done for the high-speed Tokaido line trains in Japan. It is our understanding that the cost is significant and the sealing system requires continual attention. British Rail is considering sealing their proposed high-speed trains. The sealing requirements they established are more severe than for current passenger airplanes.

The train car's air-conditioner system must be isolated from the outside during the pressure pulse period. The door sealing problem for train cars is more difficult than for airplanes. Furthermore, the door problem of a subway car, which is continually being opened, is more severe than for a train car. There is no doubt that it would be quite costly to reliably seal train cars, and even more costly to do so for subway cars. A reasonable estimate would be on the order of \$100K per car.

Although sealed cars can insure the comfort of the riders, there are definite disadvantages. The pressure pulses generated upon entry to the tunnel are imposed all along the length of the tunnel. This would affect people working in the tunnel or passengers on a platform located in the tunnel. Also, the effects of the pressure transients upon the many structural elements must be considered.

11.4

Initiate Flow in Tunnel

When a series of trains travels through single-track tunnels, air flow through the tunnel is established. This air flow can cause a significant decrease in the entry pressure pulse that the train passengers or people within the tunnel will perceive. Run 205 shows this dramatic effect. But

if the schedule of trains through the tunnel is infrequent, then an on-site ventilation system would be required to initiate the air flow. From the information derived during a study for the DOT (Reference 11), the cost of adding such a system would be at least \$500K if done in a conventional ventilation shaft manner. The capital cost could probably be decreased by designing a fan system specifically for the purpose of initiating the flow. However, many tunnels already have a ventilation system that can probably be used for this purpose with little, if any, modification. The capital and operating costs as well as the operational aspects of such an approach require considerably more study before any opinion can be formulated on the costs or effectiveness of such an approach.

11.5 Comparisons of Approaches

Only a first-cut comparison will be made. The general items which should enter into the consideration will be indicated. The assumption was made that the rate of pressure rise inside the cars will be held to a tolerable limit. In an actual case, should this not be entirely practical to do for the tailored tunnel, it can be complemented by a partial speed-restriction approach. The direct and indirect costs of each approach are estimated. These estimates should suffice to demonstrate the important trade-off principles.

The maximum instantaneous pressure pulse inside the train is limited to 0.41 kN/m^2 (0.06 psi) (Reference 13) plus a maximum rate of $0.34 \text{ kN/M}^2/\text{s}$ (0.05 psi/s). This is shown in Figure 11.1 by the line labeled "limit". From the computer results of Section 10.1, it can be seen that an entry speed of 80 mph results in a pressure pulse which exceeds the suggested limits for passengers riding in a typical train. Restricting the entry speed to 60 mph will decrease the entry pressure pulse to below the limit. The use of a

80 mph 50% Blockage
150-m Long Train
200-m Long Portal Extension

(Theoretical)

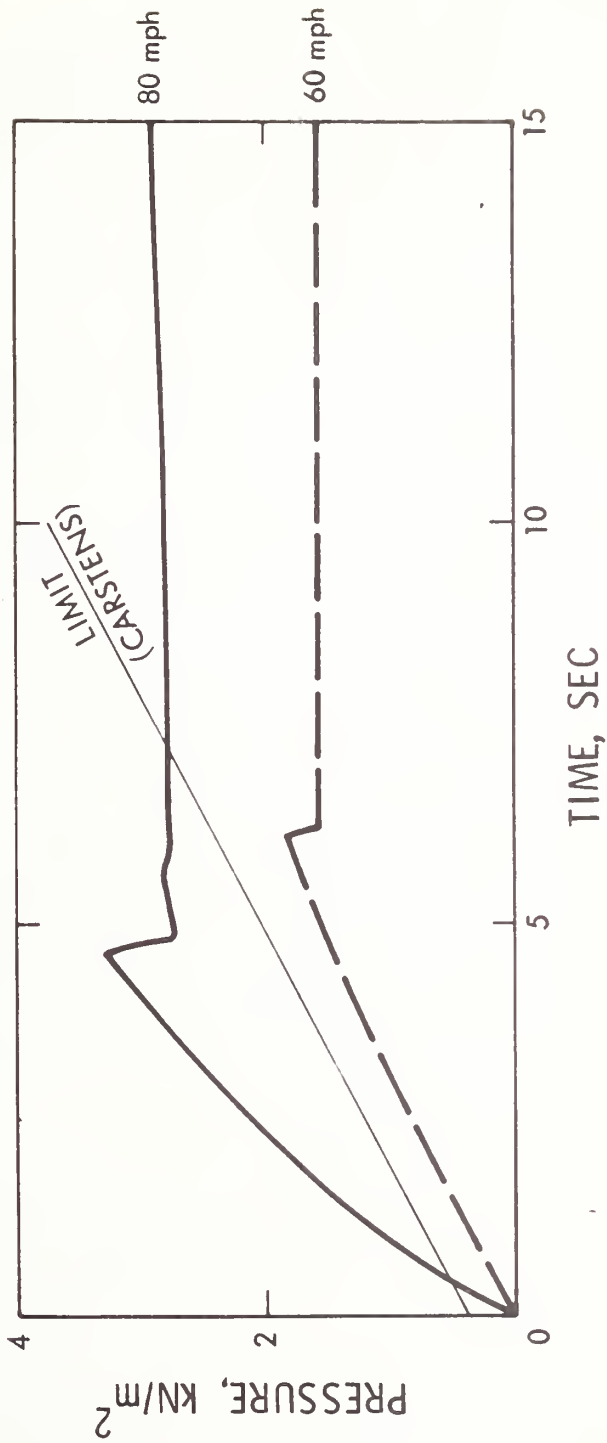


FIGURE 11-1. EFFECT OF TRAIN SPEED PRESSURE TRANSIENTS EXPERIENCED BY RIDERS ON TRAINS ENTERING TUNNELS

200-m long extension to the entry portal can keep the entry pressure pulse that the passengers sense below the suggested limit. This is shown in Figure 11.2.

The comparison of the costs of several approaches to the alleviation of the entry pressure transient is shown in Table 11.2. The "No Speed Restriction" case utilizes the 200-m long, 50% porous constant-diameter portal extension. In order to make a fair cost comparison with the restricted speed approach, it is necessary to put some arbitrary value on the time increase. This was done assuming \$5/hour for each of the 100 passengers aboard the 4-car subway train and is shown as "people".

There are two ways of restricting train speed: the first is to limit station-to-tunnel speed at 60 mph; the second is to allow train to accelerate to 80 mph; and then brake or coast to 60 mph. The least increase in time for the first is 11 seconds if there is enough distance (about 4,000 feet) for the train to attain a speed of 80 mph prior to reaching the tunnel. The other speed restriction approach could apply if the distance is great enough for the train to come up to a speed of 80 mph and then slow down to 60 mph before entering the tunnel and then back up to 80 mph. This has considerable effect on the required energy, both traction effort (TE) and braking (BE) and increases the travel time by about 5 seconds.

Costing out the TE at 5¢/kWh and the BE at half that, it is apparent that the yearly energy costs exceed the effective yearly cost (10% of the total) of the portal extension. When the cost of the passengers "lost" time is considered, the total yearly costs (direct and indirect) of the restricted-speed-approaches significantly exceed the assumed yearly amortization cost of the 200-m long perforated portal extension (by a factor of five as per the data in Table 11.6).

80 mph 50% Blockage
150-m Long Train
200-m Long Portal Extension

(Theoretical)

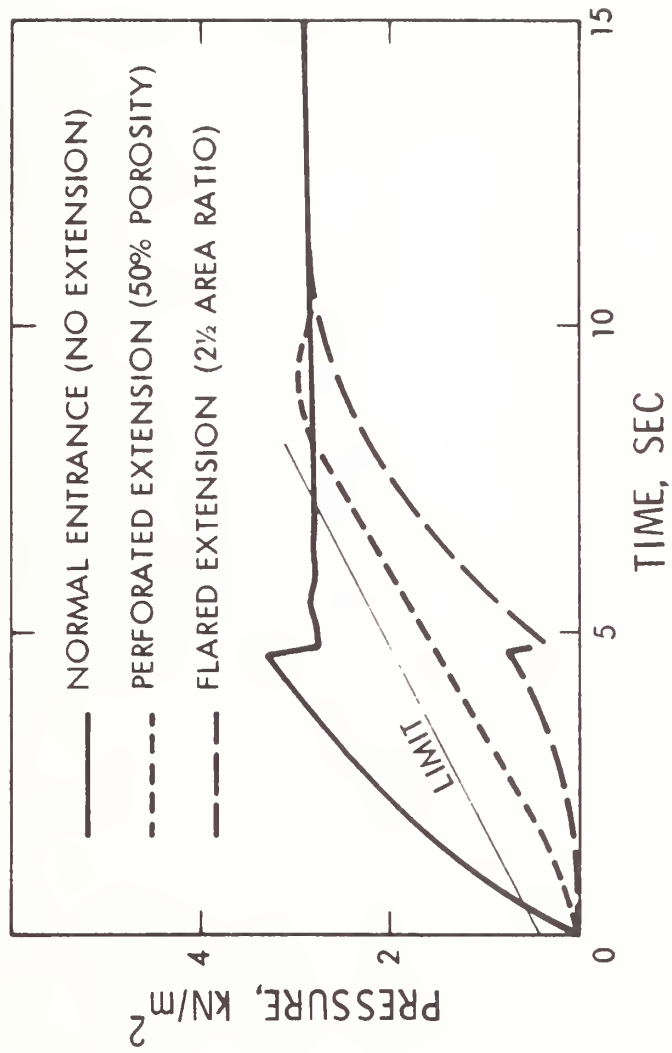


FIGURE 11-2. EFFECT OF PORTAL EXTENSION ON PRESSURE TRANSIENTS EXPERIENCED BY RIDERS ON TRAINS ENTERING TUNNELS

TABLE 11-2. TRADE-OFF STUDY COMPARISON OF APPROACHES (\$K PER YEAR)

	TE	BE	PEOPLE	CAPITAL*	Σ^{**}
RESTRICTED SPEED					
HOLD TO 60 mph TILL PAST PORTAL	-3	0	97(11) ^e	0	94
80 - 60 - 80 mph	34	18	45(5)	0	97
NO SPEED RESTRICTION	0	0	0(0)	180	18
SEALED CARS	0	0	0(0)	10000	1000

*Total (not per year)

** Σ = TE + BE + People + Capital/10

^e () Time Lost per Entry, sec

Unless there are a great many tunnels and just a few train cars, it does not appear that the sealed-car approach can be competitive with the other approaches for train speeds up to 80 mph. For train speeds of 120 mph, the costs of the other approaches will increase significantly while the sealed-car approach stays about the same. Therefore, a separate trade-off study is required for each speed regime.

12. SUMMARY

Agreement between the experimental results and the numerical predictions from the computer program has been demonstrated to be very good. This permits a high degree of confidence to be placed in both.

The experiments clearly demonstrate that very useful attenuation of the nose-entry wavefront can be achieved by equipping a tunnel with either a perforated or a flared entrance. With the former, relatively little dependence on the amount and distribution of the porosity has been demonstrated. The influence of the two entrance regions is broadly similar, but the flared entrance is considerably more effective in the elongation of the tail-entry wavefront. This leads to a reduction in the pressure magnitudes when the entrance is significantly longer than the train. In the small-scale experiments, the flare did not cause an additional reduction in the pressures expected from it acting as a diffuser, but it is still possible that a full-scale flare could be designed to yield this improvement.

Airshafts can be used to alleviate the pressure transients. Ideally they should be of a small cross-section on the order of 15% of the tunnel cross-section. If ventilation requirements dictate that large-bore shafts must be used, these should be equipped with dampers which can greatly reduce the effective shaft area.

Flow restrictions at the rear of the train and/or at the tunnel exit portal can be used to reduce or even eliminate wave activity. The built-up train rear is especially useful when a perforated tunnel entrance region is used because the latter has relatively little influence on the tail-entry wavefront. The ideal size of restrictions at the tunnel exit portal is such that the reduced area available for airflows is much smaller than the train. This

implies that the restrictions must be either removable or sufficiently flexible to allow trains to penetrate them.

The computer program has been used to extend the work to full-scale situations representative of real tunnels. Both simple and complex tunnel systems have been considered. With a simple tunnel, the use of flared or perforated entry portals has the same effect as in the small-scale tests. Additional benefit can be gained from using a small-bore airshaft in conjunction with one of these regions. The combined effect is similar to that of a longer extension. The airshaft could usefully be replaced by several very small-bore shafts which might be produced inexpensively.

In a complex tunnel system, wavefronts may be generated by trains at several different positions. Provided that these sites are not close together, it is sufficient to regard each as independent of the others when analyzing methods of alleviating the pressure transients. With this philosophy, for a tunnel system similar to the Transbay Tube under San Francisco Bay, a modification was suggested so that vehicle entry at 80 mph will not cause pressure histories on trains to violate passenger comfort criteria. The configuration considered could be improved even further if an optimization study were carried out.

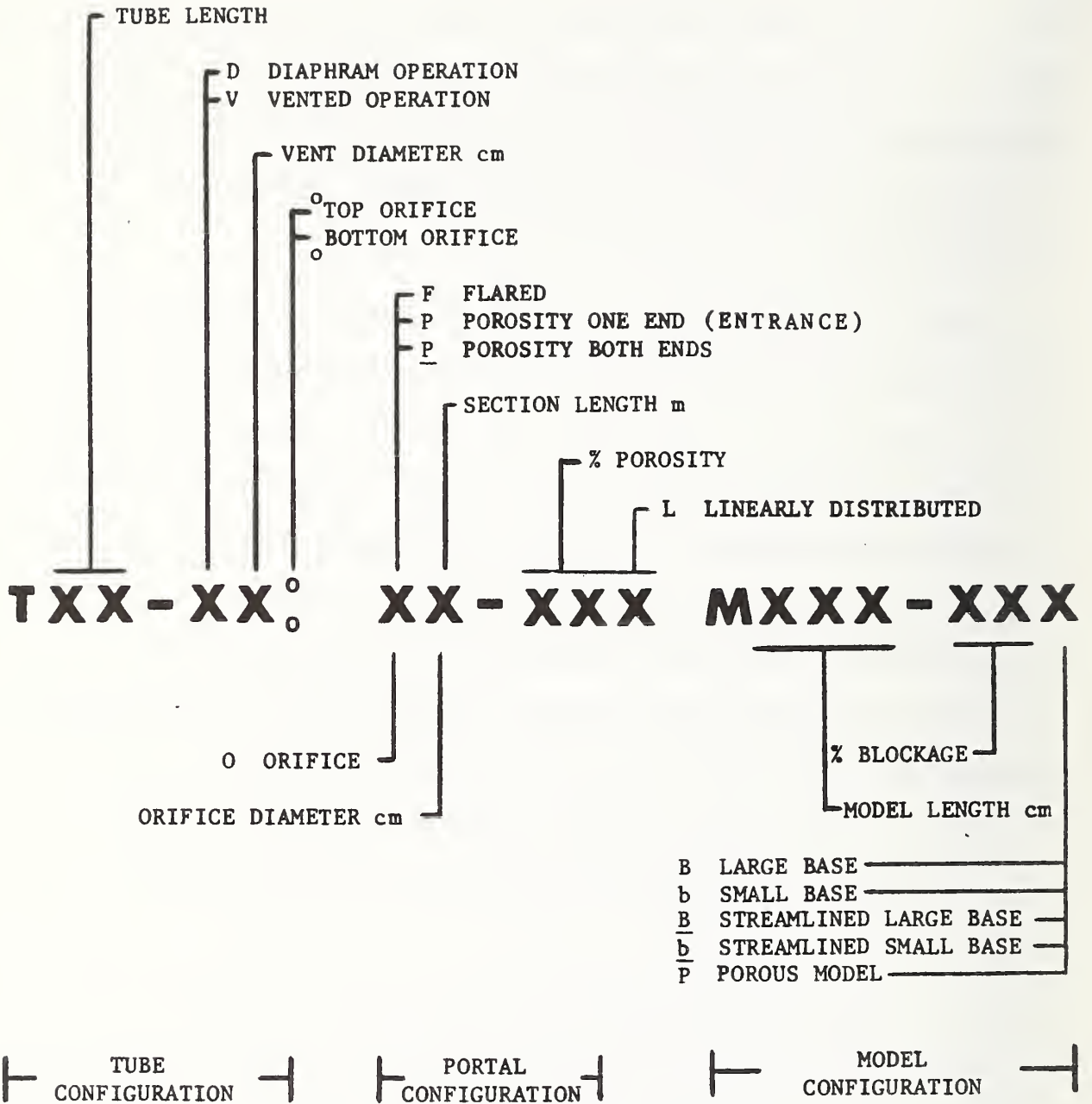
It was shown that these geometric modification approaches to alleviating the pressure transients can be cost-effective compared to the other approaches that were mentioned, including the usual one of restricting the train speed when entering a tunnel. However, additional work is required in order to insure an optimum design is obtained along with a firmly-based cost estimate.

APPENDIX A: RUN INDEX

This Run Index includes all runs that were made following the shakedown (development) phase of the facility. The prefix "C" to the run number indicated calibration runs. The model speed listed are those indicated by the photocells and should not be taken as the actual speeds through the tube. The "Indicated Settings" for the oscilloscope are to be used in conjunction with the pressure and time calibration tables in order to apply proper scales to the "Oscilloscope Trace" data.

Occasionally, the upper trace (Statham) and the lower trace (Kistler) had different settings on the oscilloscopes. This is indicated by "T" (top) for upper and "B" (bottom) for the lower trace. Normally, the Stations at which the transducers were located are the same for the entire page of the Run Index. When that is not the case, it is noted by asterisks (*) and/or in the "Remarks" column. As the comments in the "Remarks" column may be critical, they should be considered as important as any other information on the Run Index. A number of typographical errors may still exist. Any will probably show up during data analysis.

RUN NOMENCLATURE



RUN INDEX

RUN	TEST CONFIGURATION	LAUNCH SPEED m/s	Time ms/cm	INDICATED SETTINGS						REMARKS
				Pressure mv/cm						
				125	225	325	425			
C100	T19 M55-50	24.71	5	T	50	50	50			All pressure transducers located at STN 225.
				B	100	100	100	50		
100	T19 M55-50	24.71	20	T	50	50	50			Basic Run
				B	100	100	100	50		
101	T19 M55-25	24.71	20	T	50	50	50			
				B	100	100	100			
102	T19 M55-75	23.45	20	T	100	100	100			
				B	200	200	200	200		
103	T19 P 1/2-25	24.06	20	T	100	100	100			
				B	200	200	200	200		
104	T19 P 1/2-25	24.06	20	T	50	50	50			
				B	100	100	100	100		
105	T19 P 1/2-25	24.06	20	T	20	20	20			
				B	50	50	100	50		
106	T19 P 1/2-50	24.06	20	T	20	20	20			
				B	50	50	50			
107	T19 P 1/2-50	24.71	20	T	50	50	50			
				B	100	100	100	50		
108	T19 P 1/2-50	23.45	20	T	100	100	100			
				B	200	200	200	100		
109	T19 P 1-50	24.06	20	T	100	100	100			
				B	200	200	200	200		
110	T19 P 1-50	24.71	20	T	50	50	50			Basic Run (Alt)
				B	100	100	100	100		
111	T19 P 1-50	24.71	20	T	20	20	20			
				B	100	50	50	50		
112	T19 P 2-50	24.71	20	T	20	20	20			
				B	100	50	50	50		
113	T19 P 2-50	24.06	20	T	50	50	50			
				B	100	100	100			

RUN INDEX

RUN	TEST CONFIGURATION	VELOCITY m/s	Time ms/cm	INDICATED SETTINGS				REMARKS
				Pressure	mv/cm	Pressure	mv/cm	
114	T19 P2-50 M55-75	23.45	20	T 100	225	325	1372	
115	T19 P2-100 M55-75	23.45	20	B 200	200	200	100	
116	T19 P2-100 M55-50	24.71	20	T 50	50	50	50	
117	T19- P2-100 M55-25	24.06	20	T 20	20	20	20	
118	T19 P1-75 M55-25	24.71	20	B 50	50	50	50	
119	T19 P1-75 M55-50	24.71	20	T 50	50	50	50	
120	T19 P1-75 M55-75	24.06	20	T 100	100	100	100	
121	T19 P1-100 M55-75	24.06	20	B 200	200	200	100	
122	T19 P1-100 M55-50	24.71	20	T 50	50	50	50	
123	T19 P1-100 M55-25	25.40	20	B 100	100	100	100	
124	T19 P2-100 M55-25	24.71	20	T 20	20	20	20	
125	T19 P2-100 M55-50	24.71	20	B 50	50	50	50	
126	T19 P2-100 M55-75	23.45	20	T 50	50	50	50	
127	T19 P1-25 M55-75	23.45	20	B 100	100	100	100	
128	T19 P1-25 M55-50	24.71	20	T 50	50	50	50	

RUN INDEX

RUN	TEST CONFIGURATION		VELOCITY m/s	Time ms/cm	INDICATED SETTINGS						REMARKS
					Pressure mv/cm						
					125	225	425	325	425	1372	
129	T19 P1-25	M55-25	25.4	20	T 20	20	20	20	20		
					B 50	50	50	50	50	50	
130	T19	M55-50	24.71	20	T 50	50	50	50	50		Basic Run
					B 100	100	100	100	100	50	
131	T19	M55-50	24.71	50	T 50	50	50	50	50		Basic Run
					B 100	100	100	100	100		
131A	T19 P1-12 1/2	M55-50	24.71	50	T 50	50	50	50	50		Basic Run
					B 100	100	100	100	100	100	
132	T19 P1-50	M55-50	24.06	50	T 50	50	50	50	50		Basic Run (Alt.)
					B 100	100	100	100	100	100	
133	T19 P1-50	M55-50	24.71	20	T 50	50	50	50	50		Basic Run (Alt.)
					B 100	100	100	100	100	100	
134	T19	M55-50	24.06	20	T 50	50	50	50	50		Basic Run - moved both transducers from 325 to 425 for rest of test.
					B 100	100	100	100	100	50	
135	T19 P1-50L	M55-50	24.06	20	T 50	50	50	50	50		
					B 100	100	100	100	100	50	
136	T19 P1-50L	M55-25	25.40	20	T 20	20	20	20	20		
					B 50	50	50	50	50	20	
137	T19 P-50L	M55-75	23.45	20							
					200	200	200	200	200	100	
138	T19 P1-50	M55-50P	24.71	20	T 50	50	50	50	50		
					B 100	100	100	100	100	50	
138A	T19 P1-50	M55-50	26.13	20	T 50	50	50	50	50		
					B 100	100	100	100	100	50	9.75° half angle come on model nose.
139	T19 P 1/2-50	M55-50P	24.71	20	T 50	50	50	50	50		
					B 100	100	100	100	100	50	
140	T19 P 1/2-50	M55-50B	24.71	20							
					200	200	200	200	200	100	
141	T19 P 1/2-50	M55-50b	24.06	20							
					100	100	100	100	100	50	

RUN INDEX

RUN	TEST CONFIGURATION	VELOCITY m/s	Time ms/cm	INDICATED SETTINGS				REMARKS
				Pressure	mv/cm	Pressure	mv/cm	
142	T19 M55-50b	24.71	20	125	225	425	1372	
143	T19 M55-50P	24.71	20	T	50	50	50	
				B	100	100	100	50
144	T19 P2-50 M55-50P	24.06	20	T	50	50	50	
				B	100	100	100	50
145	T19 P2-50 M55-50B	24.71	20	T	50			
				B	200	200	200	50
146	T19 P2-50 M55-50b	24.06	20	T	50	50	100	
				B	100	100	200	50
147	T19 M55-50	27.71	20	T	50	50	50	9.75° half-angle C one on nose.
148	T19 P1-50 M55-50b	24.71	20	R	100	100	100	
				T	50	100	50	
149	T19 P1-50 M55-50B	24.71	20	B	100	100	100	
				T	200			
150	T19 M55-50B	24.06	20	B	50	200	200	100
				T	100			
151	T19 03 M55-50B	24.06	20	B	500	100	100	100
				T	100	100	100	
152	T19 01 M55-50B	24.06	20	B	50	50	50	100
				T	100	100	100	
153	T19 01 M55-50b	24.06	20	B	50	200	200	100
				T	100	100	100	
154	T19 03 M55-50b	24.06	20	T	100	100	100	
				B	50	200	200	50
155	T19 01 M55-50	24.06	20	T	100	100	100	
				B	50	50	50	50
156	T19- V5 M55-50	24.71	20	T	20	20		
				B	200	200		20

RUN INDEX

RUN	TEST CONFIGURATION	VELOCITY m/s	TIME ms/cm	INDICATED SETTINGS			REMARKS
				T	B	PRESSURE mv/cm	
157	T19-V5	26.31	20	20	20	1372	
158	T19-V5	24.06	20	50	100	200	
159	T19-V2	24.06	20	50	100	200	
160	T19-V2	24.06	20	50	50	50	
161	T19-V2	25.40	20	20	20	20	
C161A	T19	24.71	5	T 50 B 100	50 100	50 100	All pressure transducers located at Station 225
C161B	T19	24.71	20	50	50	50	
C161C	T14	24.71	20	50	50	50	
162	T19-V5 _o	24.06	20	50	50	50	
163	T19-V5 ^o	24.06	20	50	50	50	
164	T19-V5 ^o	24.06	20	100	100	100	
165	T19-V5 _o	24.06	20	100	100	100	
166	T19-V5 P1-50	24.06	20	50	50	50	
167	T19-V2 P1-50	24.06	20	50	50	50	
168	T19-V2 P1-50	24.06	20	100	100	100	

RUN INDEX

RUN	TEST CONFIGURATION		VELOCITY m/s	TIME ms/cm	INDICATED SETTINGS			REMARKS	
					PRESSURE	mv/cm			
169	T19-V5	P1-50 M55-75	24.06	20	125	225	425	1372	
170	T14	P1-50 M55-75	24.06	20	T	200	200	200	Downstream pressure transducer is in removed portion of tube.
171	T14	1-50 M55-50	24.06	20	B	100	100	100	
172	T14	P1-50 M55-25	25.40	20		100	100	100	
173	T19	F1-0 M55-50	24.06	20		50	50	50	
174	T19	F1-0 M55-75	26.13	20		100	200	200	100
175	T14	F1-0 M55-75	24.06	20		100	200	200	
176	T14	F1-0 M55-25	24.71	20		20	20	20	Downstream pressure transducer relocated @ STN 1125.
177	T14	F1-0 M55-50	24.71	20		50	50	50	Downstream pressure transducer relocated @ STN 1125.
178	T19	F1-0 M55-50	24.71	20		50	50	50	
179	T19	F1-0 M55-25	24.06	20		20	20	20	
180	T19	F1-25 M55-25	24.71	20		200	20	20	
181	T19	F1-25 M55-50	24.06	20		50	50	50	
182	T19	F1-25 M55-75	24.06	20		100	50	50	
183	T18	M110-50	17.93	20		50	50	50	125, 225, 425, pressure transducers moved 100 cm for all T18 to keep same distance from entrance as T19. STN 1372 not moved and is at 1272 cm from entrance.

RUN INDEX

RUN	TEST CONFIGURATION	VELOCITY m/s	TIME ms/cm	INDICATED SETTINGS			REMARKS	
				PRESSURE mv/cm ^{1/2}	ms/cm	ms/cm ^{1/2}		
184	T18 M110-50	25.40	20	125	225	425	1372	
185	T18 P1-25 M110-50	25.40	20	50	50	50	50	
186	T18 P1-50 M110-50	26.13	20	50	50	50	50	
187	T18-P1-50 ~ 01 M110-50	26.13	20	50	50	50	50	
188	T18 P 1/2-50 M110-50	25.40	20	50	50	50	50	
189	T18 01 M110-50	26.13	20	50	50	50	50	
190	T18 P1-50 M110-50	26.13	50	100	100	100	100	
191	T18 M110-50	25.40	50	100	100	100	100	
192	T18 M55-50	24.06	50	100	100	100	100	
193	T19 P1-50 M55-50	25.4	20	T B	50 50	50 100	50 100	Transducers 125 @ 225 cm, 225 @ 325 cm, 425 @ 525 cm from entrance.
194	T19 P1-50 M55-25	24.71	20	20	20	20	20	All positions as listed.
195	T19 P1-50 M55-50	24.71	20	100	200		100	
196	T19 P1-50 M55-50	24.71	20	50	50	50	100	
C196A	T19 M55-50	25.4	5	50	50	50	50	
C196B	T19 M55-75	25.4	5	200	200	200	100	All pressure transducers at STN 225

RUN INDEX

RUN	TEST CONFIGURATION	VELOCITY m/s	TIME ms/cm	INDICATED SETTINGS			REMARKS
				125	225	425	
G196C	T19 M55-25	25.4	5	20	20	20	All pressure transducers at STN 225
197	T19 M55-50	20.78	20*	50	50	50	*STN 1372 set at 5MS/CM this run only Basic Run.
198	T19 M55-50	26.13	50	50	50	50	Basic Run
199	T19 P1-50	26.13	50	50	50	50	Basic Run
200	T19 P1-50	26.13	20	50	50	50	
201	T19 P1-50	26.13	20				Statham transducer from STN 425 installed at STN 1372
202	T19 M55-50	25.40	20				50
203	T19 P1-50	26.13	20	50	50	50	Kistler pr. transducer from STN 425 along with old kulite
204	T19 M55-50	26.13	20	50	50	50	8 holes inadvertently left open near entrance of tube installed at STN 25
205	T19 + Flow M55-50	26.13	20	50	50	50	Positive flow in tube prior to model entering.
206	T19 M55-50	26.13	20	T 50 B 100	50	50	
207	T19 M55-50B	25.4	20	T 100 B 200	100	100	
208	T19 M55-50b	25.4	20	T 50 B 100	50	50	
209	T19 M55-50	23.0	20	T 50 B 100	50	100	

RUN INDEX

RUN	TEST CONFIGURATION	VELOCITY m/s	INDICATED SETTINGS		REMARKS
			TIME ms/cm	PRESSURE mv/cm	
210	T19-D		20	225 525 1825	Shakedown with new transducer locations STN 125 to 225, STN 225 to 525, STN 425 to 825 At .094 ATM (Above Atmosphere)
211	T19-D		20	100 100 100	At .094 ATM
212	T19-D		20	100 100 100	At .094 ATM
213	T19-D		20	200 200 200	At .048 ATM
214	T19-D		20	100 100 100	At .046 ATM
215	T19-D		20	100 100 100	At .046 ATM
216	T19-D 01		20	100 100 100	At .046 ATM
217	T19-D 03		20	100 100 100	At .046 ATM
218	T19-D *		20	100 100 100	At .046 ATM * Closed entrance
219	T19-D *		20	200 200 200	At .094 ATM * Closed entrance
220	T19-D P1-50		20	100 100 100	At .046 ATM
221	T19-D P1-50		20	100 100 100	At .046 ATM
222	T19-D P1-50		20	100 100 100	At .046 ATM
223	T19-D P1-50		20	200 200 200	At .094 ATM

RUN INDEX

RUN	TEST CONFIGURATION	VELOCITY m/s	TIME ms/cm	INDICATED SETTINGS PRESSURE mv/cm		REMARKS
				225	525 825	
224	T19-D P1-50		20		200 200	At .094 ATM (Above Atmosphere)
225	T19-D P1-50		20		200 200 200	At .094 ATM
226	T19-D P2-100		20		200 200 200	At .094 ATM
227	T19-D P2-50		20		200 200 200	At .094 ATM
228	T19-D P 1/2-25		20		100 100 100	At .047 ATM
229	T19-D p 1/2-50		20		100 100 100	At .047 ATM
230	T19-D P1-50L		20		100 100 100	At .047 ATM
231	T19-D P1-50L		20		200 200 200	At .094 ATM
232	T19-D F1 -25		20		100 100 100	At .047 ATM
233	T19-D F1-0		20		100 100 100	At .047
234	T19 M55-50	24.06	20	T B 50 50*		* New Kulite pressure transducer all at STN 225
C234	T19 M55-50	24.71	5	T B 100 50*		* New Kulite pressure transducer all at STN 225
235	T19 M55-50	25.40	50	T B 50 50*		*New Kulite pressure transducer all at STN 225
236	T19 M55-25	24.71	20	T B 50 20*		* New Kulite pressure transducer all at STN 225
237	T19 M55-75	24.06	20		200 200*	* New Kulite pressure transducer all at STN 225

RUN INDEX

RUN	TEST CONFIGURATION	VELOCITY m/s	TIME ms/cm	INDICATED SETTINGS			REMARKS
				TIME	PRESSURE	mv/cm	
238	T19 P1-50 M55-75	24.71	20	T B T	225 200 200	225 200*	
239	T19 P1-50 M55-50	24.71	20	B T	100 20	50* 20*	
240	T19 P1-50 M55-25	24.71	20	B	50	20*	
241	T19 P1-50 M55-50	24.71	50		50	50*	Basic Run (Alt)
242	T19 P 1/2-50 M55-50	24.71	20		50	50*	
243	T19 P2-50 M55-50	24.71	20		50	50*	
244	T19 P1-50 M55-50	21.7	20		50	50*	Low entry speeds
245	T19 P1-50 M55-50	20.32	20		50	50*	
246	T19 P1-50 M55-50	14.51	20		50	50*	
247	T19 M55-50	15.5	20		50	50*	
248	T-7 M55-50	25.4	20		50	50*	Basic Run
249	T-7 P1-50 M55-50	24.06	20		50	50*	Basic Run (Alt)
250	T19 P2-75L M55-50	24.06	20		50	50*	0-1m 50%, 1-2m 25%
251	T19 P2-100L M55-50	24.06	20		50	50*	0-1/2m 50%, 1/2-1m 25%, 1-2m 25%
252	T19 P2-112L M55-50	24.06	20		50	50*	0-1/2m 50%, 1/2-1m 37%, 1-2m 25%

APPENDIX B: EXAMPLES OF RAW DATA

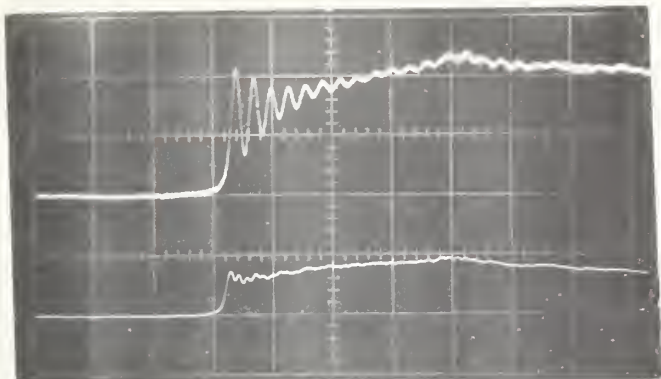
This appendix contains examples of the raw oscilloscope data. The sheet for Run C161A (Figure B.1) typifies the reruns made to relate the pressure calibration factors to the directly calibrated Statham transducer normally placed at Station 225. As all seven gauges were located at Station 225 for the run with an approximate time sweep of 5 ms per cum (major grid spacings), the comparison between the response of the Kistler and Statham transducer as well as their calibration factors can be readily determined.

The normal data run is typified by the oscilloscope sheets in Figure B.2 which are for the two basic runs: the M55-50 model entering the normal tube and the tube with the P1-50 perforated extension. Figure B.3 (Runs 101 and 179) show examples of what is considered to be the poorest data obtained during the experimental program. It is caused by having to increase the signal sensitivity a substantial amount for the 25% blockage model. Usually, the data for this model is more useable than this, but with a flared portal (Run 179), the effective blockage ratio at the moment of entry is about 10%.

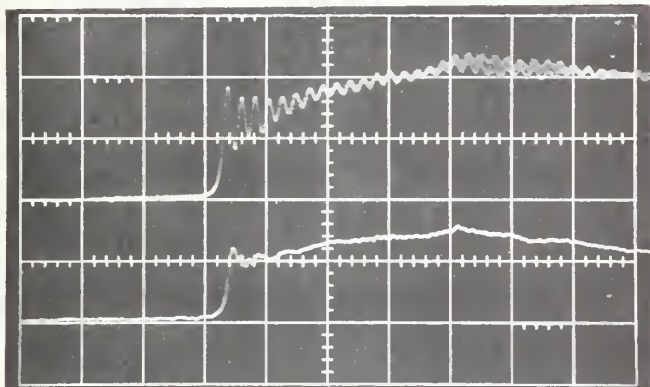
On the other hand, the quality of the pressure data was considerably improved toward the end of the test program when a newly-acquired Kulite transducer was obtained. Not only did it have excellent response time and could make absolute measurements, it was specifically matched for the pressure range expected. The data for this transducer which was located at Station 225 is included in its entirety in Figure B.4 (Runs 234-252).

A series of runs were made by bursting a diaphragm that sent a controlled pressure pulse down the tube in order to investigate wave reflection off of the tube end. The downstream portion of the tubes was sealed, pumped up to a fixed

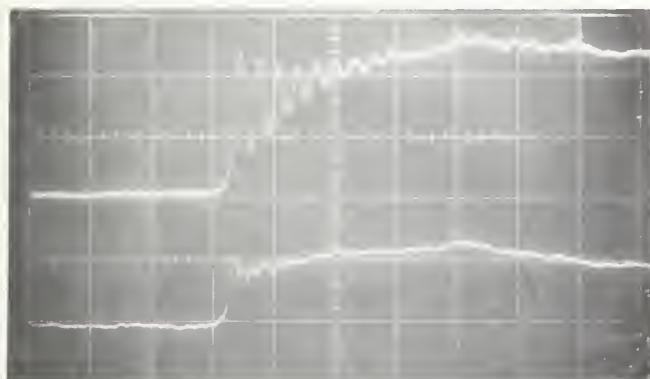
pressure somewhat above atmospheric. Then the milar diaphragm was ruptured by heating a nichrome wire which encircled it. Examples of this type of data appear in Figure B.5 (Runs 212 and 214). As the repeatability was not ideal (that for the model runs was), many repeats were run. None of this data has been analyzed.



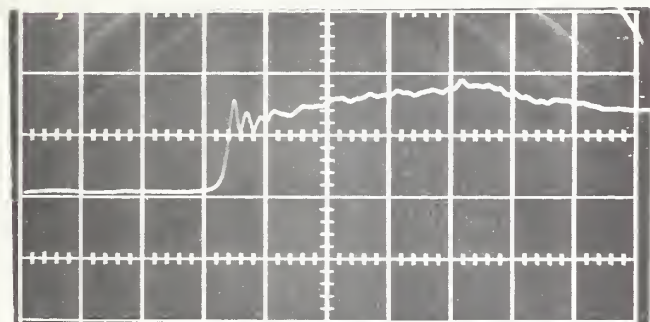
STATION 125



STATION 225

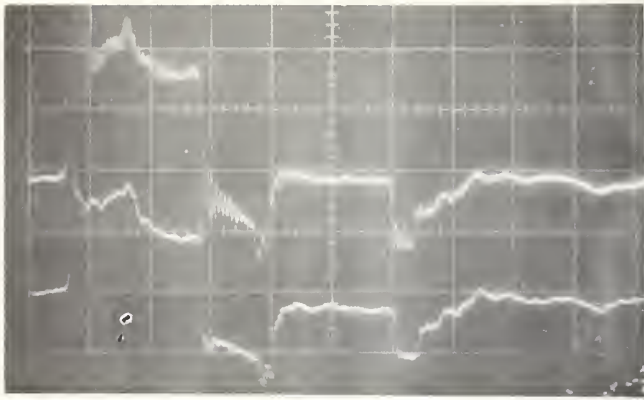


STATION 425

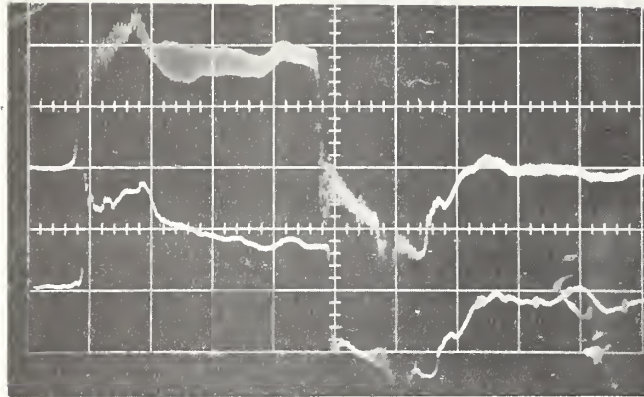


STATION 1372

FIGURE B-1. CALIBRATION TRACES



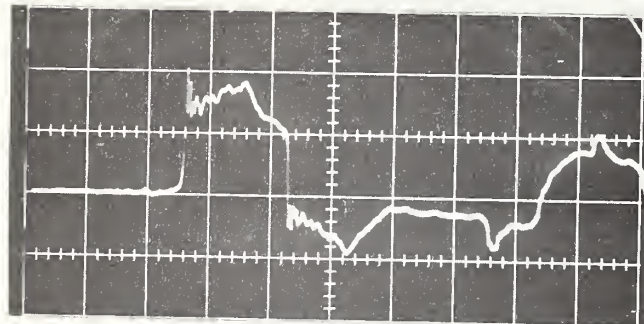
STATION 125



STATION 225

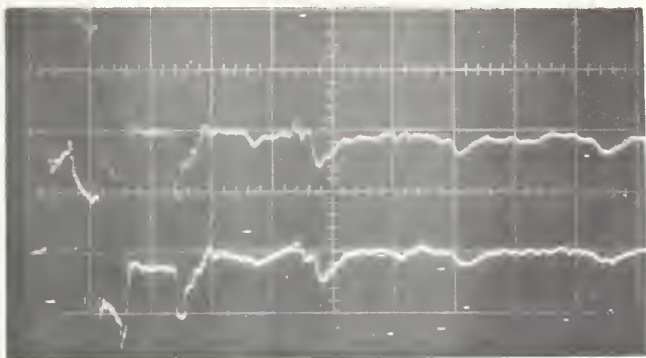


STATION 325

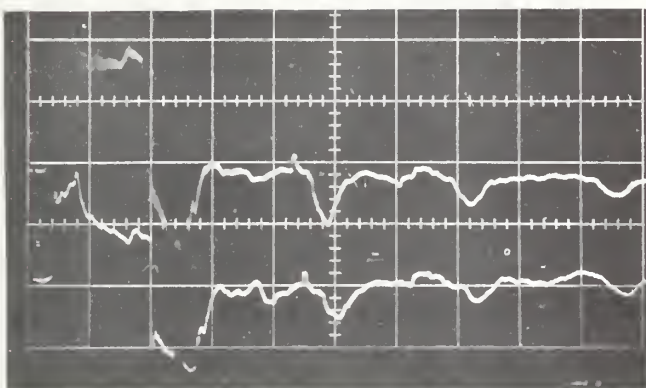


STATION 1372

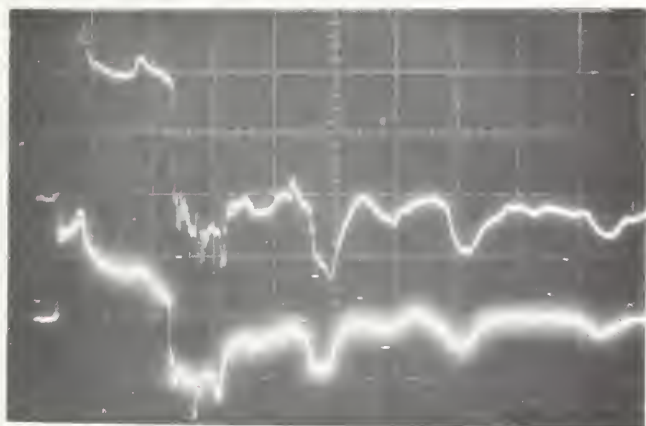
Figure B-2a. TYPICAL TRACES



STATION 125

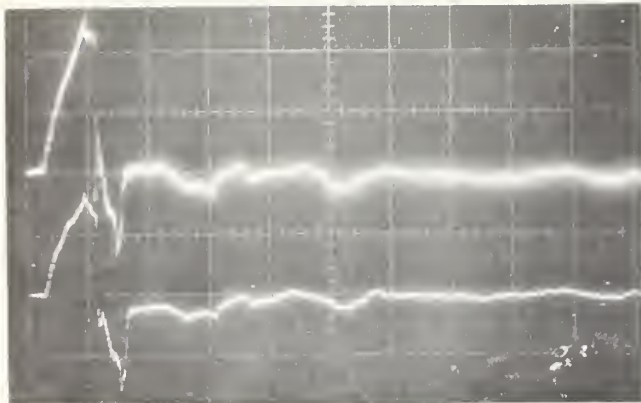


STATION 225

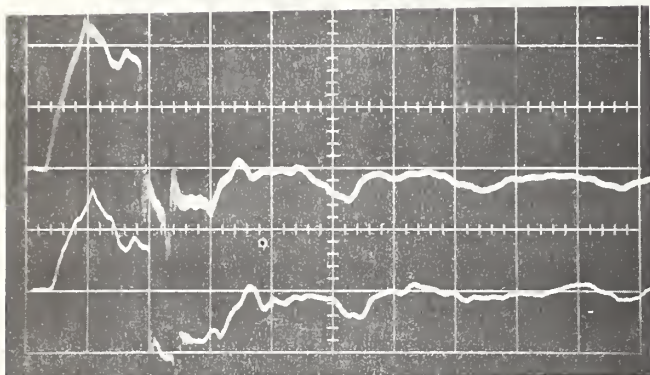


STATION 325

FIGURE B-2b. TYPICAL TRACES (Cont.)



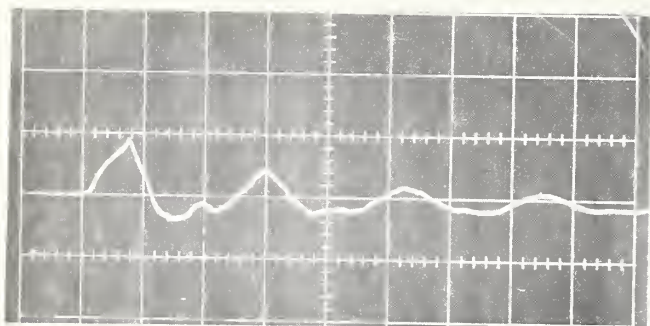
STATION 125



STATION 225

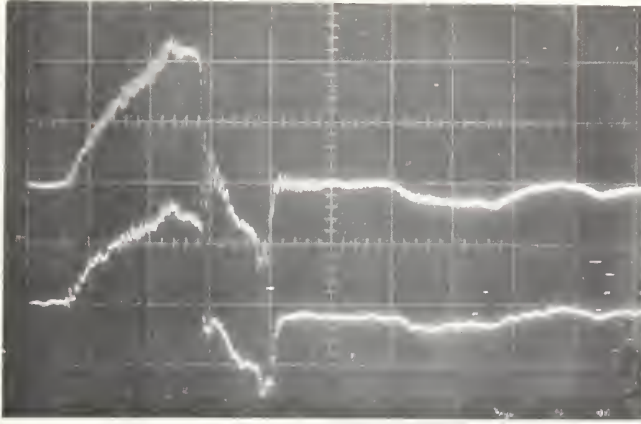


STATION 325

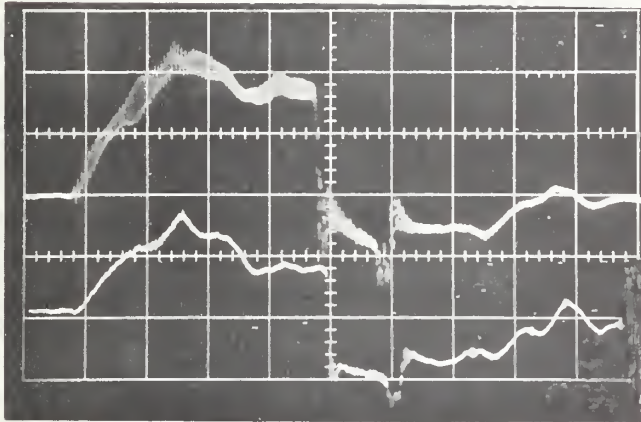


STATION 1372

FIGURE B-2c. TYPICAL TRACES (Cont.)



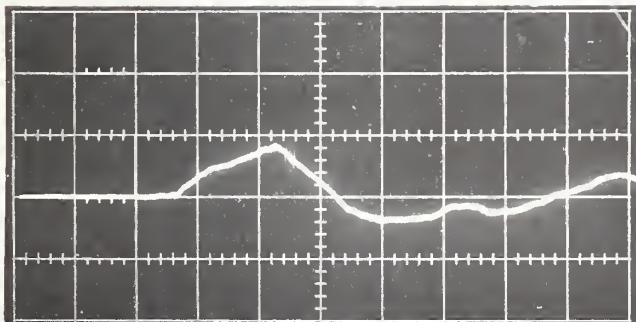
STATION 125



STATION 225

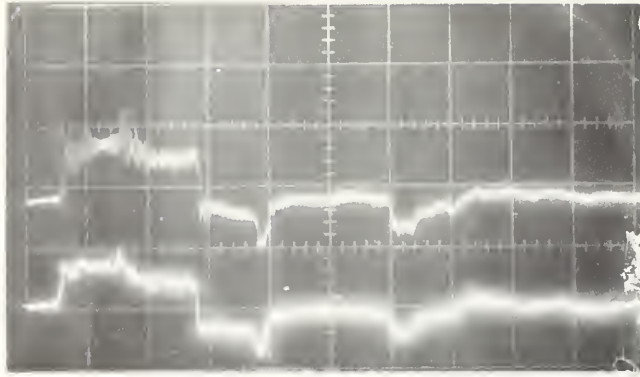


STATION 325

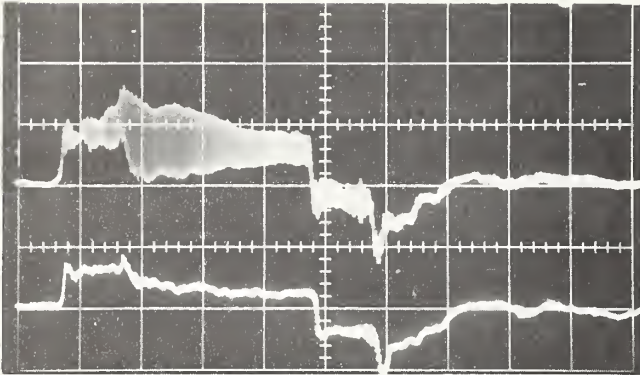


STATION 1372

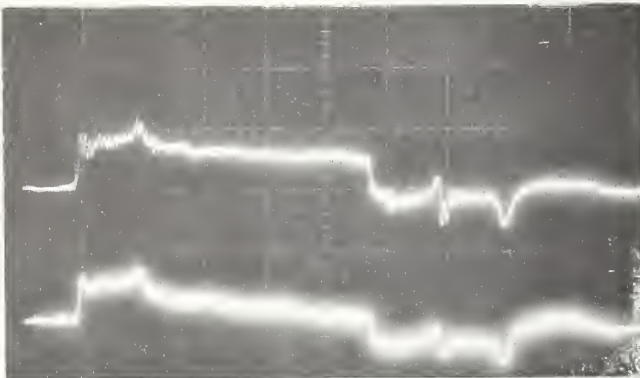
FIGURE B.2d. TYPICAL TRACES (Cont.)



STATION 125

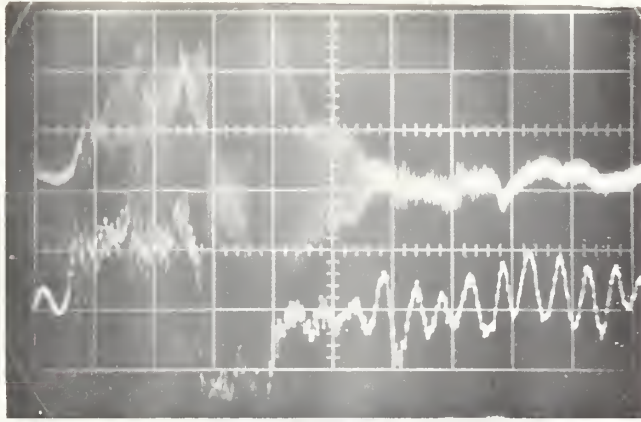


STATION 225

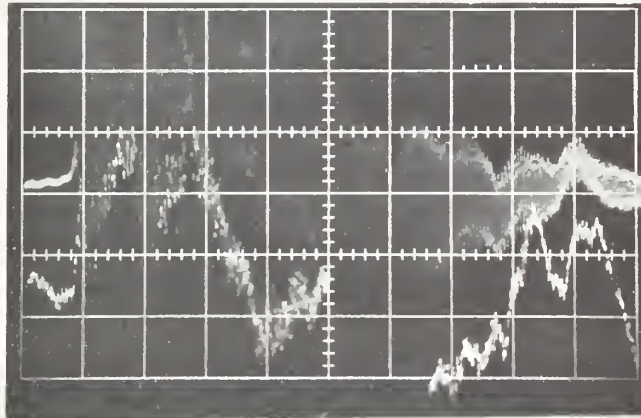


STATION 325

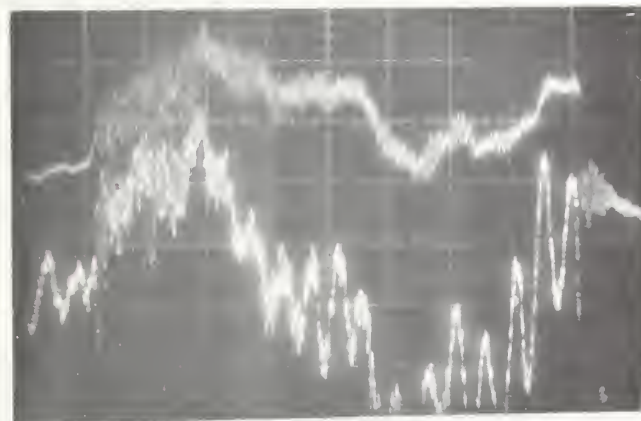
FIGURE B-3a. LOW BLOCKAGE TRACES



STATION 225

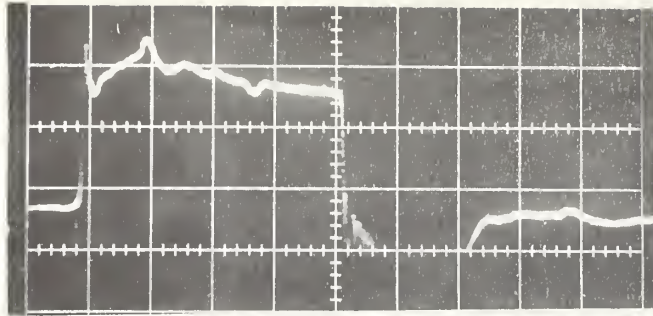


STATION 425

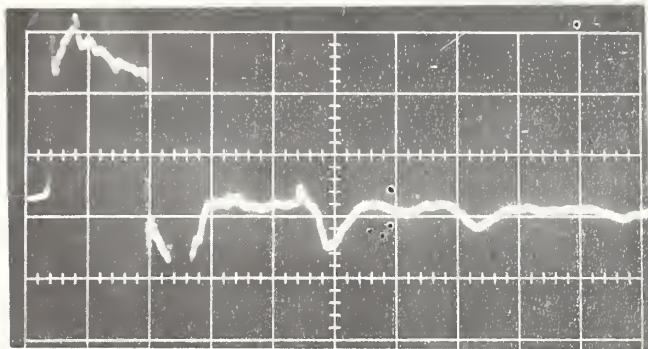


STATION 1372

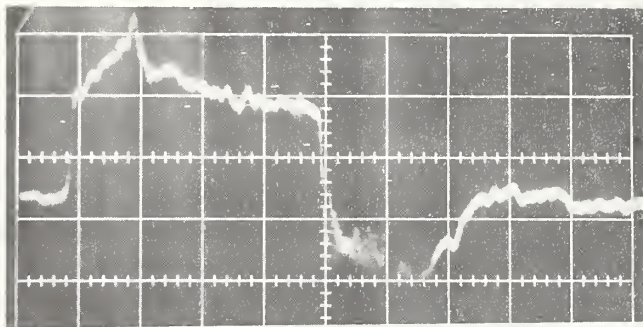
FIGURE B-3b. LOW BLOCKAGE TRACES (Cont.)



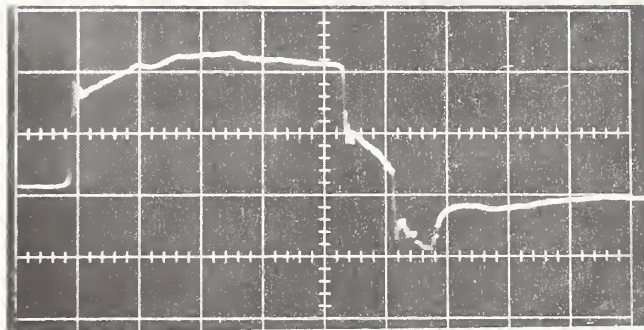
RUN 234



RUN 235

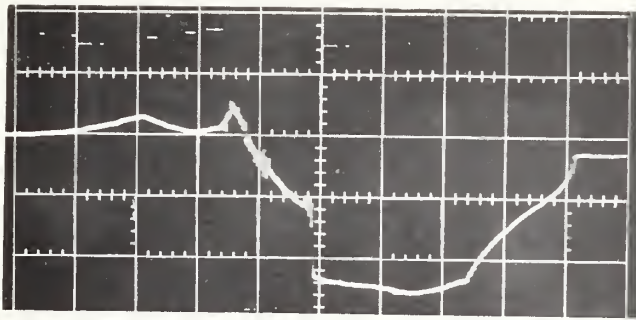


RUN 236

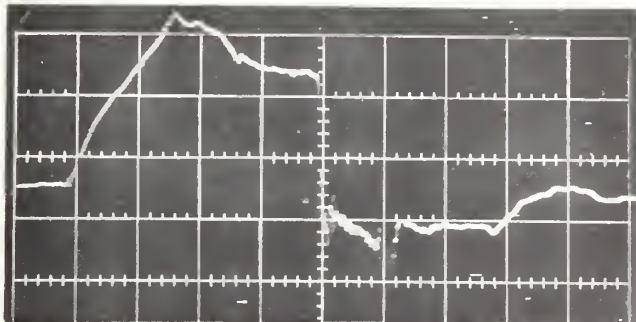


RUN 237

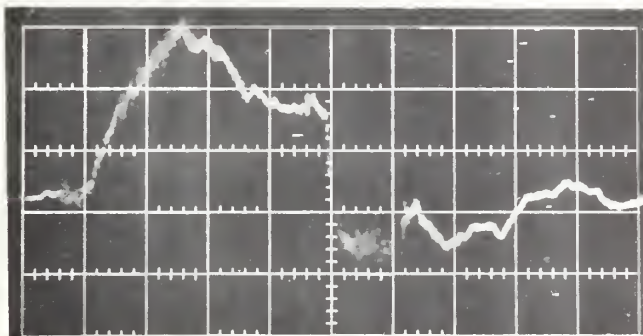
Figure B-4a. KULITE TRACES



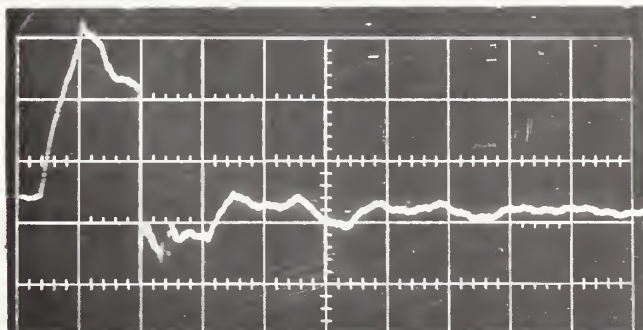
RUN 238



RUN 239

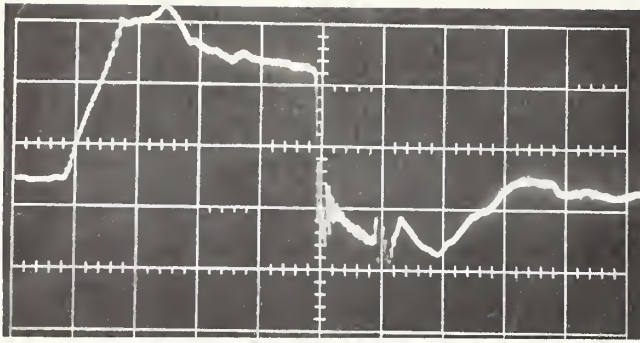


RUN 240

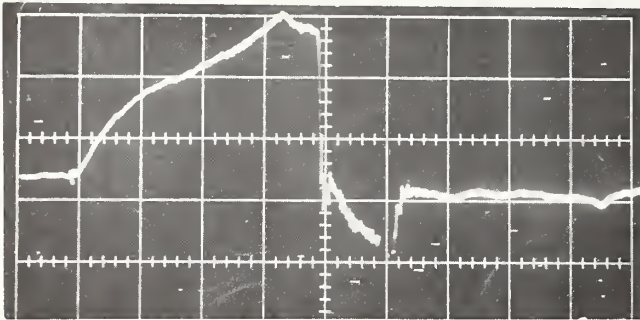


RUN 241

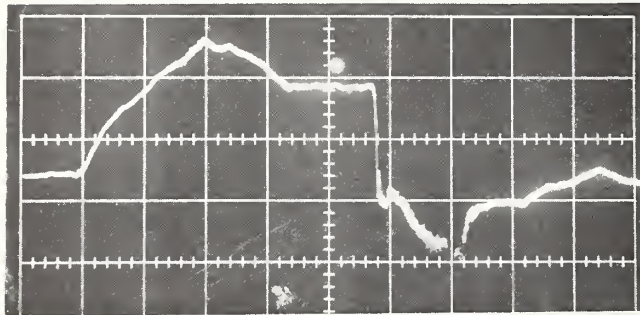
FIGURE B-4b. KULITE TRACES (Cont.)



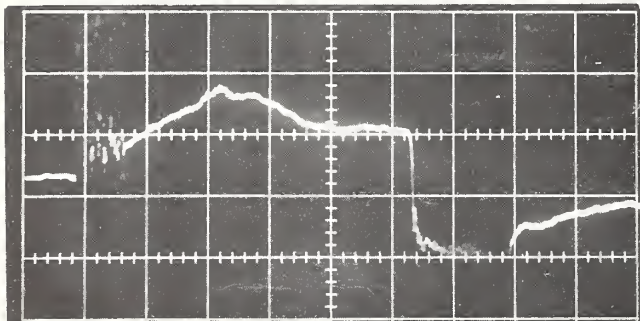
RUN 242



RUN 243

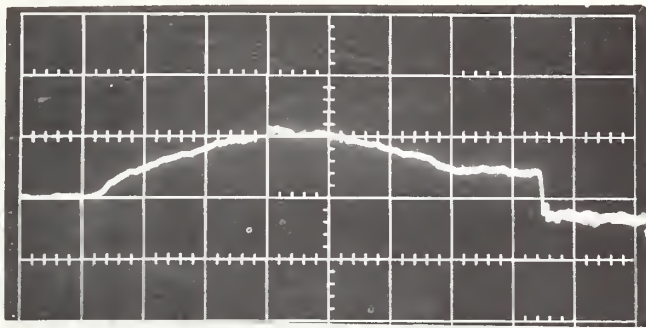


RUN 244

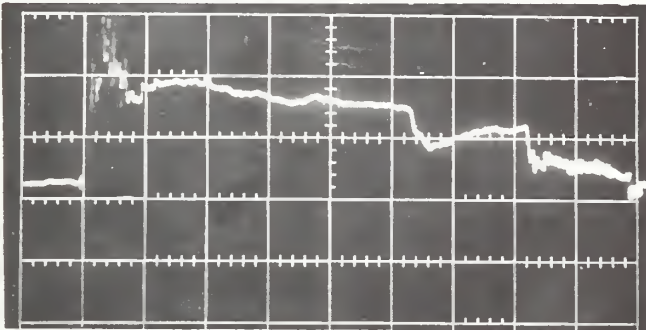


RUN 245

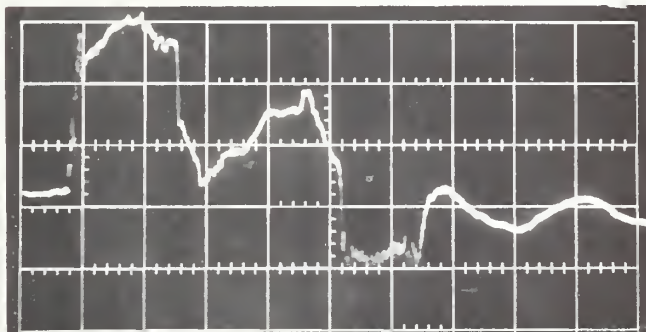
FIGURE B-4c. KULITE TRACES (Cont.)



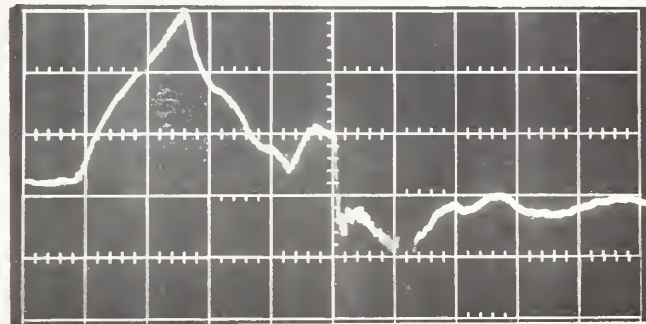
RUN 246



RUN 247

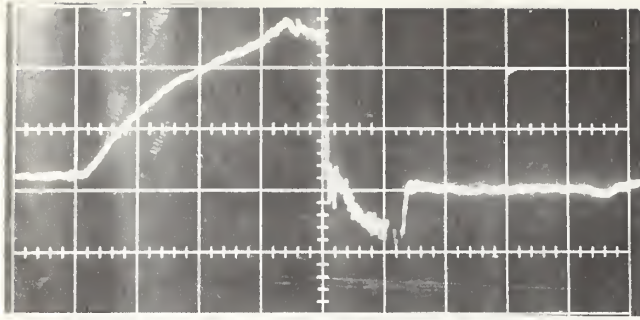


RUN 248

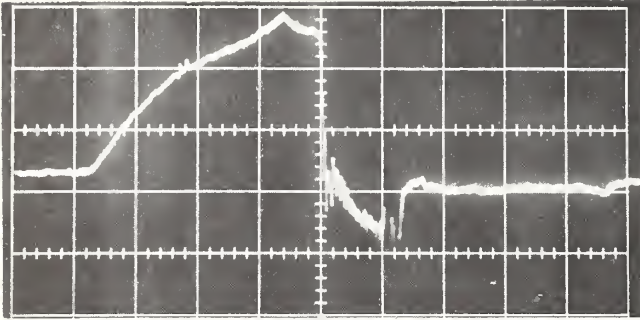


RUN 249

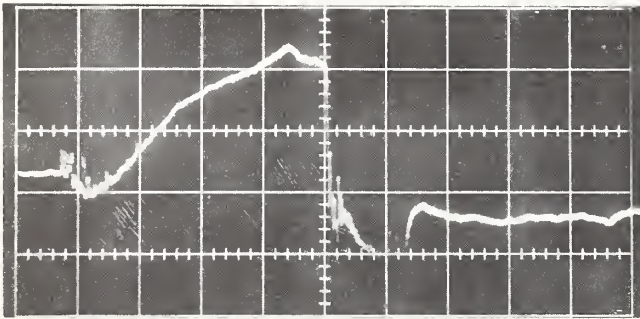
FIGURE B-4d. KULITE TRACES (Cont.)



RUN 250



RUN 251

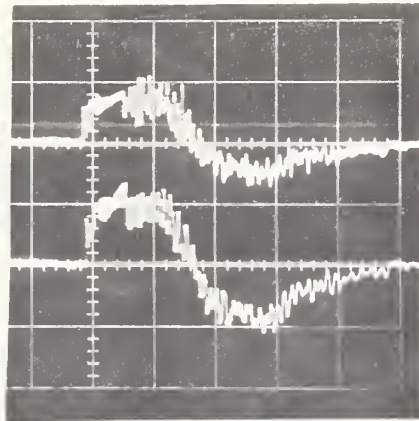
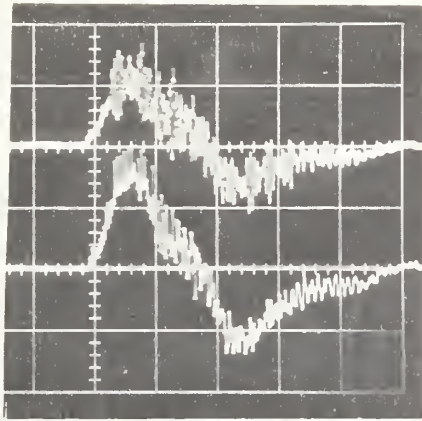


RUN 252

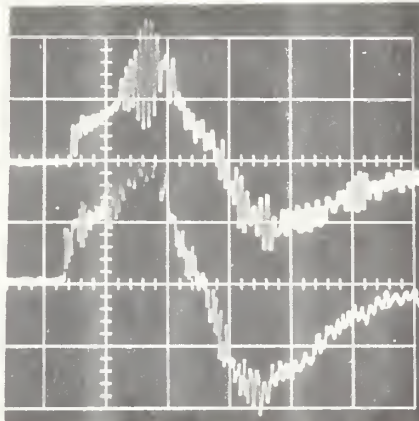
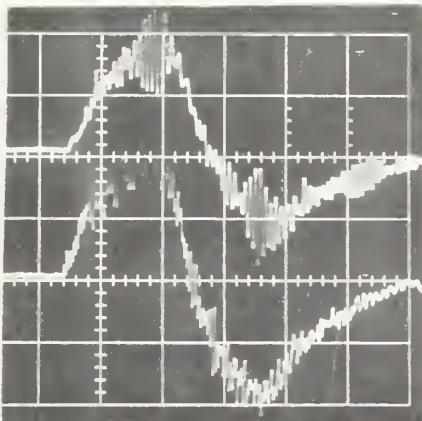
FIGUER B-4e. KULITE TRACES (Cont.)

RUN 212

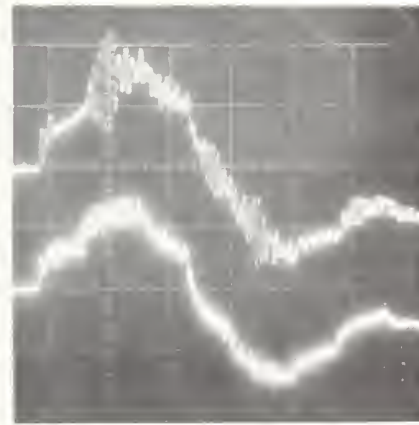
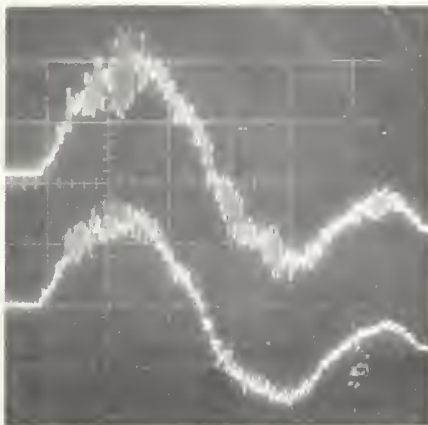
RUN 214



STATION 225



STATION 525



STATION 825

FIGURE B-5. TYPICAL DIAPHRAGM BURST TRACES

REFERENCES/BIBLIOGRAPHY

REFERENCES

1. Fox, J.A., and Vardy, A.E., "The Generation and Alleviation of Air Pressure Transients Caused by the High Speed Passage of Vehicles Through Tunnels," Proceedings of the International Symposium on the Aerodynamics and Ventilation of Vehicle Tunnels, British Hydromechanics Research Association of Fluid Engineering, Paper 63, April 1973.
2. Barrows, T.M., "Tunnel Entry Pressure Transients," International Conference on Transportation, Los Angeles, California, July 1976.
3. Vardy, A.E., "Ventilation Approach Regions for Railway Tunnels," Transportation Engineering Journal, ASCE, Volume 101, No. TEA, Proc. Paper 11691, November 1973, pp. 609-619.
4. Hara, T., "Aerodynamic Force Acting on a High Speed Train at Tunnel Entrance," Railway Tech. Res. Inst. Quarterly Report (Japan), Vol. 2, No. 2, 1961.
5. Yamamoto, A., "On the Gradual Pressure Rise by a Flared Tunnel Entrance," Railway Tech. Res. Inst. Quarterly Report (Japan), Vol. 6, No. 4, 1965, PP. 50-52.
6. Dayman, B., et al, "Alleviation of Pressure Pulse Effects for Trains Entering Tunnels: Experimental Data," JPL Publication No. 78-73, July 1978.
7. Barrows, T.M., "Wave Reflections from Slotted Tunnel Portals," Journal of Sound and Vibration, Vol. 50, No. 4, 1978, pp. 571-585.
8. Vardy, A.E., "Tunnel Entry Pressure Transients, Part 1: State-of-the-Art," University Engineering Department, Cambridge, U. K., May 1977.
9. Hammitt, A.G., The Aerodynamics of High Speed Ground Transportation, Western Periodicals Company, 1973.
10. Hammitt, A.G., and Broadwell, J.E., "Transient Response of Fluid Systems," Journal of the Aerospace Sciences, Vol. 29, No. 7, July 1962.

11. Dayman, B. et al, "Alternative Concepts for Underground Rapid Transit Systems - Volume II C: Supporting Studies - Capital Equipment," Report DOT-TST-77-31, IIC, March 1977.
12. Mathews, A.A., "Alternative Concepts for Tunnel Transit Systems: Cost Estimates of Mined Tunnels," for JPL, November 1977.
13. Carstens, J.P., "Literature Survey of Passenger Comfort Limitations of High Speed Ground Transportation," PB168 171, 1965.

BIBLIOGRAPHY

The following list is by no means exhaustive. However, it will provide a useful starting point for a literature survey. More comprehensive lists are included in Refs. 7-10.

Associated Engineers: "Subway environmental design handbook," v1, U.S. Dept. Transportation Report, No. UMTA-DC-06-0010-74-1, 1975.

Benson, R.S. and Ucer, A.S.: "An approximate solution for non-steady flows in ducts with friction," Int J of Mech Sci, v13, 1971, pp. 819-324.

British Hydromechanics Research Association: "Proc First Int Symp on the Aerodynamics and Ventilation of Vehicle Tunnels," Canterbury, U.K., 1973.

British Hydromechanics Research Association: "Proc Second Int Symp on the Aerodynamics and Ventilation of Vehicle Tunnels," Cambridge, U.K., 1976.

Edgell, G.J.: "Pressure transients in tunnels; extension of theory to irreversible non-adiabatic flow," University of Leeds Report, U.K., 1974.

Giovanni, R: "Design standards for Europe's first 250 km/hr railroad," Railway Gazette International, 1971, pp. 169-272.

Hammit, A.G: "Aerodynamic analysis of tube vehicle systems," AIAA Journal, v10, 1972, pp. 282-290.

Hammit, A.G: "Unsteady aerodynamics of vehicles in tubes," AIAA Journal, v13, 1975, pp. 497-503.

Hara, T. et al: "Aerodynamics of high speed trains," Int Railway Congress Association Bulletin, v45, 1968.

Henson, D.A. and Fox, J.A.: "Transient flows in tunnel complexes of the type proposed for the Channel Tunnel," Proc. Inst. Mech Engrs, v188, (2 papers), 1974, pp. 153-167.

Kurtz, D.W. and Dayman, B., Jr.: "The importance of aerodynamics in the design of intra-urban trains traveling in tunnels," High Speed Ground Trans Journal, v7, 1973, pp. 381-399.

Shapiro, A.H.: "The dynamics and thermodynamics of compressible fluid flow," v1 and v2, The Ronald Press Co., 1953.

Vardy, A.E.: "The reduction of pressure transients in railway tunnels," Sixth Thermodynamics and Fluid Mechanics Convention, Inst Mech Engrs, Durham, U.K., 1976.

Vardy, A.E. and Fox J.A.: "A new airshaft design for railway tunnels," Railroad Tunnel Ventilation Symp. ASHRAE, Halifax, Nova Scotia, 1977.

Woods, W.A. and Gawthorpe, R.G.: "The train and tunnel--A large unsteady flow machine," Second Int JSME Symp: Fluid machinery and fluidics, Tokyo, Japan, 1972.

HE 18.5 . A37 N

ALLEVIATION OF
PULSE EFFECTS

Form DOT F 1720.2 (8
FORMERLY FORM DOT F 170

DOT LIBRARY



00196238

**U.S. DEPARTMENT OF TRANSPORTATION
RESEARCH AND SPECIAL PROGRAMS ADMINISTRATION**

TRANSPORTATION SYSTEMS CENTER
KENDALL SQUARE, CAMBRIDGE, MA. 02142

OFFICIAL BUSINESS
PENALTY FOR PRIVATE USE, \$300

POSTAGE AND FEES PAID

U.S. DEPARTMENT OF TRANSPORTATION

613

